



10 Years of
Technology
Innovation

2007 - 2017

About KOMtech

Launched in December 2007, Keppel Offshore & Marine Technology Centre (KOMtech) is an extension and strengthening of Keppel Offshore & Marine's (Keppel O&M) research and development initiatives. KOMtech comprises two arms, Shallow Water and Deep Water. The Shallow Water segment looks into Arctic jackup designs, offshore wind solutions, LNG applications, environmental and drilling solutions for the oil and gas industry; while the Deep Water segment looks into ultra-harsh environment semisubmersibles, tension leg platforms, innovative ship designs, as well as shipyard technology to improve shipyard processes and productivity.

KOMtech complements and augments the work of the existing four design and engineering units within Keppel O&M - Offshore Technology Development (OTD), Deepwater Technology Group (DTG), Marine Technology Development (MTD), and Gas Technology Development (GTD). Leveraging existing and proprietary technologies, and in collaboration with universities, research institutes and industry partners worldwide, KOMtech continues to develop innovative solutions that are commercially viable and adaptable to the needs of the industry.

Image on cover: Celebrating 10 years of technology innovation. These images were showcased in past years' Technology Review editions, highlighting the technology research milestones over the decade.

CEO's Message

Technological advances throughout the world are changing rapidly, disrupting and affecting industries in myriad ways. Businesses must constantly adapt to market trends which can either be a threat to companies or an opportunity to push ahead of competitors.

Keppel Offshore & Marine Technology Centre (KOMtech), which turns 10 this year, was set up as a technology foresight centre specifically for this purpose. Since KOMtech was launched in December 2007, we have held steadfast to our promise of making prudent investments in research and development (R&D) to enhance our core competencies. We have filed over 180 patents, and developed improved technological offerings for existing and new markets.

Over the years, Keppel Offshore & Marine (Keppel O&M) has consistently sharpened its capabilities by focusing on innovation and technology so that we can continue to provide cutting edge solutions which meet the evolving needs of the market.

Through the Technology Review publication, we have showcased our R&D developments and planted the seeds of research and innovation which have yielded significant results. For example, we have formulated and applied various solutions in LNG transportation, production and storage.

Technology Review 2017 showcases the depth of KOMtech's multi-disciplinary research by covering an extensive range of topics such as automation and digitalisation, as well as other themes such as sustainability. We also look into other novel technologies that can future-proof our products and services.

In the current challenging market conditions, we have expanded our R&D into non-oil and gas solutions. One of the concepts explored is translating offshore knowledge and capabilities into new products such as creating livable cities along the shores which will transform city skylines dramatically.

My appreciation goes to Mr Michael Chia, Managing Director (Marine & Technology), as well as KOMtech's team of capable researchers, guided by Aziz Amirali Merchant, Executive Director, KOMtech, Dr Foo Kok Seng, Executive Director (Shallow Water Technology), and Mr Charles Sim, Technical and Projects Director (Gas Technology and Offshore Production). Keppel O&M's Technology Division brings together the different units in Keppel O&M responsible for R&D, product development and commercialisation. It is also responsible for developing process technology aimed at improving productivity in all our yards.

We appreciate the contribution from our research partners and customers who are also leaders in this industry. We hope this publication continues to inspire innovative breakthroughs, ignite ideas and propel us to continue delivering valuable and practical solutions to the market. Let us look forward to celebrating more years of successful innovation.

Yours sincerely,



Chris Ong
AG CEO
Keppel Offshore & Marine

CEO's Message

Technological advances throughout the world are changing rapidly, disrupting and affecting industries in myriad ways. Businesses must constantly adapt to market trends which can either be a threat to companies or an opportunity to push ahead of competitors.

Keppel Offshore & Marine Technology Centre (KOMtech), which turns 10 this year, was set up as a technology foresight centre specifically for this purpose. Since KOMtech was launched in December 2007, we have held steadfast to our promise of making prudent investments in research and development (R&D) to enhance our core competencies. We have filed over 180 patents, and developed improved technological offerings for existing and new markets.

Over the years, Keppel Offshore & Marine (Keppel O&M) has consistently sharpened its capabilities by focusing on innovation and technology so that we can continue to provide cutting edge solutions which meet the evolving needs of the market.

Through the Technology Review publication, we have showcased our R&D developments and planted the seeds of research and innovation which have yielded significant results. For example, we have formulated and applied various solutions in LNG transportation, production and storage.

Technology Review 2017 showcases the depth of KOMtech's multi-disciplinary research by covering an extensive range of topics such as automation and digitalisation, as well as other themes such as sustainability. We also look into other novel technologies that can future-proof our products and services.

In the current challenging market conditions, we have expanded our R&D into non-oil and gas solutions. One of the concepts explored is translating offshore knowledge and capabilities into new products such as creating livable cities along the shores which will transform city skylines dramatically.

My appreciation goes to Mr Michael Chia, Managing Director (Marine & Technology), as well as KOMtech's team of capable researchers, guided by Aziz Amirali Merchant, Executive Director, KOMtech, Dr Foo Kok Seng, Executive Director (Shallow Water Technology), and Mr Charles Sim, Technical and Projects Director (Gas Technology and Offshore Production). Keppel O&M's Technology Division brings together the different units in Keppel O&M responsible for R&D, product development and commercialisation. It is also responsible for developing process technology aimed at improving productivity in all our yards.

We appreciate the contribution from our research partners and customers who are also leaders in this industry. We hope this publication continues to inspire innovative breakthroughs, ignite ideas and propel us to continue delivering valuable and practical solutions to the market. Let us look forward to celebrating more years of successful innovation.

Yours sincerely,



Chris Ong
AG CEO
Keppel Offshore & Marine

Contents

About KOMtech

CEO's Message	1
Managing Director's Message	4

Advanced Manufacturing & Engineering

We explore the impact of how significant technological advancements in automation & robotics as well as additive manufacturing can propel the offshore and marine sectors to re-invent themselves to stay ahead in the extremely dynamic market environment.

Adopting Automation and Robotics to Propel Advanced Manufacturing Industries to the Next Level	7
---	----------

Identifying Additive Manufacturing Trends and Opportunities in the Offshore and Marine Space	13
---	-----------

Arctic Technology

We continue to focus on developing technologically advanced sustainable solutions for the Arctic by tapping on the strong academic and industry partnership that yields innovative research findings which are industry relevant.

Singapore and the Arctic: A Partnership between Academia and Business through Research & Innovation	23
--	-----------

Deepsea Mining

In the face of rising interests in seabed mineral mining amidst international strict regulations and control, we explore sustainable methods through developing core competencies in deep-water exploration survey techniques for the establishment of an environmental baseline.

Delving Into Deepsea Mining	33
------------------------------------	-----------

Digitalisation

Digital technologies are rapidly being integrated into the offshore and marine industries. One such area includes analysing computational fluid dynamics to improve vessel sea-worthiness in extreme conditions calculating methods to optimise hull designs.

Computing Second Order Wave Load Effects for Coupled Tension Leg Platform and Tender Assisted Semi-Submersible	43
---	-----------

Comparing the Performance Standards of a Tension Leg Platform and Tender Assisted Drilling between Linear Frequency Domain Versus Non-Linear Time Domain Methods	51
---	-----------

Computational Fluid Dynamics Study on Drillship Moonpool Added Resistance	67
Computational Fluid Dynamics Study of Air-Gap and Wave Impact on Semi-submersibles	75
Computational Fluid Dynamics Analysis Applied to Evaluate and Identify B-Series Propellers to enhance Ship Performance	85
Optimising Semisubmersible Hull Design to Minimise Motion and Load in Wave	99
Generating Reliability-Based Vibration Predication using Finite Element Modelling Methods	109
Evaluating Ballast Water Management Plan of a Floating Dry Dock Using Visual Basic for Applications	117

Repurposing Technology

Breaking away from conventional methods of using offshore technology, we expand the application of the innovative and rich technology expertise beyond the offshore and marine space.

A Cost Effective and Versatile Platform Solution for Global Deployment: Keppel Self-Installing Platform	125
Expanding Offshore and Marine Technologies Beyond Current Capabilities	131

Rig of the Future

This is a game changer for the offshore business with research and novel technology infused into rig product and process capabilities to transform the way rigs are being deployed in the next generation.

Improving Energy Efficiency Through New Concept of Energy Storage System for Drilling Rigs and Vessels	135
Enhancing Business Capabilities through Future Digital Rigs : Keppel RigCare™	139
Improving Cargo Handling on Floating Platforms Using Dynamic Lift Monitoring and Predictive Decision Support System	141
Introducing a Novel Mechanical System for Coupling Two Offshore Floating Structures	145
Acknowledgment	151

Managing Director's Message

2017 marks a remarkable ten years of growth for Keppel Offshore & Marine Technology Centre (KOMtech).

Through extensive research and development (R&D), KOMtech has over the past ten years produced enhanced solutions and designs, augmenting the commercialisation work of Keppel O&M's design and engineering units - Offshore Technology Development, Deepwater Technology Group, Marine Technology Development and more recently, Gas Technology Development. We will strive towards continuously raising the benchmark for innovation in our core competencies to support Keppel O&M in always being one step ahead as a market leader.

With the current weakened market conditions, it is an opportune time to review, calibrate and augment our R&D so that Keppel O&M can sharpen its edge in technology solutions, diversify its offerings and boost its presence in key markets. We are constantly thinking out of the box to develop improved technological offerings for existing and new markets. Our team of world-class engineers, researchers and scientists at KOMtech is focused on creating innovative, robust and flexible technology solutions which meet the complex needs of our customers.

KOMtech's technology foresight drives Keppel O&M into new markets and opportunities with innovative solutions that are commercially viable and adaptable. For example, KOMtech has been working with key partners and business leaders to leverage technological advancements in automation & robotics, digitalisation in the offshore and marine industry, as well as additive manufacturing, to stay ahead in an extremely dynamic market environment.

Technology Review 2017 looks into how novel technologies can define the rig of the future, and in this process, create awareness for the need to transform how industry players are currently operating rigs. We introduced the Keppel Self Installing Platform- a suite of multi-functioned fixed platform designs- which brings robust, cost effective and multi-functional alternatives to standard platform designs.

Sustainability, which is growing in importance in this industry, is one of KOMtech's priorities and we are eager to meet the growing needs in this market. One of our key products is the dual fuel propulsion system that allows greener, safer and more cost efficient operation. This innovative design led to the 65-tonne Liquefied Natural Gas (LNG) dual-fuel Azimuth Stern Drive tug receiving the Outstanding Maritime R&D and Technology Award at the 2015 Singapore International Maritime Awards.

Another key strategy for KOMtech is researching how our well-developed technology and innovation can be repurposed beyond the oil and gas industry. For example, by leveraging our in-depth knowledge of arctic environments and ship designs, we can provide luxury cruise ship designs for the arctic environment, a potential game changer for the tourism market constantly in search for its next novel experience. We also examine opportunities in non-conventional energy resources such as designing innovative wind turbines that better harness wind energy at sea.

Such research concerns the industry at large, and this highlights the importance of collaborating with industry organisations, as well as national and higher learning institutions. These partnerships combine the best of industry experience, national strategic direction and strong academic research, resulting in high quality research findings that are relevant to businesses.

We are happy to announce that we have formed a new collaboration with Lloyd's Register and Nanyang Technological University in the area of additive manufacturing for offshore & marine applications. This is a fast expanding area of research, especially when embarking on super vessels in the near future, and we are excited to see this collaboration come to fruition.

We have also received industry recognition for our efforts in Computational Fluid Dynamics (CFD) at the Inaugural National Supercomputing Centre Singapore (NSCC) Awards in March 2016. KOMtech won the NSCC Outstanding HPC Industry Application Award, as well as an honourable mention for its efforts in collaborating with national and industry partners to promote CFD innovation.

Through Technology Review, we hope to kickstart unconventional dialogues amongst industry partners and customers, and bring to focus innovative concepts that are of value to the offshore and marine technology community.

As we embark on the next decade, KOMtech shall build on this momentum and go from strength to strength in the expansion of its research and technology innovation capabilities.

I would like to convey my appreciation to the board of directors, researchers and employees of KOMtech, the editorial committee of the Technology Review, as well as our valuable industry partners for contributing to our achievements over the past ten years, and for making this publication a success.



Michael Chia
Managing Director
Keppel O&M Technology Centre

Editorial Committee

Advisors:

- | | |
|-----------------|------------------|
| Mr Michael Chia | Mr Aziz Merchant |
| Dr Foo Kok Seng | Mr Charles Sim |

Editorial members:

- | | |
|--------------------|-------------------|
| Ms Marianne Goh | Mr Wu Wenjin |
| Mr Tan Kim Pong | Mr Anis Hussain |
| Mr Ankit Choudhary | Ms Sreekala Kumar |
| Mr Matthew Quah | Dr Michael Perry |
| Dr Bernard How | Mr Roy Tan |
| Mr Brian Lee | |
-

Adopting Automation and Robotics to Propel Advanced Manufacturing Industries to the Next Level

- | **TAN Kim Pong**^{*}, CEng, MSc, FRINA, FSNAMES
- | **Josiah SNG Wei En**^{*}, B.Eng (Mech)
- | **CHEW Chee Meng**^{**}, PhD (MIT), SM (MIT), MEng (NUS), BEng (1st Hon) (NUS)
- | **Abdullah Al MAIMUN**^{**}, B.Tech (Hons), PhD (NUS)
- | **LU Weng Feng**^{**}, PhD (Minnesota), MSc, BSc
- | **Noor Hazman Bin SULAIMEE**^{*}, B.Eng (Mech)
- | **Muhd Azlan Bin ISMAIL**^{*}, B.Eng (Mech)
- | **Subramaniam VELUSAMY**^{**}, B.Eng, M.Eng (NUS), and SM (MIT), PhD (MIT)
- | **Justin PANG**^{**}, B.Eng, M.Eng, PhD (NUS)

^{*} Keppel Offshore & Marine Technology Centre

^{**} National University of Singapore

Many production processes in marine and offshore engineering are labour intensive and highly skills-based. Productivity improvement is crucial to sustaining profits while reducing foreign worker dependency. The Productivity Enhancement of Yard Operations Group consisting of researchers from Keppel Offshore & Marine Technology Centre (KOMtech) and the National University of Singapore (NUS) has been tasked to look into the use of technology to improve the productivity of three processes in yard operations, namely, the high value steelwork fabrication in the area of stub piece to chord welding, blasting operations for ship repair as well as welding operations in confined spaces. The problems posed are particularly challenging and the solution sought for each project is the improvement of quality, consistency and repeatability of the processes while at the same time achieving productivity improvement and safety for the shipyards. The research is at the half way mark.

Introduction

At the time of writing this paper, the Productivity Enhancement of Yard Operations Group consists of five researchers, a 3D software engineer from KOMtech, and eight researchers, four PhD students, one technician and five academic staff from NUS. The Group is working on three projects, each with dedicated researchers and Principal Investigators. All three projects started on different dates in 2014 and will run for a maximum duration of five years.

Three sub-themes under this research theme are: (1) High Value Steelwork Fabrication, (2) Blasting and Painting Operations, and (3) Semi-automated Operations in Confined Spaces. Each project has achieved some results and these will be reported in this paper.

High Value Steelwork Fabrication – Stub Piece to Chord Multi-pass Welding (see Figure 1)



Figure 1(a) Before



Figure 1(b) After

Problem Statement and Technical Challenges

Keppel FELS is the world's leading rig builder of jack-ups and semi-submersibles. Certain high value steelwork fabrication in Keppel FELS yard, such as jack-up leg fabrication, welding of jack-case, and thick panels is complex, labour intensive and a highly specialised and skillful process. Most of these operations are carried out manually. It is highly desirable to explore ways to increase the productivity in these areas, and to capture the knowledge of experienced welders and foremen. The project focuses on the stub piece chord welding where more than 70 passes of welding runs have to be performed.

Work Progress

Algorithms have been developed for automated work piece detection and motion planning of the robotic

welding manipulator. Precise determination of the work piece position and orientation is necessary as a new work piece will not be placed at exactly the same position due to cutting tolerances. In addition, this will ensure that the welding will be consistent for every work piece, with the welding passes beginning, ending, and overlapping at the same position. An RGB-D sensor and a laser sensor are used, all of which are commercially available. Based on the operational range of the sensors, the process of work piece detection is divided into coarse detection and motion planning to approach the work piece, followed by accurate detection based on laser scanning results. Coarse detection is carried out using the RGB-D sensor, while accurate detection is carried out using a laser sensor. The Bidirectional Transition-based Rapidly exploring Random Tree (BiTRRT) algorithm is currently used for motion planning to approach various welding quadrants of the work piece, and weld seam tracking trajectories are generated from laser scanning and applying well-known edge detection techniques.

Robotic welding parameters for the stub-to-chord work piece have been determined and a single filling pass has been welded. Based on other welding tests carried out using bevel joints, the results show that the same set of welding parameters can be used for up till eight subsequent passes. Future works include verification of the welding parameters for the subsequent welding passes on the stub-to-chord work piece.

The robotic multi-pass welding system has to be robust and generate uniform weld beads in the presence of uncertainties such as effects of gravity and variation in weld geometry due to the assembly process. A filling control strategy is proposed based on the similarity between multi-pass welding and the self-servo track writing process in the manufacturing of hard disk drives. Using the developed filling control strategy, the wire feed-rate and torch travel speed will be adjusted at specific intervals to ensure that inconsistencies in the width of each welding pass will have minimal effects on subsequent welding passes. In order to compensate for the effects of repetitive disturbances, disturbance estimation is carried out based on probability mass functions assigned to every sampled position along the x-axis. Future works include experiments to verify the effectiveness of the proposed algorithm.

Key Challenges

The key challenge is to integrate the industrial robot with the laser scanner, the vision sensor and the weld pool camera, both the hardware and the software. The edge detection from the scan results as well as the 3D elliptical profile of the stub piece also pose challenges for the researchers to resolve.

Future Work

The targets respectively for this project are by December 2016, June 2017, December 2017 and June 2018 are the installation of semi-automatic linear multi-pass welding with the gantry robot using depth sensor and the robot maker's technologies at KFELS yard; semi-automatic complex geometry welding at Keppel-NUS Corporate Laboratory; automatic single pass welding with the gantry robot at KFELS yard; and automatic multi-pass welding gantry robot at KFELS.

New Applications

Robotic welding can be readily deployed for welding of high pressure pipe spools, complicated but repeated outfits, thick plates, lattice structures in civil construction and many other areas.

Blasting and Painting Operations (see Figure 2)



Figure 2(a) Before



Figure 2(b) After

Problem Statement and Technical Challenges

Blasting and painting operations are tedious and involve heavy consumption of materials such as blasting grits and paint. These operations are necessary for ship hull maintenance. Currently, both blasting and painting are manual operations that are strenuous and hazardous. Any form of automation will result in substantial reduction of labour and health hazard with an increase of safety.

Work Progress

Commercial products for automating the blasting process are explored and studied. The advantages and disadvantages of climbing robot-based and cherry picker-based blasting systems are also examined.

A blasting experiment had been carried out to determine the effects of the blasting parameters on blasting quality and efficiency.

The first prototype for cherry picker mounted operation which sets the blasting nozzles in a weaving motion had been fabricated for visualisation and further development. A vision system based on image processing techniques for monitoring the blasting process and examining the blasting quality are being developed.

The second prototype for cherry picker mounted operation has been developed and is currently being fabricated for testing in the workshop and subsequent testing at site.

Key Challenges

The key challenge is to design and manufacture within 200 kg all the components of the blasting chamber inclusive of the blasting hose and the exhaust systems. Another challenge is the control of the cherry picker which currently does not permit the movement of the prime mover if the controls are effected from the ground. For a ground control system to be effective the control must be able to move the boom as well as the prime-mover. Image processing under different lighting conditions outdoors is equally challenging for the team.

Future Work

The targets respectively for this project are by December 2016, June 2017, December 2017 and June 2018 are the construction of proto-type blasting system for testing at shipyard; delivery of prototype to shipyard after testing and refinement; development of semi-automated painting system; delivery of semi-automated painting system after lab and field tests.

New Applications

This application can be extended to be used for blasting and painting public and private apartments and other land structures, aircrafts and other large vehicles.

The problems posed are particularly challenging and the solution sought for each project is the improvement of quality, consistency and repeatability of the processes while at the same time achieving productivity improvement and safety for the shipyards.

Semi-automated Operations in Confined Spaces (see Figure 3)

Problem Statement and Technical Challenges

Operations within confined spaces are difficult for humans and automated welding systems. Standard welding robots are not able to operate in confined spaces due to their large footprint and the volume of space swept by the arm.

The types of operations in confined spaces may include various production and repair works, such as the welding of profiles in jack cases, blasting and painting of surfaces and cleaning of tanks. A semi-automated welding system to assist the worker to perform such jobs in confined spaces will improve safety standards and reduce the fatigue-induced inconsistency in quality.

Modular and reconfigurable design of the welding system to suit different confined environments is novel and a design challenge. It has to be compact and yet able to contain most of the moving elements and controls, as well as carrying the welding and other accessories.



Figure 3(a) Before

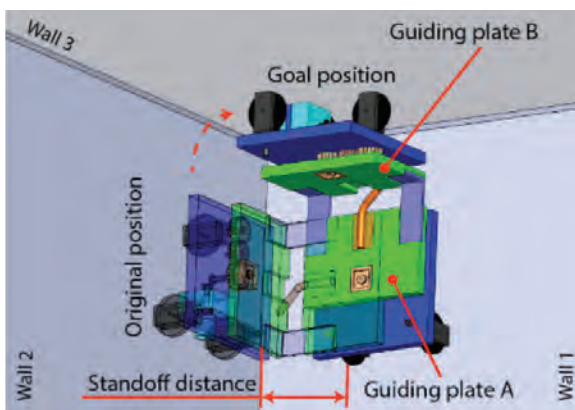


Figure 3(b) After

Work Progress

Three wall climbing prototypes have been proposed, one which can only travel in one direction and two with capability of travelling and transiting in the x-y-z directions so that welding can be performed in a confined space.

Two of the wall climbing robots have been fabricated and the second robot has been selected for further development after testing successfully without load in transiting and travelling in the x-y-x directions.

An end-to-end mechanism with smallest footprint is designed. As such, the welding platform will occupy a smaller amount of space on the robot.

Key Challenges

The key challenges include the ability to design a sufficiently compact climbing robot which is able to carry sufficient payload for the welding operation. In addition it must have sufficient mobility to carry out end to end welding of corners.

Future Work

The targets respectively for this project are by December 2016, June 2017, December 2017 and June 2018 are the implementation of vertical climbing with payload at Keppel-NUS Corporate Laboratory; vertical single pass end to end welding at Keppel-NUS Corporate Laboratory; horizontal multi-pass end to end welding at Keppel-NUS Corporate Laboratory; and vertical multi-pass end to end welding at Keppel-NUS Corporate Laboratory.

New Applications

Climbing robots can be used in other applications such as inspections of pipelines, tanks, tall steel structures; for blasting and painting; for carrying out non-destructive-testing in welds of pipe lines and difficult to reach structures.

Conclusions

These three projects have demonstrated that although the problems are complicated and complex to solve, progress has now been made towards finding the appropriate solutions.

In carrying out these projects we have acquired expertise in robotics and automation technology. In addition to that we have contributed towards additional knowledge in these areas by the publication of 13 papers at various conferences.

We have filed a joint patent, Singapore application number 10201605583Q, for Climbing Robot Surface Transition on Capability for Confined Space Application.

The saving in manpower is considerable for each of the three projects which is translated into productivity improvement and consistently good repeatable quality end products.

Finally with introduction of technology, the requirement for manpower is less, hence exposing risk to fewer workers giving an improvement in safety.

References

1. R. Haghghi, M. Rasouli, C. K. Pang, and C. M. Chew, "Fragment-Based Recognition Based on Clustered Centerpoint Feature Histogram (CCFH) and Extreme Learning Machine (ELM)," ICRA 2017, submitted.
2. S. M. Ahmed, Y. Z. Tan, G. H. Lee, C. M. Chew, and C. K. Pang, "Object Detection and Motion Planning for Automated Welding of Tubular Joints," in Proceedings of the 2016 IEEE/RSJ International Conference on Intelligent Robots and Systems (IROS), WeAT6.1, pp. 2610–2615, Daejeon, Korea, October 9–14, 2016.
3. S. Xia, Y. Z. Tan, C. K. Pang, and C. M. Chew, "Design of Feedforward Filling Control for Joining Thick Materials Using Robotic Welding Systems," in Proceedings of the IEEE 14th International Workshop on Advanced Motion Control (AMC 2016), pp. 247–252, Auckland, New Zealand, April 22–24, 2016 (invited).
4. S. Keshmiri, X. Zheng, W. F. Lu, C. K. Pang, and C. M. Chew, "Application of Deep Neural Network in Estimation of the Weld Bead Parameters," in Proceedings of the IEEE/RSJ International Conference on Intelligent Robots and Systems (IROS 2015), WeDT14.1, pp. 3518–3523, Hamburg, Germany, September 28–October 2, 2015.
5. S. Keshmiri, Y. Z. Tan, X. Zheng, S. M. Ahmed, Y. Wu, W. F. Lu, C. M. Chew, and C. K. Pang, "Identification and Reconstruction of Complex Weld Geometry Based on Modified Entropy," in Proceedings of the IEEE/RSJ International Conference on Intelligent Robots and Systems (IROS 2015), WeDT14.1, pp. 3512–3517, Hamburg, Germany, September 28–October 2, 2015.
6. S. M. Ahmed, J. Yuan, Y. Wu, C. M. Chew, and C. K. Pang, "Collision-Free Path Planning for Multi-Pass Robotic Welding," in Proceedings of the 2015 ETFA, Luxembourg, September 8–11, 2015.
7. Y. Wu, J. M. G. Zhen, S. M. Ahmed, W. F. Lu, C. M. Chew, and C. K. Pang, "Automated Bead Layout Methodology for Robotic Multi-Pass Welding," in Proceedings of the 2015 ETFA, Luxembourg, September 8–11, 2015.
8. S. Keshmiri, Y. Z. Tan, S. M. Ahmed, Y. Wu, C. M. Chew, and C. K. Pang, "3D Reconstruction of Complex Weld Geometry Based on Adaptive Sampling," in Proceedings of the IEEE/ASME International Conference on Advanced Intelligent Mechatronics (AIM 2015), FrBT7.6, pp. 1795–1800, Busan, Korea, July 7–11, 2015.
9. Xin Zheng, Guojie Lan, Chew Chee Meng, Lu Wen Feng*, "A Mathematical Model for Surface Roughness of Ship Hull Grit Blasting", ETFA Sep 6-9, 2016
10. Xin Zheng, Guojie Lan, Chew Chee Meng, Lu Wen Feng*, "A Design of Semi-Automatic Enclosed Robotic Apparatus for Ship Hull Surface Abrasive Blasting and Cleaning using Copper Grits", ETFA Sep 6-9, 2016
11. Yue Wu, Xiao Teng, Guo Jie Lan, Chee-Meng Chew, "Cubic-Climber: A Compact Magnetic Climbing Robot with Bidirectional Surface Transition & Turning on Spot Abilities", 2016
12. SiBao Wang, Yue Wu, Xiao Teng and Chee Meng Chew, "Optimization and comparison for three kinds of straight line mechanism". 2016
13. SiBao Wang, Yue Wu, Xiao Teng and Chee Meng Chew, "An L-shaped Climbing Robot with Surface Transition Capability for Confined-space Welding, CLAWR, Sep 12-14, 2016.

Acknowledgement

We wish to record our thanks and appreciation to NUS and all the team members for the collaboration in carrying out the three research projects. Initially all the work were carried out at the KOMtech Laboratory and KFELS Training Centre and thereafter from 15 January 2015 at the Keppel-NUS Corp Laboratory Workshop when the laboratory facilities were transferred from KOMtech Laboratory to the Keppel-NUS Corp Laboratory.

Author's contact

- | KimPong.Tan@KOMtech.com.sg
 - | chewcm@nus.edu.sg
 - | a.almamun@nus.edu.sg
 - | justinpang@nus.edu.sg
 - | mpelwf@nus.edu.sg
 - | velusamy.subramaniam@nus.edu.sg
-

Identifying Additive Manufacturing Trends and Opportunities in the Offshore and Marine Space

| WU Wenjin[#], B.Eng (Hons, Mech)

| Sharine TAN Ying Jia^{*}, B.Eng (Mat)

| LEE Yuan Hao^{*}, B.Eng (Hons, Mech)

| Aziz MERCHANT^{*}, CEng, MSc, FRINA, FIMarEST, FSNAMEs

^{*} Keppel Offshore & Marine Technology Centre

[#] Nanyang Technological University

Adapted from original article "State of the art review on selective laser melting of steel for future applications in shipbuilding" presented at the 2nd International Conference on Progress in Additive Manufacturing (Pro-AM 2016) 16-19 May 2016, Singapore

This paper presents a general trend analysis of 3D Printing, also known as Additive Manufacturing (AM), particularly in the areas of technology, material and application. A review on the properties of stainless steel processed using AM will also be presented, providing evidence on the feasibility of the technology. Potential and technical challenges in AM of stainless steel for the marine industry are discussed. The paper concludes with identifying cost and certification as recommendations for future work.

Introduction

Background

Additive Manufacturing (AM, also known as 3D Printing) is a process of making three dimensional solid objects from a digital file. The creation of a 3D printed object is achieved using additive processes. In an additive process, an object is created by laying down successive layers of material until the object is created. Each of these layers can be seen as thinly sliced horizontal cross-sections of the object.

AM has evolved significantly over the past few decades, transitioning from a technology for prototyping to functional end-use parts. It also allows for complexity free manufacturing, enabling re-design of components to realise improved mechanical performance and functionalities. These played critical roles in transforming the way products are now designed, prototyped and manufactured; achieving better, stronger parts built in a more resource efficient environment with reduced production times.

Despite all the controversy on the role of AM in the future of manufacturing, industry experts believe that metal AM have passed the valley of death that is often seen in the progress for the maturity of a certain technology. Challenges like metal density and the general quality of the metallurgy have long been overcome and metal AM produced products could also reach densities of 99.9%. With this, it has allowed companies like General Electric and Airbus to produce small turbine blades and airframes components. For the offshore and marine industry, Sciaky has recently produced submarine parts with its very own EBAM (Electron Beam AM) process.

General Trends

AM technology is a relatively new technology compared to other manufacturing technologies, but has evolved considerably during the past few decades. Beginning as a technology to fabricate accurate prototypes and verification tools, AM technology can now make high quality parts that can be directly installed for end-use applications. Aerospace companies have positioned themselves as first movers with AM, with numerous instances of directly manufactured end-use parts. But early followers from many other industries have also recognised the benefits and are keeping up the pace. It is these demands and needs from the industries that spur the technological advancement. In just 2013 alone, sales of metal 3D Printers have increased sharply by 75% (see Figure 1), evidence that AM adoption is on the

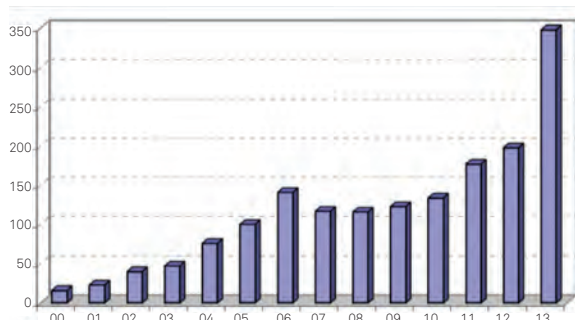


Figure 1 Sales for metal 3D printer (Y-axis) over the years (X-axis)

rise. An analysis on the general trends in the technology, materials and application will enable better appreciation of the technology.

Trends in AM Technology

Trends in AM technology include increased installation of metal based systems, increased demand for large build volume systems, and increased development in higher productivity machines. Significantly more machines now boast faster build rates and ability to build larger parts. Manufacturers of AM machines are also producing more cost effective machines, driving down the cost of AM technology. Research institutes are also developing new technologies to target specific applications, such as the Wire-Arc AM (Figure 2) technology for building large aerospace structural components.



Figure 2 Wire+Arc Additive Manufacturing Machine

AM allows users the design of AM process in concurrence with the design on the geometry of a part. In general, the quality and properties of AM manufactured components are strongly dependent on the following factors:

- AM processing technology (powder bed, power feed, wire feed)
- Energy transfer (Laser, e-beam)
- Beam shape
- Processing conditions
- Scanning strategy (Machine types)
- Scanning parameters (hatch distance, layer thickness)
- Alloy powder shape, grain size and size distributions
- Powder impurities

In order to improve AM technology, several other areas of development have also seen increased activities. In-situ AM process monitoring allows for accurate and reliable fabrication of metal and polymer components, addressing the problem of lack of controls to assess the quality of a part only until post processing inspection stage or risk having to stop the entire print halfway. The trend then is for companies to develop integrated solutions for in-situ monitoring. Some of the developments are listed in Table 1.

Trends in Materials for AM

The developments in metal AM have now led to increase in variations for metal powder production. Increasing interest in using metal AM for direct manufacturing is motivating powder makers to produce powders for actual end-use parts. Small businesses with the intention of joining the AM platform have slowly led the market to invest money into building newer and better powder production

Table 1 Trends on in-situ monitoring for AM processes

Lasers	Sensors to monitor the laser power and temperature across the various critical components in the systems.
Input Air Flow Levels	Sensors located in the build chamber and sieving stations to track the input air for constant flushing or input air to avoid leakage in the system.
Meltpool	Meltpool monitoring system from Concept Laser is used to develop 2D and 3D plots which can be superimposed with the 3D CAD file to identify the problematic areas. Similarly, SLM and EOS offers similar meltpool monitoring solutions.
Coater Consistency	Concept Laser allows the capture of before and after pictures to assess the consistency of coating thickness across the build area. Subsequently, the information will be used for feedback and adjustment for subsequent coating thickness.

equipment and optimising the design of the equipment to produce powder solely for AM. This challenges existing equipment with low yields and a high mark-up value.

This trend spurs the testing of new powder production processes, leading to new developments over traditional atomisation processes. Evolution of the AM industry is observed to approach a more advanced and serial manufacturing concept in industries like aerospace, automotive, medical and many more [1]. Looking at the powder metallurgy (PM) production in Asia across five major countries, Takashi Saito of Japan Powder Metallurgy Association presented an overview on the PM industry

in Asia (see Figure 3, Figure 4). The findings showed that China is the largest PM producer since it overtook Japan in 2009. [2]

As materials go through processing, the interaction with the heat source would lead to a formation of microstructures in the build part which gives the performance and part integrity of the material. This leads to an increasing interest in the materials science aspect of AM largely, focusing on varying material microstructures and properties at different component locations by manipulating process variables during the built process. By using an assembly of small scale microstructures to achieve varying properties, Disney Research has demonstrated the use of microstructures to fabricate deformable objects through AM.

Referencing activities in the material science aspect for additive manufacturing, it is observed that the research is moving towards the development of new alloy materials to exploit the high cooling rates of the AM processes. During typical AM processes, the energy generated is highly centralised and focused, leading to concentrated heat affected areas (ultra-high temperatures) in a very narrow and small region while the other areas remain at normal temperatures. Based on this, the highly non-equilibrium metallurgy process would serve as a platform to lead the research into producing alloys with exceptional performances at extremely high temperature conditions.

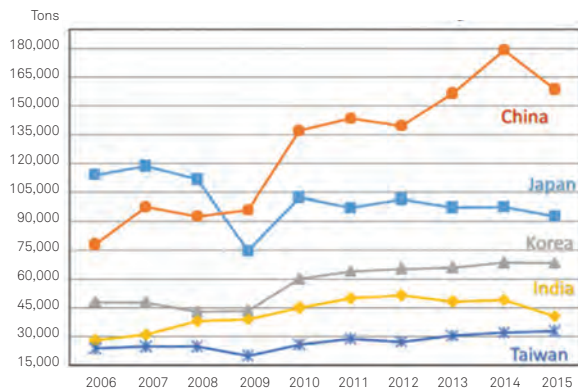


Figure 3 PM Production in the 5 major areas

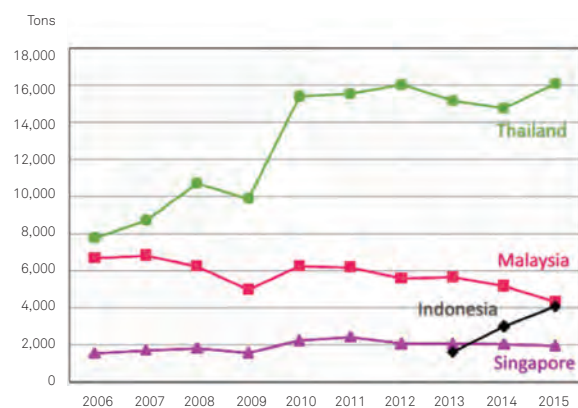


Figure 4 PM Production in the other areas

Some of the notable applications include NASA's rocket engines which can withstand a high temperature of 3315°C [3]. Since then, there has been several researches exploring the production of various types of alloys. In more recent news, US based QuesTek Innovations have been awarded a project from the US Navy and Army to develop technologies and new alloys tailored to AM [4].

Trends in AM Applications

The offshore and marine industry is slowly gaining traction in the adoption of AM as one of the technologies that will help in production. Currently the industry is looking at a few main areas, including but not limited to components that require repairs, long lead time components as well as those that require either assembly, a lot of manpower or has a lot of processes involved in the fabrication of the component.

Shell has a technology centre in Amsterdam that houses a 3D printer. The 3D printer is used to make unique components to aid in Shell's research and development projects. Advantages include cost effectiveness, potential to speed up delivery times and ability to make components on demand. One of the challenges highlighted was for engineers to rethink in terms of layers instead of taking material away^[5]. Shell has since utilised additive manufacturing as a prototyping tool. Conventionally, one portion of a project would require putting hundreds of the foam pieces into a puzzle-like geometry. With the help of additive manufacturing, they were able to make the prototype quickly (see Figure 5)^[6]. The prototype was used to demonstrate to authorities and inspectors on how Shell will be using the system. Consequently, Shell was able to anticipate any problems and issues which they could resolve ahead of time, instead of discovering them only during the project.



Figure 5 Using AM for prototyping by Shell

Port of Rotterdam has had a pilot project for 3D printing of marine spares. The project was focused mainly on printing metal spare parts in the maritime applications^[7]. As the project members were relatively new to AM, six work packages were devised – part selection and (re) design, material selection and data base, production and finishing, testing and quality, cost and return on investment, and project management^[7]. These work packages highlight some of the obstacles that the offshore and marine industry face. Some of the components studied during the project include propeller, spacer ring and hinges.

Maersk is exploring AM by having a 3D printer installed on board their vessels. They face challenges such as the need for the procurement team to deliver parts to the vessel quickly, high transportation cost of parts and the time required to locate the component, getting it to the next



Figure 6 Maersk's example on onboard vessel 3D Printing

port-of-call and chartering a boat to make the delivery^[8]. With a 3D printer installed on board, Maersk is exploring the number of parts that can be printed on board and the limitless possibilities and savings that it could bring (see Figure 6)^[8].

Tru-Marine in Singapore has 3D printed a nozzle ring for marine turbochargers. This is deemed the world's first 3D printed nozzle ring for turbocharger repair application. The premature erosion of nozzle rings is a problem which results in unplanned down times as well as emergency services^[9]. Spare parts are usually unavailable, have high costs and long lead times. With the aid of AM, Tru-Marine is able to repair the damaged components at a fraction of the time needed by conventional methods (see Figure 7). This is achieved as AM enables reconstruction at only the worn out areas directly on the original component. Other several advantages of additive manufacturing includes the ability to manufacture components with densities of greater than 99.5%, enhanced properties and performance^[9]. The 3D printed nozzle has yielded positive results from laboratory examinations and tested to be suitable for turbocharger applications^[9].



Figure 7 Tru-Marine's 3D Printed nozzle ring (right) vs worn (left)

Even classification societies have noted that AM is a disruptive technology that will come to the offshore and marine industry. Some have started to work on standards to implement for components that will be built with AM. Lloyd's Register has announced Joint Industry Projects and is inviting companies from across the world to tackle the various issues that are faced by manufacturers. Lloyd's Register identified four challenges which are the Qualification of technology, Confidence in the supply chain, Competent and qualified workforce and Safety enhancements^[10]. DNV GL has published a paper covering AM which states that while the technology is able to bring in innovative manufacturing, there are some risks present and should be considered^[11]. DNV GL determined that the distributed nature of AM would deem that the product manufactured at one location is different as compared to one manufactured at a different location. This could be due to software differences, hardware differences or other factors^[11]. Apart from the manufacturing portion for AM, DNV GL concluded that the rise in adoption might impact the overall demand for shipping of goods as well.

Additive Manufacturing Of Stainless Steel

AM of stainless steel materials has been a widely researched area. Stainless steels have good properties especially in corrosion resistance, where it differs from other steels (such as carbon-manganese and low-alloy steel) in its use of chromium as a substantial alloying element to enhance its atmospheric corrosion resistance properties^[12]. These materials are commonly used in

high value applications such as aerospace, biomedical, automotive, architectural, jewelry, dentistry and marine [13-23]. The corrosion resistance characteristic of stainless steels allows for marine applications such as protection against mechanical removal of material [23] and chloride stress corrosion cracking [22].

Stainless steels come in several types depending on their microstructure. Austenitic stainless steels contain at least six percent nickel and austenite (carbon-containing iron with a face-centered cubic structure) and have good corrosion resistance and high ductility (the ability of the material to bend without breaking). Ferritic stainless steels (ferrite has a body-centered cubic structure) have better resistance to stress corrosion than austenitic, but they are difficult to weld. Martensitic stainless steels contain iron having a needle-like structure.

Duplex stainless steels, which generally contain equal amounts of ferrite and austenite, provide better resistance to pitting and crevice corrosion in most environments. They also have superior resistance to cracking due to chloride stress corrosion, and they are about twice as strong as the common austenitics. Therefore, duplex stainless steels are widely used in the chemical industry in refineries, gas-processing plants, pulp and paper plants, and sea water piping installations.

Density

The attainable density after AM process is important and critical in determining the mechanical performance of the AM built part. Kruth et al. described the density as having a direct influence on the component performance in [52]. The objective in AM is to obtain 100% dense parts, as this will provide mechanical performance of the AM

built part as close to the bulk properties as possible. In [52], Kruth et al. has shown that the maximum achievable density for AM produced parts can be 99%. As a comparison, casting components typically have densities of 82% - 95% [53]. A compilation of some of the relative densities (versus bulk density) of AM built stainless parts are shown in Table 2. The results show that AM processed stainless steels can generally obtain very high relative density values.

Table 2 Relative densities of stainless steels processed by SLM

Material	Type	Relative Density (%)
SS304L	Austenitic	92.5 [54], 99.2 [58]
SS316L	Austenitic	99.86 [68]
SS420	Martensitic	99.95 [62]
2507SS	Super Duplex	90.8 [55]

Mechanical Properties

A summary of the mechanical properties of selected stainless steels are presented in Table 3.

The toughness performance of selected stainless steels in Table 3 is based on Charpy V-notch impact toughness tests performed at room temperature. Based on the limited literature on stainless steel 316L, it can be seen that as-built stainless steel 316L components generally have lower toughness performance than conventionally produced ones.

Table 3 Mechanical properties of selected stainless steels

Material	Process	Toughness (J) (Charpy V-notch @ Room Temperature)	Elongation at break (%)	Ultimate Tensile Strength (MPa)	Yield Strength (MPa)	Hardness
SS304L	SLM	-	25.9 [54], 40 [58]	393 [54], 655 [58]	182 [54]	192 HB [54]
	Casting	215 [69]	58 [69]	565 [69]	210 [69]	82 HB [70]
SS316L	SLM	60 [52], 56.8 [50]	30 [50]	595 [60], 688 [50]	670 [50]	238 HB [59]
	Casting, Annealed	103 [69]	55 [69]	560 [69]	235 [69]	146 HB [69]
SS17-4 PH	SLM	-	50 [61], 31 [71]	944 [61], 1009 [72]	570 [61], 515.5 [72]	200 HB [72]
	Casting, H900	21 [69]	15 [69]	1365 [69]	1260 [69]	420 HB [69]
SS420	SLM	-	-	-	-	496 HB [62]
	Casting, Annealed	100 [69]	25 [69]	655 [69]	345 [69]	175 HB [69]
2507SS	SLM	-	-	-	-	421 HB [55]
	Casting, Annealed	60 [73]	35 [73]	690 [74]	515 [74]	241 HB [74]

The ductility performance of selected stainless steels is based on the elongation at break. For stainless steels 304L and 316L, the ductility of AM produced specimens has poorer ductility than the conventionally processed ones. However, for the stainless steel 17-4 precipitation-hardened steel, the AM produced specimen has better ductility performance than the conventionally processed ones.

Based on available literature on ultimate tensile strength and yield strength, Table 3 shows that AM produced components are generally stronger than conventionally produced ones. For the study on stainless steel 304L in [54], the powder used was of poor quality, and the study was focused on AM of economically available powders, and hence the values are lower.

The hardness values of selected stainless steels are based on Brinell scale. Besides stainless steel 17-4, the rest of the stainless steels generally have better hardness values than conventionally processed ones.

Microstructure

It is also known that metal parts produced by AM generally have finer grains than castings or forgings (see Figure 8), which is a desirable trait in metal working. The fine grains can be attributed to the rapid cooling rate during the SLM process, which leads of insufficient grain growth [57]. A summary of the microstructures formed by AM processed stainless steels can be found in Table 4.

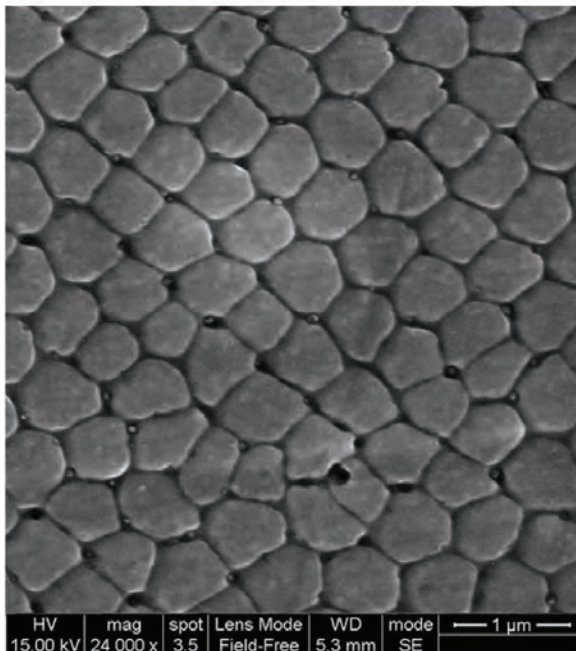


Figure 8 SEM-SE image SLM produced metal part showing fine grains [61]

AM produced components are generally stronger than conventionally produced ones.

Table 4 Summary of microstructure of SLM produced stainless steels

Material	Process	Type
SS304L	SLM	Austenitic [54]
SS316L	SLM	Austenitic [59], [60]
SS17-4PH	SLM	Austenite + Martensitic [61]
SS420	SLM	Austenite + Martensitic [63]
2507SS	SLM	Ferrite + Austenite [55]

Table 5 List of common stainless steel grades [65]

Stainless Steel Type	Common/ ASTM Name	UNS
Austenitic	304	S30400
	316	S31600
	316L	S31603
Super Austenitic	6Mo	N08926
	254SMO	S31254
	904L	N08904
	654SMO	S32654
Martensitic	420	S42000
Ferritic	430	S43400
Precipitation-Hardening	17-4 PH	S17400
Duplex	22Cr	S31803
Super Duplex	25Cr	S32750

Stainless Steel In The Marine Industry
Types of stainless steel in the marine industry

In [65], Geary et al. reviewed the performance limits of stainless steel types used in the offshore and marine industry. In the review, the types of stainless steel used in the industry are selected based on three conditions – stress corrosion cracking (SCC), pitting and crevice corrosion (PCC) and sour environment. Both SCC and PCC may be classified under a single category – chloride environment. Based on a list of common stainless steel grades (see Table 5), the review then evaluated the grades of stainless steels used in the industry. For SSC performance, austenitic and duplex stainless steels are generally preferred. Austenitic, super austenitic, duplex and super duplex stainless steels are generally used for

PCC. Austenitic and super austenitic stainless steels are more widely recommended for performance under sour environments due to their superior resistance to sulphide stress cracking and hydrogen cracking. There are no recommendations for ferritic stainless steels, and martensitic and precipitation-hardened stainless steels have rare applications.

Applications

Stainless steels have been generally used in applications where corrosion-related service failures are of concern. Hence, piping systems, including top side modules, marine systems and drilling systems, are usually fabricated using stainless steels. These include pipework, manifolds, fittings, sealings, valves and actuators^[65]. Some other examples of components built using stainless steels include pressure vessels, instrument tubings, fastening devices and parts, heat exchangers and tanks^[65].

Challenges And Potential

In [66] Wu et al. presented a review on additive manufacturing machines and their build sizes that are relevant to the offshore and marine industry. In the review, Wu et al. discussed about powder-bed systems which have build volumes of up to 300 x 350 x 300 mm (x,y,z)^[66]. This build volume may satisfy the size requirement for smaller components such as fittings and fasteners, but may be a challenge for other larger shipbuilding components such as heat exchangers and manifolds, which may occupy a footprint of up to 800mm x 800mm to more than 2000mm by 2000mm. However, machine manufacturers are developing larger machines with build envelope up to 800 x 400 x 500 mm (x,y,z)^[67]. South African research institute the Council for Scientific and Industrial Research's (CSIR's) National Laser Centre (NLC) is also developing a large-area high-speed SLM system, also known as the Aeroswift project, which is able to produce components with maximum dimensions of 2 x 0.6 x 0.6 mm (x,y,z) from metal powders. The technology for large area AM machines has since advanced beyond what was covered in the review. These include machines by DMG Mori, Optomec, EOS, etc.

The types of stainless steels used in offshore and marine industries are generally austenitic. A large percentage of the stainless steels used, especially for piping systems, are based on the 316L grade. Based on this review study, the mechanical properties of AM produced stainless steel 316L components are better in comparison to conventionally processed ones, except for applications where toughness and ductility values are critical. The poor performance in toughness and ductility is consistent with many other AM processed iron based metals^[30,52]. Hence, post processing may often be required to recover the toughness and ductility performance if required. Nonetheless, based on the as-built properties of stainless steel 316L, there already exists many opportunities for adoption as described in the previous chapter on applications.

Conclusion

This paper described the general trends in AM, particularly in the areas of technology, materials and applications. The focus is on components typically made of stainless steels, and reviewed current AM developments in processing stainless steels. The

review showed that stainless steel components can be successfully fabricated with good mechanical properties. It can thus be concluded that it is now appropriate to start developing applications for stainless steel components in the offshore and marine industry. However, this work did not include any review on the cost and the need for certification. Hence, recommendations for future work will include comparing costs of current manufacturing and AM, identifying key areas to track to predict entry points for cost effective application of the technology. Future work will also need to include review of current certification requirements and identify the gaps and opportunities to drive adoption of AM technology.

References

1. Associates, W. Wohlers Report 2016 Published: Additive Manufacturing Industry Surpassed \$5.1 Billion. [cited 2016 April]; Available from: <http://additivemanufacturing.com/2016/04/05/wohlers-report-2016-published-additive-manufacturing-industry-surpassed-5-1-billion/>.
2. Saito, T. Global Review Overview of P/M Industry in Asia. in World PM 2016. Oct 2016. Germany.
3. NASA. NASA Tests Limits of 3-D Printing with Powerful Rocket Engine Check. 2013 [cited 2017 Feb]; Available from: <https://www.nasa.gov/exploration/systems/sls/3d-printed-rocket-injector.html>.
4. Today, M. QuesTek to develop alloys for AM. 2017 [cited 2017 Jan]; Available from: <http://www.materialstoday.com/additive-manufacturing/news/questek-to-develop-alloys-for-am>.
5. 3D PRINTING. 2016 [cited 2016; Available from: <http://www.shell.com/inside-energy/3d-printing.html>.
6. Millsaps, B.B. Gulf of Mexico: Shell Uses 3D Printed Prototype for Very Complex Planning in Stones Deepwater Project. 2016 [cited 2016; Available from: <https://3dprint.com/130436/shell-3d-printed-prototyping/>.
7. Makerspace, R., Pilot Project: 3D printing of Marine spares. 2016: Port of Rotterdam.
8. Canty, M. Spare parts – just press print. 2014 [cited 2016; Available from: <http://www.maersk.com/en/the-maersk-group/about-us/publications/maersk-post/2014-3/spare-parts-just-press-print>.
9. Matthews, S. Tru-Marine 3D prints turbocharger nozzle ring. 2015 [cited 2016; Available from: http://www.mpropulsion.com/news/view/trumarine-3d-prints-turbocharger-nozzle-ring_40585.htm.
10. LR launches a JIP in additive manufacturing. 2016 [cited 2016; Available from: <http://www.lr.org/en/news-and-insight/news/joint-industry-project-additive-manufacturing-3d-printing.aspx>.

11. SHIPPING NOVEL DESIGNS. 2016 [cited 2016; Available from: <http://to2025.dnvgl.com/shipping/novel-design-and-manufacturing/>.
12. Sedriks, A.J., Corrosion of stainless steel, 2. 1996.
13. Baddoo, N., Stainless steel in construction: A review of research, applications, challenges and opportunities. *Journal of Constructional Steel Research*, 2008. 64(11): p. 1199-1206.
14. Dewidar, M.M., K.A. Khalil, and J. Lim, Processing and mechanical properties of porous 316L stainless steel for biomedical applications. *Transactions of Nonferrous Metals Society of China*, 2007. 17(3): p. 468-473.
15. Gale, W., et al., Effect of vapour phase hydrogen peroxide, as a decontaminant for civil aviation applications, on microstructure, tensile properties and corrosion resistance of 2024 and 7075 age hardenable aluminium alloys and 304 austenitic stainless steel. *Materials Science and Technology*, 2009. 25(1): p. 76-84.
16. Inoue, Y. and M. Kikuchi, Present and future trends of stainless steel for automotive exhaust system. *High-temperature*, 2003. 950: p. 750.
17. Ling, X., et al., Creep damage in small punch creep specimens of Type 304 stainless steel. *International journal of pressure vessels and piping*, 2007. 84(5): p. 304-309.
18. Mayor, M.B., K. Merritt, and S.A. Brown, Metal allergy and the surgical patient. *The American Journal of Surgery*, 1980. 139(4): p. 477-479.
19. Merritt, K. and S.A. Brown, Metal sensitivity reactions to orthopedic implants. *International journal of dermatology*, 1981. 20(2): p. 89-94.
20. Molak, R.M., et al., Measurement of mechanical properties in a 316L stainless steel welded joint. *International Journal of Pressure Vessels and Piping*, 2009. 86(1): p. 43-47.
21. Santacreu, P.-O., et al., Design of stainless steel automotive exhaust manifolds. *Revue de Métallurgie*, 2004. 101(7-8): p. 615-620.
22. Cruz, R.P.V., A. Nishikata, and T. Tsuru, Pitting corrosion mechanism of stainless steels under wet-dry exposure in chloride-containing environments. *Corrosion Science*, 1998. 40(1): p. 125-139.
23. Neville, A., T. Hodgkiess, and J.T. Dallas, A study of the erosion-corrosion behaviour of engineering steels for marine pumping applications. *Wear*, 1995. 186-187, Part 2: p. 497-507.
24. Habashi, F., *Handbook of extractive metallurgy*. 1997, wiley-VCH.
25. Norgate, T.E., S. Jahanshahi, and W.J. Rankin, Assessing the environmental impact of metal production processes. *Journal of Cleaner Production*, 2007. 15(8-9): p. 838-848.
26. Millberg, L.S. *Stainless Steel*. 1992 [20 January 2016]; Available from: <http://www.madehow.com/Volume-1/Stainless-Steel.html>.
27. Chua, C.K. and K.F. Leong, *3D printing and additive manufacturing: principles and applications*. 2015.
28. Morgan, R., C.J. Sutcliffe, and W. O'Neill, Density analysis of direct metal laser re-melted 316L stainless steel cubic primitives. *Journal of Materials Science*. 39(4): p. 1195-1205.
29. Van Elsen, M., F. Al-Bender, and J.-P. Kruth, Application of dimensional analysis to selective laser melting. *Rapid Prototyping Journal*, 2008. 14(1): p. 15-22.
30. Kruth, J.-P., et al., Selective laser melting of iron-based powder. *Journal of Materials Processing Technology*, 2004. 149(1): p. 616-622.
31. Abe, F., et al., Influence of forming conditions on the titanium model in rapid prototyping with the selective laser melting process. *Proceedings of the Institution of Mechanical Engineers, Part C: Journal of Mechanical Engineering Science*, 2003. 217(1): p. 119-126.
32. Santos, E., et al., Microstructure and mechanical properties of pure titanium models fabricated by selective laser melting. *Proceedings of the institution of mechanical engineers, part c: journal of mechanical engineering science*, 2004. 218(7): p. 711-719.
33. Louvis, E., P. Fox, and C.J. Sutcliffe, Selective laser melting of aluminium components. *Journal of Materials Processing Technology*, 2011. 211(2): p. 275-284.
34. Brandl, E., et al., Additive manufactured AlSi10Mg samples using Selective Laser Melting (SLM): Microstructure, high cycle fatigue, and fracture behavior. *Materials & Design*, 2012. 34: p. 159-169.
35. Fox, P., et al., Interface interactions between porous titanium/tantalum coatings, produced by Selective Laser Melting (SLM), on a cobalt-chromium alloy. *Surface and Coatings Technology*, 2008. 202(20): p. 5001-5007.
36. Wu, L., et al., Evaluation of the mechanical properties and porcelain bond strength of cobalt-chromium dental alloy fabricated by selective laser melting. *The Journal of prosthetic dentistry*, 2014. 111(1): p. 51-55.
37. Pogson, S., et al., The direct metal laser remelting of copper and tool steel powders. *Materials Science and Engineering: A*, 2004. 386(1): p. 453-459.

38. Zhang, D., Q. Cai, and J. Liu, Formation of nanocrystalline tungsten by selective laser melting of tungsten powder. *Materials and Manufacturing Processes*, 2012. 27(12): p. 1267-1270.
39. Amato, K., et al., Microstructures and mechanical behavior of Inconel 718 fabricated by selective laser melting. *Acta Materialia*, 2012. 60(5): p. 2229-2239.
40. Paul, C., et al., Investigating laser rapid manufacturing for Inconel-625 components. *Optics & Laser Technology*, 2007. 39(4): p. 800-805.
41. Rombouts, M., et al., Fundamentals of selective laser melting of alloyed steel powders. *CIRP Annals-Manufacturing Technology*, 2006. 55(1): p. 187-192.
42. Badrossamay, M. and T. Childs, Further studies in selective laser melting of stainless and tool steel powders. *International Journal of Machine Tools and Manufacture*, 2007. 47(5): p. 779-784.
43. Shiomi, M., et al., Residual stress within metallic model made by selective laser melting process. *CIRP Annals-Manufacturing Technology*, 2004. 53(1): p. 195-198.
44. Liu, Z., et al. A preliminary investigation on selective laser melting of M2 high speed steel. in 5th International Conference on Advanced Research and Rapid Prototyping, Leiria, Portugal. 2011.
45. Khan, M. and P. Dickens, Selective Laser Melting (SLM) of pure gold. *Gold Bulletin*, 2010. 43(2): p. 114-121.
46. Kruth, J.-P., et al., Binding mechanisms in selective laser sintering and selective laser melting. *Rapid prototyping journal*, 2005. 11(1): p. 26-36.
47. Mercelis, P. and J.-P. Kruth, Residual stresses in selective laser sintering and selective laser melting. *Rapid Prototyping Journal*, 2006. 12(5): p. 254-265.
48. Childs, T., C. Hauser, and M. Badrossamay, Mapping and modelling single scan track formation in direct metal selective laser melting. *CIRP Annals-Manufacturing Technology*, 2004. 53(1): p. 191-194.
49. Dadbakhsh, S., L. Hao, and N. Sewell, Effect of selective laser melting layout on the quality of stainless steel parts. *Rapid Prototyping Journal*, 2012. 18(3): p. 241-249.
50. Tolosa, I., et al., Study of mechanical properties of AISI 316 stainless steel processed by "selective laser melting", following different manufacturing strategies. *The International Journal of Advanced Manufacturing Technology*, 2010. 51(5-8): p. 639-647.
51. Jhabvala, J., et al., On the effect of scanning strategies in the selective laser melting process. *Virtual and Physical Prototyping*, 2010. 5(2): p. 99-109.
52. Kruth, J.-P., et al. Part and material properties in selective laser melting of metals. in *Proceedings of the 16th International Symposium on Electromachining*. 2010.
53. Avalle, M., et al., Casting defects and fatigue strength of a die cast aluminium alloy: a comparison between standard specimens and production components. *International Journal of Fatigue*, 2002. 24(1): p. 1-9.
54. Abd-Elghany, K. and D. Bourell, Property evaluation of 304L stainless steel fabricated by selective laser melting. *Rapid Prototyping Journal*, 2012. 18(5): p. 420-428.
55. Davidson, K. and S. Singamneni, Selective Laser Melting of Duplex Stainless Steel Powders; an Investigation. *Materials and Manufacturing Processes*, 2015(just-accepted).
56. Kumar, S. Microstructure and wear of SLM materials. in *Solid Freeform Fabrication Symposium*. 2008.
57. Gu, D., et al., Laser additive manufacturing of metallic components: materials, processes and mechanisms. *International materials reviews*, 2012. 57(3): p. 133-164.
58. Brown, B., Characterization of 304L stainless steel by means of minimum input energy on the selective laser melting platform. 2014.
59. Khalfallah, I., et al., Microstructure and corrosion behavior of austenitic stainless steel treated with laser. *Optics & Laser Technology*, 2011. 43(4): p. 806-813.
60. Zhang, B., L. Dembinski, and C. Coddet, The study of the laser parameters and environment variables effect on mechanical properties of high compact parts elaborated by selective laser melting 316L powder. *Materials Science and Engineering: A*, 2013. 584: p. 21-31.
61. Rafi, H.K., et al., Microstructure and Mechanical Behavior of 17-4 Precipitation Hardenable Steel Processed by Selective Laser Melting. *Journal of Materials Engineering and Performance*, 2014. 23(12): p. 4421-4428.
62. Zhao, X., et al., Fabrication and characterization of AISI 420 stainless steel using selective laser melting. *Materials and Manufacturing Processes*, 2015. 30(11): p. 1283-1289.
63. Krakhmalev, P., et al., In situ heat treatment in selective laser melted martensitic AISI 420 stainless steels. *Materials & Design*, 2015. 87: p. 380-385.
64. Yang, Y., et al., Effect of a brief post-weld heat treatment on the microstructure evolution and pitting corrosion of laser beam welded UNS S31803 duplex stainless steel. *Corrosion Science*, 2012. 65: p. 472-480.

-
65. Geary, E.A., A review of performance limits of stainless steels for the offshore industry. 2011: Harpur Hill, Buxton Derbyshire.
 66. Wu, W., et al., Study of Additive Manufacturing in Offshore & Marine, in RAPID 2014. 2014: Detroit, US.
 67. Laser, C. X line 2000R @ Technical Data. 2016 11 February 2016]; Available from: http://www.concept-laser.de/fileadmin/branchenbilder/PDFs/1509_X%20line%202000R_DE.pdf.
 68. Kamath, C., et al., Density of additively-manufactured, 316L SS parts using laser powder-bed fusion at powers up to 400 W. The International Journal of Advanced Manufacturing Technology, 2014. 74(1-4): p. 65-78.
 69. Harvey, P.D. and A.S.f. Metals, Engineering properties of steel. Stainless and Heat-Resisting Steels. 1982: American Society for Metals.
 70. MatWeb. AISI Type 304L Stainless Steel, Mechanical Properties. 2016 12 February 2016]; Available from: <http://asm.matweb.com/search/SpecificMaterial.asp?bassnum=MQ304L>.
 71. EOS, EOS StainlessSteel GP1 for EOSINT M 270 Material Data Sheet. 2009.
 72. Luecke, W.E. and J.A. Slotwinski, Mechanical Properties of Austenitic Stainless Steel Made by Additive Manufacturing. JOURNAL OF RESEARCH OF THE NATIONAL INSTITUTE OF STANDARDS AND TECHNOLOGY, 2014. 119: p. 398-418.
 73. MatWeb. Outokumpu SAF 2507@ Duplex Stainless Steel. 3rd February 2016]; Available from: <http://www.matweb.com/search/DataSheet.aspx?MatGUID=9d24d6e734b940398ba8409d8fd52aab>.
 74. MatWeb. MetalTek MTEK 2507 Cast UNS J93404 Duplex Stainless Steel. 3rd February 2016]; Available from: <http://www.matweb.com/search/DataSheet>.
-

Acknowledgements

The authors would like to thank the Singapore Centre for 3D Printing, Nanyang Technological University, including the following co-authors of the original paper:

- | TORShuBeng, PhD, BSc (Hons), Nanyang Technological University
- | LEONG Kah Fai, MSME, MSE, B.Eng (Hons), Nanyang Technological University
- | CHUA Chee Kai, PhD, MSc, B.Eng (Mech), Nanyang Technological University

Author's Contact

- | Wenjin.Wu@KOMtech.com.sg
-

Singapore and the Arctic: A Partnership between Academia and Business through Research & Innovation

| CHEN Zhuo*, PhD, M.Eng, B.Eng

| Peter G. NOBLE#, FCAE

| Professor CHOW Yean Khow**

| Adjunct Professor Aziz MERCHANT†

| Anis HUSSAIN*, MSc, B.Eng

| YEONG Wai Seng†, MBA, BSc

| Ankit CHOUDHARY†, MSc, B.Eng

*Keppel Offshore & Marine Technology Centre

#KOMUSA

†Keppel Singmarine

**National University of Singapore

The impact of the melting Arctic Sea ice on the Arctic shipping routes, and rising demand for commodities such as energy and minerals are creating new economic opportunities, but also new environmental, social and safety challenges in the Arctic. Keppel Offshore & Marine (KOM) is fully engaged in the development of solutions for safe marine navigation in the important Northern and Southern regions of the world and is also actively engaging the Arctic community to fully understand the unique culture in this frontier region. In the present paper, a review has been conducted on the background, challenges and trends for the current Arctic developments. Some possible development opportunities have also been identified.

Introduction

The melting of the Arctic Sea ice and rising demand for commodities such as energy and minerals are creating new economic opportunities, but also new environmental, social and safety challenges in the Arctic. In a speech at the Arctic Circle Greenland Forum, Singapore Minister of State, Mr Sam Tan indicated “A warmer Arctic will undoubtedly present new economic possibilities. In particular, the opening of new Arctic channels, such as the Northern Sea Route... We believe Singapore is in a position to assist in the development of maritime infrastructure to facilitate safe shipping in the region.” (Tan, 2016)

Keppel Offshore & Marine (KOM) has been involved in the design of ice breaker and other floater types in the Arctic. At present, KOM is fully engaged in the development of solutions for safe marine navigation in the important Northern and Southern regions of the world, i.e. the Arctic and Antarctica regions. Keppel Offshore & Marine Technology Centre (KOMtech) is currently partnered with National University of Singapore (NUS) to develop new generation of Arctic floaters for various applications under the Keppel-NUS Corporate Lab. Apart from the technical research on Arctic, KOMtech is also actively engaging the Arctic community to fully understand the unique culture in this frontier area and explore the opportunities for future developments. KOM have organised a breakout session, “Singapore and the Arctic: Partnership between Academia and Business through Research & Innovation” in the Arctic Circle Assembly 2016 in Iceland. KOMtech and NUS also jointly presented a paper with the title “Research Programme on Ice-Structure Interaction for Arctic Offshore Developments” in the 4th China-Nordic Arctic Cooperation Symposium. Through these activities, a better understanding of the current Arctic development has been achieved and some development opportunities also been identified.



Figure 1 Keppel's delegations in Arctic Circle Assembly 2016

Boundary of Arctic

The Arctic covers an enormous region of around 30 million square kilometers, which includes the Arctic Ocean and the land areas around it. While it is considered a distinct region, the Arctic is not easily delineated by one boundary or definition. Most commonly, scientists define the Arctic as the region above the Arctic Circle, an imaginary line that circles the globe at approximately 66° 33' N. Above this latitude the sun remains above the horizon all day for a period during summer and stays below the horizon all day for a period during winter.

But other people use different definitions when talking about the Arctic. Some scientists define the Arctic as the area north of the Arctic tree line. In terms of climate, the Arctic is also regarded as the region where the average temperature for July remains below 10°C.

In addition, the working groups of the Arctic Council defined boundary lines for the Arctic that were relevant for their particular mandate. For example, the Arctic Monitoring and Assessment Program (AMAP) created its 'AMAP area' as the territory where it would carry out environmental monitoring under the Arctic Environmental Protection Strategy. Other Arctic Council working groups such as Conservation of Arctic Flora and Fauna (CAFF) and Emergency, Prevention, Preparedness and Response (EPPR), and the Arctic Human Development Report (AHDR) also developed their own boundaries or adapted the AMAP boundary.

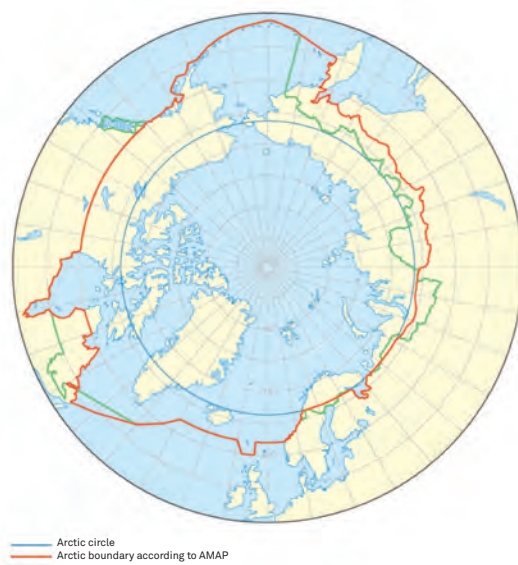
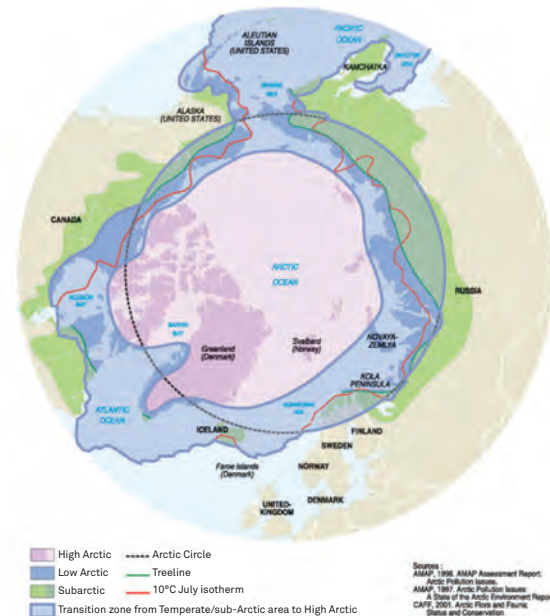


Figure 2 Various definition for the Arctic boundary (AHDR, 2004)

A warmer Arctic will undoubtedly present new economic possibilities. In particular, the opening of new Arctic channels, such as the Northern Sea Route... We believe Singapore is in a position to assist in the development of maritime infrastructure to facilitate safe shipping in the region.

International Cooperation and Treaties for Arctic

The Arctic is comprised of the northernmost territories of the eight countries—Russia, Canada, the United States, Norway, Denmark (including Greenland and the Faroe Islands), Iceland, Sweden, and Finland. Several international and regional bodies have been working together with the Arctic countries in cooperation to safely meet strategic objectives in the Arctic.

The Arctic Council (AC) is the most important forum for intergovernmental cooperation among Arctic states and indigenous peoples. The Arctic Council started functioning in 1996, which include eight Arctic state members, six permanent participants representing indigenous people and some official “observer” (non-Arctic countries, intergovernmental inter-parliamentary organisations and nongovernmental organisations). The chairmanships of AC, as well as the physical location of the AC secretariat, revolve on a periodic basis among the eight member countries.

Several other international forums with regional or broader European interests also address economic, social, and environmental issues that often relate to the Arctic, such as Barents Euro-Arctic Council, the Nordic Council, Europe Union (EU) and the Conference of Parliamentarians of the Arctic Region.

As well, International Marine Organisation (IMO) prepares regulations for vessels navigating on the Polar seas, as well as developed the Polar Code.

Another important cooperative platform is the Arctic Circle (Organisation), which is the largest network of international dialogue and cooperation between members of government, academia and the scientific community on the future of the Arctic.

Indigenous People and the Arctic development

Indigenous peoples are the longstanding permanent population of the Arctic. Their population is small and varies in proportion of total populations across the region. There are around four million people living in the Arctic and indigenous people is estimated to be near 10 percent of total population (382,000), with over 40 different ethnic groups.

Despite their relatively small numbers, Indigenous People hold significant political and moral authority within Arctic governance systems (Scott Harrison, 2015).

In the Arctic Council, Indigenous peoples' organisations have been granted status as so-called Permanent Participants (PPs), holding full consultation rights related to negotiations and decisions. These organisations include the Aleut International Association, the Arctic Athabaskan Council, the Gwich'in Council International, the Inuit Circumpolar Council, the Russian Association of Indigenous Peoples of the North (RAIPON), and the Saami Council, who are concerned primarily with human rights, environmental protection, and preservation of traditional ways of life, social and economic development, and education.

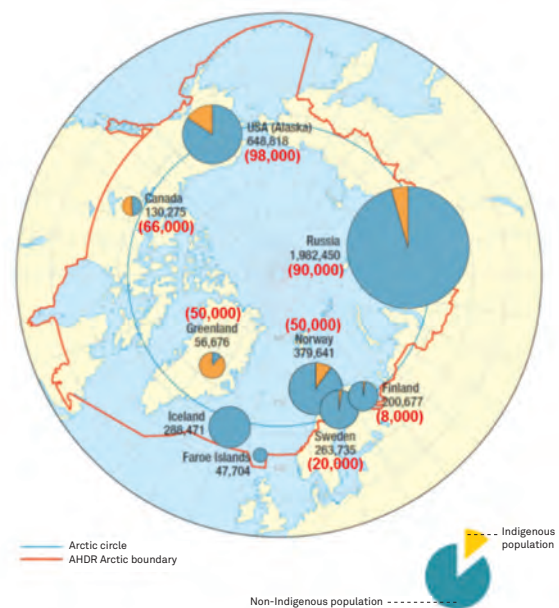


Figure 3 Distribution of indigenous people (AHDR, 2004)

Arctic Stakeholders

The Arctic stakeholders can be grouped into five categories: governments, international organisations (IGOs), civil society, private companies and academic organisations (Katie Burkhart etc., 2016).

- **Governments:** This category includes the seven AC member states and 12 AC observer countries. They are heavily investing in Arctic-related developments and play an active role in resource management, scientific research, emergency preparedness and response, maritime and aeronautical safety, and support to native Arctic communities.
- **IGOs:** Stakeholders in this category include The AC, the United Nations (UN), the European Union (EU), the World Trade Organisation (WTO), North Atlantic Treaty Organisation and Organisation of Petroleum Exporting Countries (OPEC). They all share some interests in areas like cultural conversation, economic development, energy, environmental protection, international law, resilience, scientific research or tourism in Arctic.
- **Civil Society:** this group includes the Circumpolar Inuit Council, Arctic tribal governments and regional and national non-governmental organisations (NGOs). They all have a stake in Arctic affairs and represent the interests of the indigenous peoples or the permanent protection of important onshore ecological and subsistence areas in the Arctic.

- **Private Company:** this group include companies in fishing, oil and gas, shipbuilding, shipping and tourism industry, which are interested in becoming involved in the Arctic. For example, BP, ExxonMobil, Gazprom, Rosneft and Shell are the stakeholders from oil and Gas; Samsung, Hyundai, DSME are stakeholders from shipbuilding industry.
- **Academic:** This group is comprised of research-based institutions and individuals, who are primarily concerned with scientific research related to the Arctic

Singapore’s Arctic Initiatives

Singapore has been granted permanent observer status in the Arctic Council in 2013, giving it a platform to participate in a body that shapes future policies in the icy northern region. Prime Minister Lee Hsien Loong said in a statement: “we joined the Arctic Council as an observer to find out what may happen when the northern sea-route becomes viable as the Arctic ice melts. You would not have thought an equatorial country without an interest in Arctic Affairs, but there is a reason we are there... It is relevant to us. It will not happen tomorrow. It may come to pass or it may not. But it probably will, and if it does, we will be there. These are small bets to hedge our position.” (The Strait Time, 2013). Singapore’s Arctic initiatives can be summarised as below.

- Climate Change and the impact on rising global water level on coastal states like Singapore. Much of Singapore lies only 15m above sea level, while 30 per cent of the island is less than 5m above sea level. If global temperatures continue to rise, many parts of Singapore could eventually be submerged under the water.
- Challenges and Opportunities of the new sea routes through the Arctic water. Melting Arctic ice has opened new shipping routes and ships are starting use the Northern Sea Route that bypass Singapore.
- Potential for development of the Arctic Region, such as the energy, mining, tourism and fishery.
- Singapore desire to contribute to the Arctic Community with her experience and technology solutions.

Arctic Development Trend

With the continued melting of polar ice—which will enlarge high northern international waters and the near inevitability of expanded navigation and offshore development, the geopolitical importance of the Arctic region is growing. At the same time, disputes have intensified between some Arctic states, particularly with respect to overlapping claims to areas of the northern seafloor. International “soft laws” such as the United Nations Convention on the Law of the Sea, the U.N. Fish Stocks Agreement, and the regulatory framework of the International Maritime Organisation provide areas for resolving some conflicts. Nonetheless, some experts argue that the existing system is insufficient to cope with the considerable challenges facing the Arctic in the decades to come. Both within and outside of the region, pressure is building for a stronger, more comprehensive framework for cooperative management in the Far North.

Environmental trends

The Arctic is experiencing significant changes in sea ice extent, ocean chemistry, coastal erosion, precipitation,

hydrology, and ecology, as well as extensive thawing of terrestrial ice sheets and permafrost. Ecosystem structure and function in the Arctic have been deeply influenced by these changes in both the short and long-term. This region is moving toward conditions never before witnessed.

- **Fastest warming regions** - The Arctic is warming more rapidly than anywhere else on earth – acting as an early-warning signal for the globe. In 2011, annual near surface air temperatures over much of the Arctic Ocean were 1.5°C warmer than the 1981–2010 baseline.
- **Irreversible warming** - some global climate change is locked in by current and past greenhouse gas emissions. The Arctic will continue to warm for the foreseeable future. Success in global climate negotiations under the UNFCCC would not substantially alter that outlook over the next few decades. The Arctic is already undergoing a profound and hard to reverse environmental state change.
- **Significant sea ice retreat** - The observed loss of summer sea ice has been more extreme than climate models had predicted, and this loss has been accompanied by decreases in both ice thickness and the presence of multi-year ice. Although there is some variability in ice extent from year to year, and although the annual cycle of melting and freezing continues, the overall downward trend in the September sea ice extent, recorded by the US National Snow and Ice Data Center (NSIDC) since 1979 (See Figure 3), is strong and unambiguous. Observational data and models forecast a nearly ice-free Arctic Ocean during summer before mid-century, and possibly before 2030.

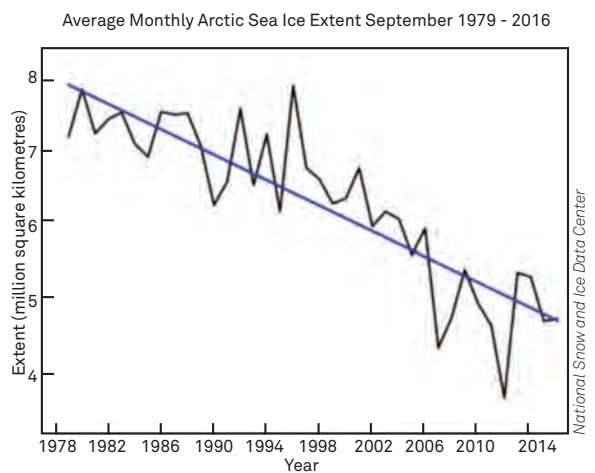


Figure 4 Decline in average sea ice extent in September, 1979-2016 (National Snow and Ice Data Centre, 2016)

- **Reduced access barrier together with new vulnerability** – more ice free area and longer ice free period will improve sea borne to the Arctic that are currently either inaccessible or accessible only by heavy ice breakers. However, the accessibility of many inland areas will be reduced because of the melting of the permafrost layer. Besides, the extreme weather such as storm will become more frequent and severe as a result of climate change.
- **Changing Ecosystem structure** – a warming Arctic probably would increase biological production but may lead to different species composition on land and

in the sea. On land, the Arctic is becoming increasingly green and there will be a tendency for pole ward shifts in major biomes and associated animals. In the sea, animals dependent on ice may be disadvantaged, such as walrus and polar bear. Ocean acidification due to increased carbon dioxide uptake in warmer seas can also harm some marine life.

Economics trends

Shipping and Logistic

Diminishing Arctic sea ice is likely to encourage growth of commercial shipping via international trans-Arctic routes. These routes may reduce transit distances between Europe and Asia by as much as 7810 km (Rotterdam – Yokohama, see Table 1). Maritime traffic in the Arctic is already considerable. In 2014, a total of 11,066 ships were detected the Arctic, which comprised 9.3% of the world's shipping traffic (Victor M. E. etc., 2016). The International Council on Clean Transportation (ICCT) also reported an average annual growth of 17 percent for cargo vessels and tugboats from 2008–2013 together with an annual growth of 64 percent for tankers in U.S. Arctic water. Year-round navigation has been maintained on the western part of the Russian Northern Sea Route (between Dudinka and Murmansk) since the late 1970s. Seasonal conditions vary across the Arctic. However, ice conditions are not necessarily worse in the Arctic than elsewhere. For example, in March 2011 ice conditions in the eastern Gulf of Finland outside the Arctic required a Russian nuclear icebreaker to be called in from the Arctic. As shipping seasons extend, Arctic shipping costs are reduced and point-to-point demand increases, traffic is expected to increase in future years.

Renewable energy

Renewable energy development and distribution in Arctic is currently limited. Remote and isolated communities in this region rely heavily on diesel or natural gas for heat, electricity, and transportation. Wind energy is currently the most feasible renewable energy source for the Arctic, due to strong winds in coastal and mountainous areas. For example, Alaska target to generate half of the state's electricity from renewable resources by 2025. Kotzebue and Nome are leading the way in the Arctic with wind turbines that have capacities of 2.28 megawatts and can

fully power up to 360 homes in each community. Several federal, state, and local entities are encouraging rural energy generation via wind turbines and solar panels. In addition, the NANA Regional Corporation, an Alaska Native association of 11 villages, is planning to expand the Kotzebue wind farm and study the potential for wind energy in other Northwest Arctic Borough communities. More recently, the Department of the Interior initiated a project with the National Renewable Energy Laboratory and several leading energy companies to explore potential development of a standardised and reliable small-scale wind-diesel renewable energy system for potential siting in small, off-grid U.S. Arctic villages.

Tourism

The Arctic has attracted tourists since the early 1800's. At the present time, vastly improved geographic and hydrographic knowledge; advancements in transport and navigational technologies; more comfortable clothing; more durable recreational equipment; significant reductions in the amount, extent and duration of sea ice; and a relatively more tolerable climate are all contributing to significant reduced "barriers to entry" for Arctic. According to a 2009 NOAA STAR report, tourism is the single largest human presence in the Arctic, with the majority of travelers visiting by ship. The cumulative impacts of these events are the following trends in today's Arctic tourism

- Growing number of Arctic destinations
- Larger numbers of tourists
- Expanding Season Length
- Duration of the tourist visit increased
- Cost of Travel Reduced

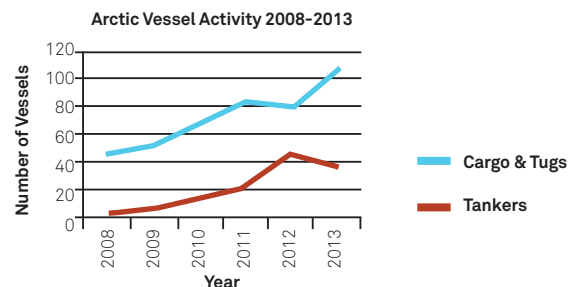


Figure 5 Vessel numbers operating in the U.S. Arctic by year (ICCT, 2016)

Table 1 Distance between major ports, using the Northwest Passage, Northeast Passage, Suez or Panama (Guy and Lasserre, 2016)

Origin-destination	Panama (km)	Northwest Passage (km)	Northeast Passage (km)	Suez and Malacca (km)
London -Yokohama	23300	14080	13841	21200
Marseilles - Yokohama	24030	16720	17954	17800
Rotterdam - Shanghai	25588	16100	15793	19550
Rotterdam - Shanghai	25588	16100	15793	19550
Rotterdam - Yokohama	23470	13950	13360	21170
Hamburg - Seattle	17110	13410	12770	29780
Rotterdam - Vancouver	16350	14330	13200	28400
New York - Shanghai	20880	17030	19893	22930
New York - Hongkong	21260	18140	20985	21570

Oil and gas

In 2008, the United States Geological Survey estimated that the Arctic contained some 412.2 billion barrels of undiscovered oil and oil equivalent. Over two-thirds of this was estimated to be natural gas – approximately 46 trillion cubic meters, representing 30% of global undiscovered natural gas (approximately equivalent to Russia's entire current proven reserves of natural gas). Some 90 billion barrels were estimated to be oil – 13% of the estimated global total of undiscovered oil, approximately three times the current total proven reserves of oil of the United States and more than three times the proven reserves of the world's largest non-state oil company, ExxonMobil. The balance of oil and gas across the Arctic will vary. In general, the Russian Arctic is considered to be more gas-prone and the offshore Norwegian and American Arctic more oil-prone. However, all these estimates are highly uncertain. In addition, the commerciality of any project or technique is based on expectations of future market prices for oil and gas. The International Energy Agency has warned that the drilling in the Arctic is not yet commercially viable, while environmental groups have warned that opening up new fossil fuel development will push the planet over the precipice into catastrophic climate change.

The outlook for Arctic natural gas is different though. In the future, European Arctic gas can be expected to reach consumers by pipeline, partly through existing Russian or Norwegian networks, and partly to compensate for declining gas production elsewhere in Europe and Russia. The scope of this market is constrained by the level of European demand. The Russian government intends to use Arctic production to allow it to keep to its European commitments while attempting to capture a part of the growing Asian gas market.

Infrastructure trends

Warming conditions in the Arctic strongly affect existing infrastructure as well as the needs and designs of future infrastructure. Permafrost thaw can undermine existing roads and buildings and, when combined with increased wave action due to reduced sea ice, accelerates coastal erosion, destroying or threatening shoreline infrastructure. In addition, design and construction of new infrastructure will require much higher engineering investments in an unstable or changing Arctic.

The vast geography and limited communications infrastructure in the Arctic significantly lengthen search and rescue and oil spill response times and create substantial challenges. In 2011, the eight member-nations of the Arctic Council signed the Agreement on Cooperation on Aeronautical and Marine Search and Rescue in the Arctic. In May 2013, these nations signed the Agreement on Cooperation on Marine Oil Pollution Preparedness and Response in the Arctic. Both agreements represent necessary steps to facilitate international cooperation in the event of a search and rescue event or marine oil spill incident in the Arctic. Successful implementation of these agreements will require appropriate response capabilities stationed strategically in the U.S. Arctic. There also is a need for more cooperative oil spill response research, development, and testing for conditions unique to Arctic environment.

Cultural and social trends

Traditional ways of life in much of indigenous population are at risk, who are facing a number of cultural and social challenges stemming from climate change as well as from economic and industrial development in the Arctic. Physical impacts to local communities from erosion, subsidence, floods, and storm surges often require emergency responses, infrastructure investments, and even full-scale community relocation.

The subsistence way of life of indigenous people relies upon natural resources for food, shelter, clothing, transportation, and the maintenance of cultural traditions. Although economic development and climate change have challenged some subsistence practices, local reliance on natural resources and traditional ways remain high.

Basic infrastructure is rudimentary or lacking in most Arctic communities. Low population densities over a vast geography, high engineering and construction costs, and lack of financial resources have led to absent or outdated water and sewer systems, a lack of passable roads between communities and locally produced electricity that is expensive and lacks a centralised energy grid.

Besides, Arctic holds many significant archeological sites, historic structures, and traditional cultural properties, which are essential to the practices that transmit culture from one generation to the next. However, climate change and modern development are affecting many of these sensitive sites, and that trend is likely to accelerate.

Opportunities For Further Development Ice capable vessel

As mentioned in previous sections, shipping in Arctic sea routine is expected to increase. However, despite relatively light ice conditions being encountered in recent years, most of these voyages have to be escorted by expensive icebreakers, which are capable of breaking through several metres of ice. The largest and most powerful icebreakers can cost up to \$1bn and take 8–10 years to build. Hiring charges vary, but the average cost to escort through the Northern Sea route is around \$200,000. If ships intending to navigate in ice infested waters could be designed as ice-capable ships to some extent, current reliance on icebreakers could be potentially significantly reduced, which in turn, could enhance shipping safety.



Figure 6 Ice capable LNG carrier by Aker
(source: <http://akerarctic.fi/>)

Carrier ships able to travel through ice of up to 1.5 metres without icebreaker support have been developed by the company Aker Arctic in Finland. As sea ice retreats and thins there is far greater prospect of Arctic shipping without icebreaker support for longer periods of the year, and ultimately all year round, in some parts of the Arctic.

Besides, the increase in traffic will also provide opportunities for specialised ship-builders and ship-designers, in the Arctic countries themselves and in new centres of ship construction in East Asia. Norilsk Nickel has invested heavily in ice-capable vessels capable of operating in 1.5 meter thick ice to ship minerals from Arctic Russia to both Europe and China without icebreaker support.



Figure 7 Ice capable vessel
(source: <http://barentsobserver.com>)

Arctic Tourism

The cruise sector, less constrained by limits on onshore tourist accommodation, has also expanded substantially. In 2003, an Association of Arctic Expedition Cruise Operators (AECO) was set up to support and establish best practice for cruises, particularly in the Norwegian Arctic. Last summer, the *Crystal Serenity*, became the largest cruise vessel to attempt to transit the Northwest Passage with 600 crew members and 1,000 passengers. It travelled from Anchorage, Alaska, to New York City in 32 days, which cost \$21,000 to \$120,000 per passenger. This trip was sold out and the 2017 trip is already waitlisted.

During Arctic Circle Assembly 2016, CEO of Lindblad Expeditions Sven Olaf Lindblad also indicated that there were many announcements early 2016 that people were entering polar marine tourism and building ships. According to him, more than 10 new expedition vessels will be delivered to various companies in 2019 and he projected an explosion of growth as related to marine tourism in Arctic commencing early 2019.



Figure 8 *Crystal Serenity* Cruise
(source: <http://www.cruise critic.co.uk/>)

Many of the challenges associated with cruise ship tourism in the Arctic are similar to those affecting commercial shipping: relatively poor knowledge of seabed features, lack of infrastructure in terms of port facilities, and the need for winterisation of vessels and the removal of deck-icing. In consideration of that, Keppel has presented a novel Arctic destination hub concept in Arctic Circle Assembly 2016 (Figure 9) based on the research work carried out in Keppel- NUS Corp Lab. In this concept, a sustainable Arctic tourism ecosystem was introduced. The system consists of,

- An Arctic Destination Hub for safe stay & research activities
- Arctic Expedition Cruise Vessels for personnel transport to local tourist attractions
- Arctic Rescue boats for safe rescue & evacuation of personnel, oil spill combat
- Arctic Crew Boats for crew transfer from Arctic islands to the Hub
- Arctic Supply Vessels for logistics supply from nearby ports to the Hub
- Arctic Ice breakers & tugs for ice management



Figure 9 Arctic Destination Hub for safe stay & research activities

Search and Rescue (SAR) infrastructure development

In contrast to the projected explosion of growth in Arctic marine activities, there is a lack of respect and experience with Arctic among those new players in this frontier region. Sven Olaf Lindblad has warned during Arctic Circle Assembly 2016 “Accident will be happened, as what has been experienced by Antarctic tourism”. A study conducted by Nord University also indicated “the probability of large scale incidents is low (in high north) but the consequences may be extremely high” while “there are severe capacity and competence gaps in marine time preparedness in most high north countries”. As Polar Code is expected to enter into force on 1 January 2017, even more strict safety requirement will be applied to vessels navigating in the Arctic water. In addition, Arctic Council reached the first legally binding, pan-Arctic Search and Rescue (SAR) Agreement in May 2011, which came into force in January, 2013. This provided a firm basis for co-operation between Arctic states.

Helicopter evacuation is considered as the preferred method of dry evacuation from a facility in an emergency situation in the High North. However, outreach (200-

300km) capacity of helicopter limits the SAR support coverage to only small parts of the Arctic water. In addition, Helicopter SAR operations are hindered by wind speed, poor visibility, fog or snow and the pilot's ability to operate under prevailing conditions. Consequently, there is a need to develop emergency response systems covering probable incidents and accidents for offshore operations shipping and tourism etc (Figure 10).

A multipurpose hub could be a floating or near shore ensuring support functions such as:

- Emergency operations/coordination
- Weather surveillance
- Hospitals/medical facilities
- Firefighting equipment
- Oil spill recovery equipment
- Additional systems and equipment for SAR
- Communications
- Helicopter base
- Telemedicine

In Arctic Circle Assembly 2016, Keppel proposed a novel near shore Mini multipurpose Hub concept (Figure 11) based on existing rig design

LNG Fuel Development for local communities

Agreement on Cooperation on Marine Oil Pollution Preparedness and Response in in the Arctic among the eight Arctic states was signed in 2013. This is the second

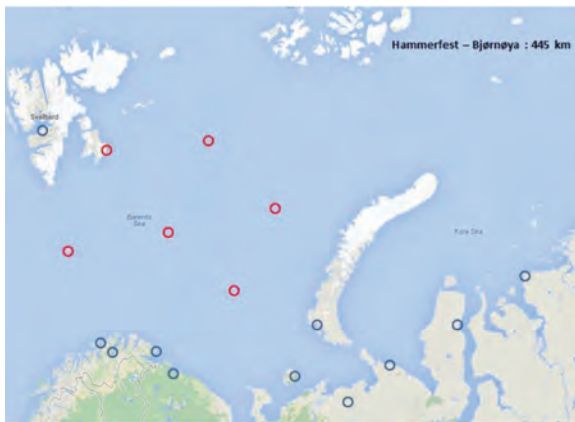


Figure 10 Multipurpose hubs with helicopter facilities (Source: North Energy)



Figure 11 Near Shore Mini multipurpose Hub

legally binding agreement negotiated under the auspices of the Arctic Council. In addition, Emission Control Area (ECA) on the coast of Norway, North Sea and Baltic Sea in effect since 1 January 2015 Furthermore, the Polar Code will enter into force in January 2017 in Arctic Water. All this enforce more and more stringent emission requirements to the Arctic marine activities and consequently alternative clean fuel need to be developed for the Arctic energy supply.

In the meantime, there are considerable natural gas resources in the Arctic Region, but at present only limited development.

In Russia on-shore arctic gas has been pipelined south for some years and current projects are underway to export LNG from the Yamal region.

In the US there is considerable associated gas with North Slope Alaska oil production but no transportation infrastructure to transport to market. Recent techno-economic studies have shown that at present it does not seem to meet business criteria to develop such infrastructure.

In Canada there have been significant gas reserves discovered in the Beaufort region and for a decade or more oil companies were working on the development of a McKenzie Valley pipeline. Unfortunately for them final approval to build this pipeline came just as the price of natural gas dropped so that again the project does not meet economic criteria.

In addition to the Beaufort region, considerable exploration has taken place in the Canadian Arctic Island north of the NW Passage, but again no infrastructure exists to bring this gas to southern markets.

A recent study by the Canadian Academy of Engineering CAE, titled Engineering in Canada's Northern Oceans - Research and Strategies for Development suggests that Arctic natural gas might be developed for local use, replacing the need to bring fuel oil shipped from southern Canada.

This would provide northern residents with a clean, green local fuel and would reduce risks to the environment through lower emissions and less risk of oil spill from tankers sailing north.

Further if developed LNG could also be used to fuel icebreakers and other vessel operating in northern waters, further providing a green fuel while also allowing more extensive missions to be carried, as current arctic marine activities are often limited by fuel availability.



Figure 12 Barge mounted LNG PreNex Plant

Conclusion

A review has been conducted on the background, challenges and trends for the current Arctic developments. Some possible development opportunities have also been identified in the present paper.

- The current infrastructure in shipping, SAR and tourism is insufficient in the Arctic to meet the expected economic development.
- If ships intending to navigate in ice infested waters could be designed as ice-capable ships to some extent, current reliance on icebreakers can potentially significantly be reduced, which in turn, could enhance shipping safety.
- The cruise sector in Arctic tourism, less constrained by limits on onshore tourist accommodation, has expanded substantially. CEO of Lindblad Expeditions has projected an explosion of growth as related to marine tourism in Arctic commencing early 2019.
- Arctic natural gas might be developed for local use, replacing the need to bring fuel oil shipped from southern Canada and Alaska.

References

- AHDR (2004). Arctic Human Development Report. Stefansson Arctic Institute, Akureyri, Iceland.
- E.J. Stewart, D. Draper¹ And M.E. Johnston (2005). A Review of Tourism Research in the Polar Regions. ARCTIC VOL. 58, NO. 4, P383– 394.
- Guy, Emmanuel and Frédéric Lasserre (2016). Commercial shipping in the Arctic: new perspectives, challenges and regulations. Polar Record, online version, janv. doi:10.1017/S0032247415001011.
- INTSOK (2014). Russian-Norwegian Oil & Gas industry cooperation in the high north. RU-NO Barents Project, Logistics and Transport-Report, 31 October 2014.
- Joe P. Clement, John L. Bengtson and Brendan P. Kelly (2013). Managing for the future in a rapidly changing Arctic. Interagency Working Group on Coordination of Domestic Energy Development and Permitting in Alaska, US.
- K. Burkhart, T.Skeadas and C. Wichmann (2016). Arctic 2030 Planning for an Uncertain Future.
- Ken Croasdale, Robert Frederking, Ian Jordaan and Peter Noble (2016). Engineering in Canada's Northern Oceans Research and Strategies for Development. Canadian Academy of Engineering, Ottawa.
- Lloyd's (2012). Arctic Opening: Opportunity and Risk in the high North. London, UK.
- Masahiko Furuichi and Natsuhiko Otsuka (2013). Cost Analysis of the Northern Sea Route (NSR) and the Conventional Route Shipping. Proceedings of the IAME 2013 Conference, Marseille, France.
- Muhammad Makki (2012). Evaluating Arctic Dialogue: A Case Study of Stakeholder Relations For Sustainable Oil And Gas Development. Journal of Sustainable development, V3, No.3.
- PMAE (2009). Arctic Marine shipping assessment 2009 report.
- Scott Harrison (2015). The indigenous factor of East Asian engagement with the Canadian arctic. <http://www.scottmharrison.com/>.
- Sam Tan(2016). Looking at the Arctic from the Outside – Prospects and Opportunities. Arctic Circle Greenland Forum, Nuuk, Greenland.
- The International Council on Clean Transportation (ICCT) (2015). A 10-Year Projection of Maritime Activity in the U.S. Arctic Region. Washington, U.S.
- Victor M. Eguíluz, Juan Fernández-Gracia, Xabier Irigoien & Carlos M. Duarte (2016). A quantitative assessment of Arctic shipping in 2010–2014. www.nature.com/scientificreports
- The Research Council of Norway (2011). Research Strategy for the Arctic and Northern Area, Hanshaugen, Noway.

Author's Contact

| Zhuo.chen@komtech.com.sg

Delving into Deepsea Mining

| Amit JAIN*, MSc, B.tech

| Anis HUSSAIN*, MSc, B.Eng

| Aziz MERCHANT*, CEng, MSc, FRINA, FIMarEST, FSNAMEs

| Lara Zalena KAMAL*, MSc, B.Eng

| WANG Rong*, B. Eng

**Keppel Offshore & Marine Technology Centre- Deepwater Technology*

Thousands of feet below the ocean's surface lies a vast untapped store of natural resources including valuable metals and rare-earth minerals hidden within an ecosystem of yet to be discovered species and seabed habitats. Technology and infrastructure development worldwide coupled with uncertain resource markets and volatile raw material prices are dramatically increasing the demand for these resources. This demand has catalysed interest in mining areas of the sea floor coming from a range of stakeholders including public actors such as states and regions as well as companies and industry organisations to explore the possibilities and to some extent to secure future resources ⁽¹⁾.

Introduction

The vast repository of minerals, including cobalt, zinc, manganese and rare earth materials that are needed for smart phones, laptops and hybrid cars, are present in three forms of ore— massive Polymetallic sulphide (SMS) deposits around hydrothermal vents, Polymetallic manganese nodules (PMN) that remain strewn across the ocean floor and cobalt-rich ferromanganese crusts that cover the seamounts (Figure 1) ⁽²⁾ found covering large areas of the oceans (Figure 2) ⁽³⁾. These ocean floor resources are key in everything from cars and modern buildings to computers and smartphones ⁽⁴⁾.

A large majority of deposits are found within deep water, which by definition starts where the continental shelf ends at depths greater than 200 metres. As such, deep-sea resources are generally found in the high seas beyond Economic Exclusive Zones (EEZ) of nation states and is thus governed by the International Seabed Authority (ISA) ⁽⁵⁾.

Established in 1994, the ISA is an autonomous international organisation established under the 1982 United Nations Convention on the Law of the Sea (UNCLOS) ⁽⁶⁾. The ISA is the only body with the legal standing responsible of managing the seabed and its resources outside of national jurisdictions. This includes the calling for global and regional cooperation, technical assistance, monitoring and environmental assessment, and the development of enforceable international rules to prevent, reduce and control pollution affecting the oceans. Since

2001, the ISA has granted 26 mining exploration contracts covering more than one million square kilometres of seabed, with 18 of these contracts granted in the last four years ⁽⁷⁾.

In 2015, Ocean Mineral Singapore Pte Ltd (OMS), a JV between Keppel and Lockheed Martin's subsidiary – UK Seabed Resources Ltd (UKSRL), was granted concession for the exploration for PMN at a site of 58,000 sq-km within the Clarion-Clipperton Zone (CCZ) of the Pacific (Figure 3). Under this license OMS intends to conduct environmental studies and to survey for deposits of PMN within the approved area which will serve as baseline data for technology development and environmental impact studies.

The success of deep-sea mining venture requires the implementation of several components. 'Exploration' invariably forms the first step towards the mining venture followed by 'Technology Development' for mining and metallurgical processing. The 'Environmental' component closely follows these so as to develop the protocol for baseline data, impact assessment and monitoring as well as the development of environmental management plans. In order to finally execute the project, a 'Techno-economic assessment' as well as a 'legal' framework would guide the decisions and actions for implementation on the basis of inputs received from earlier components. Activities under each of these components could initially be independent of each other but a close networking among these will be required to execute the project.

The success of deep-sea mining venture requires the implementation of several components. 'Exploration' invariably forms the first step towards the mining venture followed by 'Technology Development' for mining and metallurgical processing.

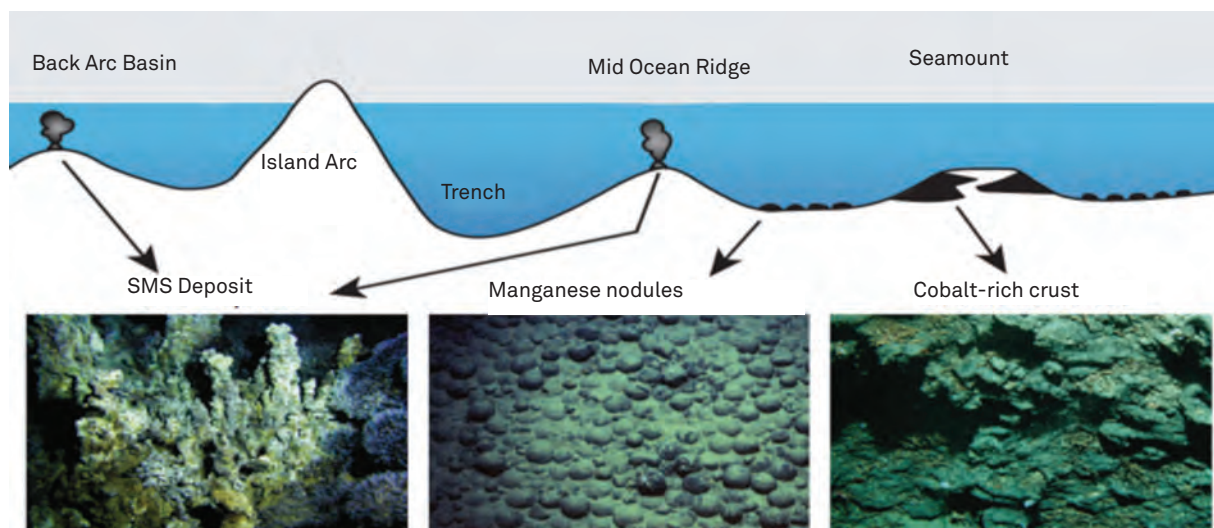


Figure 1 Type and location of ore forms found

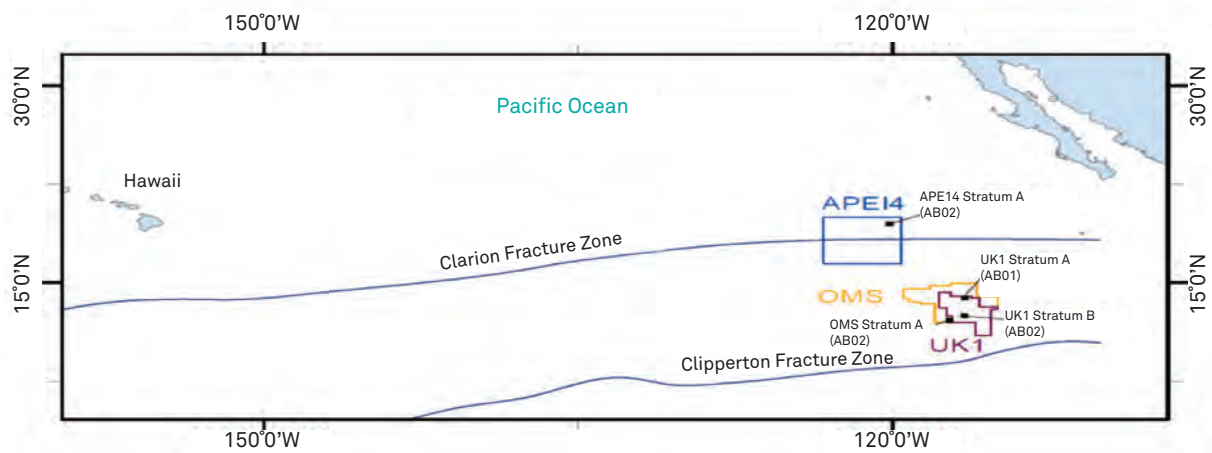


Figure 4 Location of the CCZ, UK-1, OMS and APEI-4

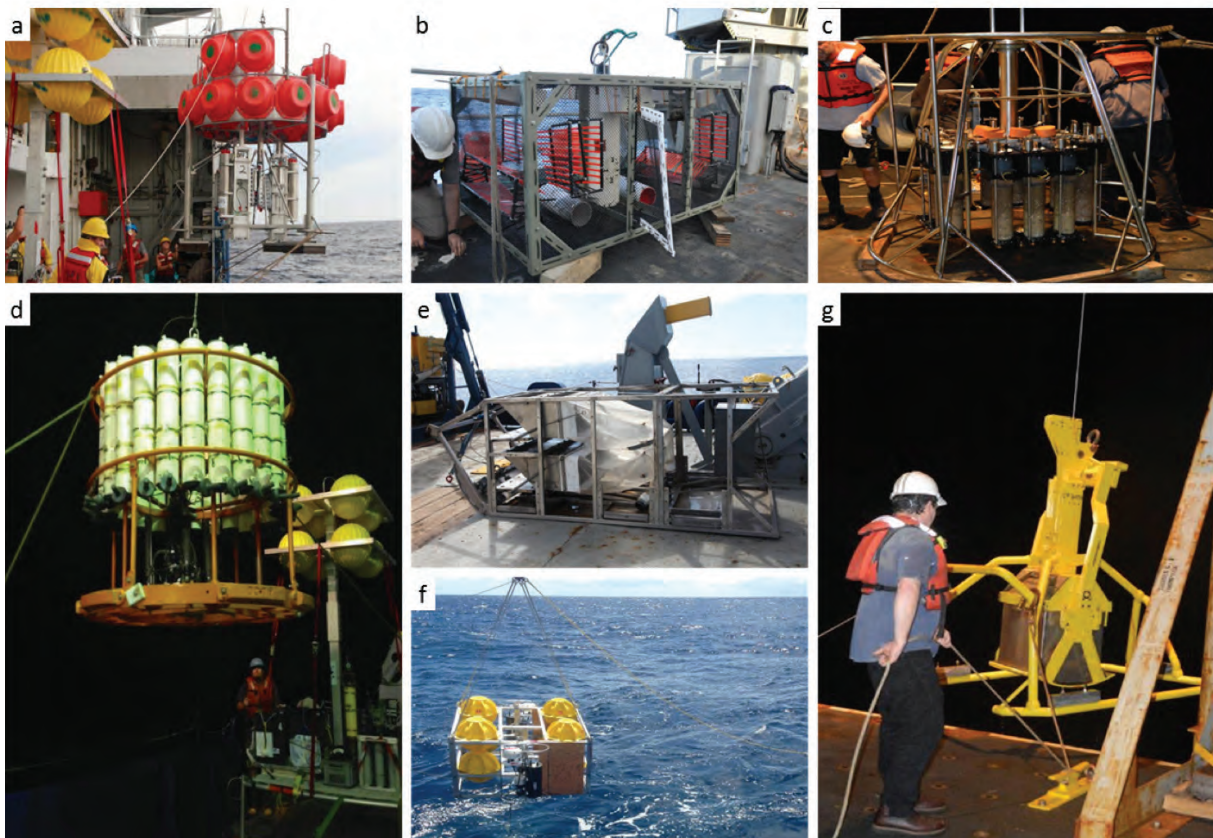


Figure 5 Sampling equipment typically used on board during an exploration cruise: (a) respirometer; (b) baited trap; (c) mega corer; (d) conductivity temperature, depth (CTD); (e) epibenthic sled; (f) plankton pump; (g) box corer.

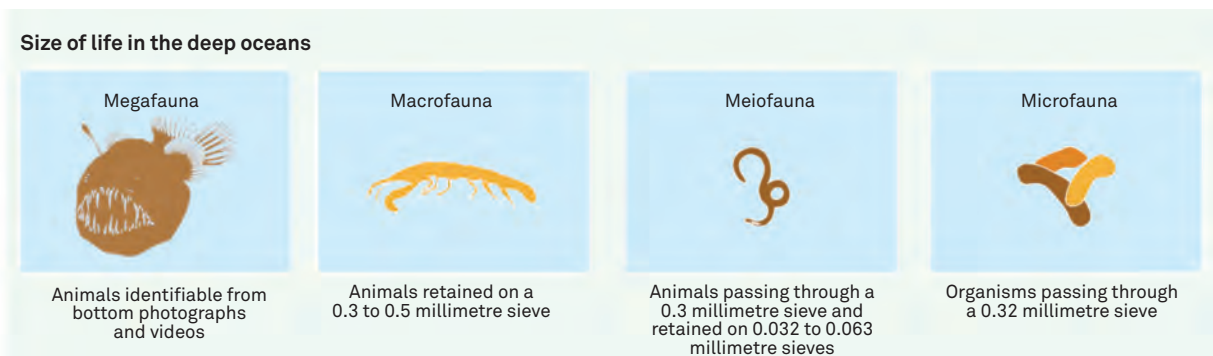


Figure 6 Deep sea communities body size classes

Introduction to Exploration

Since the establishment of the ISA ⁽⁸⁾, the ISA has kept environmental protection as one of its highest priorities and in 2000 established a comprehensive legal regime for the monitoring and protection of the marine environment ⁽⁹⁾. Environmental provisions are a major part of the obligations placed by the ISA on itself and on seabed contractors in its regulations on PMN and as such requires seabed exploration to establish environmental baselines in the areas explored. It is critical that the contractors, while conducting exploration cruises in their prospective mining areas gather as much environmental information as possible to provide baselines of the current benthic ecosystem which would become critical towards the identification of future environmental impact assessments. ISA has prescribed 44 Environmental requirements as part of the annual submittal which includes findings from geological, physical and biological oceanography survey.

Prospecting and exploration are similar in many ways to oceanographic research. The Exploration cruise are to be designed in accordance with the ISA environmental guidelines ⁽¹⁰⁾. Data are to be collected using a suite of the best available technology as well as refined and modified sampling procedures stemming directly from well-developed geological, physical and biological oceanography techniques developed for the evaluating of the benthic biological baseline (Figure 5). The data and samples gathered through this expedition will serve as a baseline for environmental impact studies and for the development of environmentally benign technologies for deep-sea mining.

Manganese nodules occur widely on the vast, sediment-covered, rolling plains of the abyssal ocean covering an estimated up to 75 per cent of the sea floor and can vary in size, abundance, and surface texture thus resulting in habitat heterogeneity, or diversity on landscape (km) scales for both hard-bottom and soft-sediment biotas, and life forms. This habitat heterogeneity leads to variations in faunal abundance and community structure. Deep sea communities are generally divided into four body-size classes for study and description: megafauna, macrofauna, meiofauna, and microfauna (Figure 6) ⁽³⁾. Megafauna are the largest animals in CCZ benthic (sea-bottom) ecosystems. These are animals large enough to be recognised in bottom photographs and range from about 2 cm to more than 100 cm in length. Megafauna include omnivorous fishes (especially rattails), cephalopods (such as octopus and squid), scavenging amphipods and deep sea shrimp, large deposit feeders such as sea cucumbers and starfish, and suspension-feeding glass sponges, anemones, and other cnidarians.

The biology associated with manganese nodules has been studied most intensively in the CCZ where sea-floor communities exist in what is known as the 'mesotrophic abyss'; a region of moderate particulate organic carbon flux and food availability by abyssal standards and where the sea floor in is heavily modified by the activities of animals in this region ⁽³⁾.

The initiative set up by the Keppel-NUS Corporate Laboratory established in 2013 with the aim to create a synergistic industry-university partnership afforded

the opportunity for local scientists to develop and build core competencies within deep-water exploration survey techniques through their participation on-board AB02.

Introduction to Geophysical Study for Resource Exploration

Exploration geophysics is an applied branch of geophysics, which uses physical methods, such as seismic, gravitational, magnetic, electrical and electromagnetic, sonar at the surface of the Earth to measure the physical properties of the subsurface, along with the anomalies in those properties. It is most often used to detect or infer the presence and position of economically useful geological deposits, such as ore minerals; fossil fuels and other hydrocarbons; geothermal reservoirs; and groundwater reservoirs.

The OMS exploration area is 58,000 sq. km in size and lies at 4500-5000 mtrs below the sea level. In order to exploit the resources, the contractor needs to explore the area first to determine the extent of the resource, i.e. the quantity of the nodule in tonnage to make a commercial decision whether exploitation is economical or not. Geophysical survey also helps to understand the terrain and thus gives key input for designing of the Nodule harvesting technology such as collector and vertical transport system. The abundance determines the size and speed of the collector. The exploration of the concession area is done using Autonomous Unmanned Vehicle (AUV) based sonar and camera, Ship based Sonar and Box core.

Sidescan sonars (SSS) use the material characteristics of reflection and absorption to image the seafloor. Some materials, such as un-weathered volcanic rock, reflect sound efficiently; other materials, such as silt and mud, do not reflect sound as well. Because of this, as an SSS ensonifies an area of the seafloor and measures the acoustic reflectivity, it is able to detect small-scale seabed features and textures. Applying the most efficient frequency sonar can greatly improve a SSS survey. Lower frequency sonars have longer ranges, but the resolution decreases as range increases. Higher frequency sonars have higher resolutions, therefore smaller objects and textures can be distinguished. However, as the frequency increases, acoustic energy is more quickly absorbed by the water and the range of the sonar decreases. Therefore, it is imperative to obtain a balance between ensonification area and resolution such that a large enough region of seafloor is surveyed while maintaining a fine enough resolution to detect features of interest on the seafloor.

Images are captured by high resolution camera mounted on AUV from different altitudes and are analysed for percent of nodule coverage on the seafloor. The nodule coverage are then plotted spatially and used to characterise regions of the seafloor for nodule distribution. These distribution maps provided ground truth data for sidescan sonar surveys.

In order to understand the characteristics of the terrain the Bathymetry data is obtained. Bathymetric data describes the depth of the seafloor and are used to create digital elevation models (DEMs). These data are collected by recording the time for an acoustic pulse, described as a beam and termed a "ping", to travel from the sonar to the seafloor and return. The range to seafloor

is calculated from the measured two-way acoustic travel times. A sonar can be mounted on any vehicle, and that vehicle can be located either on the ocean surface (i.e. a ship), or subsea (i.e. an AUV). The sonar depth, which may be zero if it is located at the ocean surface, must be combined with the calculated range-to-seafloor to determine the seafloor depth. These depth values are then assembled into a DEM.

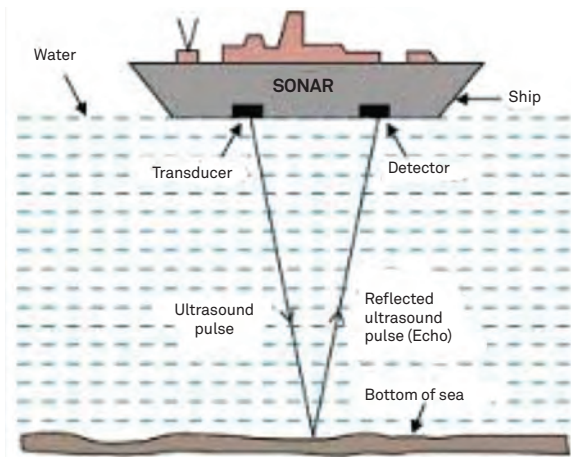


Figure 7 Image showing ship based sonar system

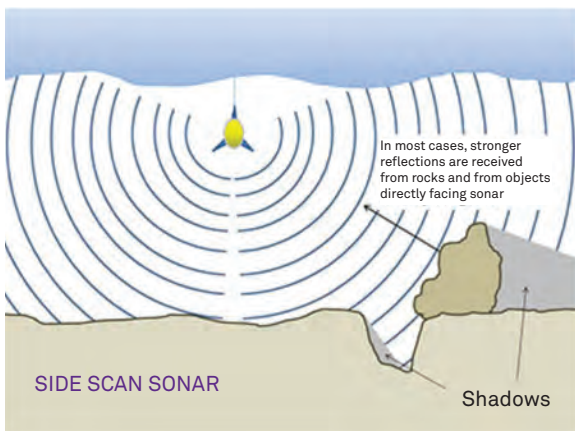


Figure 8 Image showing AUV based side scan sonar

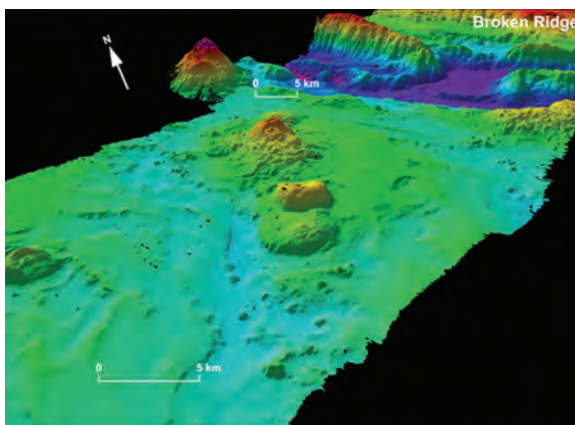


Figure 9 3D Model of sea floor terrain
Image Source: Australian Transport Safety Bureau; Geoscience Australia

Box corers are used to collect essentially intact blocks of seafloor sediment. The one used in OMS expedition cruise was approximately 0.5 m x 0.5 m x 0.6 m (L x W x D). When the box core apparatus is lowered to the seafloor, the heavy weight of the device pushes the sampling box into the sediment. As the device is lifted from the seafloor, an automatic triggering mechanism allows a large spade to secure the sample from beneath, and doors on the top of the box are shut. The device is then brought to the surface / ship with an analogous in situ sample of the seafloor.



Figure 10 AUV Photo imagery of Seabed with PMN

Estimation of Resources:

The AUV and Ship based Side scan sonar, Single Beam, Multi beam, Photo Imagery and Box Core data are used to prepare a Nodule Abundance Map for the surveyed region, based on which the estimation of resource is done. Such estimation are done by recognised experts who are skilled in the science of resource estimation.

Classification of Resources:

Mineral resource classification is the classification of mineral deposits based on their geologic certainty and economic value.

Mineral deposits can be classified as:

- Mineral resources that are potentially valuable, and for which reasonable prospects exist for eventual economic extraction.
- Mineral reserves that are valuable and legally and economically and technically feasible to extract.

Resource and Reserve Classification is an economic function and is governed by statutes, regulations and industry best practice norms. There are several classification schemes worldwide, however the Canadian CIM classification (see NI 43-101), the Australasian Joint Ore Reserves Committee Code (JORC Code), the South African Code for the Reporting of Mineral Resources and Mineral Reserves (SAMREC) and the "chessboard" classification scheme of mineral deposits by H. G. Dill are the general standards.

Mineral Resources are further sub-divided, in order of increasing geological confidence, into inferred, indicated and measured categories.

- **Inferred:** The part of a mineral resource for which tonnage, grade and mineral content can be estimated with a low level of confidence. It is inferred from geological evidence and assumed but not verified geological or grade continuity. It is based on information gathered through appropriate techniques from locations such as outcrops, trenches, pits, workings and drill holes which may be of limited or uncertain quality and reliability.
- **Indicated:** Resources that are simply economic mineral occurrences that have been sampled to a point where an estimate has been made, at a reasonable level of confidence, of their contained metal, grade, tonnage, shape, densities, and physical characteristics.
- **Measured:** Resources that have undergone enough further sampling that a 'competent person' (defined by the norms of the relevant mining code; usually a geologist) has declared them to be an acceptable estimate, at a high degree of confidence, of the grade, tonnage, shape, densities, physical characteristics and mineral content of the mineral occurrence.
- **A Proved Ore Reserve:** These are part of measured resources that can be mined in an economically viable fashion. It includes diluting materials and allowances for losses which occur when the material is mined. A Proved Ore Reserve represents the highest confidence category of reserve estimate. The style of mineralisation or other factors could mean that Proved Ore Reserves are not achievable in some deposits.

Resource Prediction

Estimation of resource is needed to determine the economic value of entire exploration area. In order to determine the resource, detailed mapping of the Nodule abundance is needed across the exploration area. Proven methods for determining the nodule abundance are AUV photo imagery, side scan data along with the box core data. Such operations are expensive and are very time consuming. Using such methods for nodule mapping across 58,000 sq.km would cost a fortune to OMS. Innovative method of finding the nodule presence probability and mapping the entire area with respect to Nodule abundance is to extrapolate the available information from few expedition cruises and historic data available in public domain.

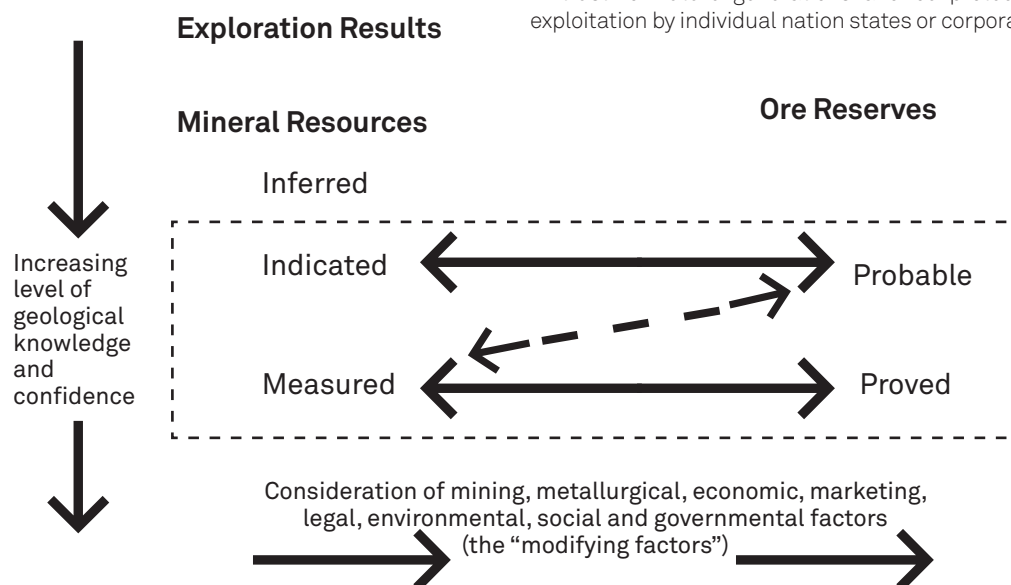
Under the Keppel – NUS corporate lab, the team has developed a Spatial Resource prediction tool based on the science of Nodule formation.

Environmental Impact Assessment:

Seabed Mineral resources in International waters are considered to be Common Heritage of Mankind (CHM). CHM (also termed the common heritage of humanity, common heritage of humankind or common heritage principle) is a principle of international law which holds that defined territorial areas and elements of humanity's common heritage (cultural and natural) should be held in trust for future generations and be protected from exploitation by individual nation states or corporations.

Mineral reserves are resources known to be economically feasible for extraction. Reserves are either Probable Reserves or Proved Reserves.

- **A Probable Ore Reserve:** These are part of indicated, and in some circumstances, measured mineral resources that can be mined in an economically viable fashion. It includes diluting material and allowances for losses which may occur when the material is mined. A Probable Ore Reserve has a lower level of confidence than a Proved Ore Reserve but is of sufficient quality to serve as the basis for decision on the development of deposit.



In order to fulfil the CHM responsibility there is a need for environment friendly technologies for Nodule Exploitation as well an efficient environment monitoring plan to make sure no adverse impact has been made on the environment.

Under societal responsibility of CHM the PMN are to be exploited in environment friendly manner. In order to fulfil the CHM responsibility there is a need for environment friendly technologies for Nodule Exploitation as well an efficient environment monitoring plan to make sure no adverse impact has been made on the environment.

Nodule harvesting from the seabed involves vertical transport of slurry (consisting of sediment, sand, gravels and nodules) from a nodule collector/harvester, through a flexible connection system to a vertical riser to a surface mining platform. Slurry processing takes place on the surface with the nodule material retained and the balance of solids returned to the seabed via tailing discharge at some pre-determined depth. This process creates sedimentary plumes from both the nodule collector/harvester and tailing pipes as shown in the image. The plumes may spread a considerable distance from the harvesting site and take a considerable time to re-settle on the seabed.

It is mandatory for an Exploration contractor to provide enough evidence in favour of the proposed technology that it does not have any adverse impact on the environment, also ISA calls for an efficient Environment monitoring plan (EMP) to monitor the effect of the exploitation activities. Having fulfilled the above mentioned requirements an Exploration contractor can be granted rights for Exploitation in the area by the ISA.

In order to meet the ISA requirements of having an efficient EMP and environment friendly technology, KOMtech

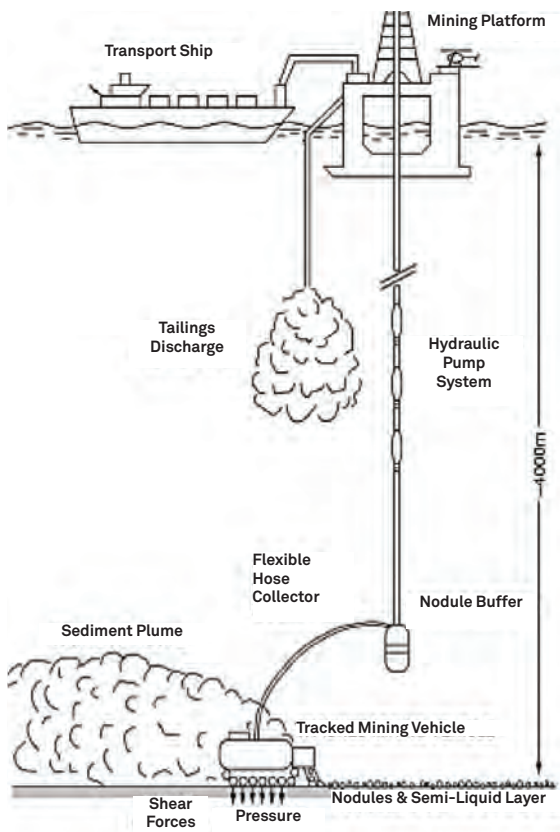


Figure 11 Image showing the plume generation and dispersion during Nodule Harvesting activities

and NUS under the aegis of the Keppel – NUS corporate laboratory are working towards development of a code based on Smooth Particle Hydrodynamics (SPH) and DPD (Dissipative Particle Dynamics) which can predict the plume generation, dissipation and dispersion in three dimensions from the source. The code predicts the generation and dispersion of the plume by assessing the spreading of sediment plume and tailing discharge caused by the technical activities by particle-based methods that respect the particulate nature of the sediment fluid. The code is capable of modelling the poly-dispersed nature of the sediment in the sediment transport process to assess the movement of different sized and shaped particles.

The impact of the research is twofold, first it provides inputs for the technology development providing the guidelines of the amount of sediment plumes generated by a particular process, further the code helps in determining the points of sediment release in order to minimise environment impact.

Introduction to Deepsea Mining Technologies

The steady rise of Deepsea Mining as a solution to depleting land resources continues to leave the engineering and research and development community with many unanswered questions. The best way forward to developing an environmental friendly and sustainable deep sea mining practice is to leverage off knowledge and experiences from adjacent industries like Deepwater Oil & Gas as well as Dredging industries. Deepwater Oil & Gas Technology deals with drilling and transportation of hydrocarbons from water depth extending up to 3000 metres, while dredging operations are carried out in shallower water and relates to the removal and transportation of sediments from seabed. Oil & Gas industries have similarities to Deepsea Mining with respect to operating depths and to dredging industries with respect to functionality. Expert consensus from around the world states that a feasible technical solution for Deepsea Mining is likely to present itself as an extension of present day Deepwater Oil & Gas and Dredging technology.

The Seabed Nodule Mining technology value chain has the following main components

- **Seabed Collector (SBC):** The equipment moving on the seabed and collects nodules and transfers it to the vertical transport system. A SBC has two parts,
 - Collector Head: The component which collects the Nodules mechanically, hydraulically or by Hybrid Means is called a Collector Head.
 - Collector Chassis: The propulsion means of the SBC is called Collector Chassis – the chassis can be a track wheel type or Archimedes Screw type or some other type.
- **Vertical Transport System (VTS):** The system which transfers the Nodules from the seabed to the sea surface is called a Vertical Transport System. The system may comprise of a typical riser and pumping system analogous to what is used in Oil & Gas Industry or it can be a batch transport system which may use Submersible robotic capsules or of some other kind.
- **On-board Handling of the collected Nodules and Waste water discharge system:** The collected Nodules are dewatered and stored on the Surface Vessel before being offloaded to a bulk carrier. A dewatering system can be a system of shakers and

conveyor belts which dewater the collected Nodules by mechanical means. The Dewatering plant can be on top of the main deck of the ship or can be inside the hull. The operational philosophy and construction methodology determines the location of the dewatering plant.

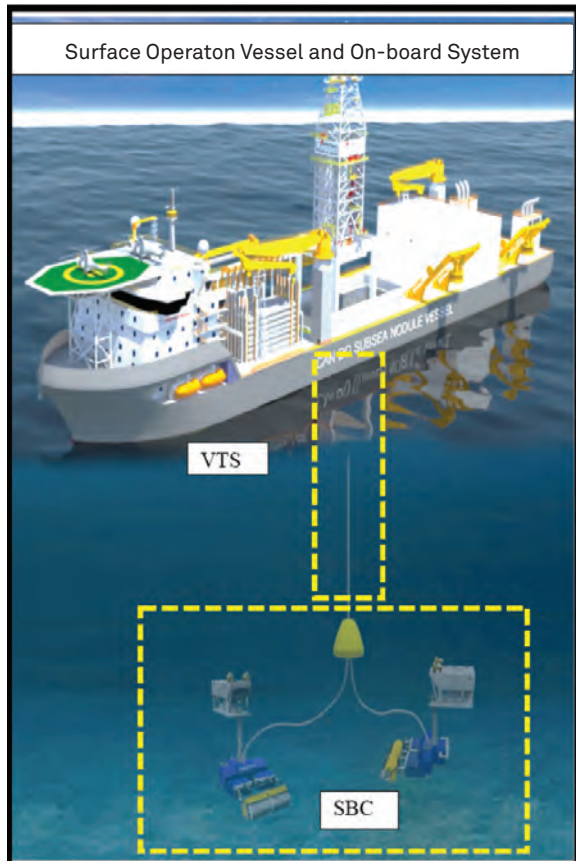


Figure 12 Image showing the various components of Nodule Harvesting Technology value chain

Considerations for Technology Development:

The subcomponents of the Mining Vessel have to be designed to operate in an unprecedented water depth of 5000 metres. Such components are not yet commercially available thus there are a lot of challenges to be overcome requiring considerable amount of research and development. The technical considerations in selection and development of a concept are as follows.

Collector Chassis:

- **Mobility Envelope** - The ability of Collector Chassis is evaluated by its Mobility Envelope Curve. On a given soil condition a chassis can carry a certain vertical load and can generate a certain traction for translational movements, enhancement in one ability adversely affects the other ability. The sweet spot lies somewhere between the two extremes. Different conditions demand different Mobility Envelope characteristics from a vehicle.
- **Slope Negotiation** - The Seabed Bathymetry is undulating which requires the Chassis to negotiate slopes while collecting the Nodules. Different Chassis have different slope negotiating capability for same amount of power consumption.

- **Turning Radius** - The Seabed Collector remains connected to the Surface Operating ship or the Vertical Transport system by means of flexible Jumpers or Hoses. This provides a limitation on excursion of the Collector requiring to turn when the excursion limit is reached. Different Chassis turn at least radius has an edge over other designs.
- **The payload carrying capacity** - The Seabed Collector needs to have an ability to store the collected Nodules for sake of redundancy. The payload carried effects the Mobility Envelope as it increases the Vertical load on the Chassis.
- **Power Consumption:** The collector chassis should be power efficient as it directly increases the OPEX.

Collector Head:

- **Efficiency of Nodule Collection:** The ability of the collector head to collect the Nodules of certain size continuously without missing out.
- **Minimum Plume Generation:** While collecting the Nodules the system which disturbs the seabed soil the least will create the least amount of Plume and thus will be preferred.
- **Power Consumption:** The collector head should be power efficient as it directly increases the OPEX.

Vertical Transport System (VTS):

- **Reliability, Availability and Maintainability** - The VTS concept should be reliable, readily available and with least maintenance requirement
- **Continuous Transportation** - The concept should have the ability to transport the nodules continuously to the Mining Ship
- **Over all Technology readiness level (TRL)** - From a contractors point of view a system with higher TRL is preferred, otherwise the gestation period of the concept will be longer which will have cost and schedule repercussions.
- **Power Consumption** - The concept should be power efficient as it directly increases the OPEX.
- **Ease of Interface between collector and the lifting means** - The simpler the interface of the VTS with the Collector and the Ship the favourable the concept will be.
- **Ease of operations** - Easier operational requirements is desirable by the contractor and operator.
- **Foot Print on Seabed** - Concept with least interaction with seabed will cause less plume generations and hence will be more environment friendly. Thus the concept with lesser footprints will be favoured over other concepts
- **Safety** - Concepts with least operational risk in it will be preferred over other concepts

On-board Handling of the collected Nodules and Waste water discharge system:

- **Reliability, Availability and Maintainability** - The concept should be reliable, readily available and with least maintenance requirement.
- **Fines losses in the system while transporting-** The concept should allow minimum wear and tear to the nodules resulting in minimum fines losses.
- **Power Consumption** - The Concept should be power efficient.

Regulatory Development and ISA Engagement

The ISA responsible of managing the seabed and its resources outside of national jurisdictions plays a vital role in encouraging for functional collaboration in resource management by creating a new basis for the participation in the development of ocean resources for the benefit of the common heritage of mankind and as such have taken a proactive approach in building its base of information and crafting the rules and regulation through the engagement with numerous stakeholders. Although the ISA continues to heed the advice of The Legal and Technical Commission (LTC), an organ of the Council of the International Seabed Authority consisting of members with qualifications relevant to the exploration, exploitation and processing of mineral resources, oceanography, economic and/or legal matters relating to ocean mining and related fields, inclusion and outreach with all stakeholder groups beyond the LTC have been important and key to the quality of work done by the ISA.

Through these ISA-stakeholder engagements the ISA often issues stakeholder survey questionnaires aimed at soliciting relevant information for the development of a regulatory framework critical for the management of minerals within ISA jurisdiction areas and more recently for the development of a fair and transparent exploitation regime relevant to the drafting of the mining code. The stakeholder survey is the first in a series of stakeholder engagements anticipated by the ISA to begin the development of a regulatory framework which will incorporate contemporary best practice and from which the ISA expects to benefit from the in-depth views, analysis and opinions from experts on activities within areas of the ISA jurisdiction.

OMS actively engages with the ISA to keep abreast of regulatory development whilst also ensuring fairness in the development of an exploitation regime favourable to both contractors while keeping the interest of the common heritage of mankind in check. OMS has thus submitted its response to the ISA working draft of its exploitation regulations issued by the ISA on 15 July 2016 to highlight a number of key areas for concern like the need for a clear timeline and schedule to further encourage heavily invested contractors on the possibility of moving to an exploitation regime. A total of 43 contributors have submitted their response to the ISA.

OMS also actively participates in community engagement activities:

- i. Active participation in the review of draft ISA regulatory codes and stakeholder surveys conducted by ISA
- ii. The team made a joint presentation with UKSRL on the Exploration Cruise during the ISA session in July 2015
- iii. Jointly organised the CIL- ISA workshop in June 2015.
- iv. Presented on Seabed Mining Technology Overview during the CIL- ISA workshop in June 2015.

Reference

1. Stone, Maddie. Gizmodo. <http://gizmodo.com/the-future-of-technology-is-hiding-on-the-ocean-floor-1764122967>. [Online] 05 04, 2016. <http://gizmodo.com/the-future-of-technology-is-hiding-on-the-ocean-floor-1764122967>.
2. Instrument, National. A National Instrument for the Standards of Disclosure for Mineral Projects within Canada. 43-101 .
3. Deep Sea Minerals: Manganese Nodules, A Physical, Biological, Environmental and Technical Review. Baker, Elaine and Beaudoin, Yannick. s.l. : SPC, 2013, Vol. 1B.
4. Worden, Sara. Protecting the Deep Sea: A Call for Balancing Mining and Ecosystem Protection. Stanford Woods Institute for the Environment. [Online] July 8, 2015. <https://woods.stanford.edu/news-events/news/protecting-deep-sea-call-balancing-mining-and-ecosystem-protection>.
5. ECORYS. Study to Investigate State of Knowledge of Deep Sea Mining. Rotterdam/Brussels : s.n., 2014.
6. International Seabed Authority. About The National Seabed Authority. International Seabed Authority. [Online] <https://www.isa.org/jm/authority>.
7. —. Deep Seabed Minerals Contractors. International Seabed Authority. [Online] <https://www.isa.org/jm/deep-seabed-minerals-contractors>.
8. —. Structure and Mandate of the Council. International Seabed Authority. [Online] <https://www.isa.org/jm/authority/council-structure-mandate>.
9. Protection of the Seabed Environment. International Seabed Authority. ENG4,
10. International Seabed Authority - Legal and Technical Commission. Recommendations for the guidance of contractors for the assessment of the possible environmental impacts arising from exploration for marine minerals in the Area. Kingston, Jamaica : s.n., 2013. ISBA/19/LTC/8.

Author's Contact

- | amit.jain@komtech.com.sg
- | larazalena.fk@komtech.com.sg
- | Anis.Hussain@KOMtech.com.sg
- | aziz.merchant@keppelom.com
- | wang.rong@KOMtech.com.sg

Computing Second Order Wave Load Effects for Coupled Tension Leg Platform and Tender Assisted Semi-Submersible

| Miguel Angel Moya RAMIREZ[†], Ms.C.

| Antonio Carlos FERNANDES^{*}, Ph.D.

[†]BrasFELS

^{*}LOC-COPPE/UFRJ

The motions of floating moored structures are affected by first order wave loads proportional to the wave amplitude and associated to the wave frequency, and second order wave loads proportional to the square of the wave amplitude and related to a pair of frequencies of the irregular sea. Although the second order loads are usually smaller compared to the first order loads, these loads can excite resonance motions in frequencies that the system has very low damping. Therefore, second order wave loads have particular importance in the design of mooring systems.

The multi-body system composed by Tension Leg Platform (TLP) and Tender Assisted Drilling (TAD) are particularly sensitive to second order effects due to their natural frequencies of horizontal and vertical modes.

This work presents a numerical study of second order wave loads on the TLP-TAD multi-body system. An extensive hydrodynamics analysis focus on the hydrodynamic interactions between the floaters was performed using frequency domain approach. The second order quadratic transform function (QTF) were evaluated using two different methods, the indirect and the direct methods. In addition to that, the accuracy of Newman approximation for the low frequency QTF is assessed.

Introduction

Wave loads on floating bodies submitted to irregular seas are commonly grouped in contributions of first order, second order and even higher orders^[1].

The second order loads are proportional to the wave amplitude and associated with the wave-wave and wave-body interactions^[2]. Thus, these forces contain terms corresponding to frequencies equal to sums and differences of the elementary wave frequencies. i.e. wave drift loads (low frequency effects) and sum frequency loads (high frequency effects)^[3].

Figure 01 presents a typical distribution of the energy of the irregular wave sea in the frequency domain. Vertical lines represent the natural frequencies of the TLP and TAD. Note that, TLP has very low natural frequencies in horizontal modes (Surge, Sway and Yaw) and very high natural frequencies in vertical modes (Heave, Roll, and Pitch). On the other hand, TAD presents very low natural frequencies of horizontal modes and low natural frequencies on the vertical modes.

Note that these natural frequencies are out of the high-energy region where first order loads are predominant. However, these are located in the areas where second order loads are predominant. Therefore, possible resonant motions due to second order loads must be investigated and considered in the moored system design.

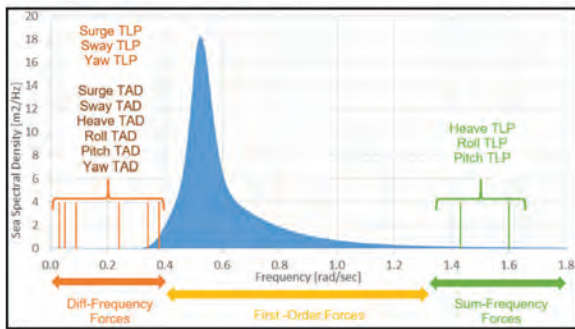


Figure 1 Typical wave energy spectrum and natural frequencies of TLP-TAD multi-body system.

Background

Second order wave loads are usually represented through the quadratic transfer function (QTF)^[4]. The QTF can be decomposed as a contribution of two parts as shown in Eq. 1. The first part F_1 contains quadratic terms due to the products of first order quantities, consequently it only depends on the first order wave potential. The second part F_2 is a consequence of the solutions of the second order wave potential^[5].

$$F(f_1, f_2) = F_1(f_1, f_2) + F_2(f_1, f_2) \tag{1}$$

where F is the second order load and f_1 and f_2 are two elementary wave frequencies.

The first term is also known as the mean drift force, and there are three formulations for calculating this term: The near-field method^[6], The far-field method^[7] and the middle-field method^[8]. The second term can be formulated as shown in Eq. 2^[5].

$$F_2 = \frac{(-i\rho)}{g} (\omega_2 - \omega_1) \int_H^{\infty} (\phi_I^{(2)} + \phi_D^{(2)}) \eta dS \tag{2}$$

where $\omega_1 = 2\pi f_1$, ρ is the water density, g is gravity, H is the body surface, $\phi_I^{(2)}$ is the second order wave incident potential and $\phi_D^{(2)}$ is the second order wave diffracted potential. Since $\phi_I^{(2)}$ is well described by an analytical expression^[6], the last challenge is to calculate the second order wave diffracted potential. The following approaches were proposed to determine this integral.

Indirect Method

This method, proposed by^[5], calculate the second order wave diffracted potential in an indirect manner using first order quantities by introducing an assisting velocity potential ψ which is the solution of the first order radiation problem at the sum or difference frequency as shown in Eq. 03. This approach is similar to the Haskind relation used to determine the first order wave diffracted potential.

$$\int_H^{\infty} (\phi_D^{(2)} \eta dS = - \int_H^{\infty} \left(\frac{\partial \phi_I}{\partial n} - \kappa_H \right) \psi - \frac{1}{g} \int_H^{\infty} \kappa_H \psi dS \tag{3}$$

The first term of Eq. 3 is an integral over the body surface; the second term is the integral which involves integration over the free surface. The convergence of the free surface integration is slow and requires very high CPU time^[9]. In some cases, such as wave drift loads on large volumes the contribution of the free surface integral is not significant and can be neglected^[10]. On the other hand, this term is predominant on the sum-frequency component and cannot be avoided^[10].

Direct Method

In this approach proposed by^[11, 12], the full second order problem is solved directly from the Eq. 2. Consequently, the second order wave loads are obtained by direct pressure integration over the body surface.

Newman Approximation

As shown in the previous sections, the calculation of QTFs involves many numerical challenges, very high number of mathematical unknowns to be calculated, and, consequently, it is very expensive in terms of time processing^[5].

With the aim of simplifying this tremendous computational effort, several approximated methods have been developed. The most widely used is the Newman approximation^[13]. With this method, the term F_2 of Eq. 1. is estimated using the term F_1 as shown in Eq. 4.

$$F_2(f_1, f_2) = \text{sgn}(F_1(f_1, f_1)) \sqrt{F_1(f_1, f_1) \times F_1(f_2, f_2)} \tag{4}$$

Note that, this method is only applicable to the estimation of wave drift loads, and in any case, this could be used to estimate the sum-frequency component. Furthermore, the Neman approximation was proposed for very large structures such as barges or FPSOs operating in deep water with very low natural frequency^[14].

Several works^[4, 9] and^[10] have discussed the limitation of this method. Consequently, its accuracy needs to be evaluated for each situation.

Study Case

This numerical analysis considers a Tension Leg Platform (TLP) with a Tender Assisted Drilling (TAD) moored in close proximity. The TLP hull consists of four rectangular pontoons in close configuration and four square columns as shown in Figure 02. The TAD hull is composed of two rectangular pontoons connected by three circular beams and six columns as illustrated in Figure 03.

The TLP is moored with eight tendons composed by circular pipes. The TAD is moored by a semi-taut-leg system composed of eight lines with segments of chain and polyester ropes.

The mechanical connection between the platforms was performed by a hawser system to restrain the relative surge, sway and yaw motions between the platforms. This system is composed of two lines of nonlinear polyester ropes. Figure 04 shows a schematic representation of the hawser system.

Finally, Table 01 presents the natural frequencies of TLP and TAD comparing the alone and connected cases. This information is crucial to define the wave frequency pairs used to analyse the second order wave loads.

Table 1 Natural frequencies of TLP and TAD (in Hz.)

Modes	TLP	TLP	TAD	TAD
	Alone	Coupled	Alone	Coupled
Surge	0.005	0.005	0.004	0.005
Sway	0.005	0.005	0.005	0.005
Heave	0.227	0.227	0.061	0.061
Roll	0.254	0.254	0.039	0.039
Pitch	0.254	0.254	0.055	0.054
Yaw	0.007	0.010	0.015	0.017

Computational Grids

The second order wave loads were calculated using the 3D diffraction-radiation code WAMIT [15]. This code requires the physical properties of the floater and the discretisation of the surfaces of the bodies and the free surface around the floaters.

The geometry of the floaters was discretised using the low-order panel method. This method represents the body surface with a set of flat quadrilateral panels, in which the hydrodynamic properties are considered constant. Consequently, the accuracy of the low order panel method depends on the number of panels used to represent the geometries. [15]

Figures 02 and 03 present, respectively, the computational grids of TLP and TAD.

Figures 05, 06 and 07 present the grids of the free surface used for the three cases: TLP alone, TAD alone and TLP-TAD multi-body case, respectively. Note that to represent this surface the low-order panel method was used.

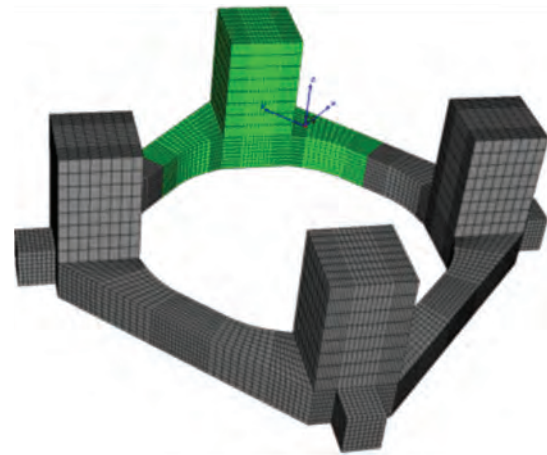


Figure 2 Low order panel method discretisation of TLP Hull.

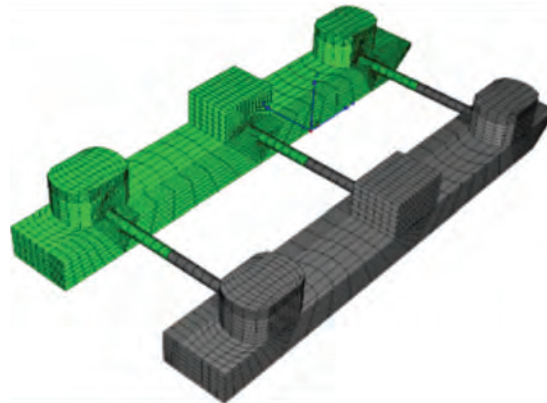


Figure 3 Low order panel method discretisation of TAD Hull.

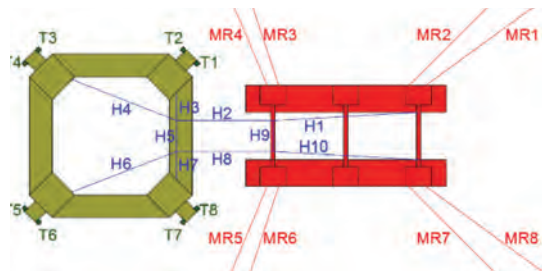


Figure 4 TLP+TAD system connected by hawser lines (H1 and H2).

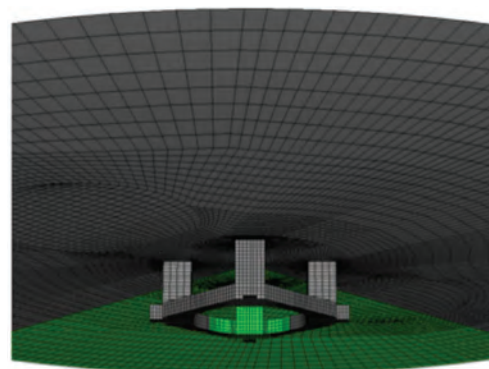


Figure 5 Free surface grid (TLP Alone).

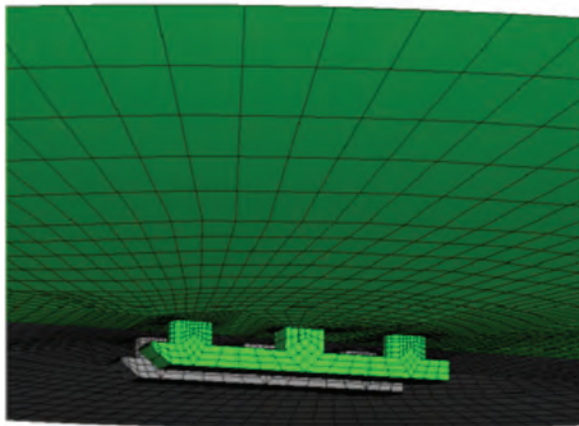


Figure 6 Free surface grid (TAD Alone).

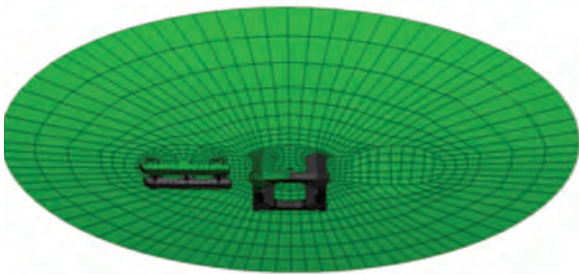


Figure 7 Free surface grid (LP-TAD multi-body system).

Grid Sensitivity Analysis

With the aim of verifying the influence of the computational grid on the calculation of second order loads, a sensitivity analysis has been performed. This study includes the calculations of the second order wave loads using the direct and the indirect methods presented in Section 2. Although these methods were developed using different numerical formulations, these are physically equivalent, and consequently, the results obtained from these methods must be the same. According to [4], the good agreement between the results achieved with the direct and the indirect method indicate that the computational grids have excellent refinement and consequently a good numerical convergence was achieved.

Tables 02 and 03 present the number of panels used to represent the floater geometries and the free surfaces.

Table 2 Number of panels of TLP and TAD

Floater	Number of Panels	Reference
TLP	3072	Figure 02
TAD	3924	Figure 03

Table 3 Number of panels of free surface

Case	Number of Panels	Reference
TLP Alone	7680	Figure 04
TAD Alone	7340	Figure 05
TLP+TAD	7870	Figure 06

Methodology

The numerical analysis includes three cases: TLP Alone, TAD Alone and TLP connected with TAD. For all cases, five wave headings were considered. 0°, 45°, 90°, 135° and 180° as shown in Figure 08. Note that the wave heading indicates the direction that waves are progressing, measured positive anti-clockwise from the global X-axis. The range of wave frequencies considered was from 0.05 to 0.25 Hz by steps of 0.001Hz. i.e. 201 wave frequencies. The second order wave loads were calculated for all the frequency combination, i.e. 20301 pair frequencies for each wave heading.

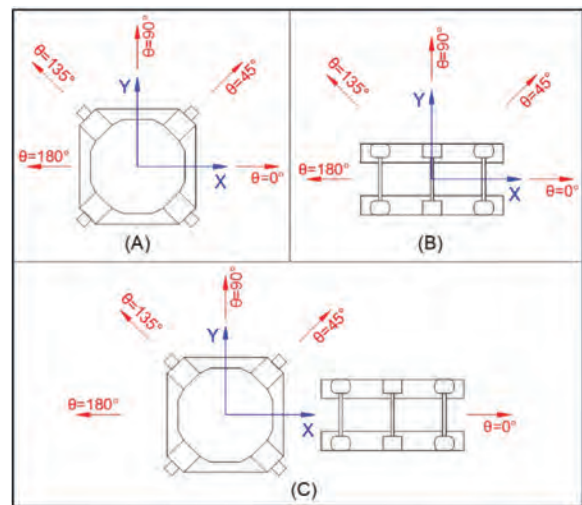


Figure 8 Global coordinate system used into the WAMIT runs.

Linear stiffness matrixes modeled mooring systems of TLP and TAD, and the connection between both floaters, moreover, the viscous damping coefficients of Table 04 were incorporated into WAMIT runs.

Table 4 Percental damping ratios of TLP and TAD

Floater	Surge	Sway	Heave	Roll	Pitch	Yaw
TLP	5	5	3	3	3	5
TAD	5	5	7	7	7	5

Significant coupling effects in the low and high-frequency second order loads were found.

The Newman approximation presents adequate predictions when the natural frequency of the floating structure is less than 0.005 Hz.

Results: Grid Sensitivity Analysis

Figure 09 presents a comparison of low-frequency QTF of TLP in Surge for a wave heading equal to 45, between following cases: (A) Alone using direct method, (B) Alone using indirect method, (C) Coupled with TAD using direct method, (D) Coupled with TAD using indirect method.

Figure 10 shows a comparison of low-frequency QTF of TAD in Surge for a wave heading equal to 45, between cases: (A) Alone using direct method, (B) Alone using indirect method, (C) Coupled with TLP using direct method, (D) Coupled with TLP using indirect method.

Note that only selected results were presented. Results of the direct and indirect methods are very similar. Not only for the alone cases, but also for the coupled cases. Therefore, the discretisation of the computational meshes of bodies and free surfaces are validated.

On the other hand, the major differences between alone and coupled cases are evidence of hydrodynamic coupled effects on the second order loads.

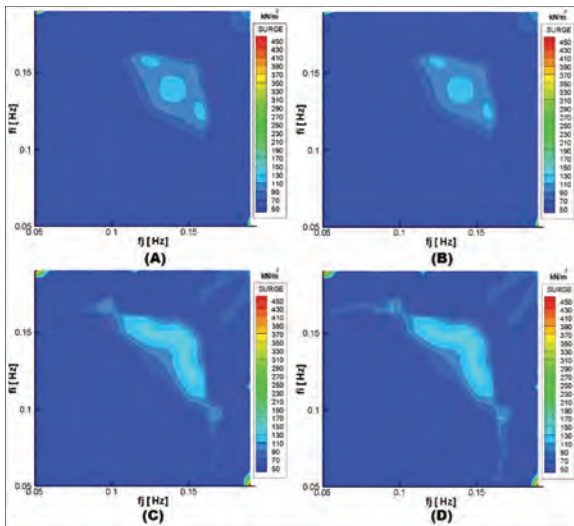


Figure 9 Low frequency QTF of TLP for Surge and $\theta=45^\circ$. (A) Alone & Direct Method (B) Alone & Indirect Method (C) Coupled & Direct Method (D) Coupled & Indirect Method

Low frequency QTF of TLP

In Figure 11, a comparison of low-frequency QTF of TLP for surge motion is presented. the considered cases are: (A) alone and $\theta = 0^\circ$, (B) coupled with TAD and $\theta = 0^\circ$, (C) coupled with TAD and $\theta = 180^\circ$. The corresponding Newman approximation surfaces are included. Note that θ is the wave heading.

The comparison between cases (A), (B) and (C) evidences strong hydrodynamic coupling effects, especially in the central region ($f_1 \approx f_2$). Note that the regions with higher forces correspond to frequencies out the diagonal, i.e. $f_1 > 0.15\text{Hz}$ and $f_2 < 0.15\text{Hz}$.

On the other hand, the comparison of QTF and the Newman approximation reveals that the last has very poor agreement in regions far from the condition $f_1 \approx f_2$.

Figure 12 presents a comparison of low-frequency QTF of TLP for Yaw motion, between cases (A) Alone and $\theta = 45^\circ$, (B) Coupled and $\theta = 45^\circ$, (C) Coupled and $\theta = 135^\circ$ and the respective Newman approximation surfaces.

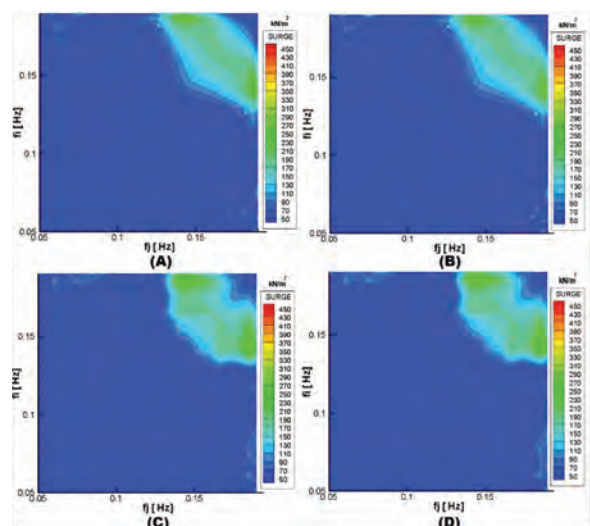


Figure 10 Low frequency QTF of TAD for Surge and $\theta=45^\circ$. (A) Alone & Direct Method (B) Alone & Indirect Method (C) Coupled & Direct Method (D) Coupled & Indirect Method

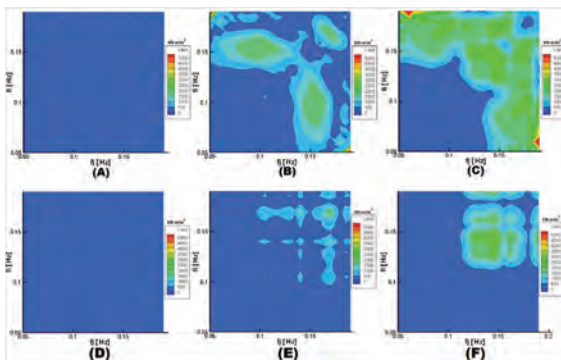


Figure 11 L. F. QTF of TLP for Surge (A) Alone & $\theta=0^\circ$ (B) Coupled & $\theta=0^\circ$ (C) Coupled & $\theta=180^\circ$ Newman Approximation for QTF (D) Alone & $\theta=0^\circ$ (E) Coupled & $\theta=0^\circ$ (F) Coupled & $\theta=180^\circ$

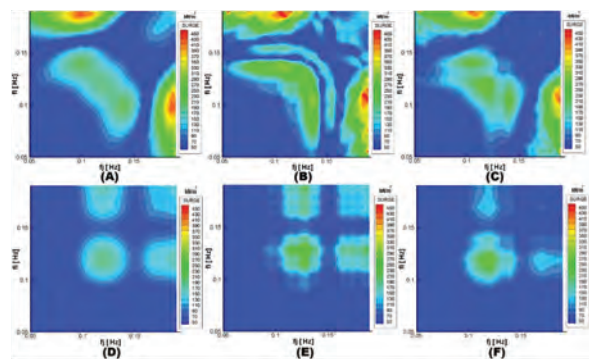


Figure 12 L. F. QTF of TLP for Yaw (A) Alone & $\theta=0^\circ$ (B) Coupled & $\theta=0^\circ$ (C) Coupled & $\theta=180^\circ$ Newman Approximation for QTF (D) Alone & $\theta=0^\circ$ (E) Coupled & $\theta=0^\circ$ (F) Coupled & $\theta=180^\circ$

As in the case of Fig. 11, significant coupling effects are observed, note that second order moment on TLP alone is almost zero, while, in coupled cases, it presents very high values.

To comparing the Full-QTFs with the predictions of the Newman approximation in a more efficient way, sectional curves of QTF surfaces with constant difference frequency df are presented below. The difference frequency df is defined in Eq. 5.

$$df = f_1 - f_2 = \text{constant} \quad (5)$$

Thus, Figure 13 presents a comparison between QTF of TLP and the respective Newman approximation for surge motion in cases: Alone with $\theta = 0^\circ$, Coupled with $\theta = 0^\circ$ and Coupled with $\theta = 180^\circ$. Note that df is equal to the surge natural frequency. i.e. $df=0.005$.

In addition, Figure 14 shows a comparison between QTF of TLP and the respective Newman approximation for Yaw motion in cases alone with $\theta = 45^\circ$, coupled with $\theta = 45^\circ$ and coupled with $\theta = 135^\circ$. In this cases $df=0.007$ is the yaw natural frequency.

Both figures, reveal significant hydrodynamic coupled effects, especially for wave headings greater than 90° i.e. when TLP is downstream.

Although Fig. 11 and 12 suggest that Newman approximation provides results with poor agreement, Fig. 13 and 14 surprisingly indicate that results of Newman approximation have a good agreement in regions with df near to the natural frequencies. Note that surge and yaw have very low natural frequencies.

High frequency QTF of TLP

Figure 15 presents the high-frequency QTF of TLP for heave motion for cases: (A) Alone and $\theta = 0^\circ$, (B) Coupled and $\theta = 0^\circ$, (C) Coupled and $\theta = 180^\circ$. In addition to that, the high-frequency QTF of TLP for pitch motion for cases: (D) Alone and $\theta = 0^\circ$, (E) Coupled and $\theta = 0^\circ$ and (F) Coupled and $\theta = 180^\circ$.

In both cases, heave and pitch, the high frequency QTF of TLP presents hydrodynamic coupling effects. The differences are relatively minor when compared with the results obtained on low frequency QTF.

In Heave, with the presence of TAD, the second order forces are smaller. It is more evident, for $\theta = 180^\circ$ in the region $f_i \geq 0.15$ Hz.

In Pitch, the multi-body case presents higher values for $\theta = 0^\circ$ in the area $f_i \geq 0.15$ Hz

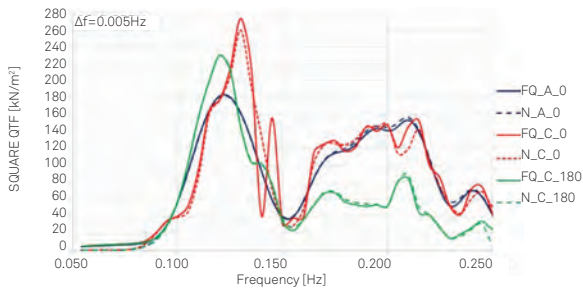


Figure 13 Full QTF (FQ) vs. Newman Approximation (N) For TLP in Surge. Alone (A) and Coupled with TAD (C). Wave headings $\theta=0^\circ$ and $\theta=180^\circ$.

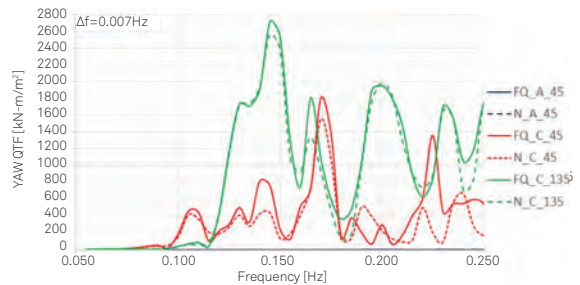


Figure 14 Full QTF (FQ) vs. Newman Approximation (N) For TLP in Yaw. Alone (A) and Coupled with TAD (C). Wave headings $\theta=45^\circ$ and $\theta=135^\circ$.

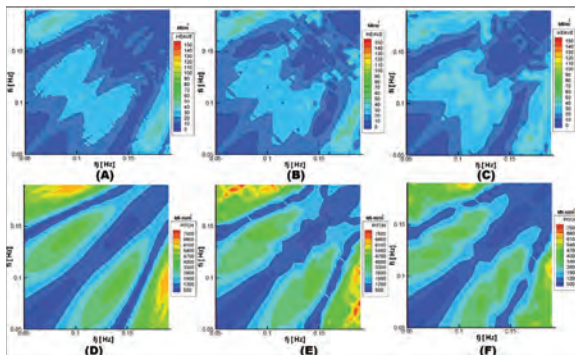


Figure 15 H. F. QTF of TLP for Heave (A) Alone & $\theta=0^\circ$ (B) Coupled & $\theta=0^\circ$ (C) Coupled & $\theta=180^\circ$ H. F. QTF of TLP for Pitch (D) Alone & $\theta=0^\circ$ (E) Coupled & $\theta=0^\circ$ (F) Coupled & $\theta=180^\circ$

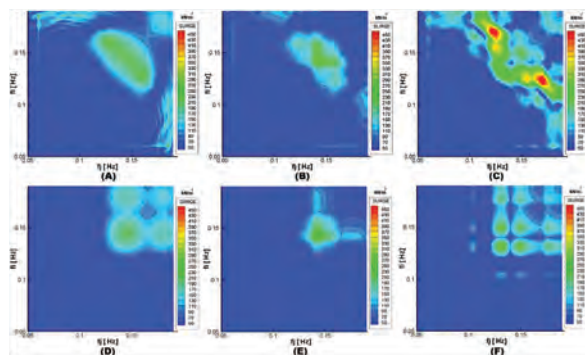


Figure 16 Full QTF of TAD for Surge (A) Alone & $\theta=0^\circ$ (B) Coupled & $\theta=0^\circ$ (C) Coupled & $\theta=180^\circ$ Newman Approximation for QTF (D) Alone & $\theta=0^\circ$ (E) Coupled & $\theta=0^\circ$ (F) Coupled & $\theta=180^\circ$

Low frequency QTF of TAD

Figures 16, 17 and 18 present a comparison of low-frequency QTF of TAD for Surge, Heave and Pitch respectively.

In all the figures the following cases were considered. (A) Alone and $\theta = 0^\circ$, (B) Coupled and $\theta = 0^\circ$, (C) Coupled and $\theta = 180^\circ$, (D), (E) and (F) present the respective Newman approximations.

In general, for the three modes (surge, heave and pitch), the comparison between cases (A), (B) and (C) reveals significant hydrodynamic coupling effects.

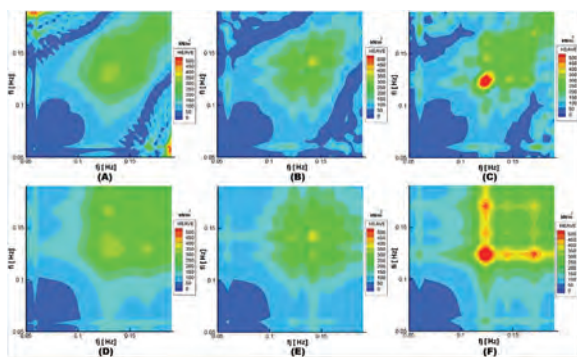


Figure 17 Full QTF of TAD for Heave (A) Alone & $\theta=0^\circ$ (B) Coupled & $\theta=0^\circ$ (C) Coupled & $\theta=180^\circ$ Newman Approximation for QTF (D) Alone & $\theta=0^\circ$ (E) Coupled & $\theta=0^\circ$ (F) Coupled & $\theta=180^\circ$

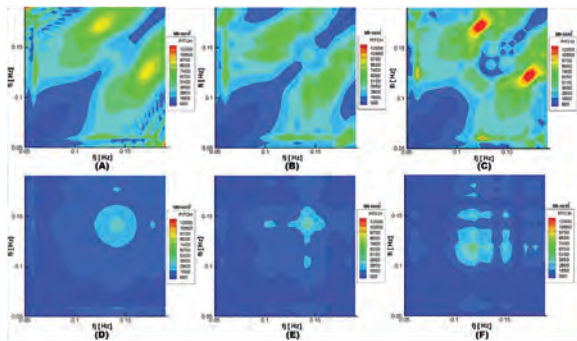


Figure 18 Full QTF of TAD for Pitch (A) Alone & $\theta=0^\circ$ (B) Coupled & $\theta=0^\circ$ (C) Coupled & $\theta=180^\circ$ Newman Approximation for QTF (D) Alone & $\theta=0^\circ$ (E) Coupled & $\theta=0^\circ$ (F) Coupled & $\theta=180^\circ$

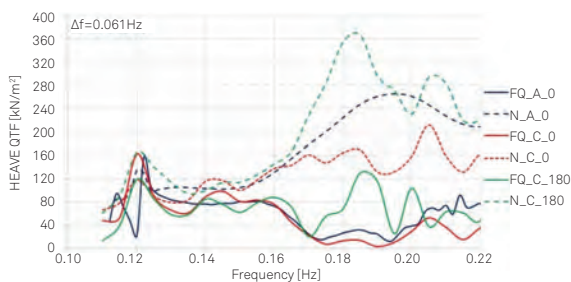


Figure 20 Full QTF (FQ) vs. Newman Approximation (N) For TAD in Heave. Alone (A) and Coupled with TLP (C). Wave headings $\theta=0^\circ$ and $\theta=180^\circ$.

The influence of the presence of TLP in second order loads on TAD seems higher.

Furthermore, the comparison between QTF and Newman approximation shows “global” poor agreement for all cases. Figures 19, 20 and 21 present a comparison between curves of QTF and Newman approximation for the cases mentioned in Fig. 16, 17, 18 respectively.

Note that d_f was selected to be the natural frequency of the respective mode.

Based on the results presented in Fig. 19, 20 and 21, the hydrodynamic coupling effects are confirmed.

The comparison between Newman approximation with the QTFs reveals good agreement for surge motions, due to the very low natural frequency. On the other hand, a poor agreement was observed for heave and pitch motion. In Heave, second order forces were overestimated. While in pitch, second order moments were underestimated.

Conclusions

Based on this extensive analysis of the second order loads on TLP-TAD multi-body system, the following conclusions were achieved:

Numerical grids of the floaters and the discretisation of the free surface were validated. Calculations using the indirect and the direct methods present very similar results. Hence, a good numerical convergence was achieved.

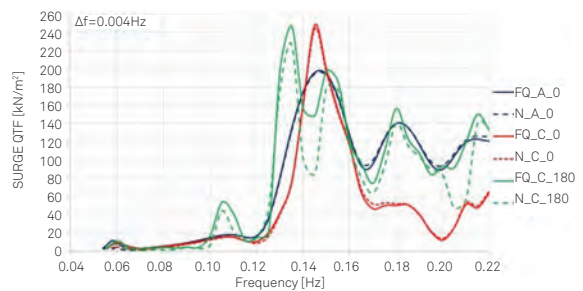


Figure 19 Full QTF (FQ) vs. Newman Approximation (N) For TAD in Surge. Alone (A) and Coupled with TLP (C). Wave headings $\theta=0^\circ$ and $\theta=180^\circ$.

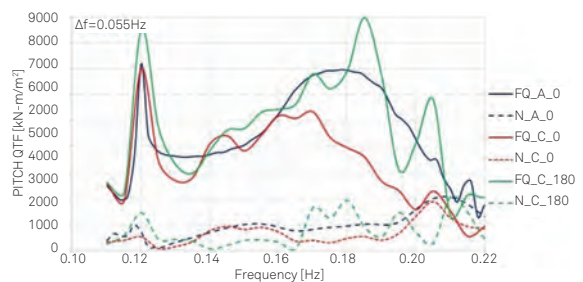


Figure 21 Full QTF (FQ) vs. Newman Approximation (N) For TAD in Pitch. Alone (A) and Coupled with TLP (C). Wave headings $\theta=0^\circ$ and $\theta=180^\circ$.

In general, significant hydrodynamic coupling effects were observed. These effects are evident in low frequency QTF of TAD. Horizontal and vertical loads present substantial variations in the presence of TLP.

Hydrodynamic coupling effects on TLP were evident on low frequency QTF of TLP. Although, the variations were slightly lower than the case of TAD. These are relevant. On the other hand, the high frequency QTFs on vertical modes of TLP present minor variations due to the presence of TAD.

The Newman approximation appears to have poor “global” agreement. However, when the predictions of the Newman approximation were compared with Full-QTF in a difference frequency equal to the natural frequency three situations were found. First, horizontal modes of TLP and TAD present good “local” agreement. Then, forces on Heave of TAD were overestimated. Finally, moments on pitch of TAD were underestimated.

In general, it is possible to conclude that Newman approximation presents adequate predictions in modes with natural frequencies less than 0.005 Hz.

References

1. Roald, L.; Jonkman, J.; Robertson, A.; Chokani, N.; 2013, The Effect of Second-Order Hydrodynamics on Floating Offshore Wind Turbines. DeepWind, Trondheim, Norway.
2. Cao, P.; Zhang, J.; 1997, Slow Motion Responses of Compliant Offshore Structures. International Journal of Offshore and Polar Engineering. Vol.7.
3. Mavrakos, S.; Chatjigeorgiou, I.; 2008, Second-Order Hydrodynamic Effects on an Arrangement of Two Concentric Truncated Vertical Cylinders. Marine Structures Vol 22.
4. Hauteclouque, G.; Rezende, F.; Waals, O.; Chen, X.; 2012, Review of Approximations to Evaluate Second-Order Low-Frequency Load, OMAE, Rio de Janeiro, Brazil.
5. Molin, B.; 1979, Second-Order Diffraction Loads Upon Three-Dimensional Bodies. Applied Ocean Research.
6. Pinkster, J.; 1980, Low Frequency Second Order Wave Exciting Forces on Floating Structure. Ph.D. Thesis.
7. Maruo, H.; 1960, The drift of a body floating on waves. Journal of Ship Research.
8. Chen, X.; 2006, Middle-field Formulation for the Computation of Wave-Drift Loads. Journal of Engineering Mathematics.
9. Rezende, F.; Chen, X.; Oliveira, A.; Menezes, F.; 2013, A Comparison of Different Approximations for Computation of Second Order Roll Motions for a FLNG, OMAE. Nantes, France.
10. Monroy, C.; Hauteclouque, G.; Chen, X.; 2013, A Practical $O(\Delta\omega)$ Approximation of Low Frequency Wave Loads. OMAE, Nantes, France.
11. Newman N.; 2005, Second-Order Diffraction in Short Waves. Journal of Ship Research.
12. Kim, Y.; Kring, D.; Sclavounos, P.; 1997, Linear and Nonlinear Interactions of Surface Waves with Bodies by a Three-Dimensional Rankine Panel Method, Applied Ocean Research.
13. Newman, N.; 1974, Second Order Slowly Varying Forces on Vessel in Irregular Waves.
14. Molin, B.; Chen, X.; 2002, Approximations of the Low-Frequency Second-Order Wave Loads. Proc. 17th IWWWFB, Cambridge, UK
15. MIT; 2008. Wamit User Manual. MIT, Massachusetts, USA.

Acknowledgments

This work is a joint effort between Wave Current Laboratory LOC – COPPE/UFRJ and Keppel Offshore & Marine Technology Centre (KOMtech).

Author's Contact

- | miguel.ramirez@kfelsbrasil.com.br
- | acfernandes@oceanica.ufrj.br

Comparing the Performance Standards of a Tension Leg Platform and Tender Assisted Drilling between Linear Frequency Domain versus Non-Linear Time Domain Methods

| Miguel Angel Moya RAMIREZ[†], Ms.C.

| Antonio Carlos FERNANDES^{*}, Ph.D.

[†] BrasFELS

^{*} LOC-COPPE/UFRJ

Tender assisted drilling (TAD) has been revealed as an efficient and effective solution in deep water installations to support drilling operations of tendon leg platforms (TLP). Although this concept is new in offshore Brazil, this has been used for more than 30 years not only in Southeast Asia but also in the Gulf of Mexico, West Africa, and the North Sea. Due to the complex scenario of two floaters moored in close proximity, an extensive and careful hydrodynamic analysis is required to guarantee a successful execution.

This work presents a numerical study of wave coupling effects on the TLP-TAD multi-body system, with the aim of investigating first-order loads, mean drift loads and wave frequency responses using frequency and time domain approaches. Hydrodynamic coefficients were calculated by the 3D diffraction-radiation panel method, the mooring systems and the mechanical connections between the floaters were modeled through stiffness matrixes. In frequency domain analysis, several relative positions between the floaters were considered. On the other hand, in time domain studies, the Finite Element Method (FEM) was used to represent moored systems and mechanical connections between the floaters. FEM allows the inclusion of drag forces, added mass and interactions between mooring lines and floaters into the non-linear dynamic simulations.

Introduction

Tender Assisted Drilling (TAD) has been used extensively for more than 30 years in very different places around the world with benign and moderate environmental conditions. Originally, TADs were barges operating with a fixed platform [1]. In 1992, the Seahawk semi-submersible was converted from mobile offshore drilling unit (MODU) to TAD, the first in the world.

Tension Leg Platform (TLP) is probably the candidate that can benefit most from the TAD concept since it is more sensitive to topside weight [3]. Additionally, small vertical motions of TLP make the connection easier with the TAD. Finally, the probability of interference between TAD mooring lines and TLP tendons is very low [4].

The advantages that TAD has versus a traditional production platform with fully functional drilling unit are described in ([1], [2], [3], [4], [5] and [6]) and summarised below.

- Decreases space requirements on production platform deck.
- Provides additional accommodation for the crew.
- Increases the storage capacity for equipment and material operations.
- Improves safety, the crew can be transferred to TAD in a risky situation.
- TADs are very versatile and same unit can be used in different projects.

Study Case

This study considers a Tension Leg Platform (TLP) with a Tender Assisted Drilling (TAD) moored in close proximity. The TLP hull consists of four rectangular pontoons in close configuration and four square columns as shown in Figure 02. The TAD hull is composed by two rectangular pontoons connected by three circular beams and six columns as illustrated in Figure 03.

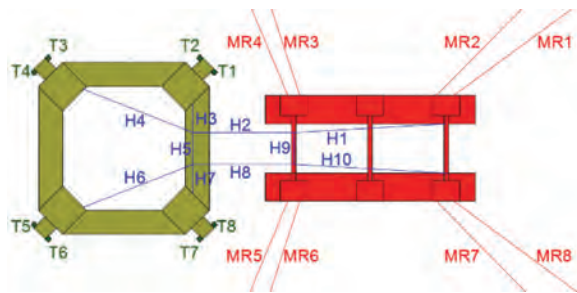


Figure 1 TLP+TAD multi-body system connected by hawser lines (H1 and H2).

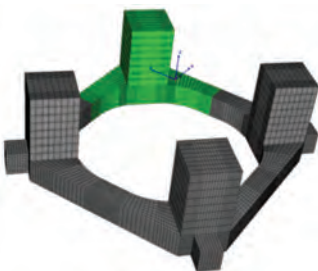


Figure 2 Low order panel method discretisation of TLP Hull.

The TLP is moored with eight tendons composed by circular pipes. Each tendon is 1155m long and has been installed with a pretension of 1232 mT. The TAD is moored by a semi-taut-leg system composed of eight lines with segments of chain and polyester ropes.

Several relative distances between the two floaters were considered in the frequency domain analysis. On the other hand, for time domain simulations, the initial position of the floaters considered into the analysis was the case (H) of Figure 08.

Finally, the mechanical connection between the platforms was performed by a hawser system to restrain the relative surge, sway and yaw motions between the platforms. This system is composed of two lines of nonlinear polyester ropes. Figure 01 presents a schematic representation of the hawser system.

Computational Grids

The hydrodynamic coefficients (added mass, potential damping, diffraction loads and mean drift loads) were calculated with the 3D diffraction-radiation code WAMIT. For that, a discretisation of the surfaces of the bodies is required.

As mentioned in [7] the geometry of the bodies can be represented by two methods: the low-order and the higher-order. The first represents the body surface with flat quadrilateral panels, and hydrodynamic properties are considered constant on each panel. On the other hand, the higher-order represents the geometry of the body by b-spline surfaces, and hydrodynamic properties are modeled in a continuous manner on each surface.

Thus, the accuracy of the low order and the higher-order methods depends on the number of panels and the polynomial degree of the b-splines, respectively. Further information can be found in [7,8,9]

Figures 02 and 03 present the grids of TLP and TAD, respectively. Note that, in the numerical calculation the low-order and the higher-order panel methods were used. However, only low order grids were shown.

In the calculation of mean drift loads, three methods were available: First, the far field method [10], which is derived by applying the momentum theorem to the fluid domain. Despite being very efficient and with very good convergence, it is restricted to three degrees of freedom (Surge, Sway, and Yaw), and cannot be used to estimate the forces on an individual body when it is part of a multi-

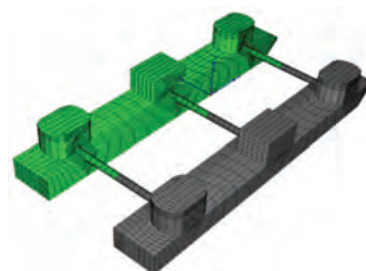


Figure 3 Low order panel method discretisation of TAD Hull.

body system ^[11]. Second, the near-field method ^[12], based on the direct pressure integration on the body surface, this approach provides the mean drift loads in six degrees of freedom and can be used for single body or multi-body case. Finally, the middle field method ^[11], which is based on the application of the Gauss theorem in limited domains by the control surface.

Per ^[11], the use of control surfaces on the estimation of mean drift loads increases the accuracy of the results considerably, especially when bodies have sharp corners. Thus, the middle-field method was used in our calculations. Figures 04 and 05 present the control surfaces used for the TLP and TAD, respectively.

Grid Sensitivity Analysis

In order to verify the influence of the grid parameters on the hydrodynamic coefficients, a sensitivity analysis has been performed. This analysis includes six grids divided into two groups: low-order grids and higher-order grids. In addition to that, three levels of refinement were considered in each group: coarse, medium and fine. Tables 01 and 02 present the refinement characteristics of the grids. The parameter considered in this analysis was the Response Amplitude Operator (RAO). The range of periods considered was from 2 to 40 sec. and wave headings from zero to 180 degrees by steps of 15 degrees. Note that, stiffness matrixes from mooring systems mentioned in Section 6 and viscous damping coefficients of Table 03 were incorporated into WAMIT runs.

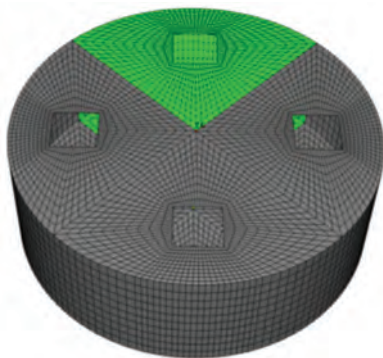


Figure 4 Control surfaces of the middle field method for TLP Hull.

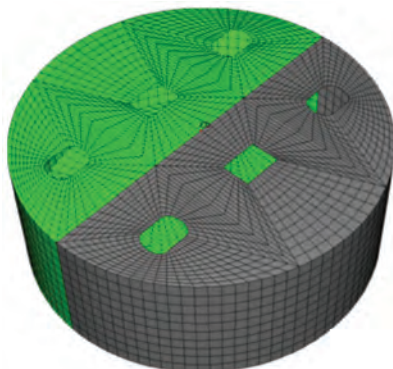


Figure 5 Control surfaces of the middle field method for TAD Hull.

Table 1 Number of panels for TLP and TAD grids (low-order method)

Code	Refinement	TLP	TAD
LO1	Coarse	768	1712
LO2	Medium	1728	2675
LO3	Fine	3072	3924

Table 2 Maximum panel size discretisation for TLP and TAD grids (higher-order method)

Code	Refinement	TLP	TAD
HO1	Coarse	20	20
HO2	Medium	10	10
HO3	Fine	5	5

Table 3 Percental damping ratios of TLP and TAD

Mode	TLP	TAD
Surge	5	5
Sway	5	5
Heave	3	7
Roll	3	7
Pitch	3	7
Yaw	5	5

Numerical Model for Time Domain Simulations

A fully nonlinear numerical model was built to study the system with static and time domain simulations. Three cases were considered: TLP Alone, TAD Alone and TLP connected with TAD as shown in Figure 06. These models were built in Orcaflex software ^[13]. This program is a 3D nonlinear time domain solver which uses Finite Element Method (FEM) to model chains, rope lines, pipes and a wide variety of moored systems.

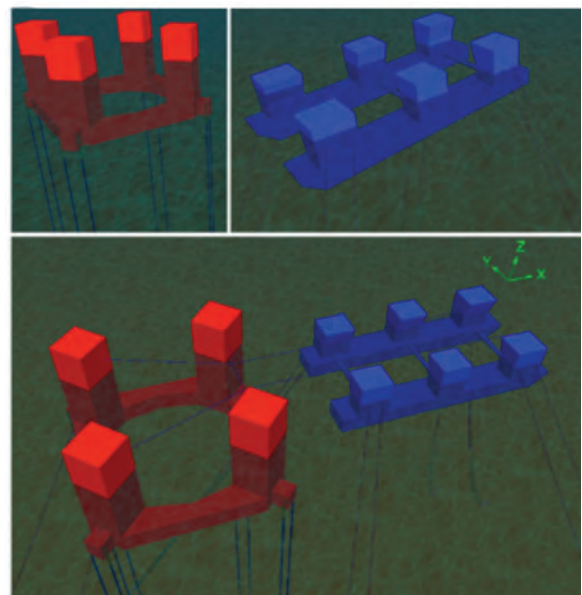


Figure 6 Numerical models of TLP Alone, TAD Alone and TLP+TAD used in Orcaflex.

In addition to the physical properties, hydrostatic data and hydrodynamic coefficients of the floaters, it is required the mechanical properties of lines (tendons, taut-leg lines, and hawsers), which can be nonlinear, to perform the simulations.

Static simulations were carried out to calculate the stiffness matrixes of the floaters. Thus, by applying a known load to the system, the displacement in six degrees of freedom is reported.

Moreover, numerical decay tests were conducted to estimate natural periods. These tests were performed given an initial displacement to the floater and then release them to move freely.

Finally, the three cases were analysed using regular waves. Note that, for each wave period, two wave amplitudes were analysed.

Table 4 Stiffness Matrix of TLP Alone (Length in meters, Force in kN and Angle in Radians)

Modes	Surge	Sway	Heave	Roll	Pitch	Yaw
Surge	79	0	0	0	-1881	0
Sway	0	79	0	1881	0	0
Heave	0	0	120056	0	0	0
Roll	0	1881	0	165131634	0	0
Pitch	-1881	0	0	0	165131634	0
Yaw	0	0	0	0	0	214368

Table 5 Stiffness Matrix of TAD Alone (Length in meters, Force in kN and Angle in Radians)

Modes	Surge	Sway	Heave	Roll	Pitch	Yaw
Surge	18	0	14	0	976	0
Sway	0	32	0	-1084	0	-452
Heave	14	0	106	0	2429	0
Roll	0	-1081	0	187783	0	-55164
Pitch	980	0	2429	0	254768	0
Yaw	0	-449	0	15077	0	252539

Table 6 Coupled Stiffness Matrix of TLP and TAD. (Length in meters, Force in kN and Angle in Radians)

		TLP						TAD					
Modes		Surge	Sway	Heave	Roll	Pitch	Yaw	Surge	Sway	Heave	Roll	Pitch	Yaw
TLP	Surge	108	0	-370	0	-1625	0	-94	0	2	0	2745	0
	Sway	0	96	0	1647	0	622	0	-31	0	296	0	656
	Heave	-370	0	120102	0	6873	0	2	0	-38	0	-1290	0
	Roll	0	1646	0	165156387	0	460738	0	293	0	-4036	0	-9308
	Pitch	-1625	0	6873	0	165279702	0	2808	0	1183	0	10579	0
	Yaw	0	622	0	460293	0	405718	0	-588	0	8188	0	6380
TAD	Surge	-93	0	1	0	-1245	0	97	0	-1	0	1510	0
	Sway	0	-31	0	249	0	-887	0	57	0	-1340	0	-1322
	Heave	1	0	-38	0	1181	0	-1	0	148	0	3196	0
	Roll	0	252	0	-4021	0	7577	0	-1340	0	186382	0	40915
	Pitch	-1217	0	-1288	0	9913	0	1510	0	3196	0	366694	0
	Yaw	0	992	0	-8620	0	6453	0	-1322	0	41418	0	372138

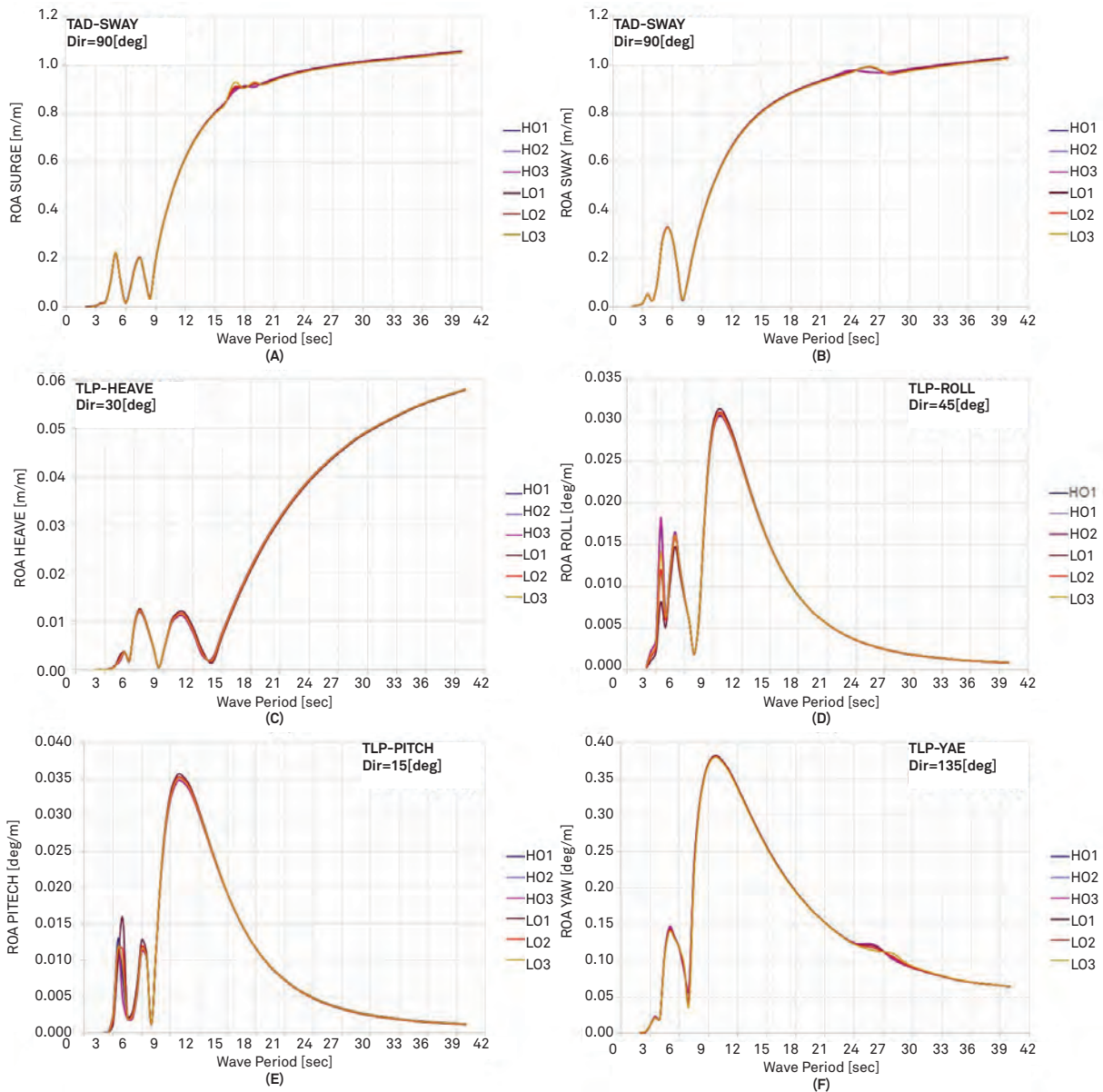


Figure 7 Grid Sensitivity Analysis for RAO of TLP and TAD.

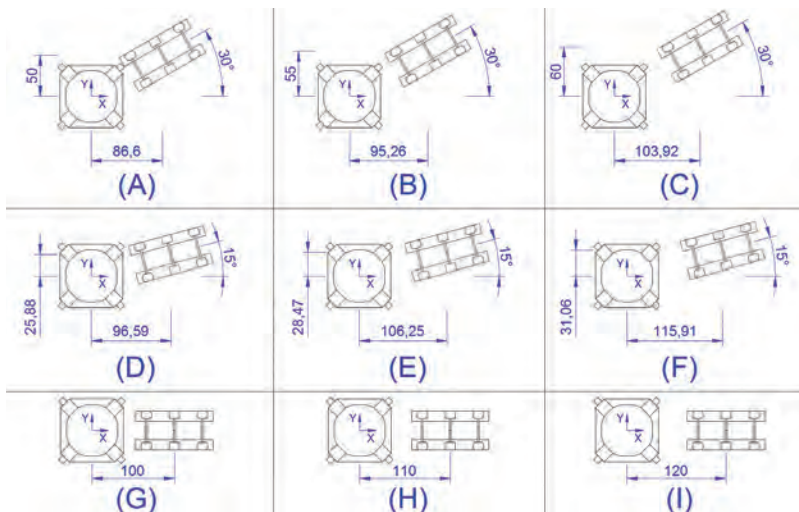


Figure 8 Relative position between the TLP and TAD for multi-body analysis (Dimensions in meters).

In order to have a better comparison of hydrodynamic interactions, results for nine multi-body cases and a single-body case were depicted together. Note that, only selected results were presented.

It is interesting to observe that the results, of both floaters, present slight differences between multi-body and the single body case.

Multi-body cases present small fluctuations for linear wave diffraction loads in low periods. However, these fluctuations were slight, and if the period increased, the fluctuations reduced until disappearing.

Response Amplitude Operators (RAOs) showed very weak coupling effects, as in the case of diffraction forces, only small differences for low periods were observed.

Finally, the spreading of the results of mean drift loads was considerably higher for low periods. For instance, yaw of TAD and yaw of TLP. However, some other modes presented minor differences. For example, heave of TLP and heave of TAD.

The fluctuations of the results of multi-body cases about the single-body case for low periods can be attributed to locally resonant waves in the confined fluid domain between the floaters^[14].

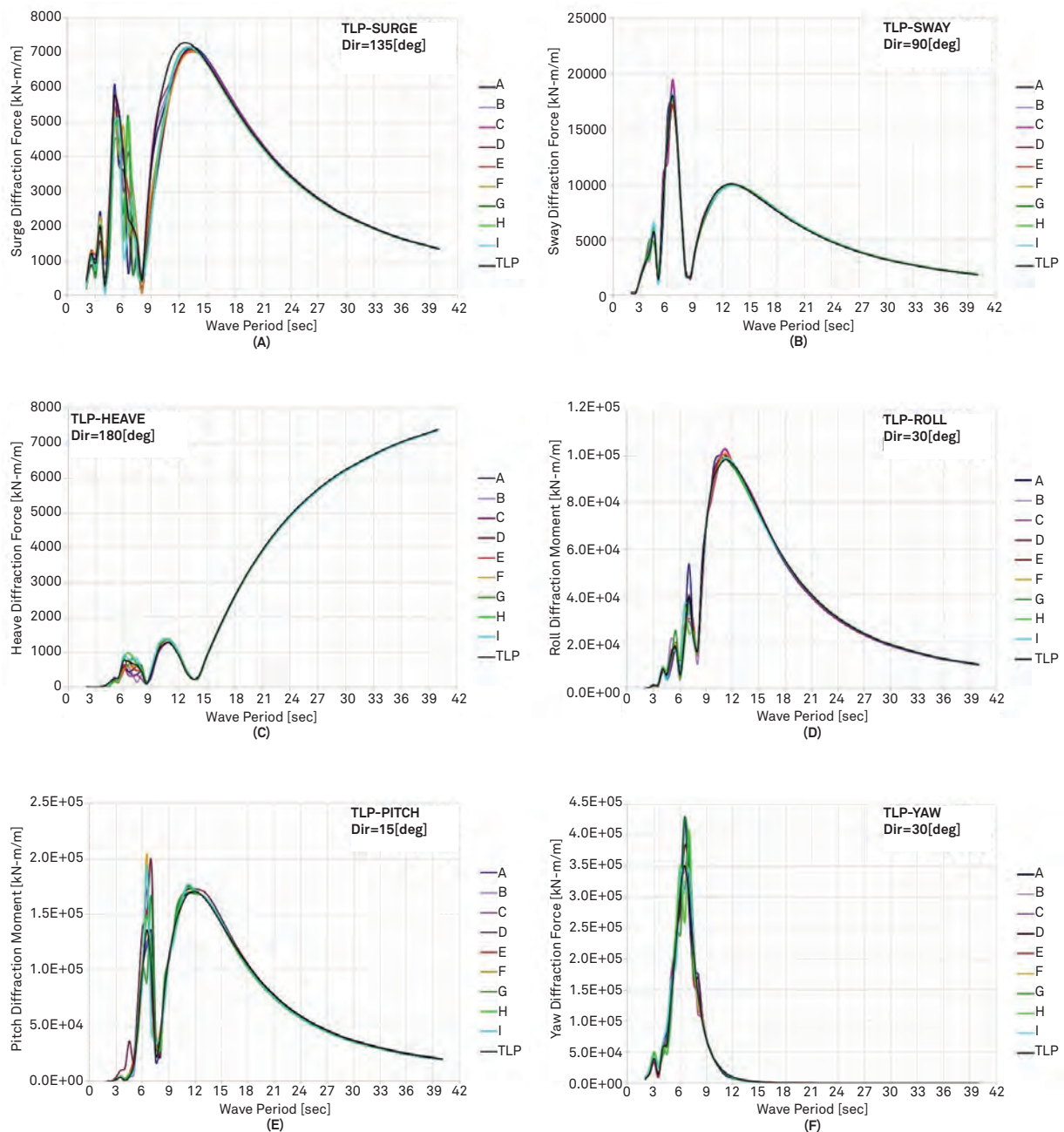


Figure 9 Diffraction forces and moments on TLP for single-body and multi-body case.

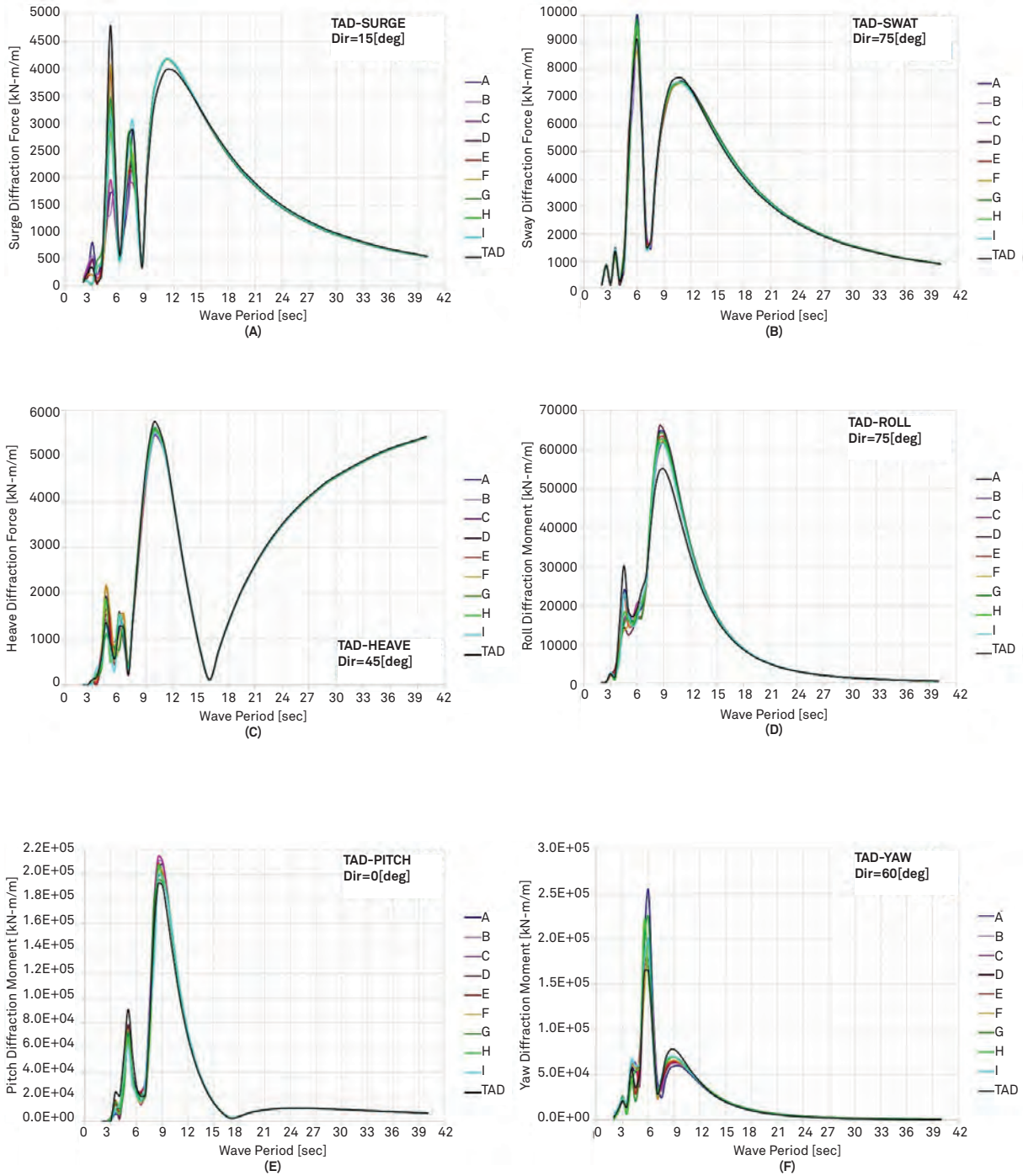


Figure 10 Diffraction forces and moments on TAD for single-body and multi-body case.

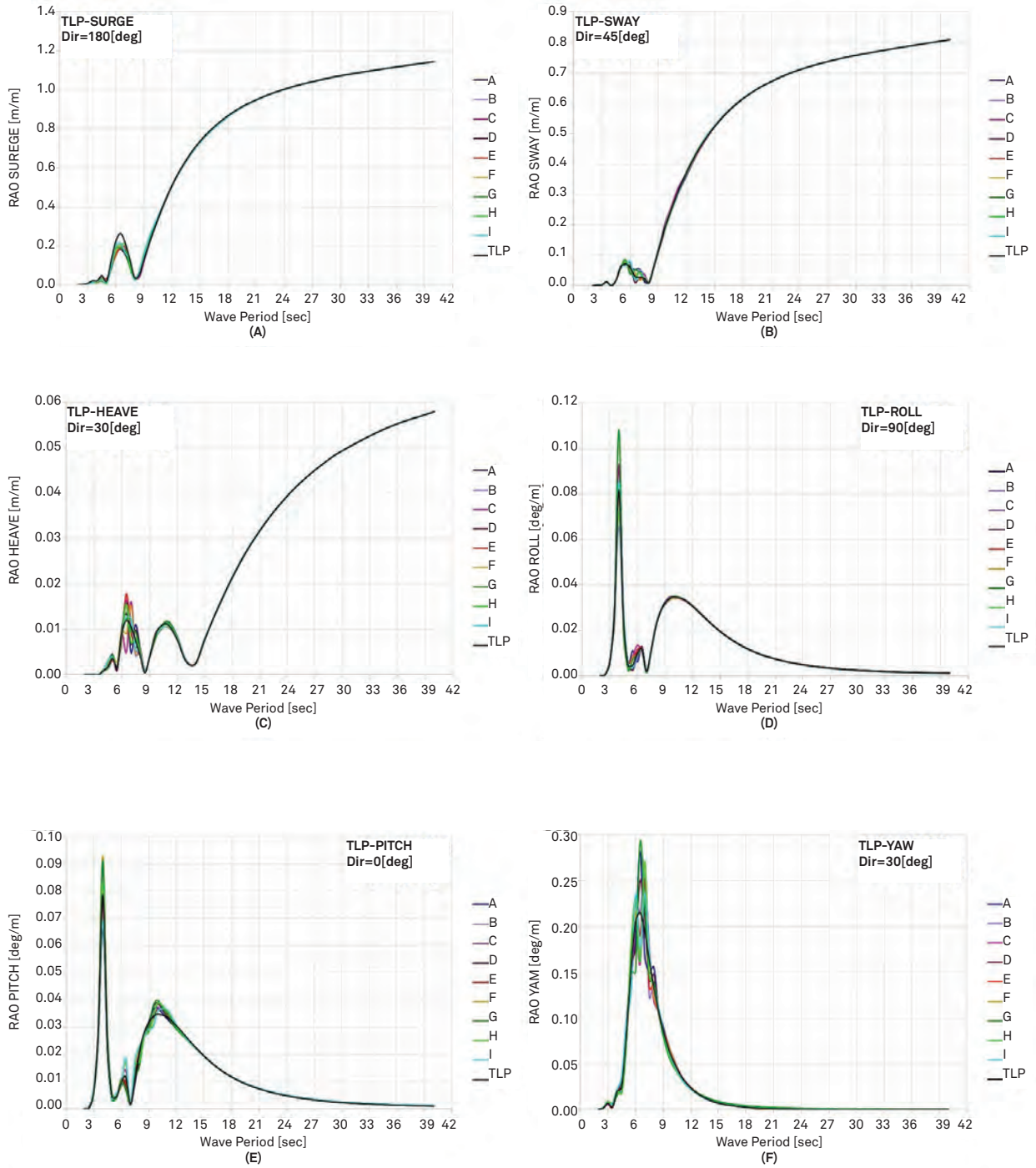


Figure 11 Response Amplitude Operator (RAO) of TLP for single-body and multi-body case.

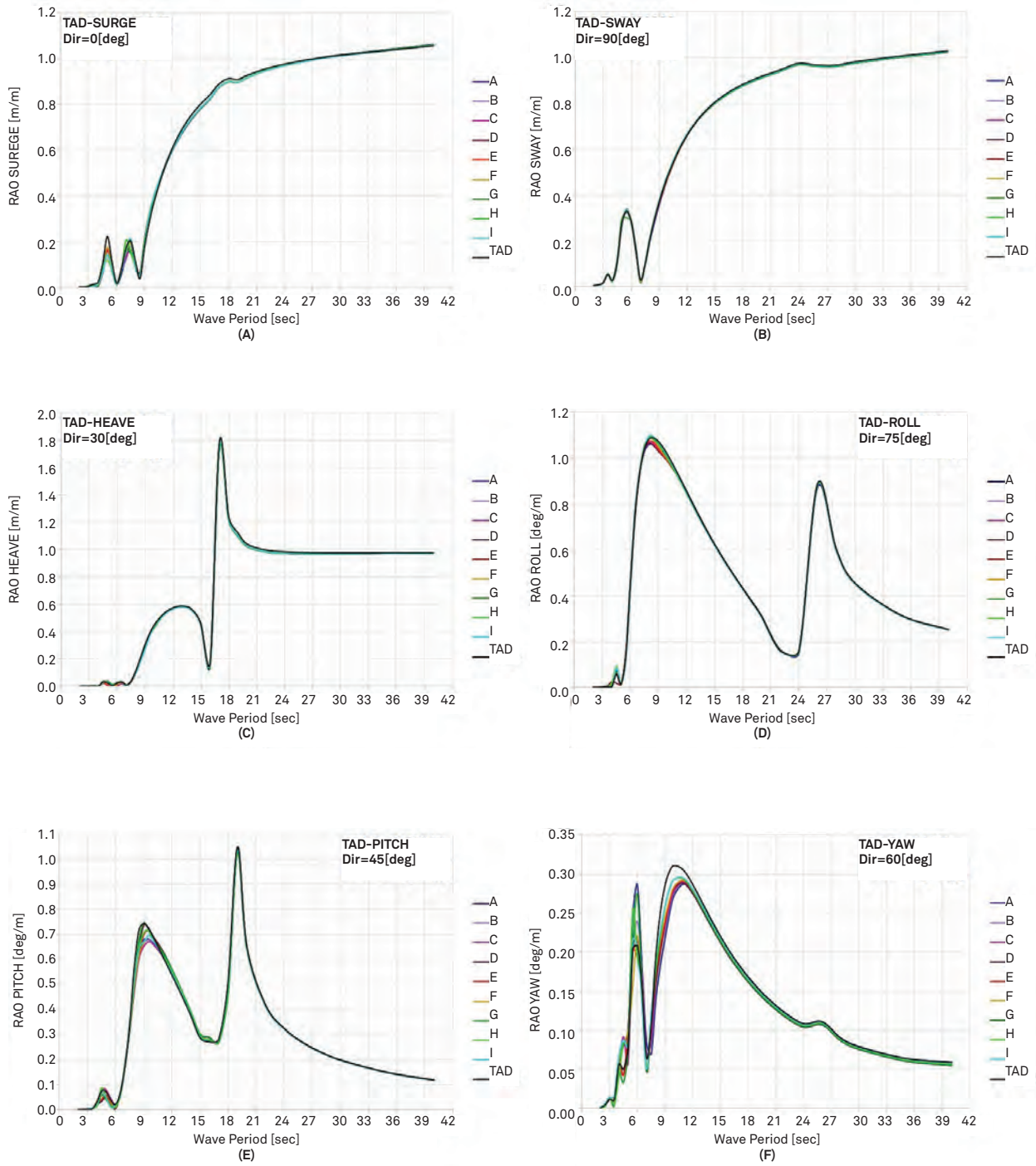


Figure 12 Response Amplitude Operator (RAO) of TAD for single-body and multi-body case.

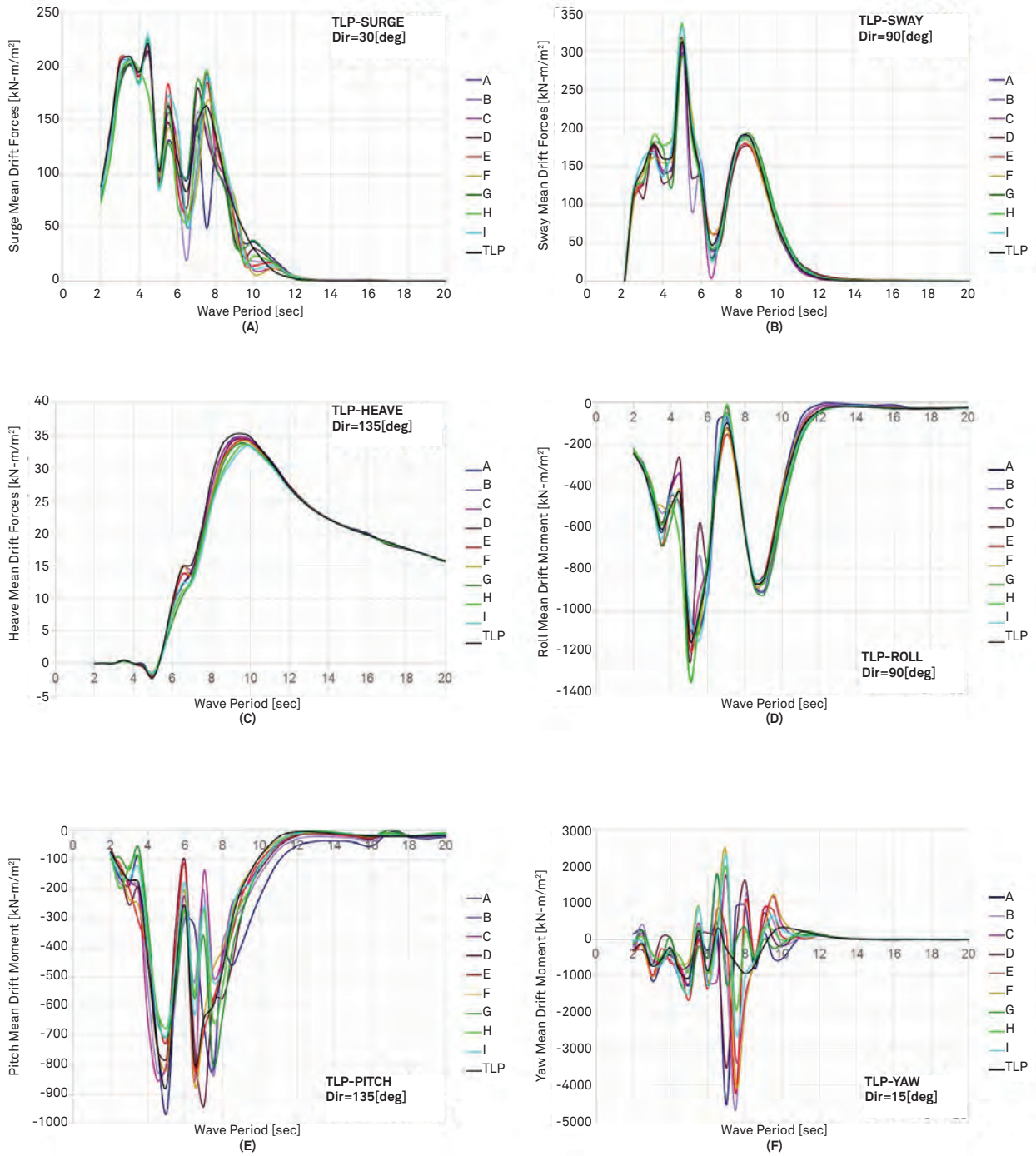


Figure 13 Mean Drift Forces and Moments on TLP for single-body and multi-body case.

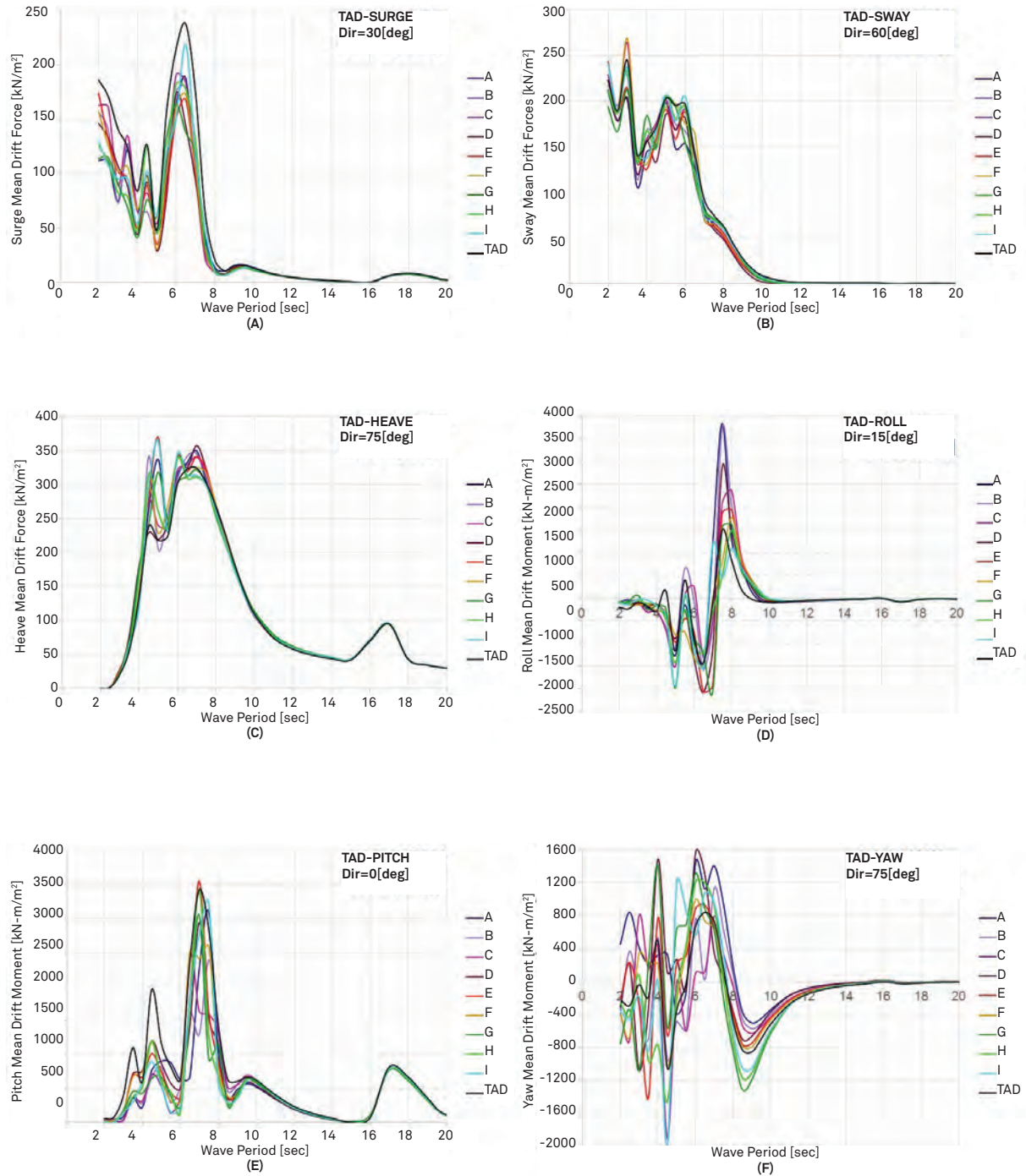


Figure 14 Mean Drift Forces and Moments on TAD for single-body and multi-body case.

Frequency domain analysis reveals that the hydrodynamic coupling effects on the TLP-TAD multi-body system are very weak.

On the other hand, Time domain simulations have proven that RAOs present nonlinear behaviour due to the nonlinear properties of mooring lines.

In general, frequency domain predictions were the most conservative.

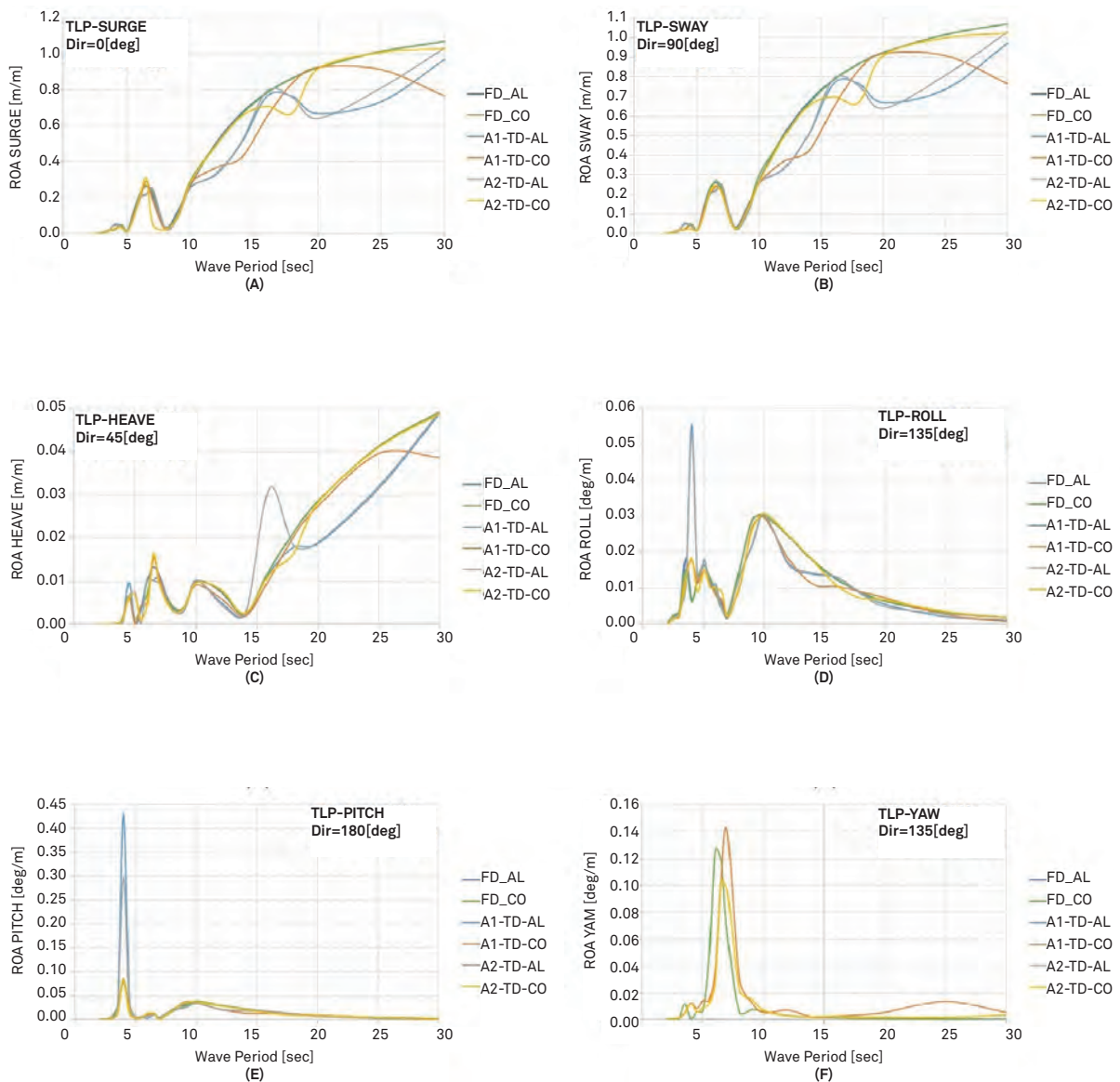


Figure 15 RAO of TLP for single and multi-body case using frequency and time domain.

Wave Coupling Effects in Time Domain

As mentioned in previous sections, the three cases (TLP Alone, TAD Alone and TLP+TAD) were analysed with time domain simulations using regular waves. Table 08 presents the wave periods and the wave amplitudes considered in the analysis. Note that, to investigate possible nonlinear effects, two wave amplitudes were taken into account for each wave period. The wave heading considered in the study were from zero to 180 by steps of 45 degrees.

Hydrodynamic coefficients were calculated for the free-floating condition. For the multi-body case, the case H of Figure 08 was considered. As in frequency domain analysis, the damping ratios presented in Table 03 were included in the time domain simulations.

Figure 15 presents a comparison of response amplitude operator (RAOs) of TLP in the following cases:

- TLP alone in frequency domain (FD1)
- TLP coupled with TAD in frequency domain (FD2)
- TLP alone in time domain with wave height H1 (TD1)
- TLP coupled with TAD in time domain with wave height H2 (TD2)
- TLP alone in time domain with wave height H2 (TD3)
- TLP coupled with TAD in time domain with wave height H2 (TD4)

Figure 16 presents a comparison of response amplitude operator (RAOs) of TAD in the following cases:

- TAD alone in frequency domain (FD1)
- TAD coupled with TLP in frequency domain (FD2)
- TAD alone in time domain with wave height H1 (TD1)
- TAD coupled with TLP in time domain with wave height H1 (TD2)
- TAD alone in time domain with wave height H2 (TD3)
- TAD coupled with TLP in time domain with wave height H2 (TD4)

Figures 15 and 16 reveal that wave amplitude has a significant influence on the response of floaters, consequently, RAOs present nonlinear behavior. In addition to that, the highest responses amplitude does not correspond to the maximum wave amplitude. In some cases, the maximum response amplitude corresponds to the lowest wave amplitude.

The comparison between single body case and multi-body cases reveals significant hydrodynamic coupling effects for long wave periods. While in low wave periods no significant differences were found.

Major differences were observed when results from the time domain and the frequency domain approaches were compared. These are clear evidence that nonlinear effects of mooring lines have a strong influence on the dynamic behaviour of the floaters.

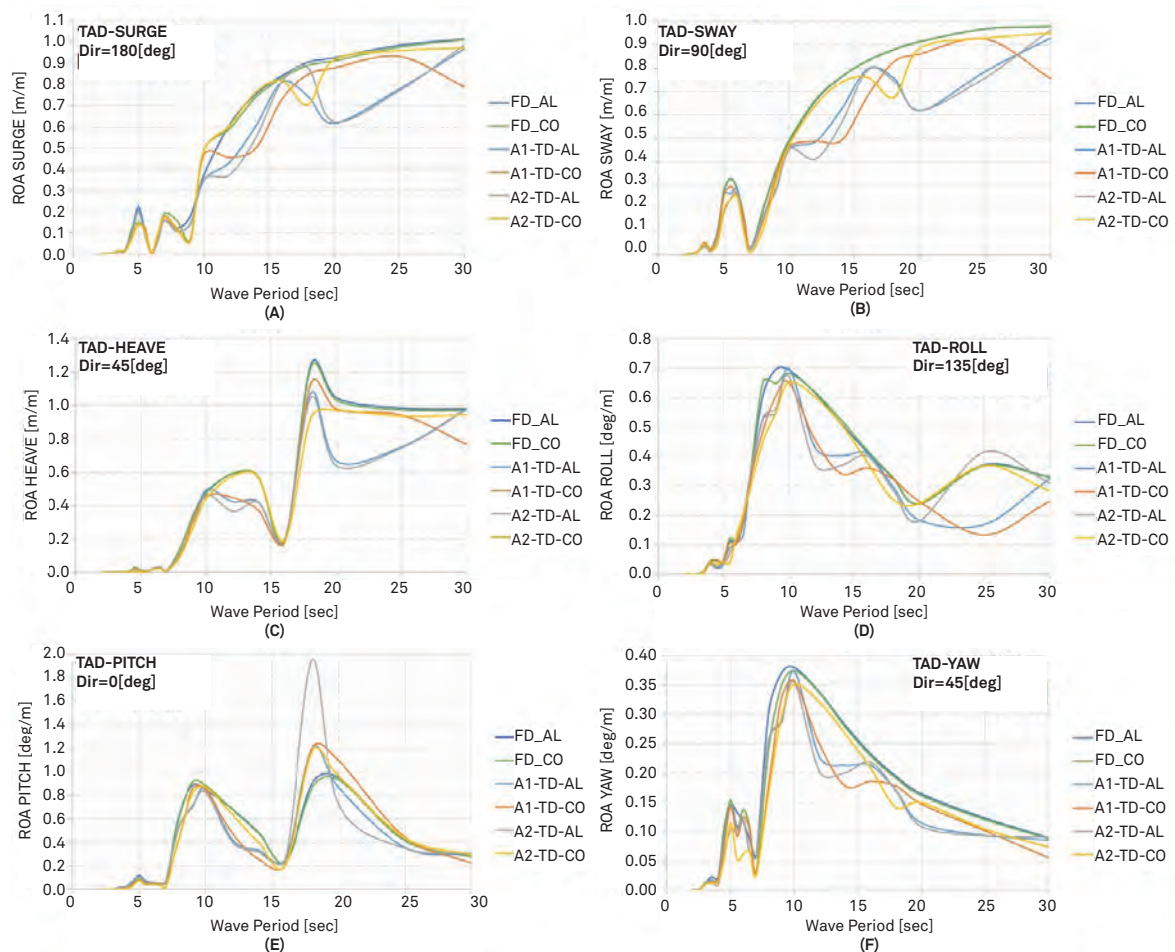


Figure 16 RAO of TAD for single and multi-body case using frequency and time domain.

Time domain simulations have shown that nonlinear properties of mooring lines and wave amplitude are very relevant to the dynamic behavior of the TLP-TAD multi-body system.

Although that frequency domain predictions were the most conservative, this work has shown that time domain approach includes the nonlinear effects in an accurate way.

Conclusions

Based on this extensive study of the TLP-TAD multi-body system, the following conclusions were achieved:

- The calculations of hydrodynamic coefficients using the low-order and the higher-order methods give very similar results. Hence, both methods have shown to be adequate to analyse this multi-body system.
- The influence of grid refinement on the hydrodynamic coefficients was very weak. Results have been shown independent of panel method discretisation.
- Frequency domain analysis reveals that the hydrodynamic coupling effects on the TLP-TAD multi-body system are very weak. Diffraction forces and RAOs present slight differences between single and multi-body cases. On the other hand, mean drift loads present moderate coupling effects.
- Time domain simulations have proven that nonlinear properties of mooring lines have a strong influence on the dynamic behaviour of the floaters. Major differences were found in comparison with frequency domain predictions, where these properties are linearised or neglected.
- The time domain simulations have also shown significant differences in the system response when it was excited with different wave amplitudes. Consequently, RAOs are not linear and must be used carefully.
- The influence of the hawser system on the horizontal modes of TLP and TAD has been confirmed. The hawser system dramatically modifies stiffness values and natural periods of Surge, Sway, and Yaw of TLP and TAD. On the other hand, vertical modes (Heave, Roll, and Pitch) presented no significant variations.
- In general, frequency domain predictions were the most conservative. However, significant differences were found when compared to time domain simulation. Therefore, frequency domain approach should be used carefully in initial stages of the design of the system. Finally, in order to represent the nonlinear behaviour of moored lines and hawser system, time domain simulations must be performed.

References

- [1] Chaudhuri, J.; 1993, Design of Semi-Submersible Tender Assisted Drilling and Workover Systems for Harsh Weather Applications. International Offshore and Polar Engineering Conference, Singapore.
- [2] Botker, S.; Karp, T.; Johannessen, T.; Chew, M.; 2001, Wellhead TLP with Tender Assisted Drilling. OTC 12988, Houston, TX, USA.

- [3] Xia, J.; Taghipour R.; 2012. Feasibility of TLP with Tender Assisted Drilling for Northwest Australian Water – A Case Study. OTC 23247, Houston, TX, USA.
- [4] Stone, B.; Treu, H.; Wybro, P.; Wu, C.; 2005. Tender Assisted Drilling on Deepwater Floating Production System. SNAME Transaction, Vol 113, pp. 418 - 427.
- [5] Mathiesen, R.; 1989. Tender Assisted Drilling – NPD Experience. SPE-19248-MS, Offshore Europe, Aberdeen, UK.
- [6] Christiansen, P.; Cuvillier, G.; Hicks, N.; 1994. Tender Assisted Drilling in the North Sea. OTC7458, Houston, TX, USA.
- [7] MIT; 2008. Wamit User Manual. MIT, Massachusetts, USA.
- [8] Newman, J. N.; Lee, C.-H.; 1992. Sensitivity of the Wave Loads to the Discretization of Bodies. Proceedings of Int'l Conf. on Behavior of Offshore Structures, London, England.
- [9] Newman, J. N.; Lee, C.-H.; Maniar, H.; Zhu, X.; 1996. Computation of Wave Loads using a B-spline Panel Method. Proceedings 21st Symposium on Naval Hydrodynamics, Trondheim, Norway.
- [10] Newman, J.; Lee, C.; 1967. The Drift Force and Moment on Ships in Waves. Journal of Ship Research Vol. 11. pp. 51 – 60.
- [11] Chen, X.; 2007. Middle-Field Formulation for the Computation of Wave Drift Loads. Journal Engineering Math. Vol. 59, pp. 61-82.
- [12] Pinkster, J.A.; Van Oortmerseen, M.; 1997. Computation of the first and second order wave forces on oscillating bodies in regular waves. Proc. 2nd Int. Conf. Num. Ship Hydrodynamics, Berkeley, pp. 136-156.
- [13] Orcina; 2005. Orcaflex Manual Version 10.0a. Cumbria, UK.
- [14] Choi, Y.R.; Hong, S.Y.; 2002. An analysis of Hydrodynamic Interaction of Floating Multi-Body Using Higher-Order Boundary Element Method. Proc. 12th Int. Offshore and Polar Engineering Conference, Kitakyushu, Japan.

Acknowledgments

This work is a joint effort between Wave Current Laboratory LOC – COPPE/UFRJ and Keppel Offshore & Marine Technology Centre (KOMtech).

Author's Contact

- | miguel.ramirez@kfelsbrasil.com.br
- | acfernandes@oceanica.ufrj.br

Computational Fluid Dynamics Study on Drillship Moonpool Added Resistance

| MA Peifeng*, PhD, M.Eng., B.Eng

| Ankit CHOUHARY*, M.Sc., B.Eng

| Deguang YAN#, PhD, M.Eng., B.Eng

| Hai GU#, PhD, M.Eng., B.Eng

| XU Haihua*, PhD, M.Eng., B.Eng

| Anis HUSSAIN*, M.Sc., B.Eng

| Hung-Pin CHIEN#, PhD, M.Eng., B.Eng

*Keppel Offshore & Marine Technology Centre

#ABS

Presented at the Offshore Technology Conference, 2-5 May 2016, Houston, Texas, USA.

While in transit, violent water motion can be generated inside a drillship moonpool, leading to added resistance which may contribute more than 50% of the total resistance and consequently increase the fuel consumption for propulsion. Unlike conventional ships that experience nearly constant resistance at a transit speed, a drillship presents a resistance with large fluctuation due to the water motion inside the moonpool. Although it is well known the large moonpool induced added resistance is mainly attributed to the vortices shedding from the moonpool front wall that enter into the moonpool and impinge on the rear wall, the physical mechanism of the vortex generation and its interaction with the moonpool are still not fully understood. This study aims at investigating the mechanism of vortex generation in a drillship moonpool using Computational Fluid Dynamics (CFD) simulations. Based on the identified mechanism, the design principles for the moonpool dimension selection and the vortex induced impinging load reduction are established as guidelines for future drillship designs.

Introduction

Water motion in a drillship moonpool could be violent in transit and significantly increase drillship resistance due to the water oscillation inside the moonpool. Such water oscillations are initiated by vortices shedding from the upstream submerged moonpool front wall. The vortices are related to the separation of a shear layer so viscous effects dominate the initiation of the oscillation. The oscillation has a dominant frequency and the amplitude increases with forward speed. The resonance oscillation mode can be piston or sloshing (Fukuda, 1977; Molin, 2001). Both types of oscillation can increase ship resistance to the same order of magnitude. Generally, the sloshing mode dominates in longer moonpools and piston mode is dominant in shorter ones.

The moonpool dimensions are an important design parameter from operational point of view. As summarised by Veer et al. (2008), the typical dimensions of existing drillships are about 7–25m in length and 8–15m in breadth. Besides, the design speed is in the range of 10 to 12knots. Theoretically, the moonpool geometry determines the piston and sloshing resonant frequency and the transit speed determines the oscillation amplitude. The natural frequency of the piston mode of a moonpool can be predicted based on formulation reported by Fukuda (1977) and Molin (2001), while natural frequency of the sloshing mode can be predicted based on formulation reported by Newman (1977), Fukuda (1977) and Molin (2001). According to the formulations which are mostly proposed by assuming a rectangular moonpool shape, the natural frequency is dependent on the moonpool geometry ratio such as the length breadth ratio and the draft breadth ratio. The estimated natural period from these formulae is about 6–8 sec and 4–6 sec for piston mode and sloshing mode, respectively.

Although the moonpool natural frequency can be estimated reliably, it still remains challenging for moonpool design in accurately predicting the moonpool added resistance and water motion resonance. The scaled model tests combined with experiences are still the reliable approach for resistance prediction in an early design phase. This approach can provide accurate resistance predictions for conventional ship hulls, but it becomes uncertain for a drillship with moonpool. In order to predict a drillship resistance in the early design stage, a reliable numerical method can be a feasible alternative. Highly efficient numerical prediction methods for resistance and water motion resonance prediction are of great interest to moonpool designers.

In order to study the strong viscous effects in the moonpool, CFD will be conducted to capture all viscous effects in turbulence flows. CFD has been proved and widely used in predicting resistance and propulsion of conventional ships (e.g. Enger et al. 2010; Larsson et al. 2013). It has also been used to study the moonpool effects on a drillship (e.g. Son et al. 2008, Hammargren and Tornblom, 2012; Wang and Quah, 2013).

The objective of this study is to investigate the impact of moonpool on drillship resistance and the mechanism of moonpool induced resistance through model test data analysis and CFD simulations. Another objective is to develop a CFD best practice based on the validation study and a guideline for drillship moonpool design.

CFD Validation and Parametric Study CFD Model Setup

In the present study, the commercial CFD software STAR-CCM+ (CD-adapco, 2016) is used to carry out all simulations, which integrates the mesh generation, simulations and post-processing into one package. The software solves the Reynolds Averaged Navier-Stokes (RANS) and continuity equations in integral form by means of the finite volume method. For temporal discretisation, the 2nd order Euler implicit scheme is employed to compute unsteady flow. In space, a second order schemes for both convective and viscous terms are applied. The pressure and the velocities are coupled by means of the SIMPLE method. Details on discretisation and solution methods can be found in literature (e.g. Ferziger and Perić, 2003; Weiss et al, 1999). The free surface is modelled with the volume of fluid (VOF) approach. In this approach, the solution domain is assumed to be filled by a single effective fluid whose properties vary locally according to volume fraction of liquid, with which the deformation of the interface between liquid and other phases of fluids can be tracked.

Computational Domain and Meshing

Half of ship geometry is considered in the present CFD computations due to the symmetry. To avoid boundary reflections, the computational domain as shown in Fig. 1 which is 5.5Lpp in the longitudinal direction, 2.1Lpp in the lateral direction and 2.8Lpp in the vertical direction. The ship is centered at the downstream of the inflow boundary about 1.5Lpp.

The trimmer grids with local refinements and prism layers near ship hull are applied in the calculations. All the grid generation are carried out based on a base grid size (e.g. mesh size in various regions, prism layer thickness and free surface etc.). To reduce unnecessary computing effort due to finer grid everywhere in the domain, local volumes of different shapes are specified based on local flow patterns as shown in Fig. 2. As depicted in Fig. 2, local refinement is conducted to the free surface layer with 20 mesh layers in the range of one wave height and 80 meshes in one wave length. In order to precisely capture ship waves, fine grids are applied in the Kelvin wave zone around the ship hull.

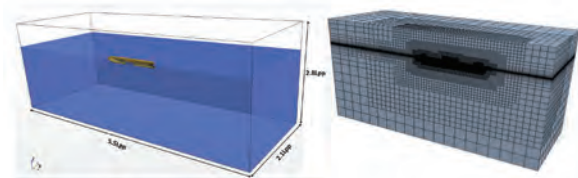


Figure 1 Computational domain and overall volume mesh

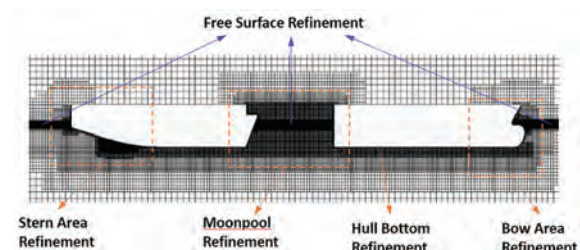


Figure 2 Mesh refinements in selected region

Besides, fine grids are also used in other regions with complicated flow such as the ship bow and stern area. The model tests reveal that the water inside moonpool can be very violent. To simulate such flows, very fine grids in the moonpool region are performed, especially in the free surface layer inside the moonpool, as shown in Fig. 2.

The prediction of wall friction and pressure depends on well boundary layer flow simulation. In the present study, the all wall y^+ treatment is applied. This y^+ value is an indicator of the distance between the hull surface and the first layer of prism layer. A reasonable prism layer setup for the turbulence layer flow field is about $20 \leq y^+ \leq 200$.

To balance the accuracy and efficiency and based on the mesh convergence analysis, the total volume mesh number of about 4 million is used in the simulations.

CFD Validation Results

To validate the CFD solver, the towing tank test data is used. Six forward speeds from 11 to 16 knots are considered in this study. Based on the CFD setup described previously, the CFD results show less than 3% difference from model test data for all the six speed cases as shown in Fig. 3. This suggests that the current CFD setup is able to well capture the drillship flow physics and yield good agreements with model test data.

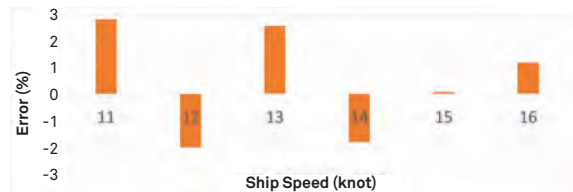


Figure 3 Differences (%) between CFD predictions and model test data

In order to gain insights from the CFD results, the case of 14 knots forward speed is presented in this study as an example. The case for the same drillship hull without moonpool is carried out to evaluate the added resistance induced by moonpool.

The wall Y^+ on the hull is shown in Figure 4, revealing that the Y^+ on the underwater part of the hull is mostly in between 20 and 50. This provides appropriate mesh inside turbulence boundary layer and makes sure the frictional resistance can be accurately computed.

The wave pattern induced by drillship with 14 knots forward speed is shown in Fig. 5a. The divergent and transverse waves are well captured. Fig. 5b is the results of drillship without moonpool. As shown in both figures, the moonpool has minor effect on bow waves. However, due to the existence of the moonpool, the stern wave height of the drillship increases, which consequently causes the better pressure recovery at the stern part compared to that of the drillship without a moonpool case.

Dynamic pressure distributions are plotted in Fig. 6 for the drillship hull and the corresponding drillship without moonpool case. Due to the vortex shedding from the moonpool, the dynamic pressure at the stern of the drillship case appears better recovery than that of the drillship without moonpool case.

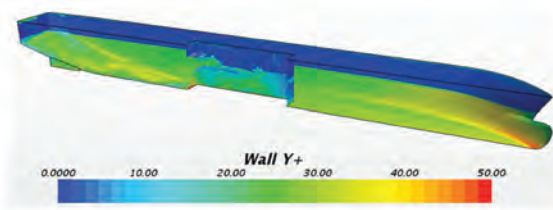


Figure 4 Wall Y^+ in the simulation

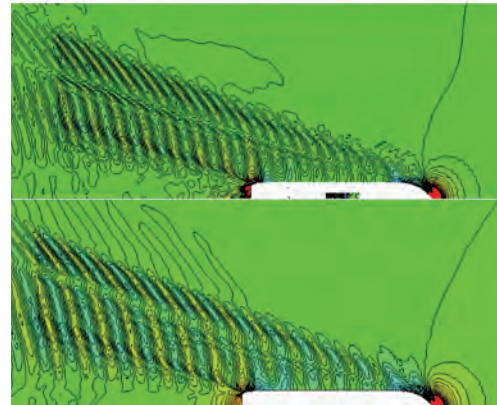


Figure 5 CFD simulated drillship waves (a) with moonpool (b) without moonpool.

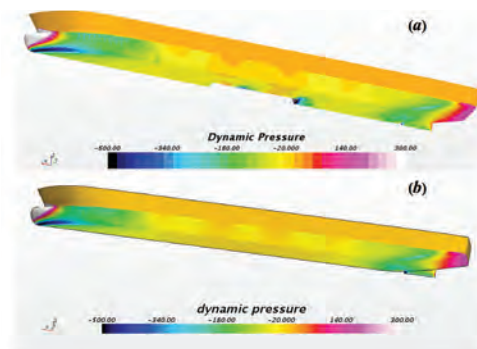


Figure 6 Dynamic pressure distributions (a) with moonpool (b) without moonpool

The unsteady vorticity and velocity vector fields as shown in Fig. 7 reveals that the unsteady flow inside the moonpool is induced by the vortex shedding from the bottom of the front wall. This unsteady flow creates time varying pressure forces on the moonpool walls and therefore the added resistance to the ship hull. At the bottom edge of the moonpool rear wall, vortices are also generated and induces vortex train under the rear part of the drillship hull as seen in Fig. 7.

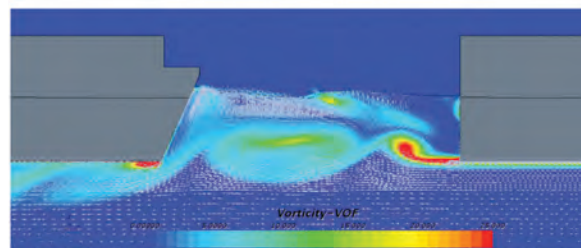


Figure 7 Vorticity field at the central plane inside the moonpool at a time instant

The resistance time history of CFD results compared with the model test measurements are shown in Fig. 8. It can be seen that the CFD simulation at the stable stage matches the model test quite well. The predicted mean resistance is in good agreement with the model test data, under-predicting 1.8%.

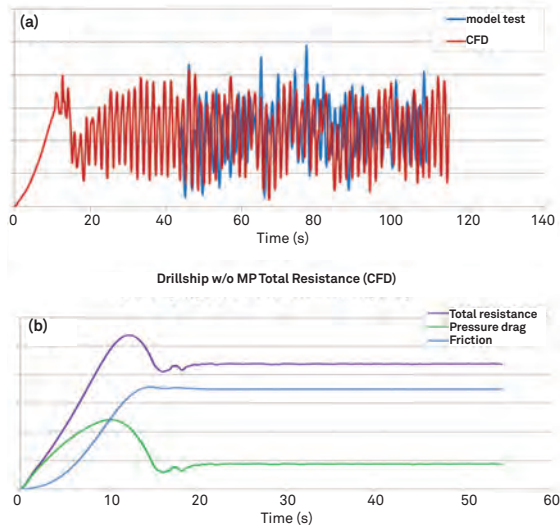


Figure 8 Resistance time history of drillship a) with moonpool; b) without moonpool

CFD predicted drillship resistance can be readily broken down into various components, e.g. the friction and pressure resistance on the moonpool and the rest of hull. The resistance induced by the moonpool is 59% of the drillship total resistance, larger than the resistance induced by the hull, which is 41% of the drillship total resistance. The friction component dominates the resistance on the hull (almost 90% of the hull resistance), meanwhile, the pressure drag dominates the resistance in the moonpool (nearly 100%). In fact, the friction force inside the moonpool is very small and insignificant compared to other components. This friction force is caused by the complex flow inside the moonpool where the flow near the side wall has a mean flow in the forward direction.

To estimate the drillship added resistance, the drillship without moonpool case has been simulated with the CFD setups same as the drillship case. The total resistance and its pressure and friction components are plotted in Fig. 8. To compare the resistance components between the drillship and the drillship without moonpool case, the pressure and friction drag components along with the moonpool induced added resistance (defined as the difference between total resistance with and without moonpool) show that the value of moonpool added resistance is 110% of the total resistance of the drillship without moonpool case. The results also show that the friction dominates the resistance of the drillship without moonpool case, which is 80% of the total resistance, as shown in Fig. 8. On the contrary, the pressure drag dominates the resistance of the drillship, which is 64% of the total resistance. CFD simulations at other transit speeds show similar results, i.e. the added resistance due to the presence of moonpool is about 100% of the resistance of the case without a moonpool.

To further investigate the added resistance from the moonpool, the time histories of the pressure force on

the front and the rear walls are analysed. As seen in Fig. 9, it suggests that the mean pressure force on the rear moonpool wall is larger than that on the front moonpool wall, indicating a drag force on the drillship hull, i.e. the added resistance.

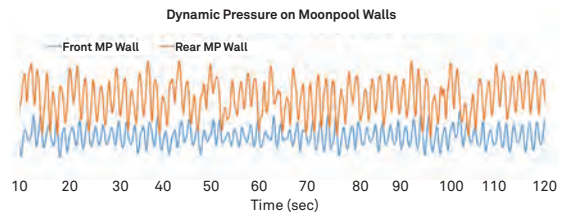


Figure 9 Time history of moonpool wall pressure (a) front wall (b) rear wall

The moonpool water elevations of CFD simulations at a centerline front point (CL) and the portside middle point (PS) are compared with model test result in Fig. 10a and 10b, respectively. From the Fig. 10, it can be seen that the amplitude of simulated water elevation is larger than that of the measurements at CL and quite close at PS. This might be caused by the violent turbulence flow and the free surface waves inside the moonpool, since the flow visualisation shows that the wave breaking occurs at the middle and rear part of moonpool. The water surface inside the moonpool at two selected time instants are shown in Figure 11, in which one is with relatively low water surface (Figure 11a) and the other with more violent water surface (Figure 11b).

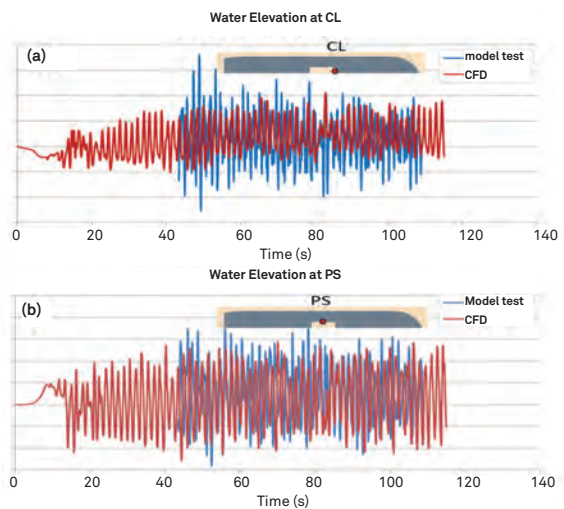


Figure 10 Time history of water elevation inside moonpool at (a) centerline front point (CL) (b) portside middle point (PS)

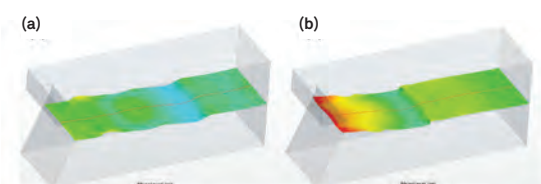


Figure 11 Water surface inside moonpool at two selected time instants, a) low water level; b) high water level

Parametric Study

Parametric study is carried out in order to find out the moonpool dimension effect on the drillship resistance, and help to understand the optimal moonpool design. Based on the original design, it is decided to evaluate the drillship resistance with the changing moonpool length and width. CFD simulations are performed for other eight cases with combinations of the base case and the other two shorter moonpool lengths and narrower moonpool breadth by using the validated model and the developed best practices. For each dimension, the resistance is evaluated under 6 speeds from 11-16 knots.

The parametric study results are summarised in Fig. 12. It is found that resistance can be reduced with narrower width or shorter length of moonpool. It can also be seen in Fig. 12 that the variation at lower speed is a bit different from that at relatively high speed. However, in overall, the optimal moonpool dimension is based on the narrowest width and shortest length.

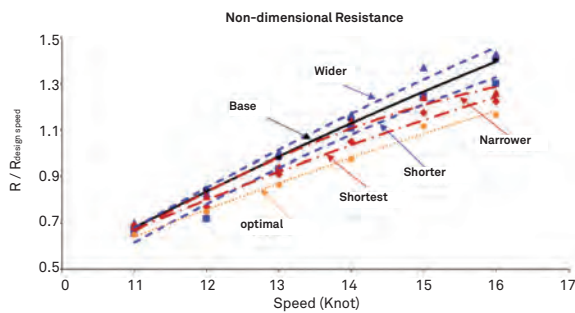


Figure 12 Drillship resistance vs speed with various moonpool dimensions

Discussions

Mechanism of moonpool added resistance

The parametric study indicates that the smaller moonpool dimension, the lower the moonpool induced resistance is. In order to find out the physics behind this phenomena, dynamic characteristics of the drillship total resistance as shown in Fig. 13a are investigated by FFT analysis to give frequency domain in Fig. 13b. It reveals obviously in Fig. 13b that shorter length and/or narrower width of moonpool result in higher shedding frequency. In other words, the smaller the moonpool dimension, the higher the vortex shedding frequency. With higher frequency, the moonpool system can accumulate less energy during a shorter period and generate smaller added resistance.

Both model tests and CFD simulations show that strong oscillatory water motions can be agitated inside the moonpool in transit at a constant forward speed. Details of flow motion can be visualised and analysed from CFD simulations and consequently the mechanism of the oscillatory motion can be investigated. In principle, the vortices periodically shed from the bottom of moonpool front wall is the origin of the oscillatory flow in the moonpool. Basically there are three frequencies in the system, i.e. the vortex shedding frequency f_1 , the dominant water elevation frequency inside the moonpool f_2 and the dominant resistance oscillation frequency f_3 , as illustrated in Fig. 14. When a stable flow state is established, the frequencies of the three phases should be identical or very close. So this flow phenomenon

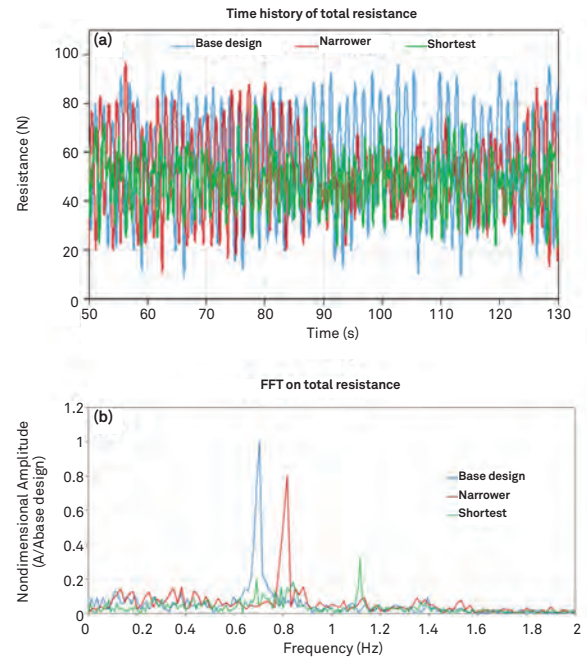


Figure 13 Resistance oscillation for various moonpool dimensions, a) resistance time history; b) resistance frequencies

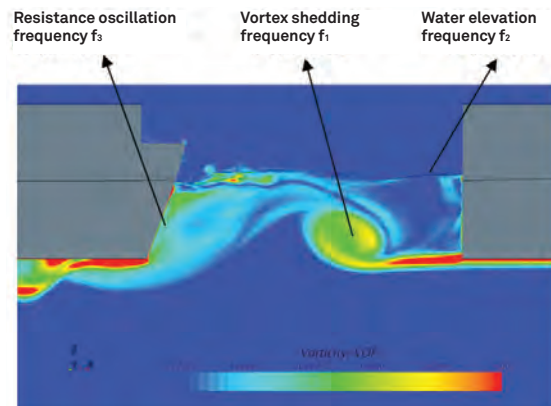


Figure 14 Vortex inside the moonpool and indication of various frequencies

can be called phase locking. This was confirmed by both the model test data and the CFD simulated results in the present study.

According to the empirical formula below (Fukuda, 1977) that estimates the moonpool natural frequency ω_n based on moonpool length L , breadth B and draft D

$$\omega_n = \sqrt{\frac{g}{D + 0.41\sqrt{L*B}}}$$

and also the present CFD simulations, it can be concluded that the shorter length L and/or narrower width B of moonpool result in higher frequency. At higher frequency, the moonpool system will accumulate less energy during a shorter period and consequently generate smaller added resistance, as observed CFD parametric study. For longer moonpool, the vortex shedding from upstream can always enter into the moonpool impinging on the rear wall to create strong pressure force on the wall, resulting larger resistance and more violent free surface flow.

Effects of trim and sinkage

In the CFD validation study, one of the main tasks is to investigate the sensitivity of the trim/sinkage motion effect on the resistance to determine if the motion could be excluded or not as it benefits a lot to reduce the CFD computational cost by excluding the ship motion computation. CFD simulations with the trim and sink motion on and off are compared in order to test the sensitivity of the trim/sinkage motion effect on the resistance. According to this sensitivity study and the model test observation, it can be concluded that the trim and sinkage effect on the drillship total resistance is insignificant and the trim and sinkage motion can be excluded from the CFD model for resistance simulation. In such measure, CFD computation time can largely be reduced.

CFD predicted resistance time history without and with trim and sinkage are shown in Fig. 15. The calculation of mean values indicate that the trim and sinkage are small, and their effects on the drillship resistance are quite minor. This means that the effect of trim and sinkage on the drillship resistance is insignificant.

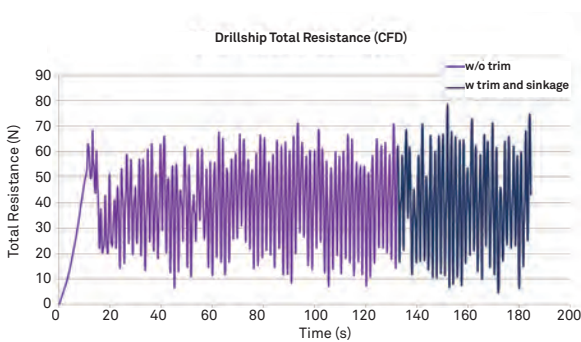


Figure 15 Time history of drillship resistnace with and without trim and sinkage

Effects of CFD solver

In developing the CFD practice applicable to the drillship problem, a variety of sensitivity tests for computational domain, grid resolution, far field damping zone, prism layer grid, trim/sinkage motion and turbulence model are performed based on the judgment and consideration of the flow physics. Some detailed analysis related to the effects of trim/sinkage motion and turbulence model on the drillship resistance are briefly discussed in this section. As a consequence, a physics based CFD practice is developed and summarised.

Although the trim and sinkage motion are set free during the model test, they are not recorded in the resistance tests except in self-propulsion tests. In the CFD validation study, one of the main tasks is to investigate the sensitivity of the trim/sinkage motion effect on the resistance to determine if the motion could be excluded or not as it benefits a lot to reduce the CFD computational cost by excluding the ship motion computation.

In order to investigate the effect of the trim and sinkage, the self-propulsion model test data is analysed as no such data for resistance tests. The results suggest that trim and sinkage at the testing speed is insignificant. These values should be even smaller in resistance tests as in propulsion tests the flow can be accelerated by the thruster and

the hull pressure on the stern will actually be decreased compared to the bare hull resistance tests and therefore cause larger trim and sink motion. CFD simulations at one design speed with the trim and sink motion on and off are compared, which show very similar simulation results. Therefore, it can be concluded that the trim and sinkage effect on the drillship total resistance is insignificant and they can be neglected in the CFD resistance simulations. As there are strong turbulence and vortex shedding in the drillship flow field especially in transit state, CFD turbulence model selection is critical to the simulation results. According to the reference (Wilcox, 2006), $k-\omega$ turbulence model can perform well in capturing the strong flow separation. In the present study, it appears that the simulated water elevation based on $k-\omega$ turbulence model always shows some discrepancies from the measurements at a low speed, even applying very fine mesh in the moonpool region. The reason might be related to the weakness of RANS model at simulating the complex vortex structure in strong wake flow such as the moonpool case. To improve the CFD simulation results of the water elevation, a more advanced model - DES (Detached Eddy Simulation) is conducted for the 11 knots case. To evaluate the DES results, the simulated water elevations at CL obtained from RANS with $k-\omega$ turbulence model and DES model are compared with the measurements, as shown in Fig. 16. As seen in the time history plots, the DES computation can improve a lot of the water elevation prediction and matched the measurements much better than that of $k-\omega$ model simulation. However, in order to perform the DES computation, finer mesh size and smaller time step with the half values used in the $k-\omega$ turbulence model are applied. This eventually causes about four times longer computation time compared to the $k-\omega$ turbulence model.

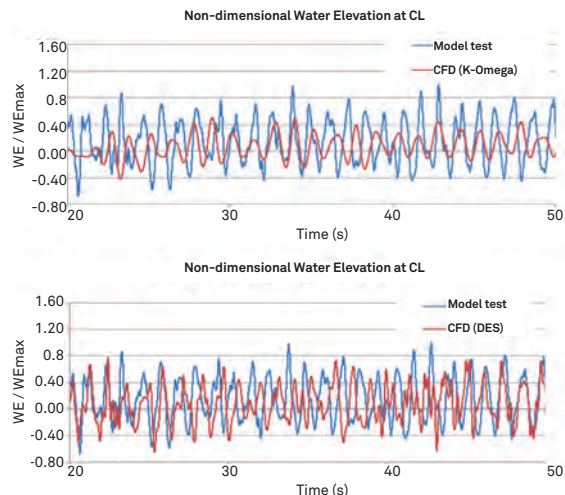


Figure 16 Turbulence model effect on predicted water elevation (a)K-Omega model (b) DES model

Physics based CFD practices for drillship resistance prediction

The physics based CFD practices for drillship resistance simulation in calm water are developed. Based on the developed best practices, the CFD simulations for drillship resistances can achieve less than 3% difference in comparison with measurements. The best practices consist of the choice of domain size, mesh refinement, time step, CFD models and numerical scheme.

The computational domain should be large enough to avoid wave reflection from upstream, downstream and side of the domain. Practically, appropriate mesh refinements should be specified in specific regions based on local flow properties. For the drillship flow problem, the critical zones include bow, Kelvin waves, moonpool, hull surface, prism layer and hull bottom.

Due to the complexity of the flow field inside the moonpool and its significance on the drillship resistances, mesh resolution inside the moonpool should be carefully controlled to ensure the accuracy of CFD simulations. It has been shown that the violent free surface and strong vortex shedding are the two dominant features inside the moonpool. Therefore, the setups of the mesh control volumes are more focused on the mesh size to capture free surface waves and the circulating flow inside moonpool.

In order to obtain an accurate CFD simulation, the surface mesh on the hull and in the wall boundary layer is very important for the friction prediction. Also, to maintain the accuracy of the hull shape, sufficient mesh refinement should be applied, especially in the areas with high curvatures. To use a wall function approach, the first cell should be appropriately located in the fully developed turbulence boundary layer. The corresponding wall y^+ value is $20 \leq y^+ \leq 200$.

In addition to the hull surface mesh and the prism layer mesh, the zone beneath the hull bottom also requires mesh refinement since the vortex shedding from the moonpool will affect the flow field underneath the hull bottom.

Conclusions

The analysis of measurements and CFD simulations was performed to investigate the mechanism of added resistance induced by the drillship moonpool. The drillship moonpool makes the resistance of drillship fluctuate substantially, which is different from conventional ships that experience nearly constant resistance in a given sea condition. This fluctuation is mainly induced by the violent water motion inside the moonpool. Flow details from CFD simulations reveal that, while a drillship is in transit at a constant forward speed, vortices shedding from the moonpool front wall can evolve into the moonpool and impinge on the rear wall to create high pressure and therefore generate additional pressure force on the drillship. Meanwhile, the water inside the moonpool is agitated by the vortices and oscillatory water motion is induced on the surface inside the moonpool.

The CFD tool was benchmarked against the model test data. Simulation results suggest that the fluctuating resistance was well captured and the predicted mean resistances agree very well with the measurements, yielding less than 3% difference for the range of speeds. A physics based CFD best practice was developed based on the domain setup, mesh refinement and various CFD model selection etc. This validated CFD tool and setup were then applied to carry out the parametric studies in order to investigate the effects of moonpool dimension on the drillship resistance.

In the parametric study, a variety of moonpool dimensions were investigated. It is revealed that smaller moonpool dimensions results in smaller added resistance. In

addition, it was found that the vortex shedding from the moonpool front wall causes higher pressure on the rear wall of moonpool and therefore contribute larger moonpool induced added resistance. FFT analysis of the CFD results showed that the oscillation frequency of the moonpool induced resistance is same as the vortex shedding frequency, which is controlled by the moonpool dimension. Larger moonpool dimension can result in longer vortex shedding period, which can accumulate more energy and consequently generate higher added resistance based on longer shedding period.

In this study, the results of parametric study reveal that moonpool dimension has significant effects on the drillship resistance, especially at relatively high transit speed (>13 knots). The resistance increase with the increasing moonpool size is more significant at higher speed. A physics based CFD best practice is established for industry applications. Based on the parametric study results, a design principle is proposed to guide drillship moonpool design.

References

- [1] CD-adapco, 2016. User Guide – Star-CCM+ version 11.04.
- [2] Enger, S., Peric, M., and Peric, R., 2010. Simulation of flow around KCS-hull. The Gothenburg 2010 Workshop on Numerical Ship Hydrodynamics, Gothenburg, Dec 8-10, 2010.
- [3] Ferziger, J.H. and Perić, M. 2003. Computational methods for fluid dynamics. 3rd Ed., Springer Verlag, Berlin, Heidelberg.
- [4] Fukuda, K., 1977. Behavior of water in vertical well with bottom opening of ship and its effects on ship motion. Journal of the Society of Naval Architects of Japan, Vol.141, pp. 107-122.
- [5] Hammargren E. and Tornblom J., 2012. Effect of the moonpool on the total resistance of a drillship. Master of Science Thesis, Chalmers University of Technology, Gothenburg, Sweden.
- [6] Larsson L., Stern F. and Visonneau M., 2013. Numerical ship hydrodynamics, an assessment of the Gothenburg 2010 workshop. Springer Dordrecht Heidelberg London New York.
- [7] Molin, B., 2001. On the piston and sloshing modes in moonpools. Journal of Fluid Mechanics, Vol.430, pp. 27-50.
- [8] Newman, N., 1977. Marine hydrodynamics, The MIT Press, Cambridge.
- [9] Son, H., Choi, S., and Kim, M., 2008. Drag reduction of recess type moonpool under vessel's forward speed. Proceedings of ASME 27th International Conference on Offshore Mechanics and Arctic Engineering. Estoril, Portugal.
- [10] Veer R.v. and Tholen H. J., 2008. Added Resistance of Moonpools in Calm Water. Proceedings of ASME 27th International Conference on Offshore Mechanics and Arctic Engineering. Estoril, Portugal.
- [11] Wang, S., and Quah, M., 2013. CFD simulation of water oscillation in the moonpool of a drillship. SNAME 34th Annual Journal 2012-2013, pp. 50-69.
- [12] Weiss, J., Maruszewski, J.P., Smith, W.A., 1999. Implicit solution of preconditioned Navier-Stokes equations using algebraic multigrid. AIAA J., 37, pp. 29-36.
- [13] Wilcox, D. C., 2006. Turbulence modeling for CFD, 3rd edition. DCW Industries, Inc., La Canada CA, 2006.

Author's Contact

| peifeng.ma@komtech.com.sg

Computational Fluid Dynamics Study of Air-Gap and Wave Impact on Semi-submersibles

| XU Haihua^{*}, PhD, M.Eng., B.Eng

| LIU Jing^{*}, PhD, M.Eng., B.Eng

| Anis HUSSAIN^{*}, M.Sc., B.Eng

| Youngkook KIM[†], M.Eng, B.Sc

| MA Peifeng^{*}, PhD, M.Eng., B.Eng

| Ankit CHOUHARY^{*}, M.Sc., B.Eng

| ZHANG Yali[†], Ph.D, M.Eng., B.Eng, B.Acc.

| Andrew Pang[†], Ph.D, B.Eng

^{*}Keppel Offshore & Marine Technology Centre

[†]Lloyd's Register Global Technology Centre

This paper presents part of the research work done in the Joint Industry Project (JIP) of extreme wave impact on semi-submersibles collaborated with Lloyd's Register Energy. This research is also partially supported by Singapore Maritime Innovation & Technology (MINT) Fund. The purpose of the project is to study the motion and air gap of semi-submersible under extreme waves using Computational Fluid Dynamics (CFD) method. In order to achieve this, the 2nd order NewWave^[1-5] is implemented in Star-CCM+ by user code functions to generate the focused extreme wave at designed wave height, focus time and focus location. The CFD capability of semi-submersible motion prediction is benchmarked against extensive in-house model test data through simulations of free decay and the vessel motion under regular waves. The simulation results show very good agreements with model test data. Through the extensive benchmark study, a best practice of CFD simulation of extreme wave generation, semi-submersible decay and motions under waves has been developed.

Introduction

Extreme waves, sometimes known as “hundred year waves” or “thousand year waves” (due to the probability of their occurrence) while uncommon, is an important ocean phenomenon which has to be modelled due to the significant damage. It can cause on an offshore structure. Some key wave properties that need to be considered in extreme waves include unsteadiness, directionality, and nonlinearity.

The properties of extreme real ocean are difficult to define numerically due to irregular wave, strong non-linearity, non-Gaussian statistics, transient dynamics and wave breaking. So far, only model test is able to predict this behaviour. However, it is not cost-effective to investigate a large number of extreme events and hoping to have that one of these events will produce most extreme events. Secondly, the model test also cannot produce this extreme wave at a location that can cause maximum damage. Thirdly, the model test is carried out at a model scale at which the effect of extreme waves could be under or over predicted due to scale effect.

In this project, 2nd order focused NewWave^[1-5] is applied in Computation Fluid Dynamics (CFD, Navier-Stokes equation) with motion of semisubmersible. Currently, simpler tools (e.g. linear potential flow code) were used by industry which is less accurate than the 2nd order NewWave with CFD due to various assumptions made in potential theory. As a convenient yet more economic method, numerical simulation on full size model using state-of-art CFD techniques has started to receive attention. Similarly, the effect of random sea states can now be captured through fluid dynamic simulation tools such as CFD. The flow around semisubmersible platforms gives rise to a number of non-linear motions such as non-linear roll through vortex induced motion.

In the current study, the non-linear NewWave method is used to generate the extreme wave, which represents the same wave spectrum as the designed sea state. The generated non-linear NewWave is input to the CFD software (OpenFOAM, Star-CCM+, etc) as the inlet boundary condition. Inside the simulation domain, the Navier-Stokes equation which considering the viscosity, turbulence, and motion of the semi-submersibles are solved.

Different from the other researchers focused on the NewWave with offshore fixed structures, the current project extended to the offshore floating platform (semi-submersible). The difficulty of the project is significantly increased due to the motion of the semi-submersible. This is because the air gap of the semi-submersible not only related to the extreme wave height but also related to the motion of the semi-submersible under the extreme wave. Hence, the simulation needs to simulate both the extreme wave and semi-submersible motion accurately. By introducing the non-linear NewWave in Star-CCM+, the project extends the capability of the commercial software to generate the extreme sea condition.

Over a period of time, Keppel has accumulated an extensive model test database of semi-submersibles which is available for various extreme events which captures both

motions and relative wave height with respect to the vessel motion (airgap). This database has been made available for validation of this novel method to arrive at best practice method in CFD tool. This has not been done by any research institution before due to the combination of technology and database required to undertake such initiative.

The project first benchmarks the extreme wave generation and propagations. After that, a series of semi-submersible motion benchmarks are carried to validate the motion in the CFD simulation. These motion benchmarks include pitch, heave and surge decay simulation, semi-submersible motion under the regular wave. The extreme wave simulation and semi-submersible motion are created to guide the industry in the application of CFD for simulation of the impact of the extreme wave on a semi-submersible.

This paper will first introduce the 2nd order NewWave implementation and benchmark in Star-CCM+. After that, the CFD simulation of semi-submersible decay and the motion under the regular wave will be discussed. The conclusion will be made at last part of the paper.

Extreme wave generation and propagation

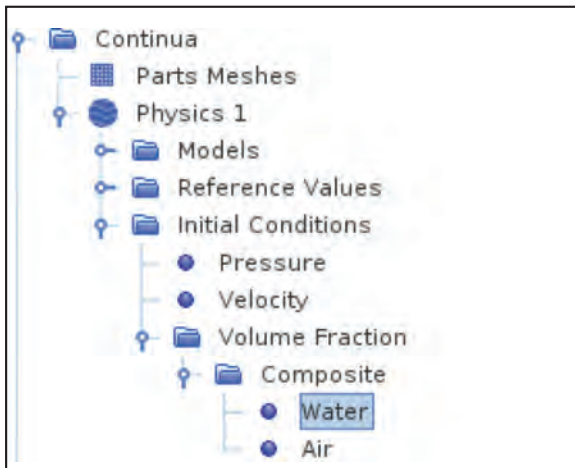
In this part, the extreme wave is generated by 2nd order NewWave method^[1-5]. The wave generation will be presented and discussed. Subsequently, a test case will be carried out for the NewWave implementation and the results will be compared with OpenFOAM results.

2nd order NewWave implementation in Star-CCM+

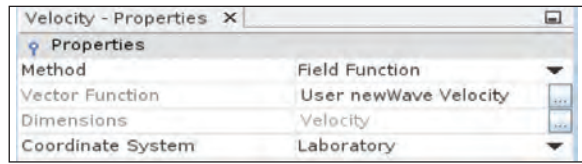
In Star-CCM+, the wave superposition method can only be adopted for linear wave superposition. For the 2nd order NewWave^[1-5], other methods are needed for the implementation. The user code function in Star-CCM+ allows functions to be compiled into a library which can be accessed by each simulation model. The user code can be written in compiled languages such as C, C++ or Fortran and compiled to a dynamic library (*.dll file in Windows and *.so file in Linux). In the current project, the 2nd order NewWave theory is implemented by this user code function in Star-CCM+^[6]. The NewWave user code functions are obtained by converting the available NewWave code in OpenFOAM (written in C++) and compiling it into a *.so library in the Linux environment.

In Star-CCM+, user code takes the form of one or more user libraries that are attached to Star-CCM+, each of which contains one or more user functions and a library registration function. When a user library has been attached, its user functions are available to use and are provided in drop-down lists for any operation needed. These functions can be used to specify values on a region or a boundary as well as for domain initialisation and visualisation.

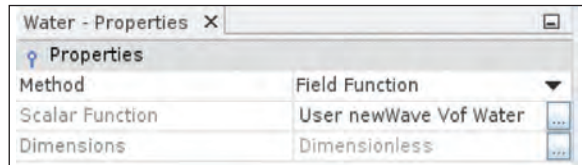
Once the library is loaded, the field function can be accessed similar to other field functions and the profile function can be accessed at the boundaries by switching to the user code. The simulation domain can be initialised by the scalar and vector field user code function as shown in Figure 1. The inlet boundary setting (utilising the boundary profile user code) is shown in Figure 2.



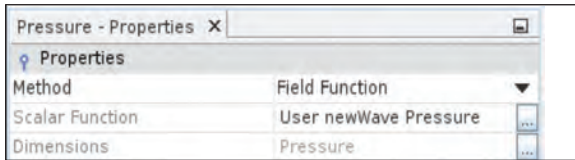
(a) Domain initialisation setting



(c) Velocity properties



(d) VOF water phase properties

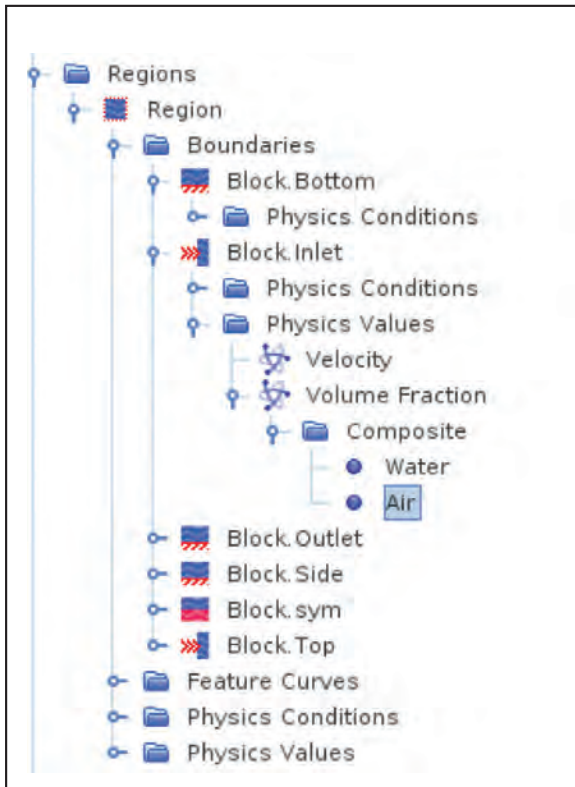


(b) Pressure properties

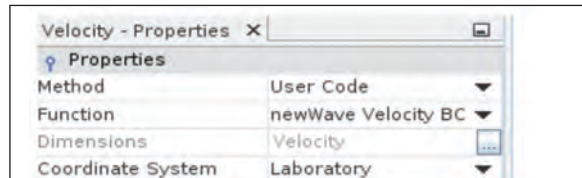


(e) VOF water phase properties

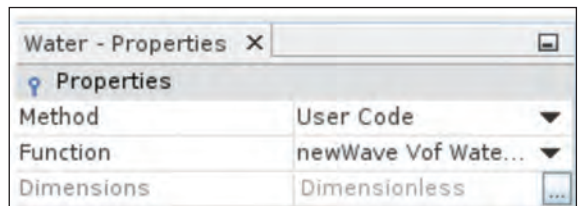
Figure 1 Screenshot of simulation domain initialisation setting by NewWave user code library in Star-CCM+.



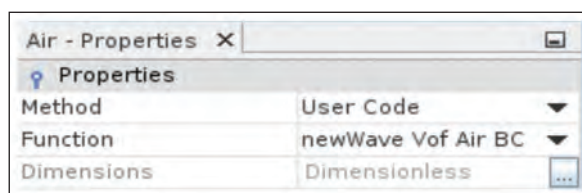
(a) Inlet boudary setting



(b) Velocity setting



(c) VOF water phase setting



(d) VOF air phase setting

Figure 2 Screenshot of inlet boundary setting by NewWave user code library in Star-CCM+.

Extreme wave generation and propagation

The NewWave implementation in Star-CCM+ is compared with the simulation of NewWave propagation in the wave flume with OpenFOAM [3]. The wave flume is 10m in length, with a water depth of 0.5m. The designed focus point is set to $x_0=3.0\text{m}$ and focus time $t_0=9.2\text{s}$. The linear input amplitude is $A=\eta^1_{\text{max}}=0.0632\text{m}$. The corresponding theoretical 2nd order amplitude at the focal point is $A=\eta^2_{\text{max}}=0.0677\text{m}$. The NewWave parameters are listed in the following table.

Table 1 NewWave parameters in Wu et al. (2013) [3]

Frequency band(Hz)	Input Amplitude (m)	No. of wave components	Peak frequency (Hz)	Peak wave period Tp(s)	Characteristic wave length λ_p (m)
0.6-1.3	0.0632	16	0.833	1.2	2.0

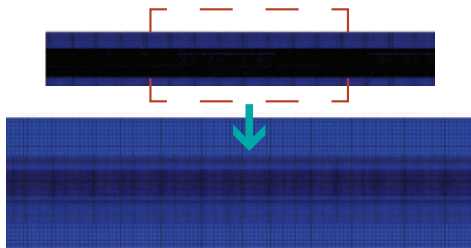


Figure 3 Screenshot of meshing setting for NewWave in Star-CCM+

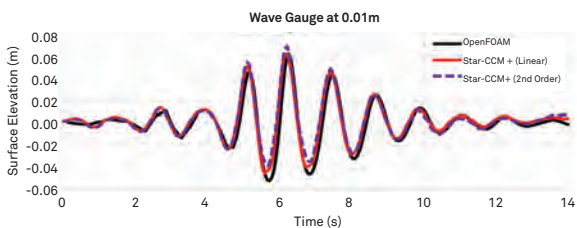


Figure 4 Time history of surface elevation at inlet ($x=0.01\text{m}$) for OpenFOAM and Star-CCM+

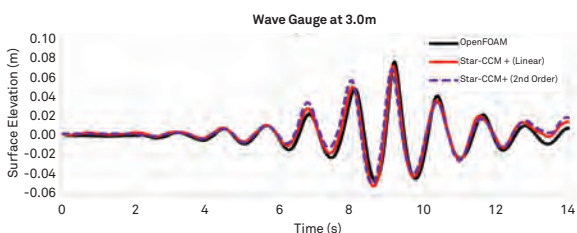


Figure 5 Time history of surface elevation at designed focused point ($x=3.0\text{m}$) for OpenFOAM and Star-CCM+.

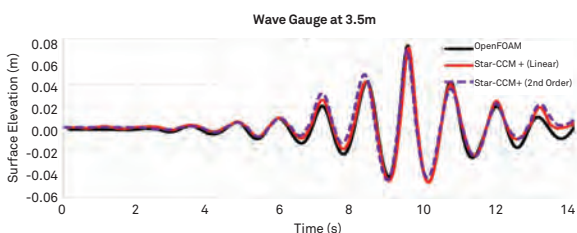


Figure 6 Time history of surface elevation at actual focused point ($x=3.5\text{m}$) for OpenFOAM and Star-CCM+

The mesh of the simulation domain is shown in Figure 3. Figure 4 - Figure 6 show the surface elevation comparison of Star-CCM+ with OpenFOAM at the inlet, designed focus point, and actual focus point. The results show that the Star-CCM+ results agree well with the OpenFOAM results. Some differences can be observed at the inlet. This may be due to the approach whereby Star-CCM+ applies boundary conditions on the face of the inlet while OpenFOAM applies relaxation schemes at the inlet zone.

At the designed focus point $x_0=3.0\text{m}$, the results of the linear and 2nd order NewWave are very close. The surface elevation of Star-CCM+ simulation is relatively smaller than OpenFOAM. At the actual focus point, both linear and 2nd order NewWave of the Star-CCM+ simulation is close to that of the OpenFOAM results. Furthermore, the linear wave superposition method is closer to the OpenFOAM 2nd order NewWave results. This may be due to the nonlinearity effect being not significant for this case.

Simulation of decay tests

The motion, which may influence the load of mooring lines and the fatigue of riser, is one of the most important parameters for semi-submersible design. The motion is determined by many parameters and the damping is one of the key parameters. The damping of a semi-submersible contains both linear and quadratic contributions. The linear contributions are partly of potential (wave radiation) and viscous (friction) origin. The quadratic contributions are the mainly viscous (drag) origin, which is due to the turbulence effect. Hence, accurate estimate the damping coefficient is important for motion analysis.

In this project, the semi-submersible heave, pitch and surge decay motion are simulated by the Star-CCM+ and OpenFOAM [8,9]. In all of the three motion decay, the pitch decay is most challenging. This is mainly due to the pitch motion which involve large mesh distortion and the CFD software may find it difficult to handle this large distortion. Hence, this part will focus on the pitch motion decay simulation and skip the heave and surge decay. Both the Star-CCM+ and OpenFOAM simulation will be discussed.

Star-CCM+ Pitch Decay Simulation

The simulation domain (as shown in Figure 7) is 20m in length, 5m in width and 14m in height. The water depth is 10m. In the current study, the domain is discretised by trim mesh (hexahedral shape). When the semi-submersible pitches, the simulation domain pitches with the semi-submersible at the same angular speed. The intersection region of simulation domain and free surface covers a wedge shape region as shown in Figure 8. In order to capture the free surface and reduce the number of cells, the free surface refinement is carried inside the wedge shape region (A) as shown in Figure 8. Another transient region (wedge shape region B) is defined to allow the mesh to grow inside the region B.

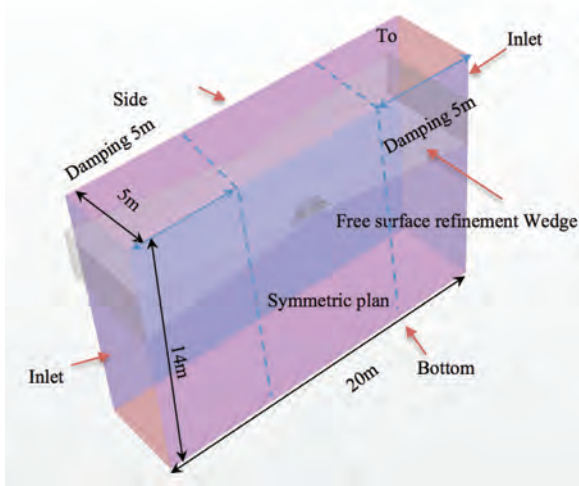


Figure 7 Star-CCM+ of domain configuration of pitch decay simulation in Star-CCM+

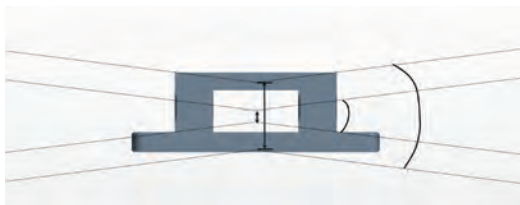


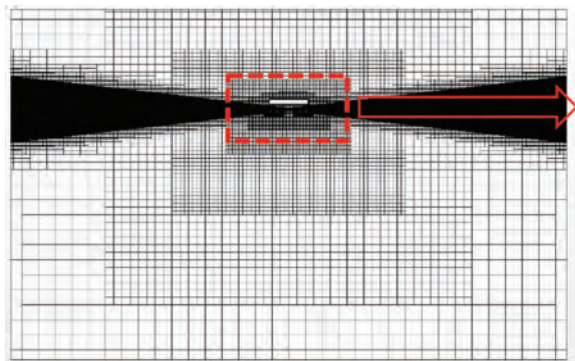
Figure 8 Star-CCM+ of free surface refinement region of pitch decay simulation in Star-CCM+.

The mesh sensitivity study of pitch decay test was performed for a coarse mesh (approx. 2M), medium mesh (approx. 4M) and fine mesh (approx. 6M). The details of the three mesh setting are listed in Table 2 and the snapshot of mesh configurations are shown in Figure 9.

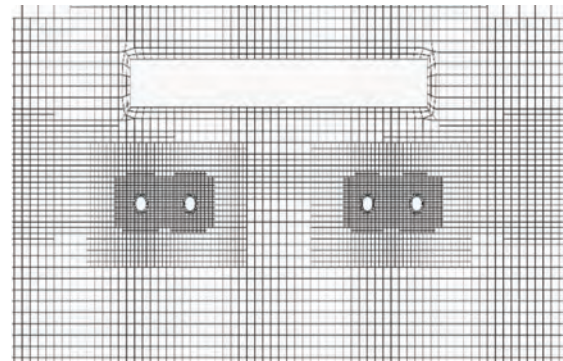
In the simulation domain, the flow is solved by the Navier–Stokes equations and the Volume Of Fluid (VOF) [7] method is used to capture the free surface. Only the laminar flow is simulated and the turbulence effect is neglected. The force and motion of the semi-submersible are simulated by Dynamic Fluid Body Interaction (DFBI) model in Star-CCM+. The 2nd order implicit time stepping scheme is used and the time step size is 0.005s.

OpenFOAM Pitch Decay Simulation

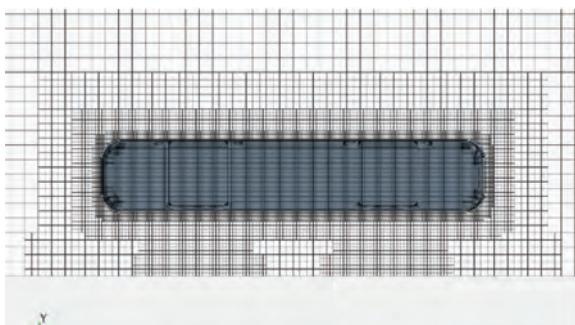
The pitch decay is also carried out by OpenFOAM to compare the accuracy and efficiency of the two software. As shown in Figure 10, the simulation domain is 14m in length, 3m in width and 14m in height. Three mesh of around 2 million (2M), 4 million (4M) and 6 million (6M) cells have been built for the pitch decay simulation. Each mesh has been refined around the semi and braces as shown in Figure 11. In the simulation domain, the flow is solved by the Navier–Stokes equations and only the laminar flow is simulated. The force and motion of the semi-submersible are solved by waveDyMFoam solver. The adjustable time step is used with the Max Courant Number for free surface equal to 0.2.



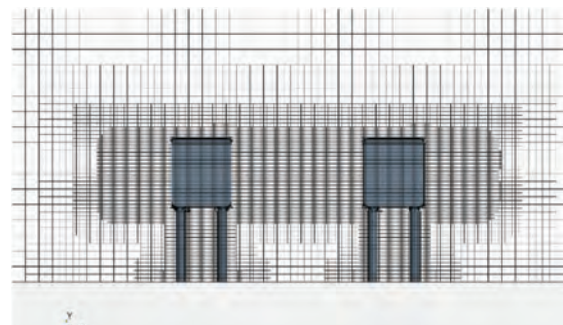
(a) Front View



(b) Front close View



(c) Ponton level close



(d) Column level close

Figure 9 Star-CCM+ mesh configuration of pitch decay for coarse mesh

OpenFOAM is an opensource CFD software and many parameters need to be tuned to achieve acceptable results. For decay simulation, several parameters may influence the results and the effect of these parameters has been investigated. In this project, OpenFOAM-3.0.1 has been used. The rigid body motion framework uses a specialised motion solver which uses an interpolation of displacement and rotation based on the distance to the object to move. The interpolation method is the spherical linear interpolation or Slerp which enforces smoothness and the distance function has a cosine profile to preserve the shape of cells close to the moving surface. The six degrees of freedom rigid body solver allows the user to specify an innerDistance and outerDistance parameter. These control how the sixDoF solver morphs the mesh. For the pitch decay simulation, it was identified that the ideal inner and outer distance for this pitch decay simulation were 0.2 and 2.0 respectively.

The parameter nAlphaCorr specifies the number of corrections to execute on the dispersed phase fraction per each PISO/PIMPLE corrector step. It was identified that changing this parameter results in big changes to the time history of the pitch decay. This change is due to small waves generated around the semi-submersible during the decay test and these waves are unable to be damped out when nAlphaCorr is set to 2 or 3. In this project, nAlphaCorr equal to one is used.

It was also found that the numerical simulation for the time history of the pitch motion could not go back to the zero position. It is suggested that this is due to the uneven distribution of the grid around the semi submersibles when the grid is generated for the initially tilted semi-submersible. Hence, a pre-step which generate the grid for the upright semi-submersible with an evenly distribution of the grid around the semi-submersible, and use dynamicMotionSolverFvMesh to rotate the grid to the initial pitch angle and subsequently let the pitch angle decays freely is employed. It was found with the pre-step treatment the results is improved and the semi-submersible pitch goes back to zero positon.



Figure 10 OpenFOAM simulation domain and simulation domain of pitch decay for coarse mesh.



Figure 11 Example of mesh refinement for 2M, 4M and 6M of the pitch decay simulation in OpenFOAM

Table 2 Mesh setting information for pitch decay simulation in Star-CCM+

Mesh	Coarse Mesh	Medium Mesh	Fine Mesh
Mesh Type	Trim	Trim	Trim
Hull size (mm)	9.375	7.5	6.25
Hull Refiment A (mm)	9.375	7.5	6.25
Hull Refiment B (mm)	18.75	15.0	12.5
Hull Refiment C (mm)	31.2	30.0	25.0
Hull Refiment D (mm)	62.4	60.0	50.0
Hull Refiment E (mm)	124.8	120.0	100.0
Hull Refiment F (mm)	249.6	240.0	200.0
Domain BC size (mm)	1200	960	800
Free Surface A (mm)	18.75	15.0	12.5
Free Surface B (mm)	31.2	30.0	25.0
Total Mesh (Million)	2.21	3.96	7.18

Results and discussion

Figure 12 shows the comparisons of a time history of pitch decay motion for OpenFOAM(OF) and Star-CCM+(CCM) with model test data. The difference of averaged natural period and decay ratio are listed in Table 2. In the figure, the time axis is normalised by semi-submersible natural period and the pitch angle axis is normalised by initial pitch angle. As shown in the figure, the Star-CCM+ results agree very well with the model test data. A small difference can be observed in terms of the natural period after four decay cycles. For medium and fine mesh (6M), the difference of natural period with the model test is about 1% and the difference of decay ratio with the model test is less than 5%. The results suggest, as refining the mesh the results of Star-CCM+ can be improved and the mesh convergence is verified. The OpenFOAM can get acceptable results. The natural period is relatively smaller than the model test results. The difference of natural period is about 5% and the difference of decay ratio is about 10%. Different from the Star-CCM+ results, the results of OpenFOAM didn't improve as the mesh refinement.

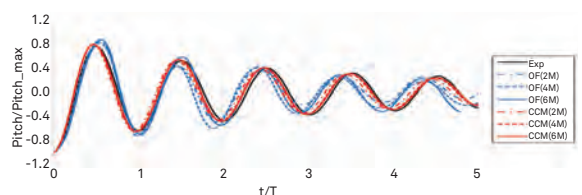


Figure 12 Comparison of semi-submesible pith time history for openFoam (OF), Star-CCM+(CCM) and model test

The snapshots of pitch decay simulation for Star-CCM+ and OpenFOAM simulations are shown in Figure 13 and Figure 14, respectively.

Simulation of regular wave with floating semi-submersible

The abilities of OpenFOAM and Star-CCM+ in handling single DOF motion have been tested in the decay simulations. In this part, the three DOFs (heave, surge and pitch) of motions will be tested simultaneously with the

regular wave. In the simulation, the semi-submersible is subjected to regular wave in the heading direction (180°) and the heave, surge and pitch motion are simulated by Star-CCM+.

The computational domain is 18m long in the upstream and 30m long in the downstream from centre of the semi-submersible platform. Only half-domain is considered in the cross flow direction in order to save computational resource and time, and the domain width is 3m. The water depth is 10m and above the free surface is 3m. The domain dimension is illustrated in Figure 15 which consists of two regions: background region and overset region. The overset region is 3.6m long, 1.2m wide and 1.3m high. Overset mesh technique is used to deal with fluid and structure interaction. In the present case study, background mesh is created for solving far flow field and overset mesh embedded semi-submersible platform is for near flow field. The overset mesh is moving together with the platform body to realise dynamic motion of floating body while the background mesh is fixed. Overset mesh interface is created at the outer boundary of the overset region where the same mesh size is generated to reduce errors. Exchange of the momentum between the two regions is realised at the interface through linear interpolation. The simulation is carried with three sets of meshes to study the grid sensitivity. The three sets of mesh are coarse mesh with 2 Million (2M) cells, medium mesh with 4 Million (4M) cells, and fine mesh with 6 Million (6M) cells. The two mesh regions are presented in Figure 15. Mesh setting details for fine mesh are summarised in Figure 16.

Table 3 Difference of natural period and decay ration with model test

CFD Setting	Averaged Natural Period Difference (%)	Averaged Decay Ratio Difference (%)
Star-CCM+(2M)	-0.43%	-5.02%
Star-CCM+(4M)	0.57%	-4.55%
Star-CCM+(6M)	1.11%	-3.59%
OpenFOAM(2M)	4.57%	7.28%
OpenFOAM(4M)	6.20%	7.70%
OpenFOAM(6M)	5.54%	10.13%

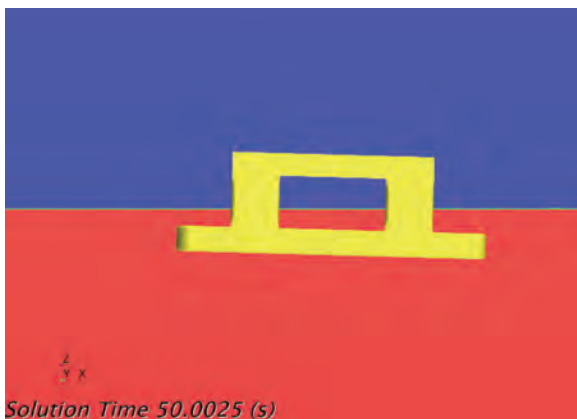


Figure 13 Snopshots of pitch decay simulation by Star-CCM+

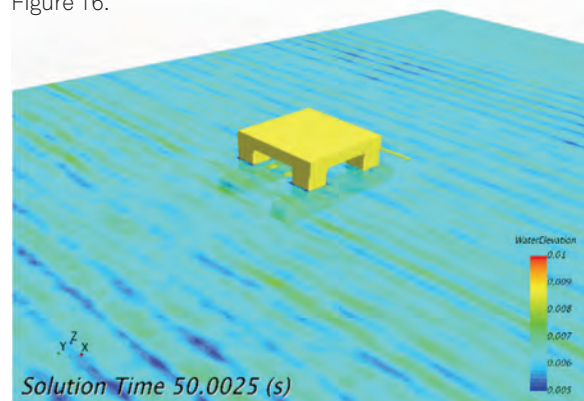


Figure 14 Snopshots of pitch decay simulation by OpenFOAM

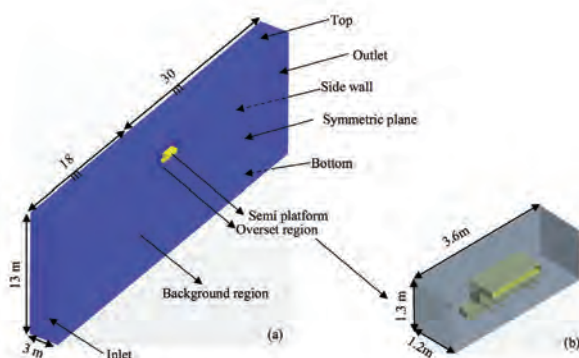


Figure 15 Computational domain for regular wave case 2: (a) background region and (b) overset region.

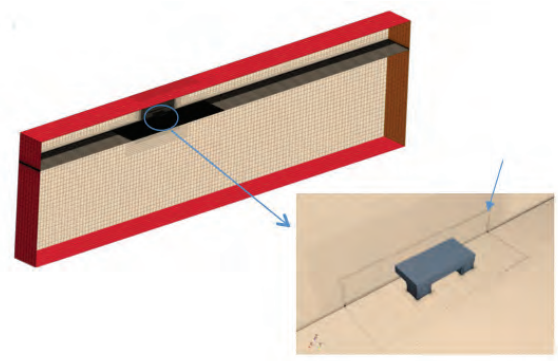


Figure 16 Created mesh in the computational domain (a) and the zoomed in mesh around semi-submersible platform (b)

Table 3 Mesh setting in model scale for the regular wave case 2 in Star-CCM+

Mesh Type		Trim
Background	Domain Size (X,Y,Z)	(48m, 3m, 13m)
	Mesh cell size	Maximum 0.4 m
	Free surface size	$\Delta x = 0.02\text{m}$ (near), 0.05m (far) $\Delta y = 0.04\text{m}$ (near), 0.08m (far) $\Delta z = 0.005\text{m}$ (near), 0.01m (far)
	Number of mesh	4.86 mn
Overset	Domain Size (X,Y,Z)	(3.6m, 1.2m, 1.3m)
	Mesh Cell size	Maximum 0.05 m
	Free surface size	$\Delta x = 0.02\text{m}$ $\Delta y = 0.04\text{m}$ (near), 0.08m (far) $\Delta z = 0.005\text{m}$ (near), 0.01m (far)
	Semi Wall size	0.025m
	Number of mesh	1.26 mn

Table 4 Computational time of different mesh counts for the regular wave case 2 in Star-CCM+

Regular Wave Case 2	2 mn	4 mn	6 mn
Physical time	707 sec	707 sec	707 sec
Computational time	83 hours	158 hours	300 hours
No. of CPUs	24 (Intel Xeon E5-2680v3 2.5G Hz)	24 (Intel Xeon E5-2680v3 2.5G Hz)	24 (Intel Xeon E5-2680v3 2.5G Hz)

Velocity inlet condition is applied to the inlet, top and bottom boundaries. Pressure outlet condition is used at the flow exit boundary. The symmetric condition is for symmetric plane. Overset mesh interface is created between background region and overset region for data exchanging by linear interpolation. First order wave will propagate into the computational domain from the inlet boundary which is defined as the velocity inlet condition. Hydrostatic static pressure of first order wave is specified as the pressure condition at the outlet boundary. The wave damping length 2λ (λ is wavelength) was suggested as best practice numerical method. Its effect on the prediction of the wave induced motion will be discussed in the following section. Laminar flow was used in the present study since no wave breaking happens and hence turbulence effect is negligible. Temporal discretisation is 2nd order. Time step is 0.005s with 10 inner iterations.

The simulation is carried on the KOMtech workstation with 24 cores. The computational time is listed in Table 4 and the comparison of wave induced motion between model test results and CFD results are shown in Figure 17. According to the results, the computational time is proportional to the mesh count. However, the number of mesh cells has insignificant effect on the wave induced pitch and surge motion as shown in Figure 17. For fine mesh, the heave motion is more accurately predicted compared with that with coarse and medium mesh. In

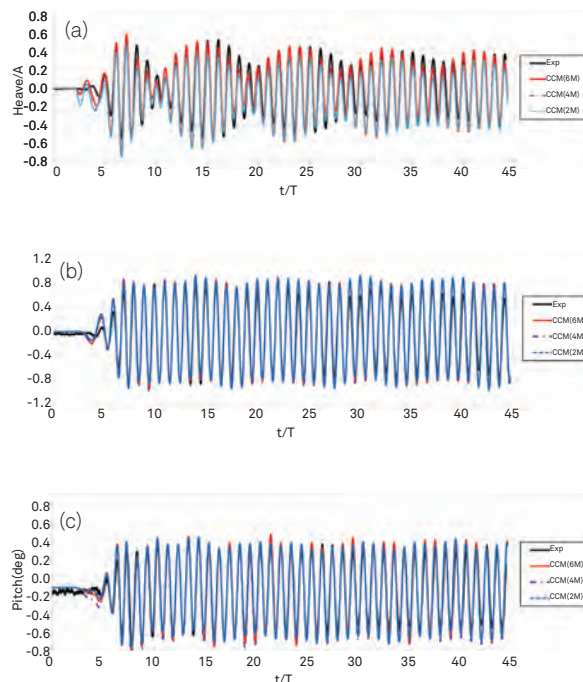


Figure 17 Comparison of wave induced motion between model test results and CFD results for regular wave

With this numerical capability, CFD simulations can be performed prior to the actual model test to help floater designers further optimise the design and improve the floater performance.

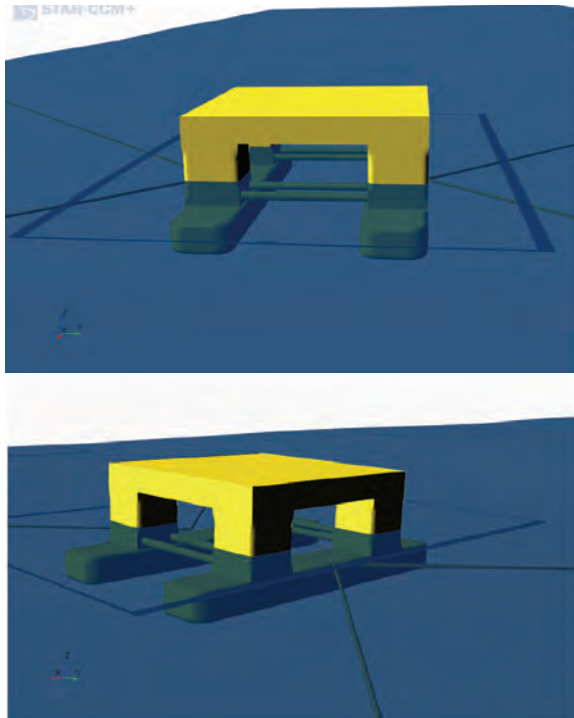


Figure 18 Snapshots of Semi with regular wave at tow view angles.

order to quantify the motion period and amplitude of the CFD results, FFT analysis was performed on the motion time history and the results are given in Table 5. Model test results and CFD results show a good agreement on the wave period with $<0.1\%$ difference. The amplitude of heave motion is accurately predicted with fine mesh. However, there is nearly 15% difference on surge and pitch motion compared with model test results. In a word, in this grid sensitivity study, it was found that coarse mesh is fine enough to capture wave induced surge and pitch motion. The finer the mesh, the more accurate heave motion can be obtained.

Conclusion

The purpose of the project is to study the semi-submersible motion and air gap under extreme wave by CFD tool. In order to achieve this purpose, the CFD tool needs to have the two capabilities which are the extreme wave generation and simulation capability and the floating structure motion simulation capability.

For the extreme wave generation and simulation capability, the current project implemented 2nd order NewWave in the Star-CCM+ by user code functions in Star-CCM+. By introducing the 2nd order NewWave in Star-CCM+, the project extends the capability of the commercial software and able to generate the focused extreme wave at designed

Table 5 Comparison of FFT analysis results on semi-submersible motion between CFD results and model test results

		Period Difference (%)	Amplitude Difference (%)
Heave	Model Test	-	-
	Coarse Mesh	0.01	-10.92
	Medium Mesh	-0.02	-8.94
	Fine Mesh	0.04	-0.60
Pitch	Model Test	-	-
	Coarse Mesh	0.05	14.38
	Medium Mesh	0.06	14.58
	Fine Mesh	0.03	14.78
Surge	Model Test	-	-
	Coarse Mesh	0.00	14.01
	Medium Mesh	0.01	14.57
	Fine Mesh	-0.01	14.51

wave height, focus time, and focus location. The generated extreme wave is compared with the OpenFOAM results and achieve very good agreement.

The motion capability is benchmarked by the semi-submersible pitch decay simulation and semi-submersible pitch, heave and surge motion under regular wave simulation. The semi-submersible motions are compared with model test data and get very good agreement. With this numerical capability, CFD simulations can be performed prior to the actual model test to help floater designers further optimise the design and improve the floater performance. With the assistance of the offshore numerical basin, it is possible to reduce the number of model test, which can significantly save the basin time and reduce the cost.

The above simulations benchmark the CFD models and generate the best practices to study the semi-submersible motion and air gap under extreme wave event.

References

- [1]. Hu, Z.Z., Causon D.M., Mingham C.G. and Qian L., 2011. Numerical simulation of floating bodies in extreme free surface waves. *Nat. Hazards Earth Syst. Sci.*, 11, 519-527.
- [2]. Westphalen J, Greaves D., Williams C., Zang J., Taylor P., 2008: Numerical simulation of extreme free surface waves, ISOPE-2008-QWM-11
- [3]. Wu Y.L., Stewart G., Chen Y., Gullman-Strand J., Kumar P. and Lv X., 2014, *Advanced in Computational hydrodynamics applied to wave-in-deck loading*. ICCM
- [4]. Chen Y., Wu Y.L., Bahuguni A., Gullman-Strand J., Zhang Y.L., Stewart G., Lv X., 2016. *Advances in Computational hydrodynamics applied to wave-in-deck*. Offshore Technology Conference.
- [5]. Lu X., Kumar P., Bahuguni A. and Wu Y.L., 2014. A CFD study of focused extreme wave impact on decks of offshore structures. OMAE
- [6]. Cd-Adapco. STARCCM+ Manual. 2016.
- [7]. Hirt CW, Nichols BD. Volume of Fluid (VOF) Method for the Dynamics of Free Boundaries. *Journal of computational Physics*. 1981;39:201-225.
- [8]. Devolder, B., Schmitt, P., Rauwoens, P., Elsaesser, B., & Troch, P. (2015). A Review of the Implicit Motion Solver Algorithm in OpenFOAM® to Simulate a Heaving Buoy. Paper presented at 18th Numerical Towing Tank Symposium (NuTTS'15), Cortona, Italy.
- [9]. Jacobsen, N. G., Fuhrman, D. R. and Fredsoe, J., 2012. A Wave Generation Toolbox for the Open-Source CFD Library: OpenFoam®. *Int. J. of Numer. Meth. Fluids*.

Author's Contact

| HaiHua.XU@komtech.com.sg

Acknowledgement

The authors thank the National Supercomputing Centre (NSCC) Singapore for providing supercomputer resource to perform Star-CCM+ simulations. This research was partially supported by Singapore Maritime Innovation & Technology (MINT) Fund.

Computational Fluid Dynamics Analysis Applied to Evaluate and Identify B-Series Propellers to Enhance Ship Performance

| Lucas do Vale Machado, M.Sc.

| Antonio Carlos Fernandes, Ph.D. (LOC – COPPE/UFRJ)

**Keppel Offshore & Marine Technology Centre*

A very interesting topic in naval architecture is the choice of propeller. The engineer team should pay attention to several characteristics of the vessel to choose properly the most effective propeller for that specific application.

At the beginning of the Second World War, the diagrams of a well-known propeller design were published, the B-Series Propellers. They were tested at the Netherlands Ship Model Basin in Wageningen and analysed with multiple polynomial regression analysis. Until today this propeller is studied because it possesses satisfactory efficiency and adequate cavitation properties. Besides that, open-water characteristics (K_T , K_Q and η_0) are easy to get.

The purpose of this work is to evaluate the usefulness of Computational Fluid Dynamics (CFD) analysis to get the main characteristics of a propeller in order to make this selection process more effective, and with its lower cost, it is possible to analyse more designs of propellers. A tool using Microsoft Excel was developed to draw any B-Series. For this work, a specific B-Series propeller, the B3.80, was used. The CFD results are verified using Richardson Extrapolation and then validated comparing with the propeller model results. The open-water characteristics are used for this purpose. Other interesting results of this propeller are shown too, e.g. the pressure distribution, streamlines and wall y^+ .

Nomenclature

$\frac{A_E}{A_0} = EAR$	Expanded Area Ratio	[-]
C_n^T, C_n^Q	Coefficients of the polynomials	[-]
D	Propeller diameter	[m]
D_E	Experimental value	[-]
E	Comparison error	[-]
GCI_{mesh}^{ij}	Grid Convergence Index	[-]
J	Advance Coefficient	[-]
K_Q	Torque coefficient	[-]
K_T	Thrust coefficient	[-]
P	Pitch	[m]
Q	Torque	[N.m]
R	Propeller radius	[m]
R_N	Reynolds number	[-]
S	Simulation value	[-]
T	Thrust	[N]
$U_{subscript}$	Uncertainty	[-]
V_a	Advance speed	[m/s]
Z	Number of blades	[-]
e_a^{ij}	Approximate relative error	[-]
h_{mesh}	Representative mesh size	[-]
n	Rate of revolution	[rps]
p	Order of accuracy	[-]
r	Section radius ($r \leq R$)	[m]
r_{ij}	Grid refinement factor	[-]
s_n, t_n, u_n, v_n	Exponents of the polynomials	[-]
η_0	Propeller efficiency	[-]
\emptyset	Pitch angle	[rad]
ρ	Water density	[kg/m ³]

Introduction

The propeller plays an important role in the design of a vessel. Proper selection of a propeller for a specific purpose depends on previous experimental data of known propellers and sometimes new experiments should be performed. This needs time and money to be spent on expensive experiments. Another way to solve this problem is to use a numerical tool, e.g. Computational Fluid Dynamics (CFD), which is more capable of trying new designs.

It does not mean that the experiments are not important and that it is possible to use any CFD code and faithfully believe the numerical results. A code validation is needed and for that, you need experimental data. After the validation it is possible to assure that the code works well for the purpose and then new propeller designs can be simulated.

A well-known propeller design is the B-series with a lot of data available. Therefore, it is a good design to be used in a validation assessment.

Goals

The main goal of this present work is to evaluate the usefulness of CFD for the problem mentioned, from the design of the propeller to the analysis of the data with a verification evaluation and the validation in the end.

A macro was created in Excel to obtain the points of any B-series propeller. The design chosen was the B3.80, where number 3 stands for the number of blades and 80 is due to the Expanded Area Ratio (EAR) that is 80%. All the characteristics of the propeller will be better described in the paper.

The experimental data were gathered at the Netherlands Ship Model Basin in Wageningen and analysed with multiple polynomial regression analysis.

A commercial CFD software based on finite volume method, STAR-CCM + (CD-Adapco) was used. Different domains were created to do a domain analysis. After that, a mesh study was done. The verification assessment was completed following the ITTC procedures and then it was possible to proceed with the validation.

Geometry

A sketch of a propeller is given in Figure 1 with some terms.

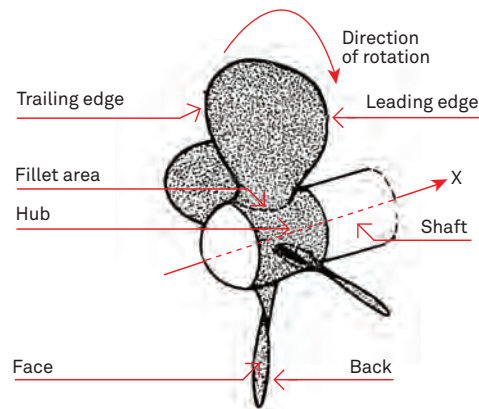


Figure 1 Sketch of a propeller [1]

The surface of the blade that is on the side of the shaft is called the propeller *back*. The opposite side is the *face* of the propeller. It is important to note that when the ship has forward speed the propeller moves with its back forward. In this case, the back side has a low pressure (*suction side*) and the face side has a high pressure (*pressure side*). There are other terms and definitions that are important to ensure they are properly defined.

The *Propeller Pitch* "P" (Figure 2) is the axial distance travelled in one full revolution and its dimension is a length.

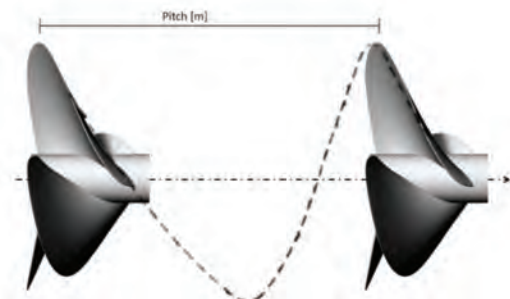


Figure 2 Pitch definition

The *Pitch Angle* "φ" is the angle between the pitch reference line and a plane perpendicular to the shaft. It is related to the pitch P by the following equation,

$$\phi(r) = \frac{P/D}{\pi r/R} \tag{1}$$

The Expanded Area Ratio (EAR) is a ratio of the actual area of the propeller blades to the area of the circle described by the diameter of the blades.

Wageningen B-Series

First of all, a propeller geometry was required for analysis. A well-known benchmark for this purpose are the Wageningen B-Series propellers. The geometry depends on some mathematical definitions and coefficients that are described by Kuiper [1]. In addition, there are a lot of data available on performance characteristics in the literature. Due to the availability of data for the creation of geometry and experimental results, this propeller profile was chosen.

Computer Program for the Design

Its geometry basically depends on three variables: pitch-diameter ratio (P/D), blade expanded area ratio (EAR), number of blades (Z).

The program algorithm is shown in Figure 3.

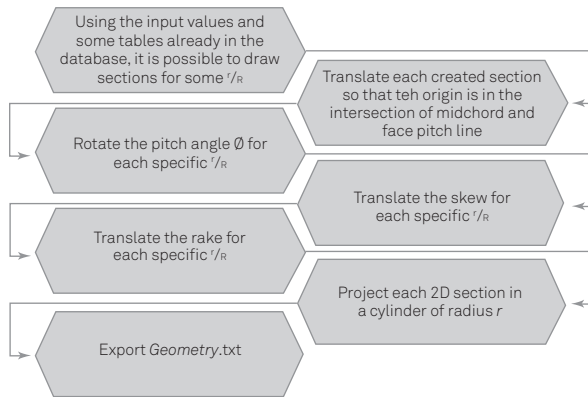


Figure 3 Algorithm of the program to draw the B-Series propeller

A macro was created in Excel (Figure 4) which does what is described in Figure 3, generating an output file called *geometry.txt* with a cloud of points that can be imported into a CAD software.

In CAD, curves are generated by an interpolated curve between points, usually called a *spline* in some software, such as Rhino and AutoCAD. Then, the surfaces are created from the network of intersecting curves.

The inputs shown in Figure 4 are related to the propeller B3.80. The final design of the B3.80 is shown in Figure 5.

The B-series have a constant pitch P at all radii (except the four bladed series), so the pitch angles θ changes for each radius.

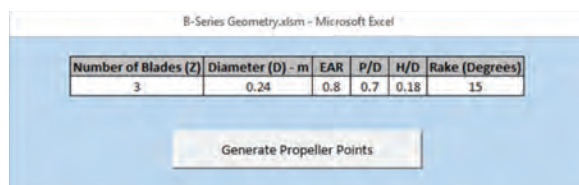


Figure 4 Program to design any kind of B-Series propeller

Experimental Results

Open-Water Test

The performance characteristics of a propeller can be studied in two ways: open water and behind-hull (self-propulsion). The open water test measures the forces and moments acting on the propeller when operating in a uniform fluid stream.

According to the ITTC Procedure 7.5-02-03-02.1 [2], for a towing tank, the propeller model must be mounted on a drive shaft. A streamlined nose cap of sufficient length to ensure that the inflow on the propeller hub is parallel to the shaft should be mounted upstream of the propeller model, as it is shown in Figure 6.

The shaft must be installed downstream to ensure that the propeller is placed in an undisturbed flow. Because of this, the surface of the blade that is on the side of the shaft is the face side (Figure 5), unlike that shown in Figure 1, which is the installation configuration in a vessel.

During the test, the following quantities are measured:

- Model speed (V_0)
- Propeller thrust (T)
- Propeller torque (Q)
- Propeller rate of revolution (n)
- Water temperature (for calculation of viscosity)

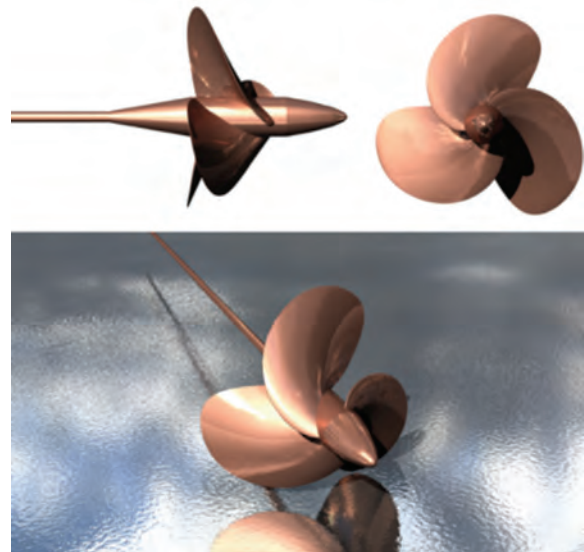


Figure 5 Final design of the B3.80

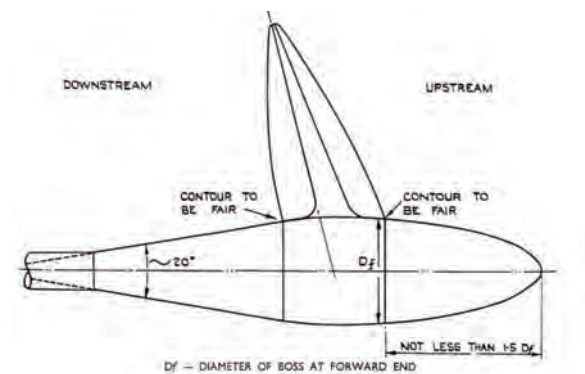


Figure 6 Propeller installation for open water test in a towing tank

The non-dimensional terms used to express the general performance characteristics are as follows:

Advance Coefficient $J = \frac{V_a}{nD}$ (2)

Thrust Coefficient $K_T = \frac{T}{\rho n^2 D^4}$ (3)

Torque Coefficient $K_Q = \frac{Q}{\rho n^2 D^5}$ (4)

Propeller Efficiency $\eta_0 = \frac{J K_T}{2\pi K_Q}$ (5)

To establish the non-dimensional groups involved in the open water test, Carlton^[3] used the principle of dimensional similarity applied to geometrically similar propellers. For the non-cavitating test, he inferred that

$$K_T = f(J, R_n), \tag{6}$$

$$K_Q = g(J, R_n). \tag{7}$$

This relation with the Reynolds number shows us that the numerical analysis is extremely important since we cannot always reproduce the same R_n of the prototype in the laboratory.

K_T and K_Q Polynomials for the Wageningen B-Series

The B-series open water test was carried out in the Netherlands Ship Model Basin in Wageningen. Oosterveld and van Oossanen published a paper^[4] presenting the open water characteristics of the B-series in polynomials obtained with the aid of a multiple regression analysis of the original test data.

The polynomials for K_T and K_Q derived with multiple regression analysis are

$$K_T = \sum_{n=1}^{39} C_n^T(J)^{s_n} \left(\frac{P}{D}\right)^{t_n} \left(\frac{A_E}{A_0}\right)^{u_n} (Z)^{v_n}, \tag{8}$$

$$K_Q = \sum_{n=1}^{47} C_n^Q(J)^{s_n} \left(\frac{P}{D}\right)^{t_n} \left(\frac{A_E}{A_0}\right)^{u_n} (Z)^{v_n}, \tag{9}$$

The coefficients C_n^T and C_n^Q and terms s_n, t_n, u_n, v_n are given in the paper^[4] for Reynolds number 2×10^6 .

It is shown in Figure 7 the open water test curves generated using the polynomials for the B3.80.

Reynolds number effect on propeller characteristics

The Reynolds number plays an important role in the characteristic curves of a propeller. Lerbs^[6] did a study on the effects of scale and roughness of propeller. In the example of characteristic curve shown in Figure 8, at the advance coefficient $J=0.225$, the percentage variations amount to:

$$\frac{\Delta K_T}{K_T} = 0.9\%, \tag{10}$$

$$\frac{\Delta K_Q}{K_Q} = -2.7\%, \tag{11}$$

$$\frac{\Delta \eta}{\eta} = 3.7\%. \tag{12}$$

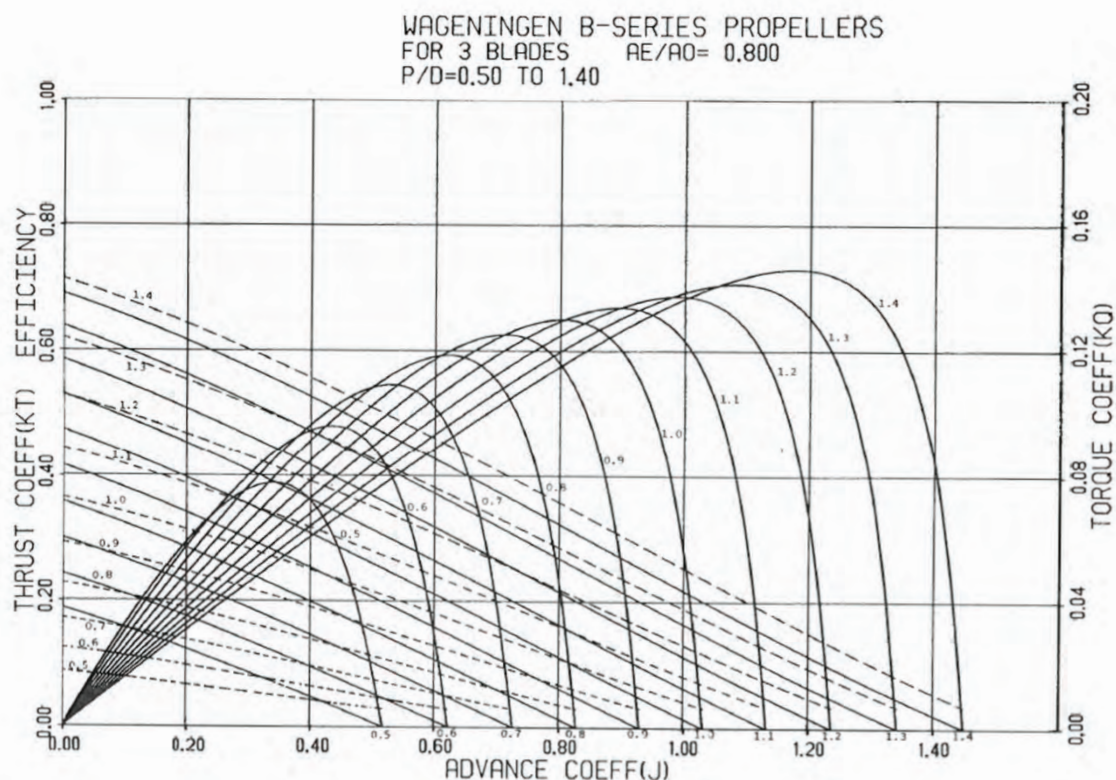


Figure 7 Open water curves for the B3.80 with different P/D , using polynomials^[5]

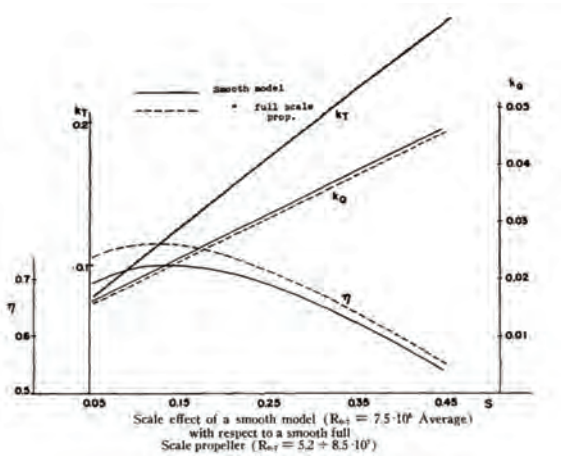


Figure 8 Open water curves for a specific propeller and its variation with Reynolds Number^[6]

That means that for a Reynolds number greater than 2×10^6 the open water characteristics should be corrected. For a Reynolds within the range 2×10^6 to 2×10^9 the following correction was derived:

$$\begin{cases} K_T(R_n) \\ K_Q(R_n) \end{cases} = \begin{cases} K_T(R_n = 2 \times 10^6) \\ K_Q(R_n = 2 \times 10^6) \end{cases} + \begin{cases} \Delta K_T(R_n) \\ \Delta K_Q(R_n) \end{cases} \quad (13)$$

Where ΔK_T and ΔK_Q are given in a polynomial form in the paper^[5] aforementioned.

These are empirical and theoretical corrections found for the B-series. The correction of the drag curve was done using the turbulent friction line as defined by the ITTC in 1957.

They are often used as benchmark, but when designing other propeller profiles we may not find so easy the curve characteristics. An experimental test may be very expensive and hardly will cover the prototype Reynolds number.

Numerical Analysis Domain

Because it is a steady-state simulation in which the Moving Reference Frame (MRF) was applied, two regions were created in the domain (Figure 9). The biggest one, called here as Static Region, is a big rectangular box containing the shaft of the propeller and the cylindrical region (Rotating Region). This smallest region contains the other parts of the propeller, i.e., the blades and hub.

Three different size domains were generated in order to do a domain study. The idea was to generate a domain that is neither too small that the boundary conditions could change the results nor too big that could increase computational cost in vain.

The domain main particulars are shown in Figure 10.

In the Table 1, the dimensions in metre of each domain analysed.

The results and which domain was chosen for the simulations will be shown later.

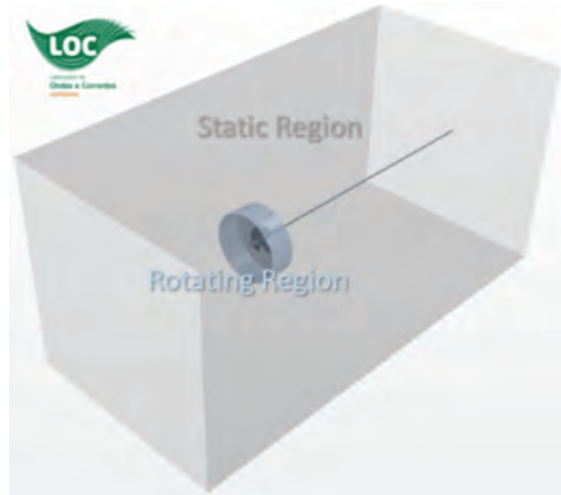


Figure 9 Domain divided in two regions

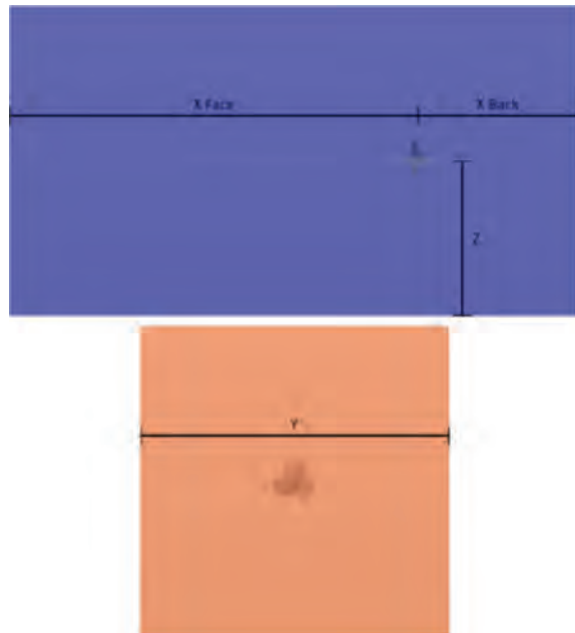


Figure 10 Main particulars of domain

Table 1 Dimensions of the three domains generated in metres (m)

	Small	Medium	Big
X Back	0.714	0.864	1.014
X Face	1.774	2.224	2.674
Y	1.2	1.68	2.16
Z	0.6	0.84	1.08

The Reynolds number plays an important role in the characteristic curves of a propeller.

Mesh

The mesh was created using hexahedral elements that are the most popular type of element as long as it brings better spatial accuracy for numerical solutions.

STAR-CCM+ works with a type of mesh that is called trimmed mesh. This method generates a high percentage of hexahedral cells and by splitting them, it is possible to quickly get a body-fitted mesh. A mesh of this type was generated in the mesh generator algorithm of STAR-CCM+ and is shown in Figure 11.

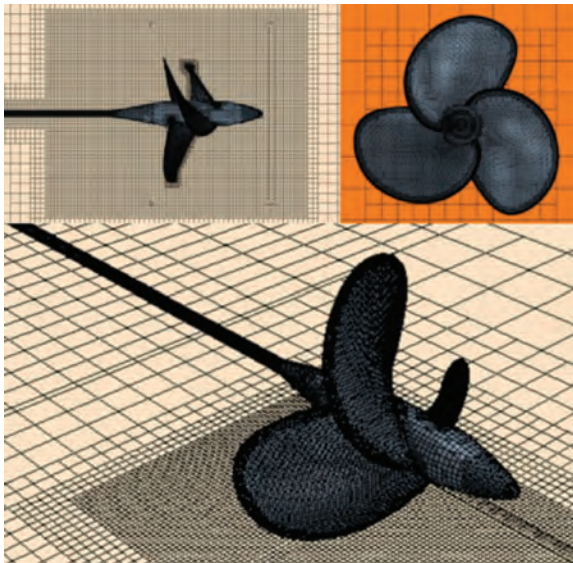


Figure 11 Trimmed mesh generated in STAR-CCM+ mesher

Some mesh parameters are shown in Table 2.

Table 2 Mesh parameters

Basic Size	8.64	mm	
Number of Prism Layer	5	-	
Prism Layer Thickness	1.728	mm	
Volumetric Control	Parameter	Value	Unit
Cylinder	Custom Size	4.32	mm

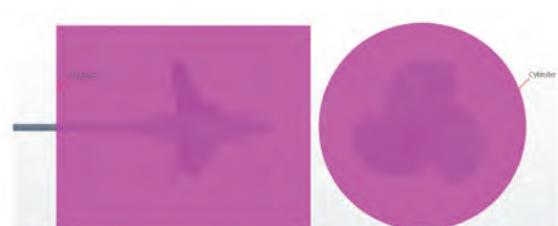


Figure 12 Volumetric controls for mesh refinement

Observing Figure 12, it is possible to understand the Volumetric Control shown in Table 2.

Due the importance of the boundary layer close to the blades and hub of the propeller, a prism mesh was created and in the Results section the values of y^+ at this region will be shown.

Turbulence Modelling

A comparison between two models of turbulence have been conducted with the same setup and geometry to choose the most suitable model to solve the studied case. The models analysed were the *Realizable* $\kappa-\epsilon$ and $\kappa-\omega$ SST. In the Results section the comparison will be shown.

Physical Setup

It is shown in Table 3 the main parameters set up for the simulation.

Table 3 Physical modelling general setup

Water	Density	997.0476
	Dynamic viscosity	8.90E-04
Time model	Steady	
Solver formulation	Segregated	
Coupling algorithm	SIMPLE	
Discretisation scheme	2nd order	
Reference pressure	1 atm	
Reference temperature	25°C	
Gravity	Diable	
Heat transfer	Isothermal	
Turbulence model	$\kappa-\epsilon$ / SST	
Motion	Moving Reference Frame (MRF)	

The Moving Reference Frame (MRF) is an efficient modelling technique for problems that involve both stationary and moving zones. It assumes that the volume has a speed of rotation and the interface is a surface of revolution.

In the Figure 13 it is shown the boundary conditions. The hub, blades and shaft are *Wall* and the far field is a *Symmetry*. The other two faces are the *Inlet* and the *Outlet*. The Table 4 presents the details of each boundary condition.

All the simulation were run using the commercial CFD software STAR-CCM+ (CD-Adapco), version 11.02.010, with double precision. They were run in a very modest computer with Windows 10 Professional (64 bits), processor Intel® Core™ i7-4790 CPU @ 3.60 GHz, 32 Gb RAM and 1 Tb of HD.

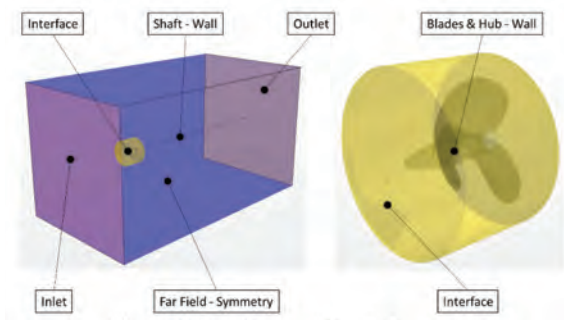


Figure 13 Boundary conditions in the domain

Table 4 Boundary conditions setup

Velocity	
V	$V_a = JnD$
V	0 m/s^2
W	0 m/s^2
Pressure Outlet	
Relative pressure	0.0 Pa
Wall	
No slip wall	
Smooth wall	

Verification And Validation

According to The American Institute of Aeronautics and Astronautics [7], the credibility of a solution in CFD is obtained by demonstrating acceptable levels of uncertainty and error. The levels of uncertainties and errors are defined through verification and validation assessments.

Verification assessment determines if the programming and computational implementation of the conceptual model is correct. It examines the mathematics in the models through comparison to exact analytical results. Verification is the process for assessing simulation numerical uncertainty U_{SN} .

Validation assessment determines if the computational simulation agrees with physical reality. It examines the science in the models through comparison to experimental results.

The ITTC [8] proposes a guideline for the overall CFD verification and validation procedures that are conveniently grouped in four consecutive steps: (1) preparation; (2) verification; (3) validation; (4) documentation.

The verification procedure is done by iterative and input parameters convergence studies that are conducted using multiple solutions with systematic parameters. The validation procedure is done comparing data and simulation values.

Verification

The recommended method for discretisation error estimation is the Richardson Extrapolation (RE) method.

Roache [9] has provided a methodology for the uniform reporting of grid refinement studies to find a Grid Convergence Index (GCI). This GCI method is based upon a grid refinement error estimator derived from the theory of generalised Richardson Extrapolation. This method can be summarised in some steps that will be described hereinafter. This sum of the method is better explained in the Journal of Fluids Engineering Editorial Policy [10]. The ITTC [11] uses a similar procedure that, at the end, led to the same result.

- Step 1: Define a representative mesh size h .
- Step 2: Select at least three significantly different set of grids, and run simulations to determine the values of key variables. Define the grid refinement factor $r_{\text{coarse, fine}} = h_{\text{coarse}}/h_{\text{fine}} > 1.3$. This value of 1.3 is based on experience and not on formal derivation.
- Step 3: Let $h_1 < h_2 < h_3$ and $r_{21} = h_2/h_1$, $r_{32} = h_3/h_2$ and calculate the apparent order p of the method.
- Step 4: Calculate the extrapolated values
- Step 5: Calculate the following error estimates, along with apparent order p :
 - Approximate relative error
 - Extrapolated relative error
- Step 6: Calculate the fine GCI

According to the ITTC [11] definition of variables, we have

$$U_G = GCI_{fine}^{ij} = 1.25e_a^{ij}/(r_{21}^p - 1). \quad (14)$$

where U_G is the grid uncertainty.

The numerical simulation uncertainty (U_{SN}) is composed of the grid uncertainty (U_G), time step uncertainty (U_T), iteration number uncertainty (U_I) and other possible parameter uncertainty (U_P), which gives the following expression,

$$U_{SN}^2 = U_G^2 + U_I^2 + U_T^2 + U_P^2 \quad (15)$$

Validation

Validation is the process for assessing simulation modeling uncertainty. It is performed by finding the comparison error $|E|$ that is given by the difference in the data D and simulation S values

$$|E| = |S - D|. \quad (16)$$

To determine if the validation has been achieved, $|E|$ is compared to the validation uncertainty U_V given by

$$U_V^2 = U_D^2 + U_{SN}^2, \quad (17)$$

where U_D is the experimental uncertainty and U_{SN} is the simulation numerical uncertainty.

If $|E| < U_V$, the combination of all the errors in D and S is smaller than U_V and validation is achieved at the U_V level. If $|E| > U_V$, the sign and magnitude of E can be used to make modelling improvements.

Results and Discussion

Domain Study

It was generated in three different domains with dimensions shown in Table 1 and the results have been tabulated as shown in Table 5

Table 5 Coefficient values for each advance coefficient and domain size

KT				10 KQ			
J	Small	Medium	Big	J	Small	Medium	Big
0.10	0.273	0.271	0.270	0.10	0.300	0.299	0.298
0.20	0.233	0.232	0.231	0.20	0.267	0.266	0.265
0.30	0.191	0.190	0.189	0.30	0.231	0.230	0.229
0.40	0.147	0.146	0.146	0.40	0.192	0.191	0.190
0.45	0.125	0.124	0.123	0.45	0.171	0.171	0.170
0.50	0.102	0.101	0.101	0.50	0.150	0.150	0.150
0.55	0.079	0.079	0.079	0.55	0.129	0.129	0.128
0.60	0.057	0.056	0.056	0.60	0.107	0.107	0.107
0.65	0.034	0.034	0.034	0.65	0.084	0.084	0.084
0.70	0.011	0.011	0.011	0.70	0.060	0.060	0.060

The relative variation can be seen in Table 6.

Table 6 Relative variation of the coefficients for each advance coefficient and domain size

KT				10 KQ			
J	Small	Medium	Big	J	Small	Medium	Big
0.10	-	-0.59%	-0.31%	0.10	-	-0.45%	-0.24%
0.20	-	-0.64%	-0.30%	0.20	-	-0.48%	-0.22%
0.30	-	-0.66%	-0.31%	0.30	-	-0.47%	-0.22%
0.40	-	-0.67%	-0.31%	0.40	-	-0.46%	-0.20%
0.45	-	-0.66%	-0.30%	0.45	-	-0.44%	-0.19%
0.50	-	-0.65%	-0.31%	0.50	-	-0.40%	-0.18%
0.55	-	-0.62%	-0.28%	0.55	-	-0.36%	-0.16%
0.60	-	-0.58%	-0.26%	0.60	-	-0.29%	-0.13%
0.65	-	-0.49%	-0.22%	0.65	-	-0.19%	-0.09%
0.70	-	0.00%	0.00%	0.70	-	0.00%	0.00%

The medium size already had a small variation in the results from the smallest domain (less than 1% for any advance coefficient). The number of cells did not change so much because most of cells are located in the very refined area around the propeller, due to this, the simulation duration time was almost the same for the three domains. The medium size was the chosen one.

Turbulence Modelling

There were tested two different kinds of turbulence model and the results are shown in Table 7 with the experimental results from the polynomials

The relative variation of the turbulence models results from the experimental results are shown in Table 8.

Table 7 Coefficient values for each advance coefficient (Different turbulence models and experimental)

KT				10 KQ			
J	K-epsilon	SST	Exp	J	K-epsilon	SST	Exp
0.10	0.271	0.271	0.266	0.10	0.299	0.300	0.312
0.20	0.232	0.232	0.228	0.20	0.266	0.266	0.276
0.30	0.190	0.190	0.188	0.30	0.230	0.230	0.236
0.40	0.146	0.146	0.146	0.40	0.191	0.191	0.193
0.45	0.124	0.123	0.124	0.45	0.171	0.171	0.172
0.50	0.101	0.101	0.102	0.50	0.150	0.150	0.150
0.55	0.079	0.079	0.080	0.55	0.129	0.129	0.129
0.60	0.056	0.056	0.057	0.60	0.107	0.108	0.107
0.65	0.034	0.034	0.034	0.65	0.084	0.085	0.086
0.70	0.011	0.011	0.012	0.70	0.060	0.061	0.066

Table 8 Relative variation of the coefficients for each advance coefficient and turbulence model

KT			KT		
J	K-epsilon	SST	J	K-epsilon	SST
0.10	1.28%	2.00%	0.10	-4.24%	-4.11%
0.20	1.51%	1.50%	0.20	-3.67%	-3.55%
0.30	0.80%	0.71%	0.30	-2.66%	-2.52%
0.40	0.03%	-0.18%	0.40	-1.35%	-1.13%
0.45	-0.42%	-0.71%	0.45	-0.75%	-0.46%
0.50	-0.79%	-1.19%	0.50	-0.26%	0.15%
0.55	-1.03%	-1.50%	0.55	-0.01%	0.52%
0.60	-1.08%	-1.64%	0.60	-0.46%	0.15%
0.65	-1.07%	-1.94%	0.65	-2.63%	-2.04%
0.70	-5.03%	-7.76%	0.70	-8.89%	-8.44%

In the thrust coefficient we can notice that the *Realizable* $\kappa-\epsilon$ had results closer to the experimental while for the torque coefficient the $\kappa-\omega$ SST had the closer ones.

The root mean square of each column has been tabulated as shown in Table 9.

Table 9 Root mean square of the relative variation for each turbulence model

KT		10 KQ	
K-epsilon	SST	K-epsilon	SST
1.91%	2.78%	3.57%	3.36%

The *Realizable* $\kappa-\epsilon$ has been recommended to study the propeller analysis in open water performance, so it has been selected in this study.

Verification

Using the domain size specified after the size study, it generated three different meshes. These meshes have different refinement and as the dimensions of the domain is the same, they have different number of cells too.

After generating the first mesh, the coarser, it was possible to calculate its representative mesh size h . Obeying the grid refinement factor r_{ij} minimum value of 1.3, the two other meshes were generated.

The setup for all the meshes were the same. After the solver process, it was possible to get the thrust and torque coefficients and the variation between each results.

Table 10 Coefficient values for each advance coefficient and refinement

KT				10 KQ			
J	Coarse	Medium	Fine	J	Coarse	Medium	Fine
0.10	0.264	0.271	0.275	0.10	0.294	0.299	0.301
0.20	0.228	0.232	0.237	0.20	0.263	0.266	0.269
0.30	0.188	0.190	0.192	0.30	0.228	0.230	0.231
0.40	0.145	0.146	0.147	0.40	0.189	0.191	0.192
0.45	0.123	0.124	0.124	0.45	0.170	0.171	0.171
0.50	0.101	0.101	0.102	0.50	0.149	0.150	0.150
0.55	0.078	0.079	0.079	0.55	0.128	0.129	0.129
0.60	0.056	0.056	0.057	0.60	0.106	0.107	0.107
0.65	0.034	0.034	0.034	0.65	0.084	0.080	0.084
0.70	0.011	0.011	0.011	0.70	0.060	0.060	0.060

It is shown in Table 10 the coefficient values for each advance coefficient and it is shown their variation in Table 11.

The simulation duration time did increase considerably due to the refinement. Since the results of the medium refinement had already less than 3% of difference from the results of the coarser mesh, for any advance coefficient, the medium refinement mesh was the chosen one.

Following the math procedure explained above, it was possible to get the GCI for thrust and torque coefficient in each advance coefficient for the medium refinement mesh. The results are shown in Table 12.

Table 11 Relative variation of the coefficients for each advance coefficient and refinement

KT				10 KQ			
J	Coarse	Medium	Fine	J	Coarse	Medium	Fine
0.10	-	2.65%	1.52%	0.10	-	1.69%	0.72%
0.20	-	1.56%	2.09%	0.20	-	1.03%	1.33%
0.30	-	1.09%	0.99%	0.30	-	0.88%	0.66%
0.40	-	0.73%	0.67%	0.40	-	0.72%	0.148%
0.45	-	0.58%	0.38%	0.45	-	0.63%	0.29%
0.50	-	0.53%	0.31%	0.50	-	0.53%	0.29%
0.55	-	0.61%	0.31%	0.55	-	0.52%	0.26%
0.60	-	0.70%	0.39%	0.60	-	0.57%	0.19%
0.65	-	0.93%	0.70%	0.65	-	0.61%	0.10%
0.70	-	2.92%	2.85%	0.70	-	0.85%	0.06%

Table 12 Grid uncertainty for each advance coefficient of the medium refinement mesh

J	KT	KQ
0.10	4.79%	1.64%
0.20	5.16%	4.18%
0.30	17.33%	3.48%
0.40	11.52%	1.82%
0.45	1.41%	0.67%
0.50	0.95%	0.83%
0.55	0.84%	0.67%
0.60	1.14%	0.37%
0.65	3.80%	0.15%
0.70	9.57%	0.09%

This calculated uncertainty is just related to the refinement of the mesh, so it is what was called the grid uncertainty (U_G). Time step uncertainty (U_t), iteration number uncertainty (U_i) and other possible parameter uncertainty (U_p), was not quantified due to the lack of machine resources to run countless simulations in a reasonable time. The most common analysis of uncertainty is based on grid refinement, so it was done. Therefore, we can infer that

$$GCI = U_G = U_{SN} \tag{18}$$

The verification procedure of assessing simulation numerical uncertainty U_{SN} was completed.

Validation

For the validation procedure, it would be necessary to calculate the experimental uncertainty. Due to the lack of data recorded from the experiments, it is impossible to calculate the uncertainty based on the equipment used and measurements done. Despite that, it is known that the tests were done with a Reynolds number lower than 2×10^6 and then the drag curve was corrected for this difference. The correction was done using the turbulence friction line as defined by the ITTC in 1957.

Table 13 Numerical and experimental coefficients for the B3.80 ($P/D=0.7$).

J	CFD		Experimental
	KT	Uncertainty	KT
0.10	0.2709	0.0130	0.2657
0.20	0.2319	0.0120	0.2285
0.30	0.1899	0.0329	0.1884
0.40	0.1462	0.0168	0.1461
0.45	0.1238	0.0017	0.1243
0.50	0.1014	0.0010	0.1022
0.55	0.0789	0.0007	0.0797
0.60	0.0565	0.0006	0.0571
0.65	0.0340	0.0013	0.0343
0.70	0.0109	0.0010	0.0115

J	CFD		Experimental
	10 KQ	Uncertainty	10KQ
0.10	0.2991	0.0049	0.3124
0.20	0.2658	0.0111	0.2759
0.30	0.2295	0.0080	0.2358
0.40	0.1909	0.0035	0.1935
0.45	0.1706	0.0011	0.1719
0.50	0.1498	0.0012	0.1502
0.55	0.1286	0.0009	0.1286
0.60	0.1069	0.0004	0.1074
0.65	0.0842	0.0001	0.0865
0.70	0.0603	0.0001	0.0662

Now, we are just concerned with the comparison between the numerical simulation and the experimental data considering just the calculated grid uncertainty. In Table 13, we can see the numerical result for the coefficients, its uncertainty and the correspondent experimental data.

The validation uncertainty is given by,

$$U_V^2 = U_D^2 + U_{SN}^2 = U_G^2 \therefore U_V = U_G \tag{19}$$

With all these values from Table 13 it is possible to complete the validation procedure. Table 14 summarises these values and confirm that some results were validated as can be noted that for the cases that $|E| < U_v$.

Most of the advance coefficients were validated just considering the grid uncertainty. If we consider that the

Table 14 Validation of the propeller B3.80 (without experimental uncertainty).

J	KT			KQ		
	E	U_v	Validated	E	U_v	Validated
0.10	0.0052	0.0130	Yes	0.0133	0.0049	No
0.20	0.0035	0.0120	Yes	0.0101	0.0111	Yes
0.30	0.0015	0.0329	Yes	0.0063	0.0080	Yes
0.40	0.0000	0.0106	Yes	0.0026	0.0035	Yes
0.45	0.0005	0.0017	Yes	0.0013	0.0011	No
0.50	0.0008	0.0010	Yes	0.0004	0.0012	Yes
0.55	0.0008	0.0007	No	0.0000	0.0009	Yes
0.60	0.0006	0.0006	Yes	0.0005	0.0004	No
0.65	0.0004	0.0013	Yes	0.0023	0.0001	No
0.70	0.0006	0.0010	Yes	0.0059	0.0001	No

Table 15 Validation of the propeller B3.80 considering experimental uncertainty (with experimental uncertainty of 0.6%).

J	KT			KQ		
	E	U_v	Validated	E	U_v	Validated
0.10	0.0052	0.0179	Yes	0.0133	0.0133	Yes
0.20	0.0035	0.0172	Yes	0.0101	0.0166	Yes
0.30	0.0015	0.0351	Yes	0.0063	0.0147	Yes
0.40	0.0000	0.0209	Yes	0.0026	0.0128	Yes
0.45	0.0005	0.0124	Yes	0.0013	0.0124	Yes
0.50	0.0008	0.00124	Yes	0.0004	0.0124	Yes
0.55	0.0008	0.0123	Yes	0.0000	0.0124	Yes
0.60	0.0006	0.0123	Yes	0.0005	0.0123	Yes
0.65	0.0004	0.0124	Yes	0.0023	0.0123	Yes
0.70	0.0006	0.0124	Yes	0.0059	0.0123	Yes

experimental uncertainty is more than 0.6% for any J , all the results will be validated, as it is shown in Table 15. In addition, there is the fact that the numerical uncertainty is not only given by the grid uncertainty. It was supposed to consider other means of uncertainties.

In this way, we can affirm that the validation was achieved.

Numerical Results
Open Water Curves

The most important result of an open water test is the graphic showing the open water curves of the propeller. It is shown in Figure 14 the experimental and numerical curves (with uncertainty) for the B3.80.

The numerical results show a fairly good agreement with the experimental data, especially for the advance coefficients around the best efficiency. There is a need to do more research in order to understand why the torque coefficient had a greater difference for lower values of advance coefficient. It may be showing the importance of a cavitation analysis for a better result in this region.

Pressure Distribution

The pressure difference between the face side and the back side is the major contribution for the thrust force. It is shown in Figure 15 the pressure distribution in the face and back side of the propeller in an advance coefficient $J=0.5$, that is in the region of the most efficient advance for the B3.80.

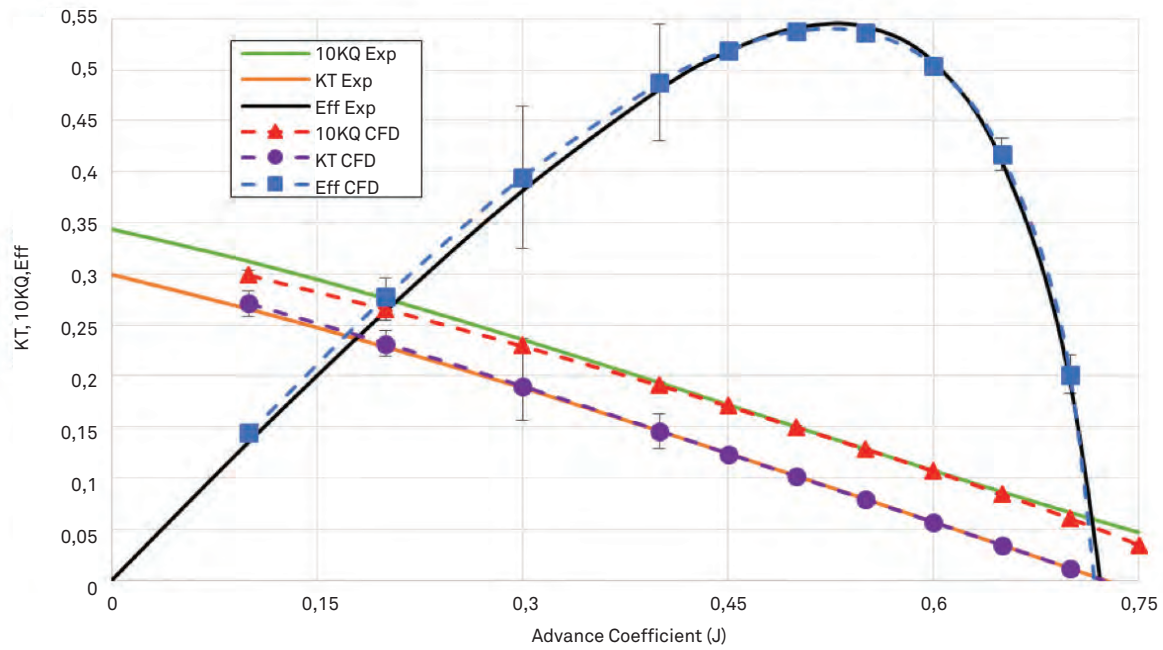


Figure 14 Experimental and numerical (with uncertainty) open water curves for the B3.80

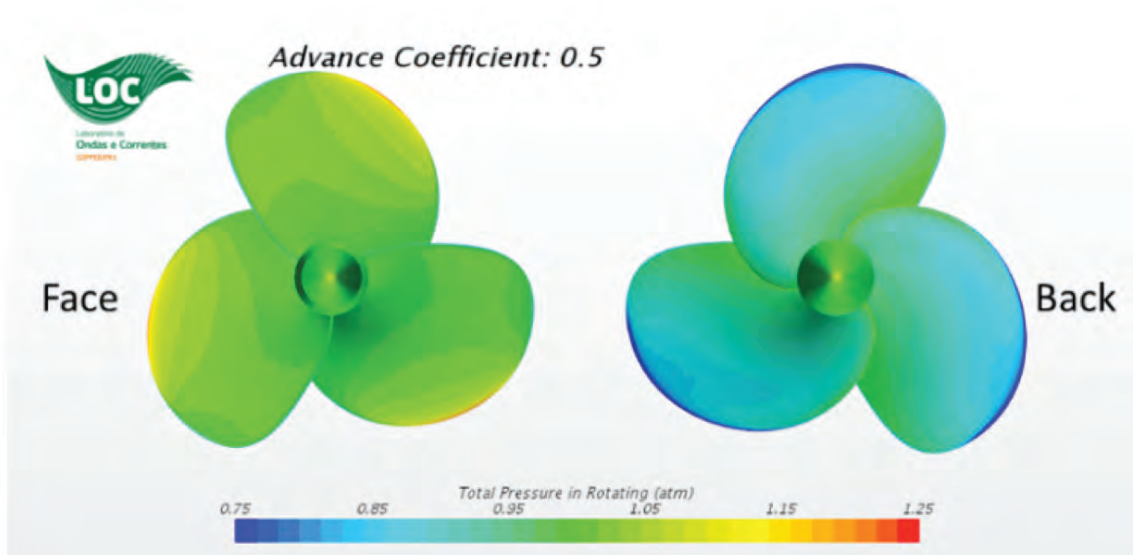


Figure 15 Pressure distribution for $J=0.5$

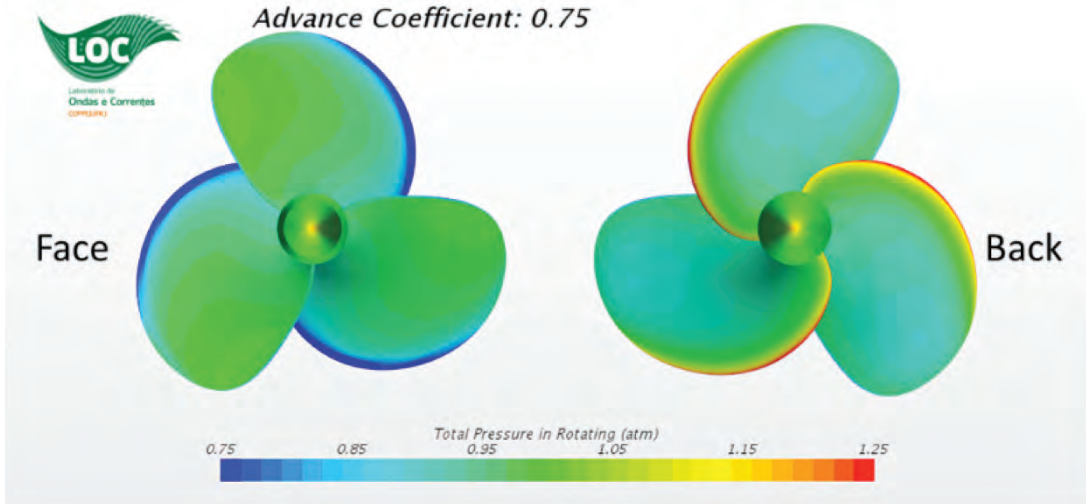


Figure 16 Pressure distribution for J=0.75

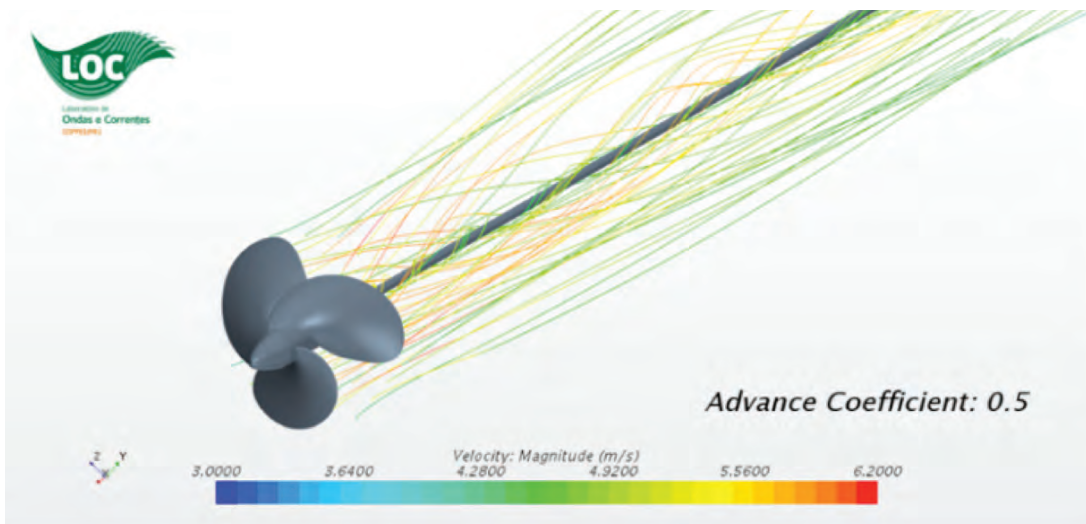


Figure 17 Streamline for J=0.5

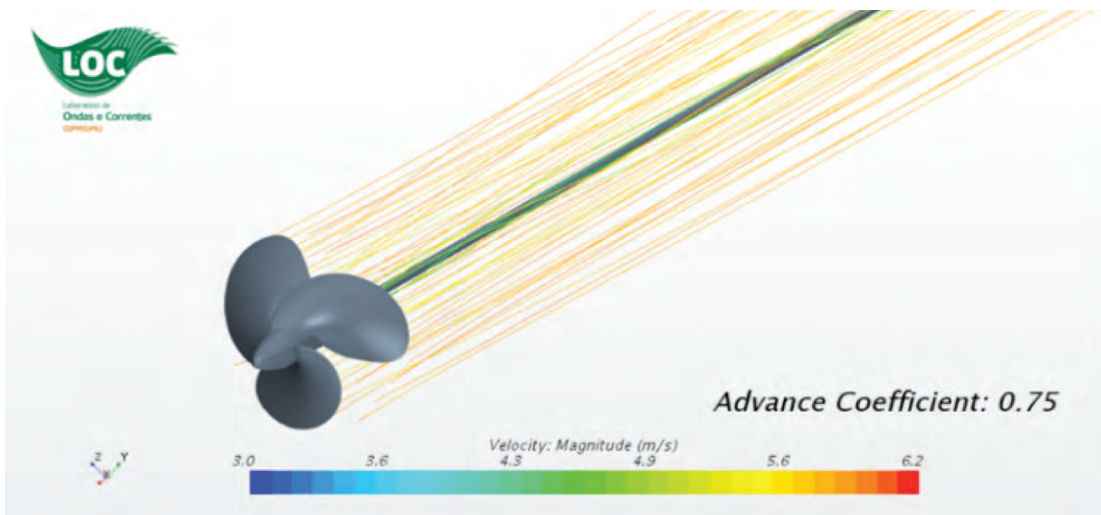


Figure 18 Streamlines for J=0.75

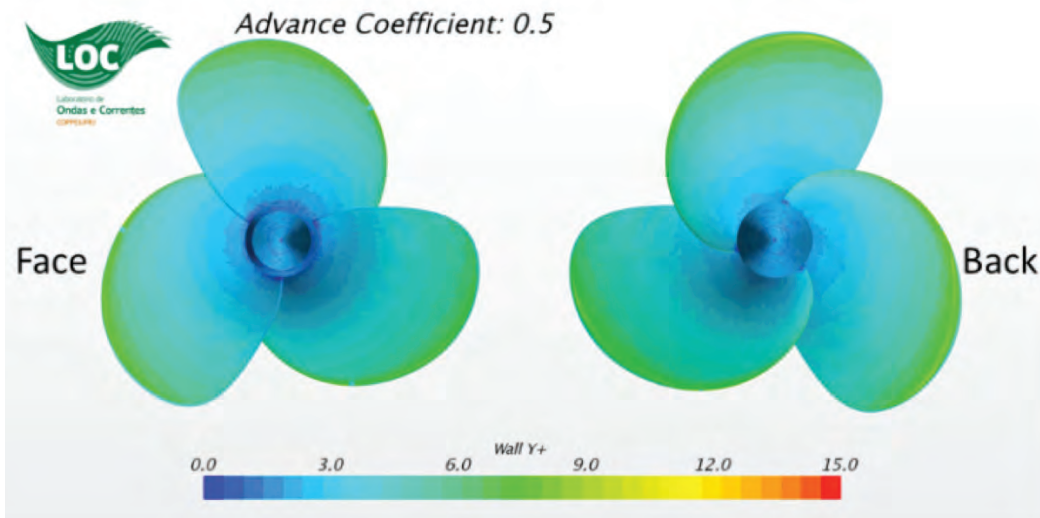
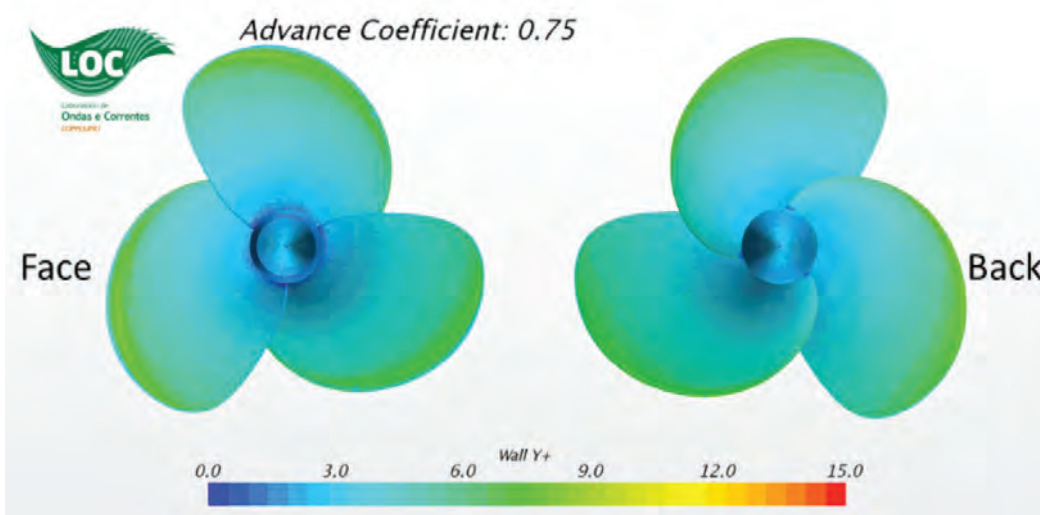
Figure 19 Wall y^+ for $J=0.5$ Figure 20 Wall y^+ for $J=0.75$

Figure 16 shows the pressure distribution for an advance coefficient $J=0.75$. In this case, we can notice that the pressure is higher in the back side. Looking at Figure 14, we can see that this is the advance coefficient which the efficiency begins to be negative.

Streamlines

Another interesting result to observe is the streamlines. In Figure 17, it is shown for $J=0.5$.

In Figure 18, it is shown for $J=0.75$. It is interesting to notice that the streamlines tend to maintain an undisturbed motion passing close to the propeller. It happens because the advance speed is getting higher as

the J gets higher and so its components are less sensitive to the rotational speed components.

Y Plus (y^+)

The importance of the y^+ is related with the capacity to solve the boundary layer in the body. It is of a big importance to have good values of y^+ at the blades and hub. In Figure 19, it is shown for the $J=0.5$ and in Figure 20, it is shown for $J=0.75$.

It is possible to see that in just a few regions the y^+ is greater than 5.0. It is a good mesh to consider that the boundary layer is being calculated.

The numerical results show a fairly good agreement with the experimental data, especially for the advance coefficients around the best efficiency.

Conclusions

The main purposes of this work were to show the importance of the numerical simulation for the propeller design and show the steps to obtain suitable results using CFD.

To perform this task the open water characteristics of a Wageningen B-series propeller were investigated. First, the propeller geometry needed to be designed and for that a tool was developed in Excel to generate the points cloud for creating surfaces in CAD software. This tool has been developed for any type of B-series propeller design, thus presenting an importance for future work.

Another detail raised in this study is the importance of analysing the Reynolds number that the prototype of the propeller will work. Rarely experiments can be done on the correct Reynolds number and some corrections may depend on empirical results. Depending on the propeller, these results may not exist.

Having demonstrated the importance of the numerical analysis, the steps to carry it out were shown. It is important to start with a domain study to be sure that your results are not being modified by the boundaries or even that it is taking a long time to converge. Then, it was shown the possibility of doing an analysis of the turbulence model to obtain better simulation results.

The verification assessment for calculating numerical uncertainty is very important, since most of the poor numerical results are due to poor mesh design and this assessment helps to avoid this.

The validation assessment is the comparison between the numerical and the real experimental result. In this work, the lack of data of experimental uncertainty did not allow an adequate interpretation of the results. In any case, even considering only the grid uncertainty, most of the numerical results were validated directly against the experimental results, thus proving that the simulation mesh and the set up are well defined.

Finally, some results that cannot be easily obtained in experiments were shown.

Future Proposals

The simulation was done in a steady state condition and for future simulation it would be interesting to see the variation when considering a transient simulation.

Considering the motion of the body rather than using a reference frame analysis is possible when doing a transient simulation also.

A multiphase simulation that considers water vapour to see if cavitation is occurring and how it can change the results.

In summary, this work brings the knowledge and the fundamentals for this kind of simulation. With that, the idea is to continue trying some new profile, trying to think of new variations that could be applicable and use it to improve the industry.

References

- [1] G. Kuiper, The Wageningen Propeller Series, Wageningen: MARIN, 1992.
- [2] ITTC, "Testing and Extrapolation Methods Propulsion, Propulsor Open Water Test," in International Towing Tank Conference - ITTC, 2008.
- [3] J. Carlton, Marine Propellers and Propulsion, Elsevier, 2007.
- [4] M. W. C. Oosterveld and P. van Oossanen, "Further Computer-Analyzed Data of the Wageningen B-Screw Series," Netherlands Ship Model Basin, Rotterdam, 1975.
- [5] M. M. Bernitsas, D. Ray and P. Kinley, "Kt, Kq and Efficiency Curves for the Wageningen B-Series Propellers," The University of Michigan, Ann Arbor, 1981.
- [6] H. W. Lerbs, "On the Effects of Scale and Roughness on Free Running Propellers," Journal of the American Society for Naval Engineers, vol. 63, no. 1, pp. 58-94, 1951.
- [7] AIAA, Guide for the Verification and Validation of Computational Fluid Dynamics Simulations, AIAA, 1998.
- [8] ITTC, "CFD, General Uncertainty Analysis in CFD, Guidelines for RANS Codes," in International Towing Tank Conference - ITTC, 1999.
- [9] P. J. ROACHE, "Verification and Validation in Computational Science and Engineering," Hermosa publishers, 1998.
- [10] B. I. CELIK, Procedure for Estimation and Reporting of Discretization Error in CFD Applications, Morgantown.
- [11] ITTC, "Uncertainty Analysis in CFD - Verification and Validation Methodology and Procedures," in International Towing Tank Conference - ITTC, 2008.

Author's Contact

- | lucas.machado@kfelsbrasil.com.br
- | acfernandes@oceanica.ufrj.br

Acknowledgments

This work is a joint effort between Keppel Offshore & Marine Technology Centre (KOMtech) and Laboratório de Ondas e Correntes (LOC – COPPE/UFRJ).

Optimising Semisubmersible Hull Design to Minimise Motion and Load in Wave

| Wei XU¹, BEng

| Shengchao JIANG², PhD, BEng

| Aziz MERCHANT¹, MSc, BEng

| Ankit CHOUDHARY¹, MSc, BEng

| Anis HUSSAIN¹, MSc, BEng

¹Keppel Offshore and Marine Technology Centre

²Department of Civil and Environmental Engineering, National University of Singapore, Singapore

Semi-submersible platforms have been widely used based on their various advantages such as wide range of operational water depth, great performance of stability and good drilling capabilities. As the exploitation of offshore oil and gas resources extends to deep water or harsh environment seas, the optimisation of semi-submersible hull form can either reduce the initial sunk cost or improve the uptime which can bring economic value to the clients. This project focuses on the heave motion and mean wave drift force optimisation of semi-submersibles. The first-order potential theory analysis is used to determine the optimal case from a number of possibilities. The parametric optimisation is carried out to study the impact of change in column shape, centre column diameter, pontoon shape, etc. This article starts with introduction of the state of art of hull optimisation and the fundamental theory used to calculate those quantities of the optimisation objectives. Then case study and application are demonstrated. The last section is the conclusion and recommendation for future work.

Introduction

Important business strategies on deepwater technology are directed towards the design of floaters to increase the operability window in challenging and harsh environments, including ultra-deep waters. To meet the challenges and increase product line, there is interest to offer a suite of drilling and production semi-submersible designs with enhanced performance by reducing motions, thereby allowing operations with larger uptime window. In this aspect, the heave Response Amplitude Operator (RAO) is quite important parameters. In addition, environmental loads, especially wave drift load, need to be minimised to reduce the cost of riser and mooring systems.

In order to reduce the heave RAO and mean drift force of a semisubmersible hull, a lot of work have been carried out in recent years. Goncalves et al. (2010) [1] investigated a new concept for a monocolumn floating unit, aimed at exploring and producing oil in ultradeep waters. Hong et al. (2013) [2] analysed the steady roll motion of a semi-submersible with shallow draft in regular waves. Voogt et al. (2002) [3] demonstrated how the findings of a series of model tests and diffraction calculations, performed to determine the motion behavior of a new semi-submersible design were used to influence the final design. Spahaier et al. (2007) [4] performed a series of tests with a model of a monocolumn platform with a moonpool, with the objective of determining the entrance area at the bottom of the moonpool that minimises vertical motion in waves.

Matsumoto et al. (2008) [5] investigated the influence at vertical first order motions using appendages in a monocolumn platform. Generally, the optimisation can be performed in two steps: (1) critical assessment of existing concepts and technologies used in various complex hull designs, and (2) development and adaptation of these design concepts and technologies to optimise existing semi-submersible designs for harsh environment. The latter one is the major target of this paper.

The aim of this paper is the reason of heave RAO and mean drift force according to optimising the semi-submersible hull. Various types of proposed semi-submersibles are carried out, including the column shape, centre column and pontoon shape. According to the optimisation mentioned above, the influence of them on heave motion and mean drift force are investigated.

Mathematical Model

Linear Potential Theory Model

A Cartesian coordinate system $\vec{X} = (x,y,z)$ is defined with $z = 0$ for the plane of the undisturbed free surface. It is assumed that the fluid is incompressible and inviscid, and the flow is irrotational. The fluid velocity potential $\phi(\vec{X},t)$ satisfying the Laplace equation in the fluid domain,

$$\frac{\partial^2 \phi(\vec{X},t)}{\partial x^2} + \frac{\partial^2 \phi(\vec{X},t)}{\partial z^2} = 0 \tag{1}$$

As in Fig. 1, the fluid depth is finite. The portion of the body below the plane $z = 0$ is referred to as the submerged surface S_B . This surface is assumed to be impermeable, with its normal velocity equal to the normal component of the fluid velocity. At far-field from the structure, the waves are composed of prescribed incident waves and outgoing waves associated with diffraction and radiation.

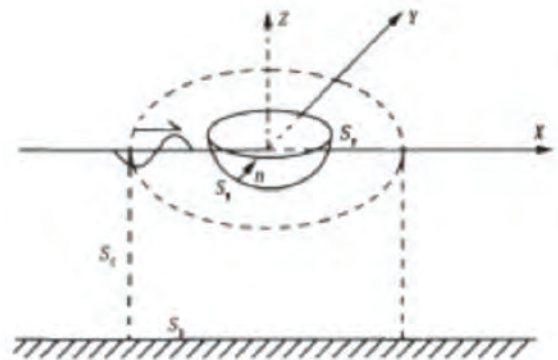


Figure 1 Definitions of computational domain and boundaries

Under the assumption of small, unsteady motions relative to the wavelength, the free surface boundary condition can be linearised about its mean position. The body boundary condition can also be linearised about its mean position if the structure is not fixed. Owing to the time harmonic dependence, the use of a complex notation for all oscillatory quantities is applied. Thus the velocity potential is expressed as:

$$\phi(\vec{X},t) = \text{Re}\{\phi e^{-i\omega t}\} \tag{2}$$

where ω is the incident regular wave angular frequency or angular frequency of body motion. The complex spatial potential ϕ , must satisfy the following linearised free surface S_F , body surface S_B and infinite seabed boundary conditions besides the Laplace equation:

$$\frac{\partial \phi}{\partial z} = \frac{\omega^2}{g} \phi, \quad \text{on } S_F \tag{3}$$

$$\frac{\partial \phi}{\partial n} = v_n, \quad \text{on } S_B \tag{4}$$

$$\frac{\partial \phi}{\partial n} = 0, \quad \text{on } S_D \tag{5}$$

where g is the acceleration owing to the gravity, n and v_n are the unit normal vector and the normal velocity of points on the body surface, respectively. Generally, n points out of the fluid domain and thus towards the inside of the body. The linearisation permits the decomposition of the velocity potential in the alternative forms:

$$\phi = \phi_i + \phi_d + \phi_r \tag{6}$$

where ϕ_i is the potential of the incident wave, defined by:

$$\phi_i = \frac{igA \cosh k(z+d)}{\omega \cosh kd} e^{ik(x \cos \beta + y \sin \beta)} \tag{7}$$

where A is the wave amplitude, and β is the incident wave angle. The wave number k is the positive real root of the dispersion relation. Except for the incident wave potential ϕ_i , all the other wave components are needed to satisfy the radiation condition of outgoing waves in the far field, i.e., the Sommerfeld condition.

In equation (6), the diffraction potential ϕ_d and the radiation potential ϕ_r , owing to the presence of the body, are subject to their boundary conditions as follows:

$$\frac{\partial \phi_d}{\partial \mathbf{n}} = -\frac{\partial \phi_l}{\partial \mathbf{n}}, \quad \text{on } S_B \quad (8)$$

$$\frac{\partial \phi_r}{\partial \mathbf{n}} = v_{n_j}, \quad \text{on } S_B \quad (9)$$

The radiation potential ϕ_r represents the fluid disturbance due to the motions of the body and can be expressed in the form:

$$\phi_r = \sum_{j=1}^6 -i\omega \xi_j \phi_j \quad (10)$$

Where (ξ_1, ξ_2, ξ_3) are the amplitudes of body translation and (ξ_4, ξ_5, ξ_6) are the amplitudes of body rotation. ϕ_j is the radiation potential corresponding to a unit body velocity in the j^{th} body degree of freedom. By substituting equation (10) into (9), the boundary condition of the body surface is then expressed in the following form:

$$\frac{\partial \phi_j}{\partial \mathbf{n}} = n_j, \quad \text{on } S_B \quad (11)$$

Where (n_1, n_2, n_3) are the unit normal vector of the body surface and $(n_4, n_5, n_6) = (\mathbf{x} - \mathbf{x}_0) \times \mathbf{n}$ are the coordinates of the rotation centre. Similarly, note $\phi_0 = \phi_i$ and $\phi_7 = \phi_d$ the body conditions of diffraction radiation potential, which can be written together as follows:

$$\frac{\partial \phi_j}{\partial \mathbf{n}} = \begin{cases} n_j, & j = 1, \dots, 6 \\ -\frac{\partial \phi_0}{\partial \mathbf{n}}, & j = 7 \end{cases} \quad (12)$$

The infinite depth free surface Green function $G(\mathbf{x}, \mathbf{x}_0)$ is used as follows:

$$G = G_T + G_H \quad (13)$$

$$G_T = -\frac{1}{4\pi} \left(\frac{1}{r_1} + \frac{1}{r_2} \right) \quad (14)$$

$$G_H = \frac{1}{4\pi} \int_0^\infty \frac{2(v + \mu)e^{-\mu d} \cosh \mu(z + d) \cosh \mu(z - d_0) J_0(\mu R) d\mu}{v \cosh \mu d - \mu \sinh \mu d} \quad (15)$$

Where $r_1 = [R^2 + (z - z_0)^2]^{\frac{1}{2}}$, $r_2 = [R^2 + (z + z_0 + 2d)^2]^{\frac{1}{2}}$ and R is the horizontal distance between field and source points. $v = \omega^2/g$ is the wave number in deep water. In the development of the Green function computation, important works on the approximation of free-surface Green functions have been instructive by Noblesse (1982)^[6] and Newman (1992)^[7]. Applying the second Green's theorem to potential Φ and the Green function $G(\mathbf{x}, \mathbf{x}_0)$, we can obtain the boundary integral equation as follows:

$$\alpha \phi_j(\mathbf{x}_0) - \iint_{S_B} \frac{\partial G(\mathbf{x}, \mathbf{x}_0)}{\partial \mathbf{n}} \phi_j(\mathbf{x}) dS = \begin{cases} -\iint_{S_B} n_j G(\mathbf{x}, \mathbf{x}_0) dS, & j = 1, \dots, 6 \\ \iint_{S_B} G(\mathbf{x}, \mathbf{x}_0) \frac{\partial \phi_0(\mathbf{x})}{\partial \mathbf{n}} dS, & j = 7 \end{cases} \quad (16)$$

Where the free term α is the solid angle coefficients. Its value changes with the position of the source point \mathbf{x}_0 and it is $\frac{1}{2}$. A set of linear equations are obtained after the integral equation (16) discretised.

Diffraction and radiation potentials on the body surface can be resolved from the set of linear equations. Then the exciting forces and hydrodynamic coefficients are obtained by Bernoulli's equation and integration of wave pressure over the body surface. The exciting forces can be written into:

$$F = \text{Re} [f^{(1)} e^{-i\omega t} + f^{(2)} e^{-2i\omega t}] \quad (17)$$

$$f^{(1)} = i\omega \rho \iint_{S_B} (\phi_0 + \phi_7) \cdot \bar{\mathbf{n}} dS \quad (18)$$

$$\omega^2 a_{ji} + i\omega b_{ji} = \omega^2 \rho \iint_{S_B} \phi_j n_i dS, \quad i, j = 1, \dots, 6 \quad (19)$$

Where a_{ji} and b_{ji} are added mass and radiation damping, respectively.

Furthermore, the mean drift force can be calculated by:

$$\bar{f}^{(2)} = -\frac{\rho}{4} \iint_{S_B} \nabla \phi \cdot \nabla \phi^* \cdot \bar{\mathbf{n}} dS + \frac{\rho \omega^2}{4g} \oint_{WL} \phi \phi^* \cdot \bar{\mathbf{n}} dS \quad (20)$$

Where ϕ^* is the conjugate of potential ϕ . Equation (20) is near-field method. Besides to this method, a far-field method can also be adopted for mean drift force:

$$\bar{f}_x^{(2)} = -\frac{\rho g A^2 C_g}{k C} \left\{ \int_0^{2\pi} \cos \theta |A_s(\theta)|^2 d\theta + 2 \text{Re} \{A_s(\theta)\} \right\} \quad (21)$$

$$\bar{f}_y^{(2)} = -\frac{\rho g A^2 C_g}{k C} \int_0^{2\pi} \sin \theta |A_s(\theta)|^2 d\theta \quad (22)$$

$$\bar{M}_z^{(2)} = -\frac{\rho g A^2 C_g}{k C} \left\{ \int_0^{2\pi} \text{Re} \left\{ A_s(\theta) \frac{\partial A_s^*(\theta)}{\partial \theta} \right\} d\theta - \text{Re} \left\{ \frac{\partial A_s(\theta)}{\partial \theta} \right\} \Big|_{\theta=\beta} \right\} \quad (23)$$

Where $A_s(\theta)$ is the amplitude of scattered wave, C and C_g is the phase velocity of wave and wave group, respectively. Generally, the far-field method is more accurate than near-field method due to avoiding of the complex space derivative computation over the body surface.

For field points in the fluid, it is straightforward to evaluate the potential as given by equation (16) with the solid-angle coefficients being unity. The appropriate representations in this case are:

$$\phi_j(\mathbf{x}_0) = \iint_{S_B} \frac{\partial G(\mathbf{x}, \mathbf{x}_0)}{\partial \mathbf{n}} \phi_j(\mathbf{x}) dS + \begin{cases} -\iint_{S_B} n_j G(\mathbf{x}, \mathbf{x}_0) dS, & j = 1, \dots, 6 \\ \iint_{S_B} G(\mathbf{x}, \mathbf{x}_0) \frac{\partial \phi_0(\mathbf{x})}{\partial \mathbf{n}} dS, & j = 7 \end{cases} \quad (24)$$

And then, the wave elevation can be written as:

$$\zeta = \text{Re}[\eta(x, y)e^{-i\omega t}] \tag{25}$$

$$\eta(x, y) = \frac{i\omega}{g} \sum_{j=0}^7 \phi_j \tag{26}$$

The mean wave drift quadratic transfer functions (QTFs) are calculated by the diffraction model. The formulae for calculating the mean wave drift force and moment are as follows:

$$F_{waves_{x,y}} = 2 \int_0^{\infty} S_{\eta}(\omega) \times QTF_{x,y}(\omega) \times d\omega \tag{27}$$

$$QTF_{x,y}(\omega) = \frac{F_{x,y}}{\eta_a^2}(\omega) \tag{28}$$

$$F_{waves_{total}} = \sqrt{F_{waves_x}^2 + F_{waves_y}^2} \tag{29}$$

$$M_{waves_{x,y}} = 2 \int_0^{\infty} S_{\eta}(\omega) \times QTF_{\phi}(\omega) \times d\omega \tag{30}$$

Where F and M are the force and moment respectively, $S_{\eta}(\omega)$ is spectral density of waves in $m^2/(rad/s)$.

Software Program

The commercial software HydroStar is used as the tool of linear diffraction tool. HydroStar is the hydrodynamic software developed in Bureau Veritas since 1991 that provides a complete solution of first order problem of wave diffraction and radiation and also the QTF of second order low-frequency wave loads for floating body with or without forward speed in deep water and in finite water depth.

Case Study

Hull optimisation twin pontoon semi – heave motion & mean wave drift force

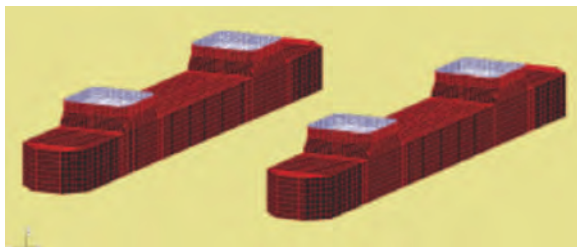


Figure 2 Panel model of semi-submersible hull

The optimisation of two important hydrodynamic behaviour i.e. heave motion and mean wave drift force under three incident wave directions - 0, 45 and 90 deg, are carried out. The objective is to obtain an improved new semi hull having lower heave second hump and lower mean drift force under irregular waves. There are

three optimising schemes, which are column shape, centre column and pontoon shape as in Figure 3. The displacement of the semi-submersible are kept the same, i.e. 3.2×10^4 m³. The radius of gyration and the COG are also assumed the same. This assumption is to simplify the optimisation work for direct comparison purpose.

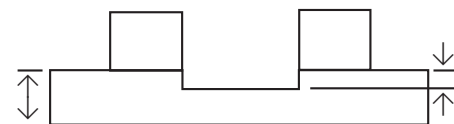
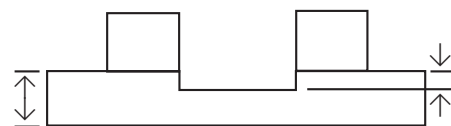
Main Dimensions of the Vessel	
Length Pontoons (m)	113
Breadth outside pontoons (m)	69
Pontoon Breadth (m)	14.5
Pontoon Height (m)	8.8
Column Breadth (m)	14.5
Column Length (m)	14.5
Draft (m)	14
Longitudinal Distance Between of Columns (m)	57
Transverse Distance Between of Columns (m)	55
Pontoon Corner Radius (Profile) (m)	4
Pontoon Corner Radius (Plan) (m)	2
Column Cornear Radius (m)	2
Centre of mass (m)	(2.53, 2.29, 7.84)
Mass of Semi-submersible (kg)	3.2×10^7
Radius of gyratio (m)	(26.9, 29.2, 33.4)



(a) Column shape



(b) Centre column



(c) Pontoon shape

Figure 3 Three optimisation schemes (a), (b), (c)

The optimisation of two important hydrodynamic behavior i.e. heave motion and mean wave drift force under three incident wave directions - 0, 45 and 90 deg, are carried out. The objective is to obtain an improved new semi hull having lower heave second hump and lower mean drift force under irregular waves. There are three optimising schemes, which are column shape, centre column and pontoon shape as in Figure 3. The displacement of the semi-submersible are kept the same, i.e. $3.2 \times 10^4 \text{ m}^3$. The radius of gyration and the COG are also assumed the same. This assumption is to simplify the optimisation work for direct comparison purpose.

Scheme (a) investigated the influence of column shapes when keeping the same heave natural period. Results in Figure 4 shows that the column cross sectional shapes have negligible change to the heave RAO. However, Figure 5 shows that the round shape column gives lower maximum mean wave drift load compared to the rectangular shape one.

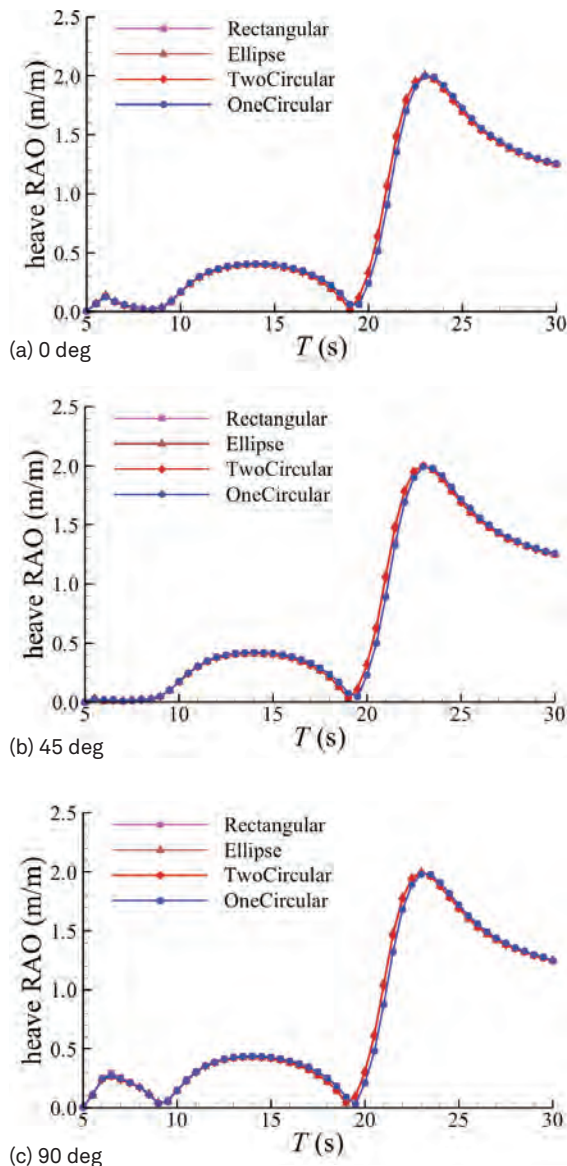


Figure 4 Heave RAOs for scheme (a) - different column shapes

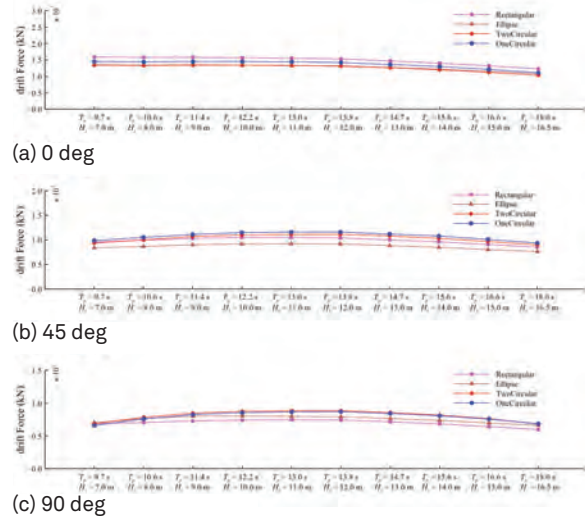


Figure 5 Mean wave drift load for scheme (a) - different column shapes

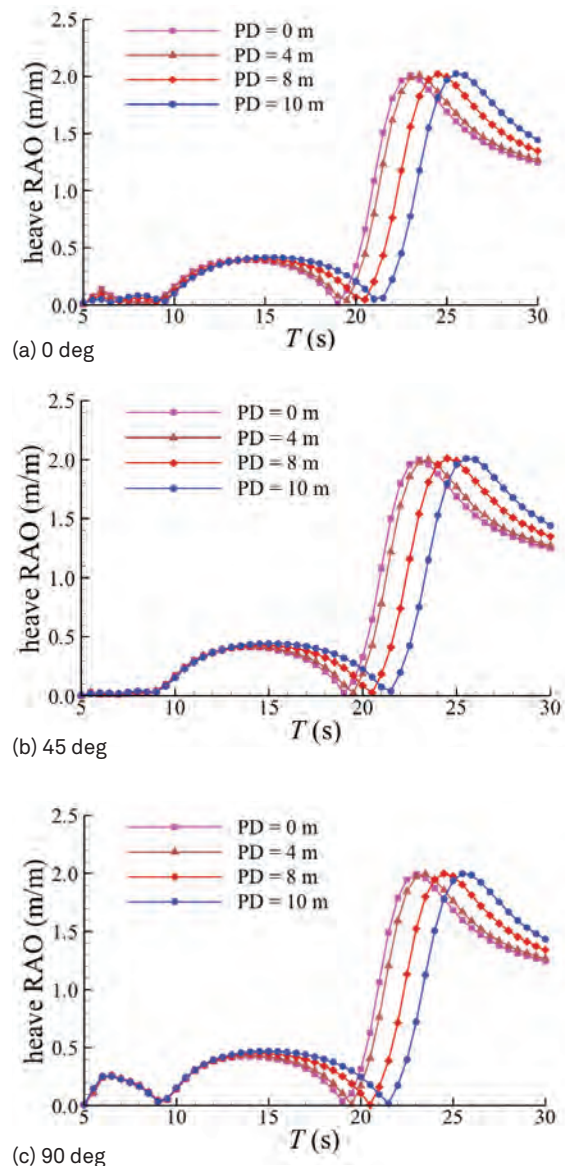


Figure 6 Heave RAOs for scheme (b) - different centre column diameters

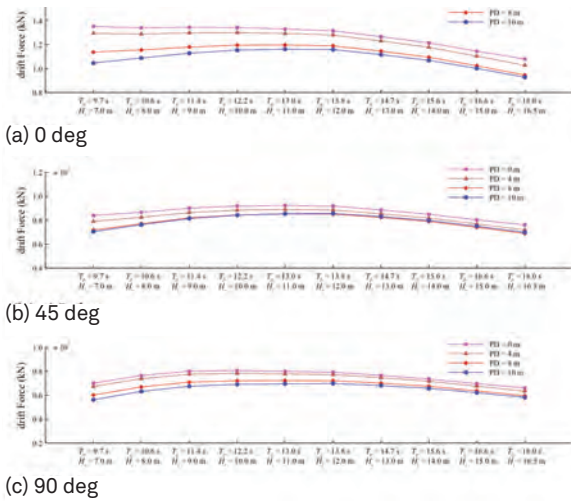


Figure 7 Mean wave drift load for scheme (b) - different center column diameters

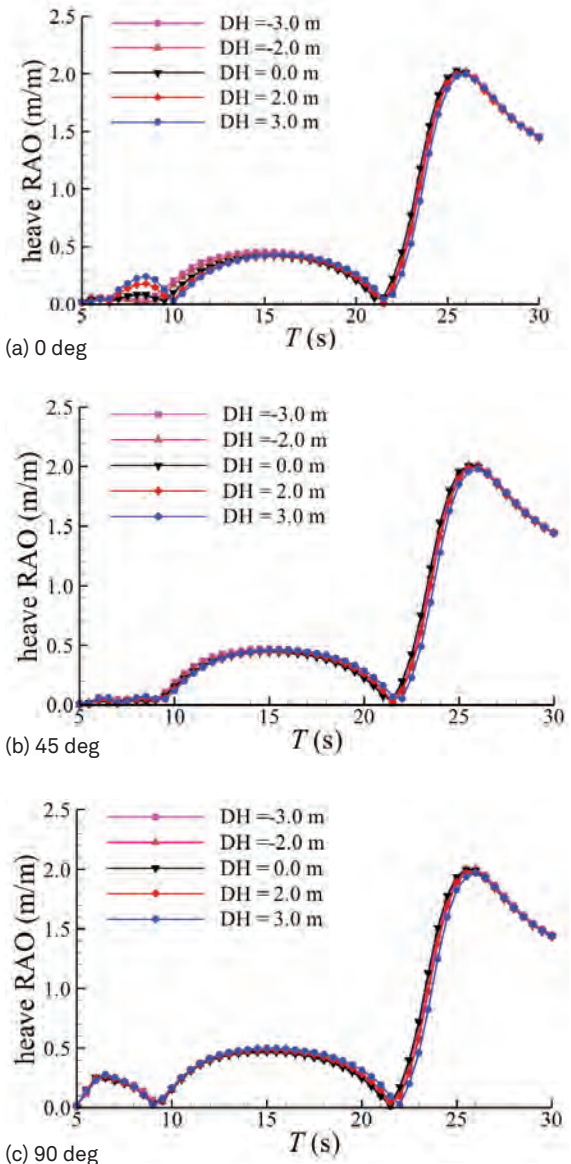


Figure 8 Heave RAOs for scheme (c) - different pontoon shapes

Scheme (b) investigated the influence of pencil column diameters. PD refers to the diameter of centre column. Figure 6 shows that the diameter have negligible change to the heave 2nd hump but the larger diameter will increase water plane area thus lower heave natural period. Figure 7 shows that larger centre column diameter gives smaller mean wave drift load by scyrfying some of the heave natural period.

Scheme (c) investigated the influence of pontoon shape change. PH refers to the pontoon height and DH refers to difference between pontoon mid-section and two ends. Positive DH means mid-section has greater height than two ends, while vice versa for negative DH. Figure 8 shows that DH have negligible changes to the heave 2nd. Figure 9 shows that the semi is subjected to minimum wave mean drift load when DH is zero i.e. the pontoon has a uniform height.

The optimisation shows that a semi-circular cross section column is preferred as it makes little impact to the heave motion but yields well balanced mean wave drift load which will benefit the station keeping design. Pencil column can help reduce the mean wave drift load, and it also can be adjusted to tune the natural period. Pontoon height can affect the heave motion. Once the optimal pontoon height is determined, it is ideal to adopt uniform pontoon height to minimise the mean wave drift load.

As the exploitation of offshore oil and gas resources extends to deep water or harsh environment seas, the optimisation of semi-submersible hull form can either reduce the initial sunk cost or improve the uptime which can bring economic value to clients.

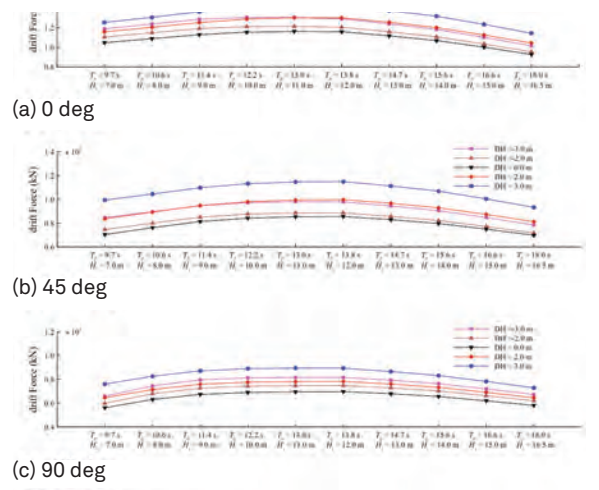


Figure 9 Mean wave drift load for scheme (b) - different pontoon shapes

Applications in Projects
Floatel Endurance with fork shaped wave diverter

Floatel Endurance is an accommodation semi-submersible deployed to work along with other offshore drilling and production platforms. The semi has suffered from imbalance mean wave drift load in surge and sway for a governing wave condition with Hs 8m and Tp 8.7s. The mooring analysis shows the mooring system may be insufficient to fulfil the design requirement during head sea when subject to a steep wave. However, the mooring system has some redundancy in beam sea. Therefore, the columns have been modified from the rectangular shape cross section to a fork shape cross section as shown in Figure 10.

After the modification, the mean wave drift force in head sea has been reduced by 600 KN and which helps on the thruster assisted mooring system. And the increase of mean wave drift load in beam sea and quartering sea doesn't affect the requirement of the mooring design.



Figure 10 Column shape modification

New design features such as pencil column, fork shaped wave diverter and super E column have been applied to real projects and potential design projects.

Table 1 Mean wave drift load of original Floatel Endurance

Heading [deg]	Wind force [kN]	Wave force [kN]	Current force [kN]
0.00	1866.99	3295.90	296.64
22.50	2135.84	2779.89	479.93
45.00	2298.61	1662.31	672.45
67.50	2016.25	1273.70	624.03
90.00	1664.11	1599.51	628.93
112.50	2069.07	1250.34	663.56
135.00	2255.26	1687.72	694.86
157.50	2012.40	2802.49	484.22
180.00	1654.20	3279.90	307.45
202.50	1983.91	2802.49	484.22
225.00	2214.39	1687.72	694.86
247.50	1993.84	1250.34	663.56
270.00	1639.20	1599.51	628.93
292.50	2033.79	1273.70	624.03
315.00	2256.06	1662.31	672.45
337.50	2047.28	2828.13	460.32

Table 2 Mean wave drift load of modified Floatel Endurance with fork shape column

Heading [deg]	Wind force [kN]	Wave force [kN]	Current force [kN]
0.00	1866.99	2669.30	296.64
22.50	2135.84	2324.93	479.93
45.00	2298.61	1575.62	672.45
67.50	2016.25	1468.05	624.03
90.00	1664.11	1849.23	628.93
112.50	2069.07	1453.26	663.56
135.00	2255.26	1587.40	694.86
157.50	2012.40	2325.60	484.22
180.00	1654.20	2657.10	307.45
202.50	1983.91	2325.60	484.22
225.00	2214.39	1587.40	694.56
247.50	1993.84	1453.26	663.56
270.00	1639.20	1849.23	628.93
292.50	2033.79	1468.05	624.03
315.00	2256.06	1575.62	672.45
337.50	2047.28	2330.42	476.19

KFELS5000HE with fork shape wave diverter and pencil column

KFELS5000HE is Keppel Offshore & Marine Technology Centre's (KOMtech's) proprietary harsh environment drilling semi design. The vessel is designed to operate in North Sea environment where the vessel is subject to large wave load due to steep waves. The application of pencil column and fork shape column can improve the heave motion as well as to reduce the max mean wave drift load in head sea to reduce the cost of thruster assisted mooring design.



Figure 11 Modification of KFELS5000HE

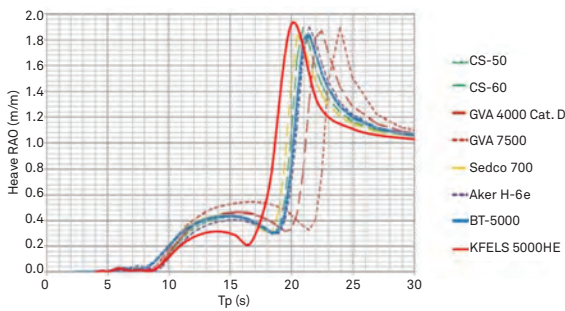


Figure 12 Heave RAO comparison in wave at 0 degrees

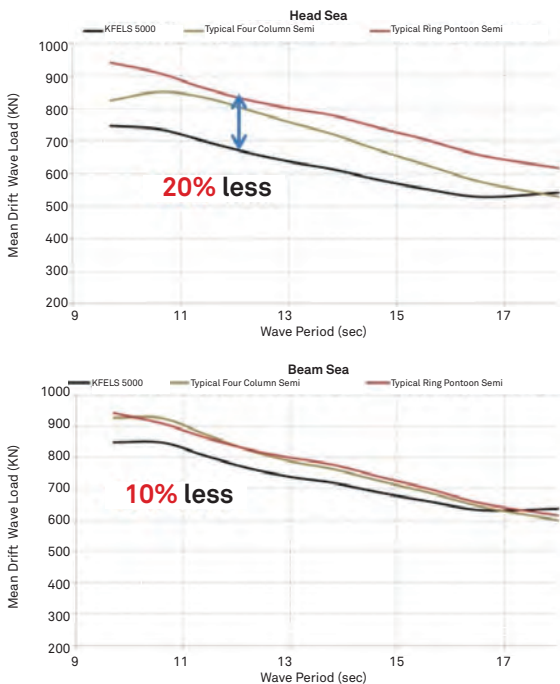


Figure 13 Mean wave drift load of KFEL5000HE with fork shaped wave diverter

Compared to other competitive designs, Figure 12 shows that the vessel is well tuned to have an optimal heave motion in wave i.e. significantly reduced heave motion in 2nd hump for operation and slightly reduced heave natural period to allow large relative motion to have positive airgap in survival condition.

Figure 13 shows that the mean wave drift load has been reduced by about 20% compared to those typical four column twin pontoon or ring pontoon semi-submersibles. For the pure mooring design, the reduced load can reduce the mooring weight which can be converted to payload. For the thruster assisted mooring design, the reduced load can reduce the size of thruster used or the fuel consumption during operation.

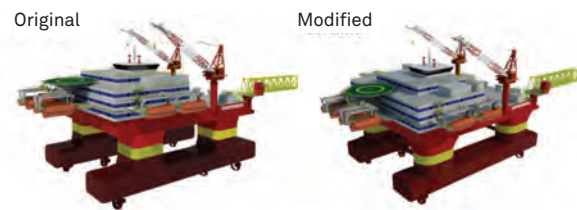


Figure 14 Modification of SMART Semi

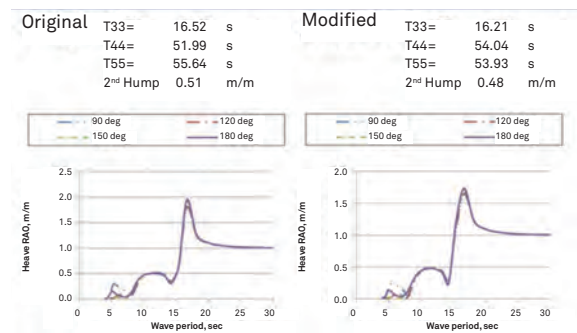


Figure 15 Heave RAO of SMART Semi

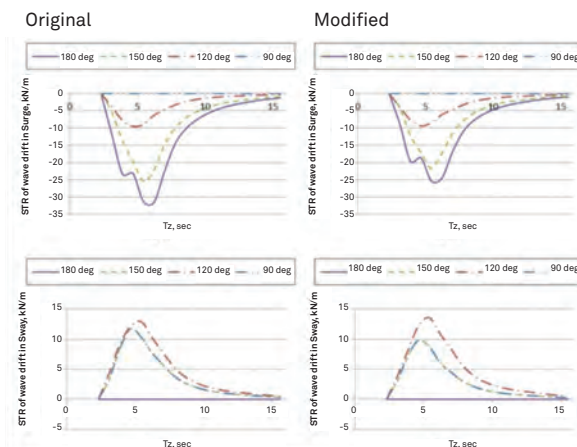


Figure 16 STR of mean wave drift load of SMART Semi

SMART Semi with super E column

The SMART Semi is an accommodation semi designed to have improved agility i.e. quick response to move with Floating Production, Storage and Offloading (FPSO) during operation. Smaller wave mean drift load and smaller added mass are preferred for the optimisation.

The rectangular column has been modified to semi-circle plus rectangular. The heave RAO in Figure 12 shows there is little change after the modification. The short term response (STR) of mean wave drift load in Figure 13 shows the mean wave drift load in head sea has been reduced significantly when wave zero crossing period is in the range of 4 – 8 seconds. The mean wave drift load in beam is not much affected.

Conclusion

The hull optimisation by modifying the hull form can improve the global performance of the semi-submersible. The study will give the designer a better understanding of the parameters which can tune the semi-submersible to better meet the client's requirement. This article has discussed the theory of the optimisation, introduced an optimisation scheme, and performed the optimisation study. New design features such as pencil column, fork shaped wave diverter and super E column have been applied to real projects and potential design projects.

However, it is worthwhile noting that this optimisation exercise is limited to linear wave diffraction and radiation program. Therefore, some non-linear impact may not be fully captured by the program. The overall performance shall be fully analysed to include the impact on other design aspects. Some more, the impact of the change in hull on the construction also should be considered to ensure any novel conceptual change will not compromise the construction feasibility.

In future, scaled model tests in the forthcoming ocean basin at National University of Singapore (NUS) will provide experimental data for validations of the developed software tools and programmes.

References

- [1] M. F. M. E. M. H. N. K. Gonçalves RT, "Conceptual Design of Monocolumn Production and Storage With Dry Tree Capability," ASME. J. Offshore Mech. Arct. Eng., 2010.
- [2] B. W. N. N. W. K. Y. S. C. Sa Young Hong, "Investigation of Nonlinear Roll Motion Characteristics of a Shallow Draft Semi-submersible," in International Ship Stability Workshop, Brest, 2013.
- [3] J. J. S. R. D. A. J. Voogt, "Mean and Low Frequency Roll for Semi-submersibles in Waves," Kitayashu, 2002.
- [4] F. T. I. M. A. C. C. L. S.H. Sphaiera, "Monocolumn Behavior in Waves: Experimental Analysis," vol. 34, no. 11-12, 2007.
- [5] F. T. G. R. T. M. E. B. d. M. H. F. N. K. & M. I. Q. Matsumoto, "The Influence at Vertical First Order Motions Using Appendages in a Monocolumn Platform," 2008.
- [6] F. Noblesse, "The Green Function in The Theory of Radiation and Diffraction of Regular Water Waves by a Body," vol. 16, no. 2, 1982.
- [7] J. N. Newman, "The Approximation of Free Surface Green Functions," 1992.
- [8] W. Cummins, "The Impulse Response Function and Ship Motions," Cardrock, Maryland, 1962.
- [9] F. John, "On The Motion of Floating Bodies II," 1950.

Author's Contact

- | Wei.XU@KOMtech.com.sg
- | Ankit.CHOU DHARY@KOMtech.com.sg

Acknowledgements

The authors thank the National Research Foundation, Keppel Corporation and National University of Singapore for supporting this work done in the Keppel-NUS Corporate Laboratory. The conclusions put forward reflect the views of the authors alone, and not necessarily those of the institutions within the Corporate Laboratory.

Generating Reliability-Based Vibration Predication using Finite Element Modelling Methods

| WANG Wenping^{*}, M.Eng, B.Eng

| Mano SUNDAR, M.Eng, B.Eng

| Ankit CHOUDHARY, M.Sc, B.Eng

| Anis HUSSAIN, M.Sc, B.Eng

**Keppel Offshore & Marine Technology Centre, Deepwater Group*

Traditionally, the structural capacity is determined based on the given extreme static loading to ensure a sufficient safety margin. In fact, uncertainties always exist in the real world. These uncertainties are due to the random character of the environment, geometric and material properties, as well as inaccuracy in prediction of loads and response. Engine room vibration predication is one suitable topic with many such uncertainties. Our experience shows that reliability based Finite Element Model (FEM) simulation approach for vibration predication provides a more reliable and less conservative response predication than deterministic extreme response vibration analysis when multi-point random source vibration excitations exist.

Offshore structures, like semi-submersibles, are typically equipped with six engines in topside engine rooms. Local vibration levels due to multiple engine excitations are quite challenging nowadays due to continuous increase in vessel output power and structures becoming lighter. Prediction of the vibration level at engine room structures at early design stage is essential for designer to propose possible modifications to ensure a reduced risk of excessive vibration. Specially, when six engines are arranged nearby, the combination of vibration responses for any location shall be illustrated with many uncertainties, such as, vibration modes, piston rotating phase angles and amplitudes, damping and tolerance. Thus, how to evaluate the combination effects to obtain maximum response within acceptable criteria becomes a critical problem.

Our approach is to generate a computational time affordable large number of input data sets based on input parameters possibility distribution density function through Monte Carlo simulation technique. The outputs, like response levels, obtained from force vibration FEM simulation are post processed with six sigma statistical methods. This predicted maximum response levels under different sigma levels are compared with shipyard experimental report to form in-house best practice.

Introduction

Offshore structures, like semi-submersibles, are typically equipped with six engines in topside engine rooms. Local vibration levels due to multiple engine excitations are quite challenging nowadays due to vessel output power increase and structures become lighter. The current vibration acceptance criteria are to be determined as appropriated specifications from owner and manufacturer. In basic design team, ISO 6954 ^[ref5] is one of widely used guidance. Prediction of the vibration level at engine room structures at early design stage is essential for designer to propose possible modifications to ensure a reduced risk of excessive vibration. Our objective for this paper is to present one reliability based prediction technique to simulate engine room vibration under multi-engine excitations.

Each engine set provided by manufacturers has been tested according to ISO 8528-9 ^[ref6]. They are supported with structural foundation with resilient mounts ^[ref7]. Due to double bottom stiffness conditions, each engine exhibits different vibration modes of “H type”, “X type” and “L type” (see figure 11) during operation ^[ref1]. To evaluate overall engine room’s performance, each engine vibration modes are modelled as force vibration source in designer’s global hull Finite Element Model (FEM). However, when six engines are arranged nearby, the combination of vibration responses for any hull location shall be illustrated with many uncertainties, such as, vibration modes, piston rotating phase angles and amplitudes, damping and tolerance. Thus, how to evaluate the combination effects to obtain reasonable maximum response becomes a critical problem to compare with acceptable criteria.

Reliability based design gives designers a solution in probabilistic way. Our approach is to generate a computational time affordable large number of input data sets based on input parameters’ probability distribution density function through Monte Carlo simulation technique ^[ref10]. The outputs, like response levels, obtained from force vibration FEM simulation are post processed with six sigma statistical methods ^[ref8]. This predicted maximum response levels under different sigma levels are compared with shipyard experimental report to form in-house best practice. This approach not only provides more reliable solution, but also gives potential cost savings to shipyards.

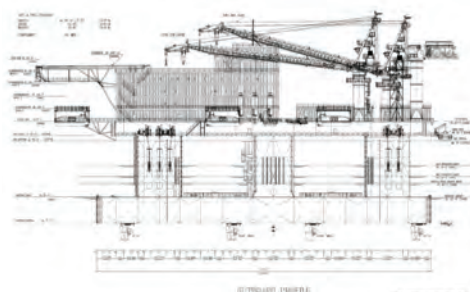


Figure 1 Overview of drillship model

Engine Room Arrangement and Acceptable Criteria

Semi-Submersible Drilling Tender (SSDT) Unit, SSDT5000NG as shown in Figure 1, is used to illustrate our method in this paper. SSDT5000NG is designed for unrestricted service at UK sector, North Sea with more than 25 years’ service life against given environmental conditions. The principal dimensions are listed in table 1.

Table 1 Principal Dimension SSDT

Length of Pontoon	112.7 m
Breadth of Pontoon	12.5 m
Pontoon Height	7.62 m
Columns (Length X Breadth)	13.07 X 10.67 m
Upper Hull Length	92.66 m
Upper Hull Breadth	40.94 m
Main Deck Height above Baseline	25.3 m

The engine room is located in the middle of deck box, mainly supported by the middle two columns. As shown in Figure 2, there are totally six engines arranged in parallel position.

Basic design team is more focussed on the overall vibration level for engine room and surrounding hull structures. Thus, local FEM as shown in Figure 4 is used for calculation purpose. The main deck is hidden to help readers to know the arrangement inside the engine room.

Engineering common practice is to control structural natural frequencies to be away from engine excitation frequency with +/- 10%. As such, when engine dominate operating frequency is at 15Hz, the structural natural frequency should be away from 13.5~16.5Hz. Nowadays, new engine model running at higher speed, such as 20Hz, are also available. If it is selected by mechanical

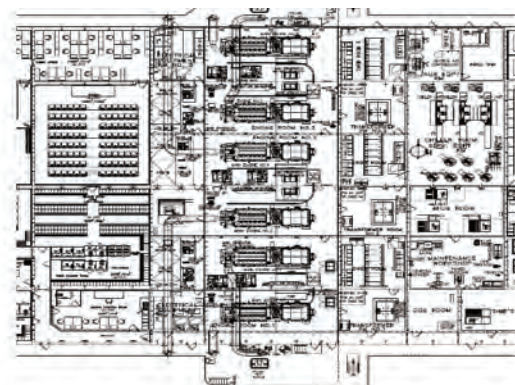
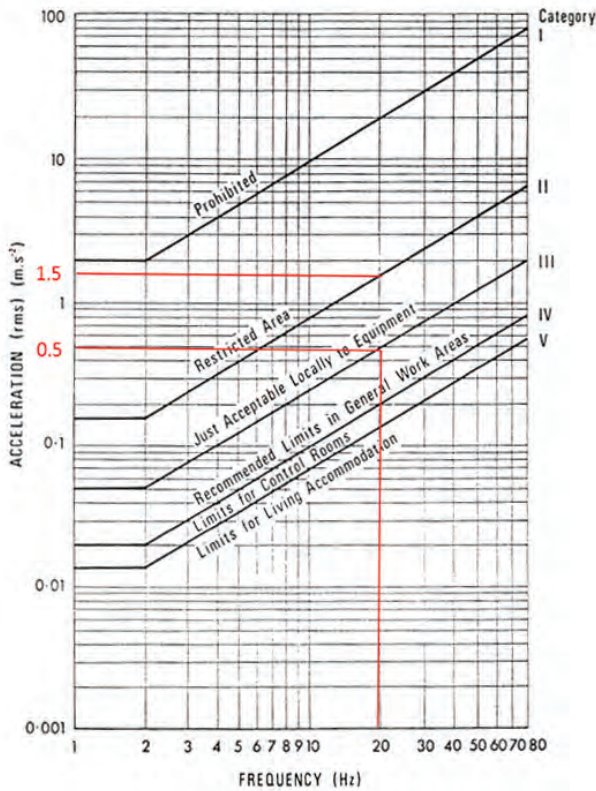
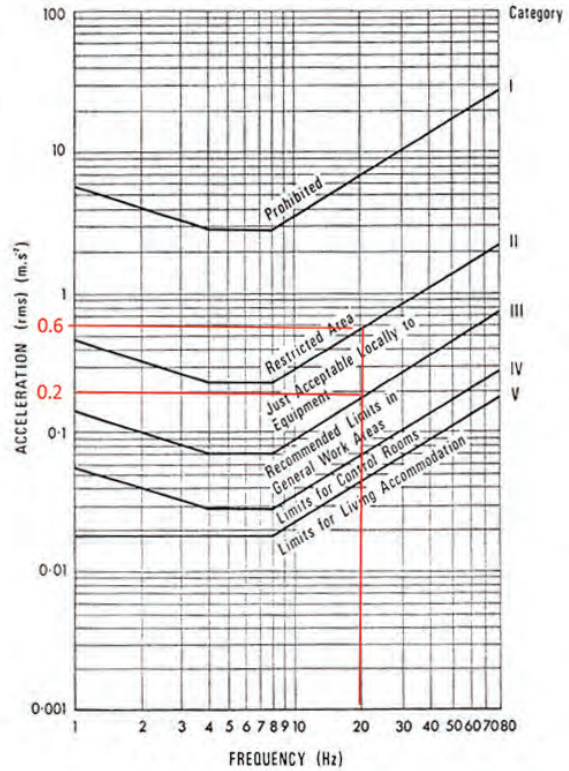


Figure 2 Engine room arrangements

Technology improvements always help company efficiency. Reliability based design technology has potential to minimise construction risk and gives valuable prediction at early design stage.



Vibration limits for Offshore Installations: 'Horizontal' axes (a_x, a_y)



Vibration limits for Offshore Installations: 'Vertical axis' (a_z)

Figure 3 UK HSE 2001/068 vibration acceptance criteria in acceleration level

designer, the immediate question is what vibration risk exist to topside hull structure. To address this, FEM study with force vibration shall be performed to predict actual vibration level.

The acceptance vibration criteria usually refer to UK HSE 2001/068 requirement [ref2] when vessel is intended to go UK sector. Engine rooms are classified as between category II to III in Figure 3. That means,

- 1) Vibration induced acceleration level on vertical (such as, decks) should be less than $0.2m/s^2$. Local extreme peak values must be less than $0.6m/s^2$.
- 2) Vibration induced acceleration level on bulkheads should be less than $0.5m/s^2$. Local extreme peak values must be less than $1.5m/s^2$.

Theoretical Background

Generally, the equation of dynamic equilibrium is written as below [ref3]

$$M\ddot{r} + C\dot{r} + Kr = R(t)$$

Where, M is the global mass matrix, C is the global damping matrix, K is the global stiffness matrix, $R(t)$ is the time dependent load vector and r is the displacement vector with its time derivatives. Engine room vibration analysis equals to how to solve this equation.

Dynamic forced response may either be computed by Modal Superposition, which involves solving a number of uncoupled equations or by direct methods which involves solving matrix equations directly [ref3].

As the direct method is more computationally expensive, modal superposition method is adapted in this paper. Meanwhile, the mode shape study in the initial step also can give an overall participation factor review for each mode shape. Furthermore, it helps to locate the problem source and mitigation method. The calculation work described can be easily achieved in the FEM tool [ref9]. However, the post-processing work is not so straight forward.

When multiple engines arranged nearby, the combination of vibration response for any location shall be illustrated in the following formula.

$$R_{loc} = \sqrt{(\sum_{i=1}^n f_{i,j} A_{i,j} \sin(\theta_{i,j}))^2 + (\sum_{i=1}^n f_{i,j} A_{i,j} \cos(\theta_{i,j}))^2}$$

Where, n is the total number of engines. $f_{i,j}$ defines the weighting factor depending on engine i at vibration mode j . $A_{i,j}$ defines the response amplitude for engine i at vibration mode j . $\theta_{i,j}$ defines the harmonic load phase angle for engine i at vibration mode j .

Deterministic Based FEM Simulation

The overall view of CAD model is shown in Figure 4. They are meshed into FEM model as shown in Figure 5. The model consists of solid element (engine blocks), shell element (plates), beam element (stiffeners and girders) and spring element (resilient mounts). Total summary of the FEM model is 12,100 elements and 10,900 nodes. Only engine foundation parts are provided with local refined meshes, this is to avoid the FEM model size is too big for office computer to handle.

The masses and centre of gravity of the main engines and generators (B374 CAT Main Gens & E-Gen) are according to vendor's datasheet [ref4]. Stiffness characteristics of the resilient mounts (60° SH.A) are shown in Figure 6. Vibration load and frequency datasheet for 900RPM engine from vendor is given in table 2.

Initial screening shows dominate modes in all directions are mode 6, 7, 13 and 24 (see Figure 7~10). Their effective mass in percentage of total mass are also reported in table 3. Please take note that mode 24 (Figure 10) is at 21.126Hz. This is close to engine operating frequency of 20Hz. This should be studied carefully with forced vibration.

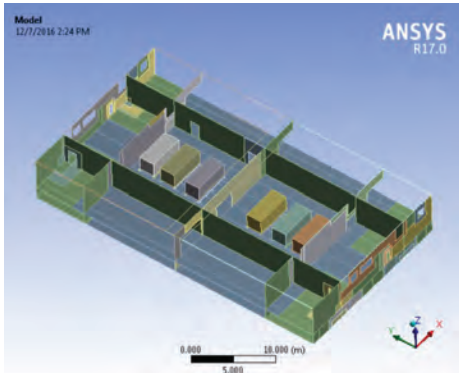


Figure 4 Overview of CAD model

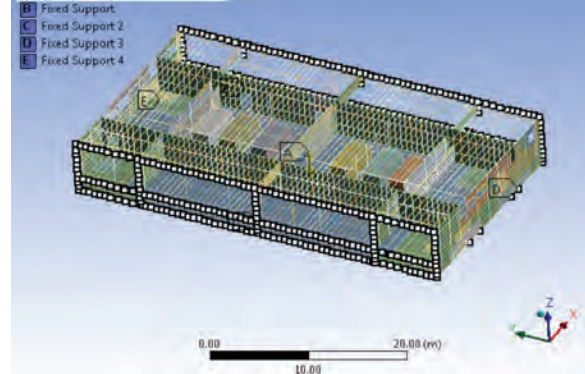


Figure 5 Overview of FE model

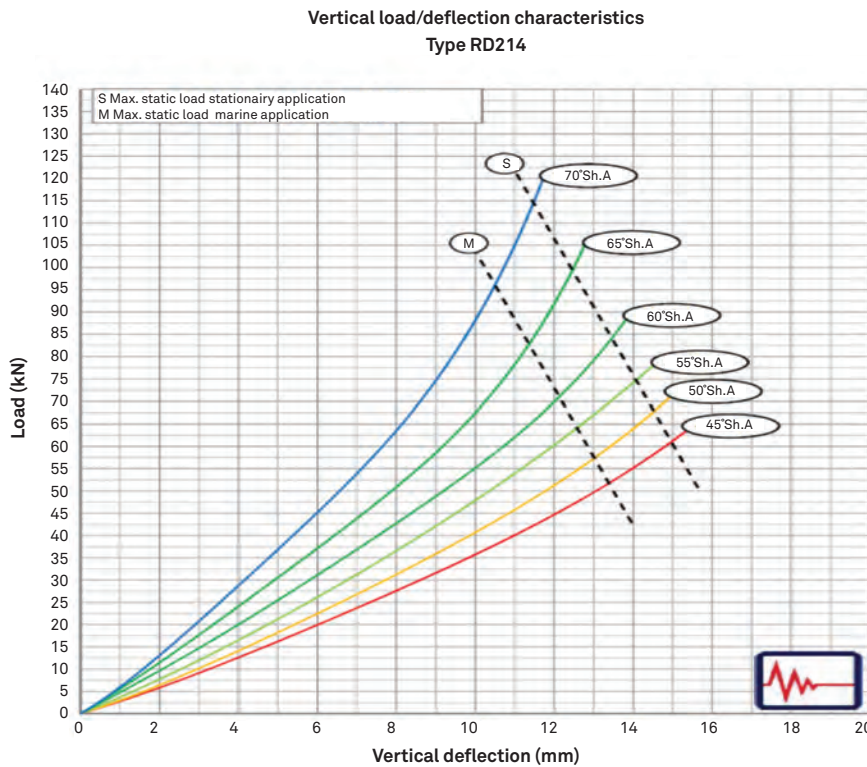


Figure 6 Resilient mount design information

Table 2 CAT main gens & E-gen design information

Engine	Speed (rpm)	Frequency (hz)	Fy (kN)	Fz (kN)	Frequency (hz)	My (kNm)	Mz (kNm)
B374 3516CHD	1200	20	5	5	20	4	4
B374 3512B	1200	20	5	5	20	4	4

Table 3 Engine room dominate modes

direction	Dominate modes	Percentage of total mass
X-dir	Mode 7	3.4%
Y-dir	Mode 6	10.8%
Z-dir	Mode 24	39.7%
Rot-X	Mode 13	14.8%
Rot-Y	Mode 24	30.7%
Rot-Z	Mode 7	5.0%

Due to double bottom stiffness conditions of engine foundation, each engine exhibits different vibration modes of “H type”, “X type” and “L type”. (See Figure 11). More detail explanation refers to [ref1].

To generate the equivalent loading conditions for engine vibration modes, the following three types of vibration loads combination are applied. Please refer to Figure 12 for load definition.

- a) Combination of harmonic load F_z and M_y
- b) Combination of harmonic load F_z and F_y
- c) Combination of harmonic load F_z and M_z

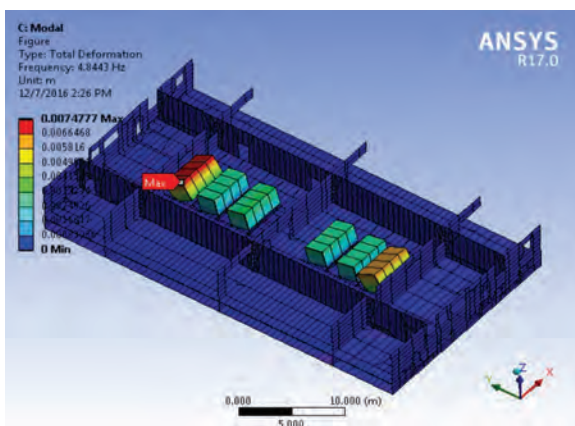


Figure 7 Vibration mode 6

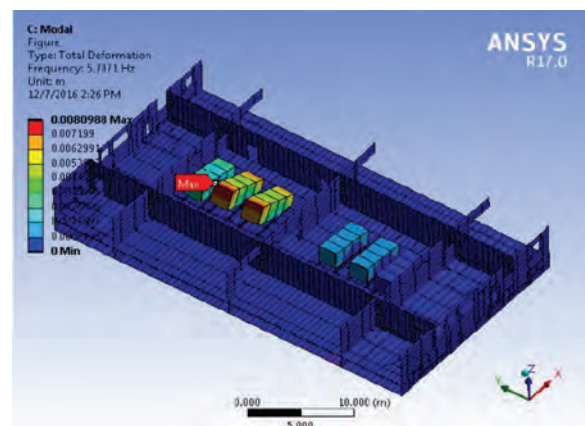


Figure 8 Vibration mode 7

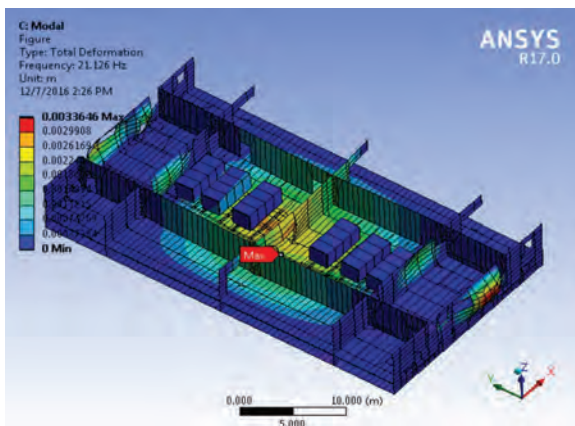


Figure 9 Vibration mode 13

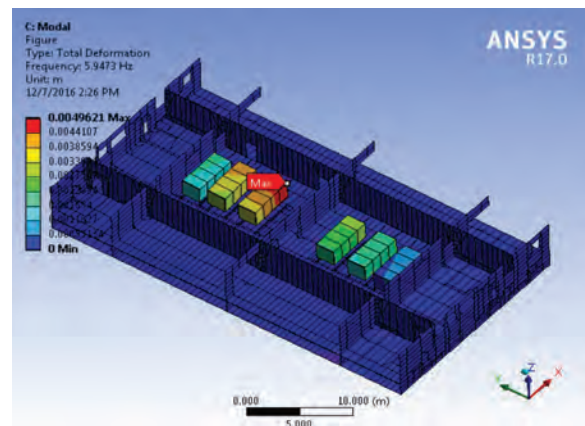


Figure 10 Vibration mode 24

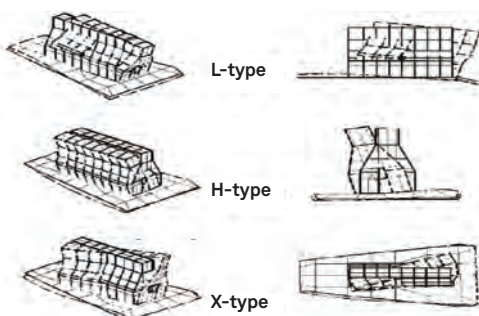


Figure 11 Engine vibration modes

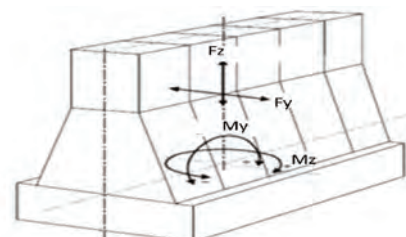
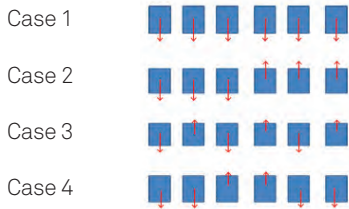


Figure 12 Load definition for engine block.

For each harmonic load combination, six engines might be at different phases. To ensure to cover all the maximum response, the following four cases are considered for each vibration type. The arrows indicate the engine starting operating phase angle.



Thus, total 12 cases (three mode x four cases) have been studied to scan through to obtain the maximum acceleration response envelop of all engine room structures. Each loading case needs to be defined as loading conditions as in Figure 13 in FEM simulation.

The result obtained can be plotted in the contour format for review. Figure 14 (a,b,c) are acceleration response plot sample for illustration purposes. Figure14a is the condition for all harmonic loads are running together in-

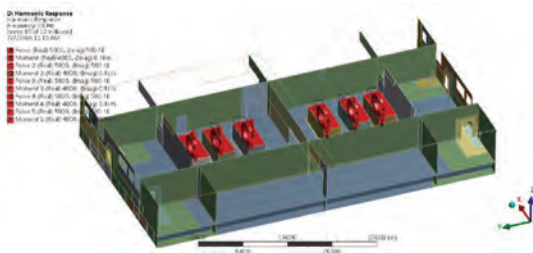


Figure 13 Loading condition model in FEM

phase. Figure14b is the condition for all harmonic loads are running together out of phase. By comparing Figure 14a and Figure14b, the reader will notice the influence of starting phase angle to the maximum acceleration response levels. As shown in Figure14c, the main deck group which gives maximum value of 0.213m/s² which is above the engine room limit of 0.2m/s². This shows the vibration for main deck group is relatively higher. Some local reinforcement might be needed.

Sensitivity studies are needed to address some uncertainty values, like constant damping ratio (Figure 15). In this way, the result can gives better confidence to designers.

Figure 16 gives a clear picture of the risk to change engine operating frequency from 13.5Hz to 22Hz. The maximum acceleration response increases significantly after 18Hz. This also indicate that 20Hz new engine might have risk for excessive vibration.

In short, not only deterministic FEM simulation requires quite a lot of load cases (12 cases) to be done, but also shows the calculation might be too conservative in selection of critical load cases.

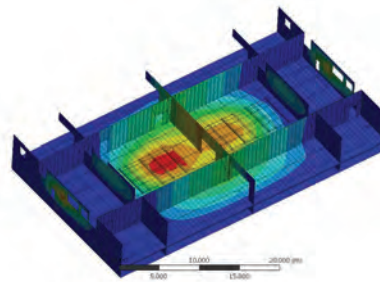


Figure 14a Sample for engine room vibration at 20Hz (L-type, case 1).

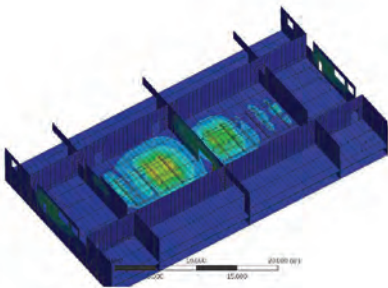


Figure 14b Sample for engine room vibration at 20Hz (L-type, case 3).

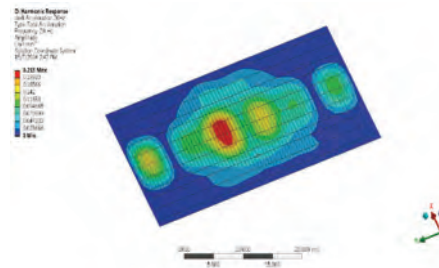


Figure 14c Main deck acceleration level for critical case (H-type, case 1)

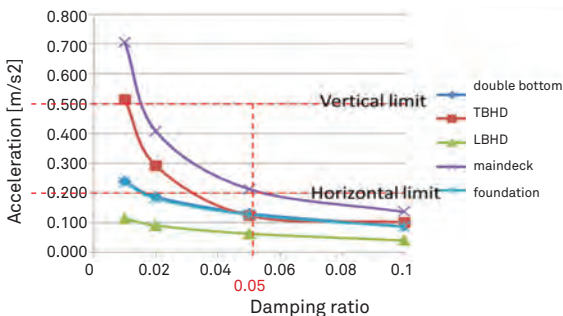


Figure 15 Sensitivity study for acceleration response vs constant damping ratio

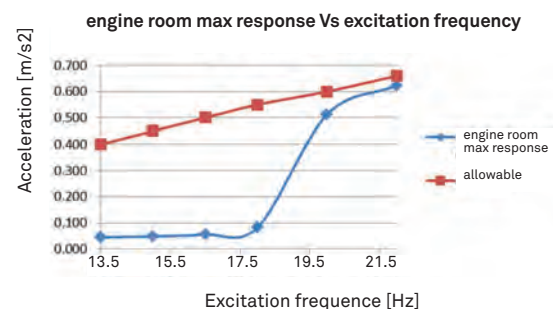


Figure 16 Sensitivity study for acceleration response vs excitation frequency

The reliability based FEM simulation approach for vibration prediction provides a more reliable and less conservative response prediction than deterministic extreme response vibration analysis especially when multi-point random source vibration excitations exist.

Reliability Based FEM Simulation

In practical situation, all engines are not possible to be working at the same modes, phase angles and amplitudes. Thus, how to evaluate the combination effects of above response formula to obtain maximum response becomes a critical problem to compare with acceptable criteria.

Our approach is to generate a computational time affordable large number of input data sets based on input parameters probability distribution density function through Monte Carlo simulation technique as shown in Figure 17.

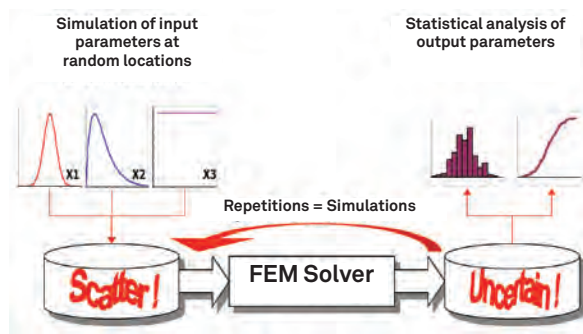


Figure 17 Monte Carlo simulation method scheme

The following assumptions are considered to generate Monte Carlo simulation input database.

- 1). All vibration Force and Moment amplitudes follow normal distribution with truncated at max/min variation of 5% of mean values.
- 2). All vibration Force and Moment phase angles follow uniform distribution from 0 to 360 degrees.
- 3). Vibration modes of “H type”, “X type” and “L type” are at equal possibility.

Our analysis limit our database to total 129 runs in the reliability based design to be time affordable. The input parameter sample is shown in Figure 18. The sensitivity level for input parameter can also be reported as Figure 19. This gives the designer a good clue for solving the problem if there is one.

The outputs, like response levels, obtained from force vibration FEM simulation are post processed with six sigma statistic methods (see Figure 20). The predicted the maximum response levels under different sigma levels are well below the deterministic extreme results.

The reliability based FEM simulation approach for vibration prediction provides a more reliable and less conservative response prediction than deterministic extreme response vibration analysis especially when multi-point random source vibration excitations exist.

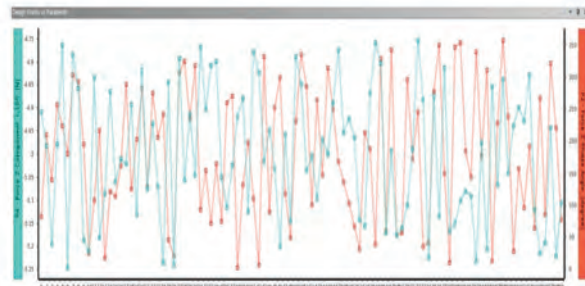


Figure 18 Sample for design point vs parameters.

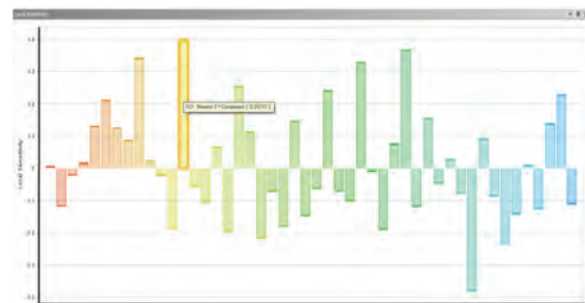


Figure 19 Sample for sensitivity study for input parameter to acceleration level at 20Hz excitation.

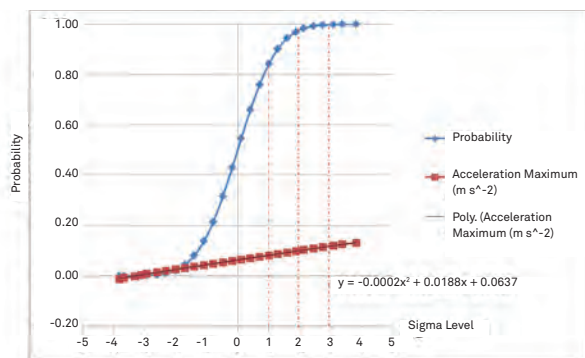


Figure 20 Sample for main deck acceleration level and probability vs different sigma level

Obviously, the reliability based approach for Semi-submersible engine room vibration prediction provides better prediction under multiple engine source vibration interactions.

The following key trends can be observed.

- 1). Reliability analysis results under three sigma levels are close to deterministic analysis results. They are at 96% agreement in average. This tells us why deterministic analysis usually is at conservative side.
- 2). Minimum acceptable criteria for the shipyard should be at one sigma level. That is about 66% of deterministic analysis results. Such as, the acceleration level for main deck group under one

sigma level is less than allowable limit of 0.2m/s^2 . But under two sigma level, it will be over the limit. Thus, the vibration risk at main deck level (Figure 14c) is one concern only. It is still acceptable. This not only provides cost savings, but also reflect the actual situation of six engine are not running at the same phase angles.

Conclusion

This paper presents a new reliability based FEM force vibration simulation method with assistance of Monte Carlo simulation techniques. The acceleration response level obtained is closer to the actual situation, which gives potential cost savings to the shipyard.

The approach also provides a unified predication method for any vessel to perform vibration analysis under multi-point vibration excitations.

References

- [1] American Bureau of Shipping & Affiliated Companies, SHIPVibration April 2006
- [2] UK HSE requirement, Noise and Vibration 2001/068
- [3] Ray W. Clough, Dynamics of structures, McGraw-Hill Companies (January 1, 1975)
- [4] B374, SSDT5000NG semi General Arrangements, Mechanical data sheet.
- [5] ISO6954, Mechanical vibration, Guidelines for the measurement, reporting and evaluation of vibration with regard to habitability on passenger and merchant ships, 2011
- [6] ISO8528-9, Reciprocating internal combustion engine driven alternating current generating sets — Part 9: Measurement and evaluation of mechanical vibrations, 1995.
- [7] Francis F. Vane, A guide for selection and application of resilient mountings to shipboard equipment, 1958
- [8] Tennant, Geoff (2001). Six Sigma: SPC and TQM in Manufacturing and Services. Gower Publishing, Ltd. p6. ISBN 0-566-08374-4.
- [9] ANSYS theory manual for Probabilistic Design, v15, 2010
- [10] Achintya Haldar and Sankaran Mahadevan, Probability, Reliability, and Statistical Methods in Engineering Design. Nov 1999.

Author's Contact

| wenping.wang@komtech.com.sg

Evaluating Ballast Water Management Plan of a Floating Dry Dock Using Visual Basic For Applications

| Rafael de Barros PASSOS*, Ms.C.

| Olivier Jean Pascal de MONTGOLFIER*, Eng.

| Miguel Angel Moya RAMIREZ*, Ms.C.

| Lucas do Vale MACHADO*, Ms.C.

* BrasFELS

This work presents a numerical tool to calculate the ballast water management plan (BWMP) for floating dry docks (FDD) using Visual Basic for Applications (VBA) from Microsoft Excel. First objective is to employ a widely used and user-friendly software in the solution of this problem. It allows cost savings reducing the need for an expensive software. Second objective is to estimate an efficient BWMP of FDD addressing the technical and safety requirements. Finally, the research is to provide versatile tool which can be used during the FDD operation to check any ballast condition in real-time.

The numerical model takes into account structural constraints, hydrostatic equilibrium, stability parameters and operational limitations in the estimation of efficient BWMP to achieve the target drafts in each stage of docking procedure. A FDD composed by one pontoon with four square columns is analysed as an example.

Introduction

In spite of recent efforts being made to reduce the need for dry dock ships, the shipping and insurance industries still consider important to move all ships, large or small, to the dock from time to time for inspection, repair or hull painting^[1].

In the past, shipbuilders used inclined launch ways, which were very economical and fitted sufficiently the demand of shipbuilding at that time. Nowadays, huge ships from naval and commercial areas are seldom built on launch ways since it has been found that cost and risks cannot be neglected for that operation. In addition, there are limitations of crane access at the head end of the built-up ways. These are some of the reasons that a great number of yards recently developed building basis of short draft for ship construction and launching by simple floating^[2].

With the continuous demand to construct more docks of large size and because of physical limitations in the basin dock concept, several shipyards have gone ahead with the construction of large floating docks.

Floating dry docks are bargelike floating structures with sufficient displacement, dimension and stability for physically lifting a vessel from water. In general, these floating dry docks have wing walls on either side of the barge pontoon structure to provide stability during docking operations and add strength to the sectional area of the dock. Concerning the docking procedures, there are usually five phases of importance to evaluate the vessel/dock intact stability, as follows:

1. Dry dock at full submergence (no vessel on board);
2. Partial lift of vessel (half of vessel draft);
3. External waterline at top of keel blocks;
4. External waterline just over pontoon deck;
5. Dock at normal operating draft.

Each of these phases must have an estimated final draft at aft and forward perpendiculars, providing appropriate trim of the floater. This work has three main objectives. First, to employ a user-friendly interface to solve the docking issues using VBA from the widely used software Microsoft Excel. Second, to find a Ballast Water Management Plan (BWMP), according to the limitations of the Floating Dry Dock (FDD) and its specific phase of docking. Third, to provide versatile tool which can be used during the FDD operation to check any ballast condition in real-time. In order to evaluate the proposed procedure a hypothetical FDD is introduced in a simplified datasheet by means of its geometrical parameters. Such a numerical tool should be able to handle hydrostatic equilibrium, intact stability and structural analyses for longitudinal and transversal forces after the user provides an appropriated keel block plan. With all this inputs in mind, a possible ballast plan is the desirable output. Figure 1 and figure 2 show some geometrical properties of the proposed example of FDD. Additionally, table 1 presents the lightweight properties of the FDD. Figure 3 shows a 3D view of the hypothetical dry dock.

Model the hydrostatic properties of the FDD at a unique datasheet provides means of evaluating different ballast plan through Excel Solver function, for non-linear problems. The equilibrium routine calculates the submerged volume

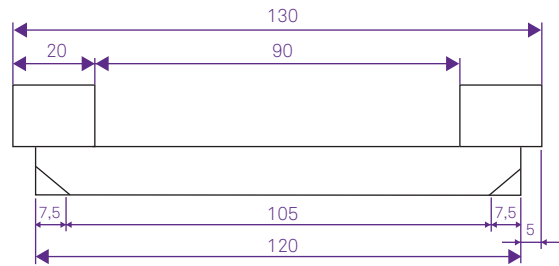


Figure 1 FDD side view, dimensions in metres

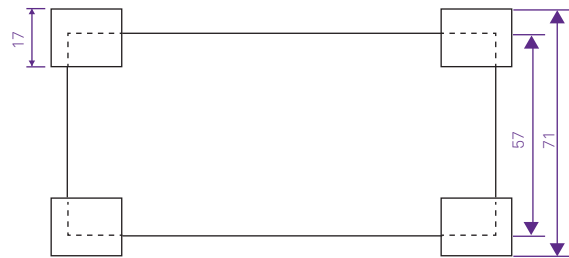


Figure 2 FDD top deck view, dimensions in metres

and centre of buoyance by numerical trapezoidal method, due to the simplified geometry of the FDD. After equilibrium is reached, it can be submitted to several constraints and, although a great number of variables are checked at each trial, a possible solution is always achieved. Previous studies for a DP vessel using Excel VBA solver^[3] indicated that it is a viable and cost saving alternative to preliminary design phases.

Property	Value	Unit
Mass	8450	[mT]
KG	8.38	[m]
Maximum draft	19.0	[m]

Table 1 Lightweight Properties of FDD

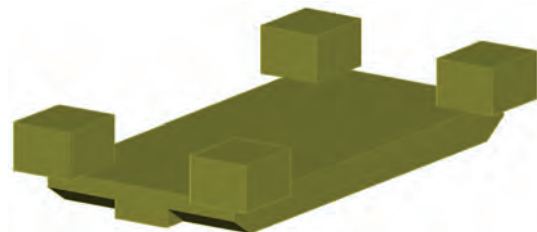


Figure 3 FDD 3D view

Spreadsheets

This section presents all data desirable for each docking procedure. In addition, it presents comprehensive description of each individual step of calculation, its assumptions and limitations to provide realistic results for the computational tool.

Block Loading Properties

This table of datasheet creates an arrangement of the keel blocks and side blocks along the FDD main deck. The user must insert a feasible blocking plan and check all constrains in order to obtain the correct load of the vessel, which is under docking analyses. Table 2 presents the properties of the vessel to be docked used as input in the case.

Table 2 Vessel under docking procedure

Variable	Description
Vessel Name	Name of the Vessel to be docked
W	Total load on blocks
LCG_v	FWD of Vessel Aft Perpendicular
VCG_v	Vertical centre of gravity
TCG_v	Vessel Transversal centre of gravity, STBD>0
LBP_v	Length between perpendiculars
d_fr_0s	Distance between dock Fr.0 to vessel Fr.0 This distance is positive when vessel Fr.0 is FWD of dock Fr.0.
h	Block Height
F_sb	Factor of Side Blocks effective area

If variable d_fr_0s is a positive value, then the vessel's frame zero is located forward the FDD frame zero. On the other hand, when d_fr_0s is a negative value, vessel's frame zero is located afterward the FDD frame zero. All the procedures developed in the current datasheet consider a single vessel docking above the FDD deck. In addition, the vessel orientation is shown in Figure 4.

Supposing the vessel is 180 degrees inverted along the FDD deck or its coordinated system is in different position from that presented in figure 4, users must convert to the currently adopted system. In addition, figure 4 emphasis variable d_fr_0s between the vessel's coordinate system and FDD aft perpendicular.

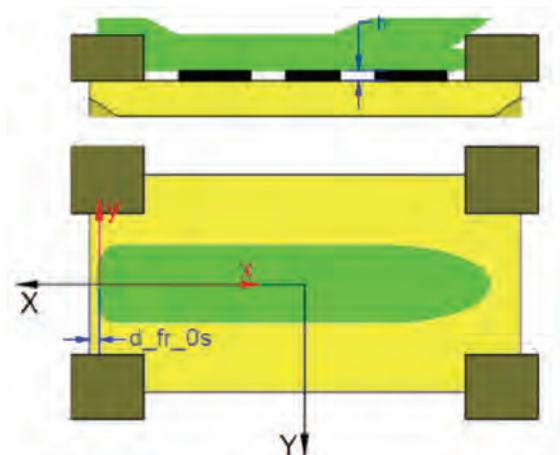


Figure 4 Vessel's coordinated system (in red) and FDD coordinated system (in black).

Table 3 shows another important input set consisting of a possible keel block plan to receive the vessel. The user must provide length, width, distance from keel block to FDD's frame zero for each block and its distance from the centre. It is assumed that the cross section of all beams used as keel blocks are identical, with a known section area (m^2) and inertia (m^4). For practical purposes, three beams of 92m length are used in this keel block plan, one is located at the vessel's centreline and the other two are placed at portside and starboard of the FDD.

Table 3 Lightweight Properties

Type	Length	Width	Dist. From frame "0"	Dist. From CL
Centre Line Blocks	92000	2200	17.0	0.0
Starboard Blocks	92000	2200	17.0	3.2
Portside Blocks	92000	2200	17.0	-3.2

Constrains checked through the docking plan are:

- Maximum linear load over the centreline bulkhead is 145mT/m;
- Maximum linear total load over the ship beam is 190mT/m;
- Maximum percent of load over the side blocks is 30% of the total mass of the vessel.

Table 4 shows some of the outputs of the keel block plan, according to [1]. Figure 5 shows a longitudinal load distribution. Previous three constrains are satisfied with this example and after that, user must go to the next sheet to add further inputs to the problem.

Main Inputs

This is the main datasheet to define the case before the equilibrium is calculated. A summary of the case is pre-analysed here, checking if the proposed case is feasible. The parameters are as shown below.

Table 4 Keel blocks output

LCG	LCG of the vessel (fwd of dock Fr.0)
A	Total block area. It considers a reduction due to the F_sb input value only for the side blocks
C_BA	Centre of Block Area (fwd of dock Fr.0)
e	Longitudinal eccentricity on loading
L_t	Total Inertia of blocks
Load on CL blocks	Percent value
Load on Side blocks	Percent value

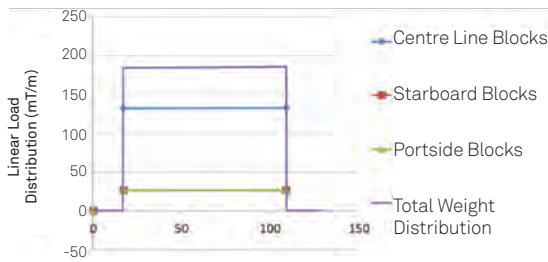


Figure 5 Linear load distribution on blocks

- 1) **Required Drafts:** The user must define which are the target drafts (aft and fwd). To achieve such drafts by static equilibrium, the computational tool adds or removes water inside the tanks, according to the correct phase of the ballast plan.
- 2) **Procedure:** According to the user needs this parameter takes the integer “1” if water ballast is only going to be added to the tanks or “0” if ballast water will only be removed from the tanks. For practical reasons, this option does not allow that a hypothetical ballast plan removes water from some tanks while adding water into others at the same phase.
- 3) **Upper Tanks:** The user has the option to configure the wing tanks (upper tanks) to search for equilibrium condition. If this integer is set as “1”, the routine considers the wing tanks as part of the equilibrium. On the other hand, if it is set as “0” the tool neglects those tanks from the analysis.
- 4) **Tanks:** define some constants of the problem such as density of ballast water (D.L.) and permeability of the tanks (Perm).
- 5) **Max H_tanks:** The user can limit a maximum water column in each ballast tank. The pontoon ballast tanks (Hmax_TL) are default 9.0m maximum water column and wing tanks (Hmax_TU) are default 7.2m maximum water column.
- 6) **Initial Condition:** Before starting any operation, the user must know the initial condition of each tank. Thus, the user fills only the yellow cells below due to transversal symmetry. Figure 6 shows nomenclature of each tank at FDD. The water column in metres is expected at each tank cell.

T6B						T1B
	6BA	5BA	4BA	3BA	2BA	1BA
	6B	5B	4B	3B	2B	1B
	6C	5C	4C	3C	2C	1C
	6E	5E	4E	3E	2E	1E
	6EA	5EA	4EA	3EA	2EA	1EA
T6E						T1E

Figure 6 Initial water level in ballast tanks

- 7) **Vessel:** During the evaluation of a complete pumping plan, there are some steps that do not have the load of the vessel to be docked yet (i.e. the beginning of the operation) and only the FDD is analysed in these cases. However, when the vessel to be docked touches the keel blocks it starts to gradually transfer load to FDD hull (i.e. middle to the end of operation). When the presence of the vessel is important in the study its draft and position of the centre of gravity is also required, to check stability and equilibrium of the rigid system vessel-FDD. This is the reason why the user must define if the presence of the vessel is considered or not in each step of the pumping plan by the computational tool.

Properties of the vessel to be docked must be available as well as its coordinated system in the convention adopted in this work.

Advanced Check of initial condition

According to the initial condition provided by the user, datasheet will perform following verifications.

- Maximum trim angle is 2.85 degrees;
- Maximum Trim (aft draft minus forward draft) is one metre;
- Maximum Draft is 19 metres at both perpendiculars of FDD.

Force equilibrium is performed as follows. If ballast water is going to be added, the total load in the initial condition must be less than the difference between the buoyance and the total mass. If this condition is not followed, a message is displayed indicating problems in the input data.

The opposite situation is observed for the removing ballast condition. In this case, the total load from initial condition must be greater than the difference between the total buoyance (FDD + vessel) and the total mass (FDD + vessel). If it is not, an error message will show that it is not possible to continue since for equilibrium this situation is only consistent with the ballasting condition. If any of the tanks in the initial condition is greater than maximum established in MAX_H_TANKS cell, than an error will be returned to the user.

Vessel Properties

In this datasheet the user must insert the hydrostatic properties of the vessel to be docked, such as equivalent draft, displacement, longitudinal centre of buoyance, KB and KMt. Linear interpolation is made whenever necessary, in order to get closer values from hydrostatic properties of the vessel to be docked.

Equilibrium of the FDD

This table brings hydrostatic properties of FDD or the coupled system FDD-vessel and a summary of constrains for running the excel solver. Figure 7 shows the target submerged condition for the case that will be solved, with correspondent drafts aft and forward at FDD simplified view. Running solver will allow the tool to search for a static equilibrium situation based on two main conditions. The first, is the classical equilibrium equation from Newton’s second law and the second is the difference between longitudinal centre of gravity (LCG) and Longitudinal centre of buoyance (LCB).

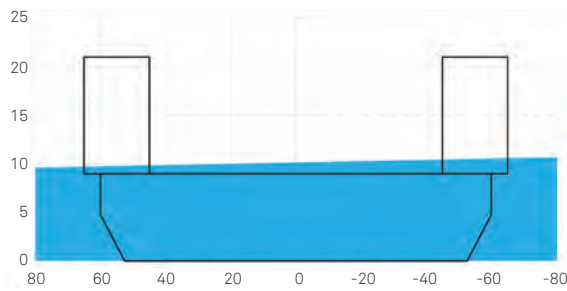


Figure 7 FDD target drafts

Discrete integration of the submerged volume is performed by the trapezoidal method, with all the sections inside the same datasheet. Equilibrium equation is given by:

$$\sum F_z = A_B + L_S + W_V - \Delta_{FDD} - \Delta_V = 0$$

Where:

- $\sum F_z$ is the sum of all forces at z direction;
- A_B is the added weight due to ballast water into the tanks, it is a variable condition to achieve equilibrium of the floating structure;
- L_S is Lightship weight of FDD which is a constant in this tool;
- W_V is Weight of the vessel to be docked. This could be "zero" if only FDD is available (in the beginning of operation, for example) or could be any parcel of the force added from the vessel to be docked. At the end of operation all loads of the vessel will be over the deck of FDD;
- Δ_{FDD} is the displacement of FDD, in mT. This parameter is defined when the user selects both target drafts over the FDD, which directly defines the total submerged volume of dry dock;
- Δ_V is the displacement of the vessel to be docked, in mT. This could be zero, total weight or only a parcel of total weight of the vessel.

The second condition, as previously mentioned, is given by:

$$LCG - LCB = 0$$

It states that no residual moment is present in the floating structure when longitudinal centre of buoyance and gravity are at the same perpendicular. Executing the solver in Microsoft Excel requires that only one "Objective Cell" is select to minimise, maximise or to reach a target constant value. In this tool the objective cell is the sum of the previous two condition residual values, forcing this cell to a minimum value of error, ideally zero. Other possible objective cells were evaluated during this work (i.e. only volume, only residual moment) but the most effective one was a linear combination from both conditions, leading to high computational efficient.

For the force equilibrium, a small tolerance value is acceptable as a percentage from total water to be distributed into the ballast tanks, in the beginning of operation. However, difference from LCG and LCB is taken as its absolute value. The solver will try to minimise both cells leading to a "zero" value for the objective cell. When it happens, equilibrium is established into FDD or FDD-vessel system.

The FDD constrains are evaluated together with classical equilibrium problem of a long floating structure due to small angles of inclination.

The variable cells are the required values of ballast water column in each tank. Symmetry is assumed from portside to starboard. Thus, a Ballast Plan is generated in each iteration, as exemplified in Figure 8. The FDD constrains are evaluated together with classical equilibrium problem of a long floating structure due to small angles of inclination.

4.47							3.17
	3.84	4.83	5.23	5.10	4.92	4.31	
	3.53	6.43	7.53	4.78	4.74	5.28	
	3.04	4.47	4.32	3.76	3.03	5.53	
	5.28	6.43	7.53	4.78	4.74	5.53	
	3.84	4.83	5.23	5.10	4.92	4.31	
3.17							4.47

Figure 8 Example of ballast plan

As the Solver tries to fulfill equilibrium conditions, it must also try to respect some other restriction, different from those related to the target condition. A description of constraints is shown below.

- Maximum head pressure between adjacent tanks ($\Delta h < 6\text{m}$);
- Minimum GM for Intact Stability ($GM > 1.5\text{m}$);
- Maximum Longitudinal Bending Moment ($LBM < 151,597 \text{ mT}\cdot\text{m}$);
- Maximum Transversal Bending Moment ($TBM < 127,464 \text{ mT}\cdot\text{m}$).

Tanks definition

34 ballast tanks are modeled, as shown in figure 9. All tanks have rectangular shape, and their volume are easily calculated. In addition, all the geometric properties of each tank are evaluated, such as centre of gravity and inertial areas. Free surface effects due to the existence of non-completed tanks is also considered for a safe operation.

Longitudinal and Transversal Structural Analysis

Due to the distributed load on the ship, the structural elements suffer with shear forces and bending moments. There are some limit values for these forces and moments depending on the type, size, and material of a member in a structure so it can support without structural failure^[4].

The FDD can be analysed in a simplified way as a beam with two fixed supports and some distributed loads. Model is shown in Figure 10, while the analytical representation of such problem can be found in any mechanical textbook.

In addition, all the geometric properties of each tank are evaluated, such as centre of gravity and inertial areas. Free surface effects due to the existence of non-completed tanks is also considered for a safe operation.



Figure 13 BrasFELS Floating Dry Dock

Table 7 Maximum Submergence ballast plan

6.86							6.69
	8.55	8.29	8.47	8.60	8.59	8.52	
	8.53	8.53	8.16	8.55	8.38	8.43	
	8.62	8.50	8.50	8.62	8.56	8.33	
	8.43	8.53	8.16	8.55	8.38	8.53	
	8.55	8.29	8.47	8.60	8.59	8.52	
6.69							6.86

Table 8 Keel Touch ballast plan

6.80							6.63
	8.46	8.16	8.40	8.48	8.51	8.42	
	8.41	8.44	8.12	8.49	8.32	8.32	
	8.52	8.40	8.42	8.50	8.47	8.20	
	8.32	8.44	8.12	8.49	8.32	8.41	
	8.46	8.16	8.40	8.48	8.51	8.42	
6.63							6.80

Table 9 5.5m Vessel draft ballast plan

6.21							5.23
	7.15	7.20	7.74	7.34	7.58	7.76	
	8.16	7.76	7.69	7.83	7.41	8.03	
	7.74	7.99	8.08	7.95	7.98	7.45	
	8.03	7.76	7.69	7.83	7.41	8.16	
	7.15	7.20	7.74	7.34	7.58	7.76	
5.23							6.21

Table 10 Top of keel blocks ballast plan

4.47							3.17
	3.84	4.83	5.23	5.10	4.92	4.31	
	3.53	6.43	7.53	4.78	4.74	5.28	
	3.04	4.47	4.32	3.76	3.03	5.53	
	5.28	6.43	7.53	4.78	4.74	5.53	
	3.84	4.83	5.23	5.10	4.92	4.31	
3.17							4.47

Table 11 Tow back/End ballast plan

0.00							0.00
	1.72	2.19	4.39	2.56	3.73	2.03	
	2.30	4.40	0.56	0.99	1.76	0.39	
	2.07	1.15	0.32	1.97	1.71	1.44	
	0.39	4.40	0.56	0.99	1.76	2.30	
	1.72	2.19	4.39	2.56	3.73	2.03	
0.00							0.00

Conclusions and future works

The development of inside solutions for equilibrium problem applied to a Floating Dry Dock (FDD) is presented in this work. The problem is established with all the constraints necessary for further operation, such as longitudinal and transversal stress force calculations, intact stability limits, and correct keel blocks plan.

The computational tool has been validated through past docking cases finding reasonable ballast plan to each of the different phases of docking procedure at a regular yard. One of the main advantages this routine is the fast confirmation of the desired equilibrium position in real time operation, without the need of other sophisticated programmes.

The entire development of this computational tool was performed using Microsoft Excel VBA and its solver function. For future improvements, data from real docking operations is required, comparing them with the predictions from this computational tool.

References

- [1] Crandall, P. S., 1976. Large Floating Dry Docks for Large Ships. Marine Technology, Vol. 13.
- [2] Heger Dry Dock Inc., 2005. Dockmaster training manual.
- [3] Passos, R. B. et. al., 2015. VBA numerical tool to analyze the capability of dynamic positioning systems. Keppel Technology Review.
- [4] Becht, Paul M., and James R. Hetherman, 2016. Introduction to Dry Docks. Design of Marine Facilities: Engineering for Port and Harbor Structures.

Author's Contact

- | rafael.passos@kfelsbrasil.com.br
- | olivier.montgolfier@kfelsbrasil.com.br
- | miguel.ramirez@kfelsbrasil.com.br
- | lucas.machado@kfelsbrasil.com.br

Acknowledgements

Authors would like to thank BrasFELS Shipyard for all support provided during the period of this research. Especial thanks to Mr. Michael Poeschmann and Mr. Too Lye from BrasFELS shipyard. Figure 13 shows an example of FDD used by BrasFELS to perform upgrade and repair for large offshore units and long vessels.

A Cost Effective and Versatile Platform Solution for Global Deployment : Keppel Self-Installing Platform

| Si Xuan HUANG*, M.Eng.

| Michael PERRY*, PhD, CEng, MIMarEST.

| Matthew QUAH**, PhD, CEng, CMarEng, FIMarEST.

| Terence LEK Wen Shiung#, B.Sc.

* Keppel Offshore & Marine Technology Centre

** Offshore Technology Development

Keppel Self-Installing Platforms (SIP) have been developed as cost effective fixed platforms for operations at marginal fields worldwide. They are multi-functional and relocatable minimal platforms that build on the core strength of Keppel jackup design and construction, with track record of more than 100 jackups delivered to date.

Main features of Keppel SIP include:

- Large topside capacity and available deck area. The base design has up to 9000MT topside capacity and 2100m² deck area, which is expandable by adding “hull wings”.
 - Self-Installing - OTD H4000 hydraulic jacking system allows easy, fast and cost effective installation without hiring offshore heavy-lift vessels. Cylinders can be removed for reuse after fixation systems are engaged.
 - Minimal platform with optimised design providing cost effective “real estate” that is easily adaptable for different uses (multi-function).
 - Modular design allows for fast and efficient design and construction. There is compatibility at subassembly level to provide modular “hull corner kits”.
 - Relocatable and adjustable for different sites, within a wide range of water depths, soil and metocean conditions.
-

Introduction

Jacket structures are currently the most common offshore structures used for marginal field developments. After being transported and positioned at site, the jacket is placed in the seabed and piles are driven through the jacket legs into the soil, before the topside modules are installed on top of the jacket.

A considerable part of the lifecycle cost of the jacket is caused by renting offshore heavy-lift vessels for installation. In addition, the installation schedule is highly restricted by availability of the heavy-lift vessels. The self-installing platform (SIP) concept becomes an attractive alternative solution for such developments as it has the great advantage that offshore installation can be done by using a lifting system, avoiding high cost of cranes and other offshore support vessels. Furthermore, conventional methods of pile driving is not required, making the installation, and eventual removal, faster and more environmentally friendly.

Keppel has developed innovative SIP solutions building on its core strength of jackup design and construction. They are multi-functional minimal platforms that can operate in offshore marginal fields worldwide, and are relocatable and adjustable for different sites.

Overview of Keppel SIP

Keppel is the world leader in the design and construction of offshore oil drilling jackups, with track record of more than 100 jackups delivered to date. The existing jackup knowledge and expertise has been leveraged in the design of Keppel SIP.

Keppel SIP has large topside capacity and wide open deck area. K4000S SIP (Figure 1), which is the base design of Keppel SIP, is able to support up to 9000MT topside weight and an available deck area of at least 2100m². The deck area is further extendable by adding "hull wings"; with hull wings of 10m in width, the available deck area can be increased to be 3428m².

K4000S SIP has a hull dimension of 50mx50m.

The design environmental parameters given in Table 1 allow it to operate in shallow water regions all around the world.

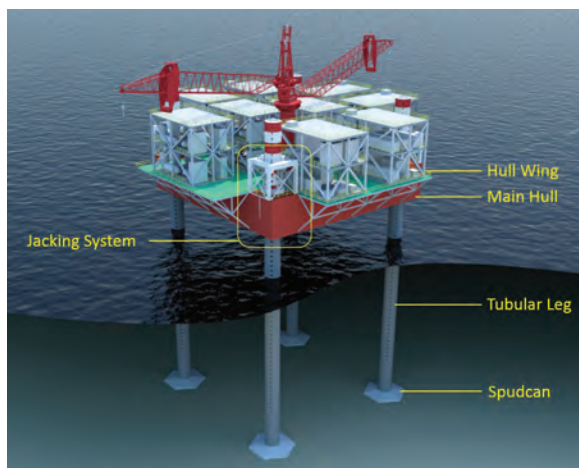


Figure 1 K4000S SIP – Keppel SIP Base design

Table 1 Design environmental conditions for K4000S SIP

Case 1

Environmental Parameter	Value
Max. water depth	50.0 m
Max. wave height	10.0 m
Wave period	10.0 s
Surface current	1.5 m/s
Wind speed (1-minute average)	30 m/s
Air gap	10.0 m
Leg penetration	3.0 m

Case 2

Environmental Parameter	Value
Max. water depth	40.0 m
Max. wave height	17.0 m
Wave period	13.0 s
Surface current	1.2 m/s
Wind speed (1-minute average)	36 m/s
Air gap	13.0 m
Leg penetration	3.0 m

Keppel's SIP design is based on the ABS Rules for Offshore Installations ⁽¹⁾ and ABS approval in principle has been obtained.

H4000 Jacking System and Fixation System

Self-installation of Keppel SIP (Figure 2) is achieved using the H4000 hydraulic jacking system developed by Offshore Technology Development (OTD).

The jacking system design leverages world leading jackup installation knowledge, and is based on strong competency in mechanical, hydraulics, electrical, instrumentation and automation.

The H4000 hydraulic jacking system provides a low cost solution for jacking. Compared to strand jacks which are commonly used for SIP installation, H4000 jacking system only requires a single system for both leg lowering and hull lifting. In addition there is no requirement for disposable items such as strands, and the jacks can be easily reinstalled in the case of relocation and removal of the platform.

K4000S SIP (Figure 1), which is the base design of Keppel SIP, is able to support up to 9000MT topside weight and an available deck area of at least 2100m².

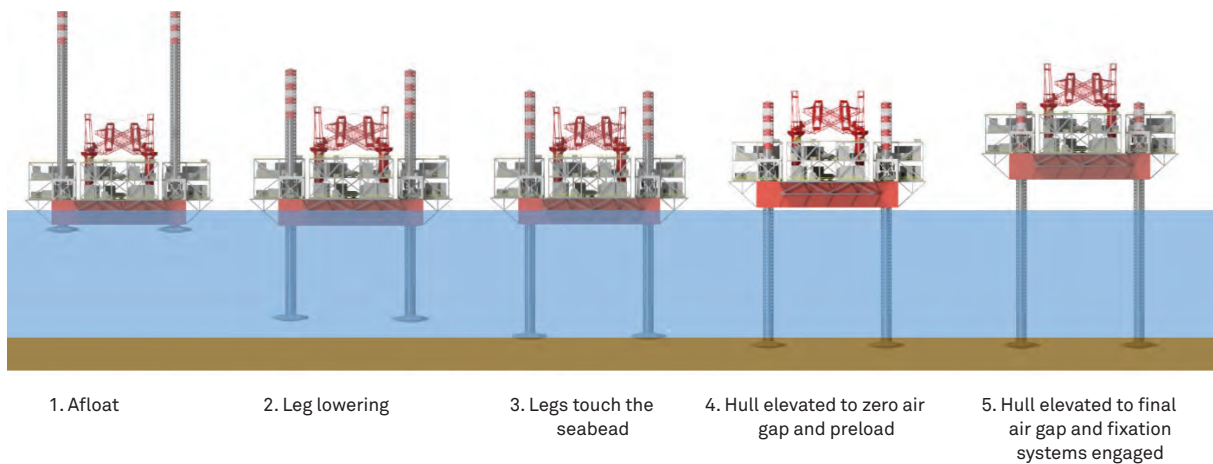


Figure 2 Self-Installation of Keppel SIP without using offshore heavy-lift vessels



Figure 3 Multiple functions of Keppel SIP

Table 2 Specifications of H4000 hydraulic jacking system

Type	Hydraulic pin & yoke
Hull jacking speed	0.1m/min
Leg jacking speed	0.2m/min
Normal jacking capacity	4,000MT per leg
Preload capacity	5,673MT per leg

Another key trait for the H4000 jacking system is that it is power self-sufficient for the entire jacking operation, removing the needs of expensive generator’s set to sustain this major operation.

Upon reaching the operational air gap, fixation system is engaged to hold the hull firmly in position. This significantly simplifies and reduces the time required for the installation, since offshore welding or grouting work is not required.

The cylinders are removable after the fixation system is engaged. Therefore the cylinders can be a temporary

(rental) equipment which makes it highly cost efficient for platforms requiring only one time jacking operation. On the other hand, ownership of the jacking system allows flexibility in installation scheduling as well as convenient reuse on multiple platforms.

Optimised Design for Multiple Uses

Keppel SIP design is optimised to create cost effective minimal platforms. Main components of the platform have a clean design, with local strengthening structures only applied at locations where needed. Internal connections and welding are therefore significantly reduced, minimising the works needed for construction and internal inspection. Fatigue performance of the platform is also improved.

All the SIP legs are located at the corners of the hull, this provides a large uninterrupted deck space with a regular shape. Different types of topside modules can be arranged on the deck with great flexibility, making the SIP easily adaptable to various uses, such as a production platform for offshore oil and gas development, a substation platform for an offshore wind farm, or an accommodation platform to provide offshore residential space for personnel. Moreover, Keppel is actively looking into solutions based on SIP concept for coastal engineering uses.

Modular Concept for Keppel SIP

The modular concept is implemented throughout the design of Keppel SIP. There is compatibility at subassembly level to provide modular “hull corner kits” (Figure 4). Besides, several SIP platforms can be combined via bridge connections, to control possible separation for example between an accommodation platform and a production platform (Figure 5). In this way the jacking components can also be reused across the units to reduce costs.

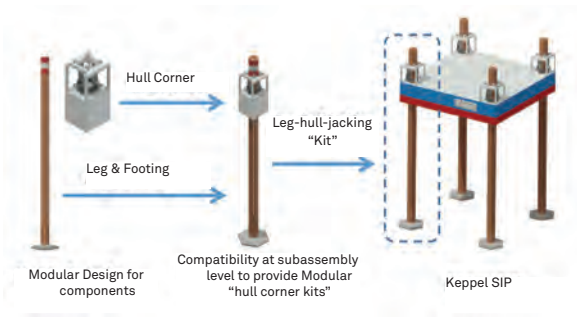


Figure 4 Modular design of Keppel SIP

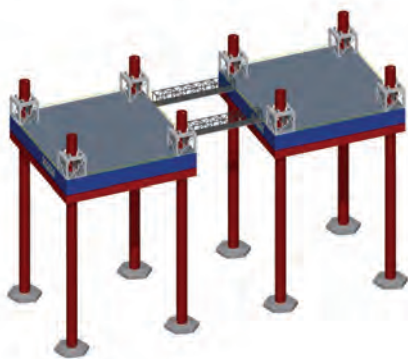


Figure 5 Possibility of combining Keppel SIPs

The modular concept allows for fast, efficient and cost effective design and construction. Different facilities can be constructed at the same time, to speed up the construction progress.

Flexible Keppel SIP Design

With the help of the jacking system, Keppel SIP is relocatable and reusable for different sites (Figure 6). Relocation of the SIP is fast and cost efficient since there is no need for mobilising large offshore support vessels. The whole SIP platform is removable, so that environmental impact is minimised. Topside and structures can be adjusted to fulfill the changes on topside requirements, water depths, metocean conditions and soil conditions.



Figure 6 Relocation and reuse of Keppel SIP

While the base design of Keppel SIP is targeted at shallow water depth, flexibility of entering deeper water regions is provided by adding a subsea frame (Figure 7). The entire hull and jacking system can remain the same as those for shallow water solutions, with the subsea frame sitting in the seabed to support the legs. The hull and the subsea frame can be constructed at different yards, to allow for flexibility on construction, or the frame can be provided as an add-on item for reuse of SIP at a new site.

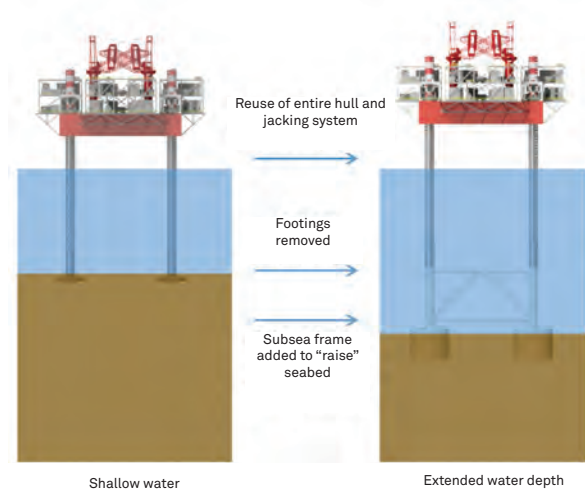


Figure 7 Keppel SIP for extended water depth

Conclusion

Compared to conventional jacket structures, SIP has the great advantage that its self-installation feature avoids high cost of cranes and other offshore support vessels; there is also greater control and flexibility with the installation schedule.

Keppel SIPs are innovative solutions building on Keppel’s core strength of jackup design and construction. They are multi-functional minimal platforms for operation at marginal fields worldwide. ABS approval on the design has been obtained.

Key features of Keppel SIP include:

- Self-Installing with using OTD H4000 hydraulic jacking system. Cylinders can be removed after engaging fixation systems.
- Minimal platform with optimised design to provide cost effective “real estate” for multiple uses.
- Large topside capacity and available deck area. It can be individually adjusted to meet different clients’ requirements.
- Modular design allows for fast and efficient design and construction. There is compatibility at subassembly level to provide modular “hull corner kits”.
- Relocatable and adjustable for different sites, with a wide range of water depths, soil and metocean conditions.

Reference

- [1] American Bureau of Shipping (ABS), "Rules for Building and Classing Offshore Installations", 1997.

Authors' Contact

| Sixuan.Huang@komtech.com.sg

Expanding Offshore and Marine Technologies beyond Current Capabilities

| WANG Rong*, B. Eng

| Ankit CHOUDHARY*, MSc, B.Tech

| Anis HUSSAIN*, MSc, B.Eng

| Sreekala Kumar*, B. Tech

| Pasumarthy S MURTHY#, - MSc, B.Eng

| Aziz MERCHANT*, CEng, MSc, FRINA, FIMarEST, FSNAMES

*Keppel Offshore & Marine Technology Centre

#Deepwater Technology Group

Many of decommissioned offshore platforms are getting a new sense of purpose such as diving resorts, cruise ship port-of-calls, recreation destinations, bio-habitats and hotels. As sea levels approach catastrophic levels, some see offshore platform architecture and other floating structures as the only viable way to survive, but they are also a great way to take advantage of beautiful oceanic settings.

Given the scarcity of land that the city-state faces, lack of space leads to skyrocketing real estate prices and impeded traffic. Mixed-use developments are seen as a successful strategy to resolve these spatial issues. Urbanisation and water retention can be combined, creating mixed-use developments and floating buildings can cope with sea level changes. More than one in every six people in the world is water stressed, meaning that they do not have access to potable water, which is due to many factors such as lack of water resources, infrastructures as well as climate change, etc. With an increased demand for smart energy storage and efficient management, Williams Advanced Engineering is working with Nissan Europe to demonstrate how electric vehicle battery storage technology from its cars can be repurposed to help power buildings in combination with solar photovoltaic (PV) energy.

Offshore platform is a large structure with facilities to drill and produce oil and/or natural gas from the seas or oceans or to temporarily store products until it can be brought to shore for refining and marketing. The offshore platform is built with a water treatment system to produce fresh water, power generator as well as provide comfortable accommodation to house the workforce. For example California coastal oil and gas platforms are proposed to be repurposed for use as large-scale fresh water production facilities. Solar arrays, mounted on the platforms, are able to provide some of the power needed for seawater desalination during the daytime.

A very large floating structure can provide a viable solution to the scarcity of land and infrastructure needs. Keppel Offshore & Marine, one of the global market leaders in the production and deployment of offshore maritime infrastructure, specifically oil rigs for oil majors would like to explore the repurposing of marine and offshore technology to build sustainable and eco-friendly solutions.

Introduction

Jack-up rig is a mobile self-elevating platform and consists of a buoyant hull fitted with a number of movable legs, capable of raising its hull over the surface of the sea since 1960s. Currently, there are jack-ups which can accommodate 150 people. There are semi-submersibles that have been developed and used since 1980s as floating hotels for up to 500 people and designed to function independently for an extended period of time to support various offshore work. These Floatels are high quality accommodations which provide recreational spaces alongside the usual facilities like catering, storage, workshops, offices, medical services, as well as lifesaving and firefighting equipment.

Translating Offshore Knowledge and Capabilities into New Products

Offshore construction and installation methods and technology have advanced over the years to make safe and reliable offshore structures to operate in extremely harsh offshore environments.

- Engineering capabilities: Technological know-how and capabilities have advanced to make it possible to design and engineer complex structures.
- Advanced facilities and infrastructure: Shipyard facilities have grown to support the construction of complex engineering structures.
- Adoption of offshore construction methods: Construction in a controlled environment and transported to be installed on site.
- Use of standardised components: Use of pre-built living spaces can result in faster and more economical construction than using stick-built on site construction techniques.

Keppel Offshore & Marine sees commercial viability in repurposing offshore technology in the following areas:

- Floating Cities
- Floating Desalination Plants
- Floating Power Solutions
- Floating Aquaculture Hubs

Making Improved Use of Sea-Space

As urban areas get more crowded, building new land and even floating homes is becoming more economic. Many small countries are in real need of additional sovereign territory. Sometimes, they even build on rotting landfills and install various kinds of expensive artificial islands. The ocean covers 71% of our Earth's surface. Countries starting early colonisation of the ocean may obtain advantages through additional territory or creating their own independent state. The best solution to this problem, is the provision of floating cities, islands, and states.

For example, a large part of Singapore's sea-space is taken up by anchorages for ships anchored by traditional methods. By repurposing some existing offshore technology such as suction piles or single point mooring technology it may be possible to tighten up mooring swing space for individual vessels allowing this sea-space to be used for alternative activities discussed previously such as offshore communities, aquaculture, offshore bunker storage and operations, offshore power plants, floating desalination plants etc.

Floating Cities

Why don't we build floating structures on the surface instead? It's not impossible. Floating villages have been around for a long time. In Cambodia, residents of the Tonle Sap freshwater lake live in floating houses. Similarly in Perus Lake Titicaca, the Uros people live on floating islands made from bundles of reeds. Around the world, architects are building more modern floating homes, especially in countries such as the Netherlands which is vulnerable to flooding.

Floating cities have been proposed by designers, researchers and organisations all over the world as a solution to the expected effects of climate change and land scarcity, or as a way to create opportunities for societal and political change. While the number of visions and designs for floating cities is impressive, the actual implementation to date remains limited to small-scale demonstration projects.



Figure 1 Floating Islands of Han River, Seoul

Waterfront living has become a worldwide trend and it presents a new and refreshing lifestyle. Near-shore or floating (or offshore fixed) platform communities and towns are a possibility of Singapore's skyline in the near future. Beyond Singapore, this is an exportable business option if we are able to refine our skills and manufacturing expertise in building offshore towns/cities.

There is reduced ecological impact and stress to the environment when compared to land reclamation. Offshore towns allow flexible town planning with varied infrastructure options combining both water and road transport. They will help reduce population strain on urban centres while opening up valuable and limited land for other land dependent uses.

Easily constructed at shipyards before being transported to their determined location, offshore towns can constantly appear dynamic and progressive. There is no disruption to the environment which land based construction projects would generate such as creation of construction pits,

Translating Offshore Knowledge and Capabilities into New Products

excavation work and noise during the construction. Even the demolition work can be done beyond current urban communities.

Offshore technology applied to offshore towns open new functions and design ideas of how land based buildings are used when at sea. Jack-ups are installed near the shore to create elevated platforms. From the spud cans, lower and upper hull to the above sea deck space, there is opportunity to weave into the design by utilising existing offshore and/or marine technology to provide fresh water, electricity, heating and waste management.

With offshore towns and cities, the possibilities of combining multiple functions and utilities can be applied to design, to create self-sufficient townships including desalination plants, fish farming, commercial, entertainment and accommodation facilities, etc.

Floating Desalination Plants

Floating desalination plant has been utilised as a temporary solution and already demonstrated many cases in several areas.

Floating desalination plants can be quickly implemented, with the capability to be incrementally added if necessary and easily deployed elsewhere after completing its expected role.

Mobility is the key word as new and existing plants are efficiently towed and relocated to any place of operation. There is minimum disruption to the supply due to the ease of replacing an old plant on-site with a new plant; the old plant can be easily decommissioned off-site. Floating desalination is a solution that can be deployed for meeting peak water demands.

A Hybrid Solution of an Offshore Plant with Land-Based Storage Facilities is also a possibility, with the flexibility to easily adapt to future advances in desalination technology by replacing the process barge.

The global desalination market is increasing as the world's growing population becomes more demanding. From Land based desalination plant builder, Israel's IDE Technologies Ltd. is in talks with Japan's shipbuilders and government to design and build off-shore desalination plants, seeking to tap rising demand for alternate sources of short-term freshwater supply. Many other designers also move into the floating desalination plant concept, such as Hyflux and BMT.



Figure 2 Floating Desalination Plant

Advantages of a Floating Desalination Plant

- Construction time is significantly shorter than a land based plant. No site mobilisation and civil work, e.g. foundations, buildings, roads, seawater intake structures are necessary.
- Turnkey delivery of the complete system to the service area saves transport over land.
- Simplified authority engineering, authorities approval procedures and customs advantages save time and money
- The rebuilding work required on the floating platform/vessel and the assembly of the seawater desalination plant is entirely performed in a well-equipped shipyard by highly skilled workforce.
- Tanks and infrastructure are already available on the floating platform/vessel, e.g. accommodation, offices, workshops, power generation, air conditioning, etc.
- Lower energy consumption for intake and brine disposal.

Floating Power Solutions

The concept of floating power barges already exists in the industry. An example is Keppel Energy's Power Barges which have been in operation in Ecuador since 2006.



Figure 3 Power barges deployment in Ecuador

Floating Power solutions provide an excellent alternative to meet the power demands of developing countries with quick implementation possibility, minimal land usage and high mobility. Floating power plants can also provide a rapid answer to increased power demand in advance of coming land based power plants.

Advantages of a floating power plant:

- Constructed in shipyards under controlled condition, relatively fast construction dependent upon equipment availability
- Can utilise any electrical generating technologies
- It provides fast supply of electricity to areas with limited infrastructure
- It is a mobile asset, possible to relocate or trade
- Provides secure power supply in the event of natural disaster (earth quakes or floods)

Floating Aquaculture Hubs

Aquaculture is the most rapidly expanding food industry in the world as a result of declining wild fisheries stocks and is a profitable business.

The Singapore Government and others have been looking at vertical farms/market gardens as a way to produce fresh fruit and vegetables in areas where land is at a premium.

One concept might be to move such vertical farms to waters adjacent to major urban centres and combine them with fish farming – a symbiotic combination as waste vegetable matter can be used for fish food and fish waste can be used as plant fertiliser. Such vertical farms can also contribute to cleaner air with plants absorbing CO2 and giving off oxygen.

Advantages of Repurposing Offshore Technology

1. Offshore platforms make for ideal construction of scalable and modular designs. Such designs make it efficient to construct, maximise gross floor space, and allow for flexibility of scale and dimensions.
2. Having designed and built large steel structures meant for long term use in the oceans we already have the technology and expertise to build sustainable floating and fixed structures.
3. Such offshore structures, using re-purposed technology, can be built entirely in the shipyards and towed out as a completed unit, thus there is no worry about construction disruption to environments they are being deployed to. Furthermore there is improved efficiency by completing construction, outfitting and commissioning at a well-equipped shipyard with skilled staff, rather than on site in the field.
4. In addition, these structures can be easily moved out for upgrading or modification or can be replaced by newer models, thus making the environment vibrant and dynamic while enhancing the seascape. The existing modules can also be quickly towed out and redeployed elsewhere or even refurbished and recycled. Note that marine steel structures, ships and offshore structures, are amongst the most recyclable. Approximately 90% of scrap steel is re-rollable to make new steel.
5. All of the above products can be built in shipyards, not only transforming how we use shipyards in the near future, but also tapping existing skills and expertise. This will refine and enhance industry standards, and further expand our knowledge of how existing concepts can be used in other non-offshore industries, while building up a manpower pool of transferable skills across the Group.
6. Coastal cities, regions and countries that are land constrained need to look to the sea for alternative resources. Singapore can become a manufacturing hub of such modular structures and platforms for the global market. Furthermore with the potential of sea level rising, the ability to build and deploy such structures which can handle such changes will be of interest in several areas of the world.

Summary

Offshore assets are in operation for a very long time used safely, efficiently & effectively in offshore oil and gas activities. They can be called offshore factories where people live and work.

Alternate use of such offshore structures and technologies for a beautiful, sustainable world is a way of amalgamating creativity with technology.

Efficient use of the sea space around various cities, islands and countries around the world can be a logical next step to the increasing urbanisation requirements.

References

1. <http://weburbanist.com/2015/04/01/oil-rigs-reclaimed-7-ways-to-reuse-obsolete-platforms/2/>
2. The Open Ocean Engineering Journal, 2010, 3, 1-11, Floating cities on Ice platform by Alexander Bolonkin*
3. <http://inhabitat.com/worlds-first-solar-powered-floating-island-opens-in-seoul/>
4. <http://www.archdaily.com/793589/this-floating-desalination-megastructure-is-designed-to-combat-californias-water-shortages>
5. <http://www.salmar.no/en/>

Authors' Contact

- | WANG Rong, wang.rong@komtech.com.sg
- | Sreekala Kumar, Sreekala.KUMAR@komtech.com.sg
- | Ankit Choudhary, Ankit.CHOUDHARY@KOMtech.com.sg
- | Pasumarthy S MURTHY, Murthy.Pasumarthy@keppelfels.com

Improving Energy Efficiency Through New Concept of Energy Storage System for Drilling Rigs and Vessels

| Afshar SHAIKH*, MSc, B.Eng.

| Dr. Bernard HOW*, PhD, B.Eng.

| Dr. FOO Kok Seng*, PhD, B.Eng.

| KOH Jin Xiang*, B.Eng.

| LEE Wey Lii#, B.Eng.

*Keppel Offshore & Marine Technology Centre

#Keppel FELS

This paper describes the introduction of an Energy Storage System (ESS) on-board drilling rigs and vessels. Various configurations, features and operation modes can be enabled by the ESS to achieve higher fuel efficiency. The ESS can enable features such as jacking and drawworks regenerative energy recovery, fuel efficient operation mode, jacking inrush current reduction, reduce drilling DC power variation, optimal discharge mode and renewable input. Benefits include reduced fuel consumption, increased spinning reserve, load leveling, reduced emission and reduction in maintenance cost for operators/owners.

Introduction

Drilling activities of an oil rig require considerable amount of power. The marine system, drilling equipment, mud pumps, drawworks, top drive, jacking, hotel etc. form the major consumers of electricity on an oil rig. The electrical demand can vary depending upon the operations being carried out and site parameters such as environment, drilling depth and soil conditions. As such, the engine may not be operating at its most fuel effective operating point. Also, energy can be recovered during jacking down operations and lowering of the drawworks.

Energy Storage System (ESS) in the form of batteries and capacitors can be introduced to improve the energy efficiency of the rig. By introducing an ESS, the engines can be operated at a fuel efficient operating point and the regenerative energy can be absorbed and stored. This stored energy can then be utilised to supply to loads when they are needed.

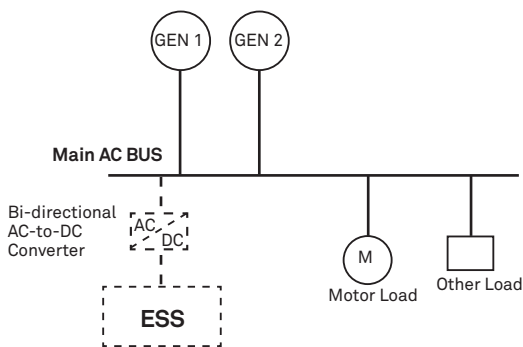


Figure 1 ESS Integration with Main AC Bus

ESS Integration and Configuration

The ESS can be designed into new builds or retrofitted into existing rigs and vessels as shown in Figure 1 to 4.

ESS Features and Benefits

The benefits of introducing the ESS features are summarised in Table 1.

Conclusion

Integrating an ESS onboard drilling rigs create benefits such as increase spinning reserve, jacking inrush current absorption, increase equipment life, reduce fuel consumption, back-up power option. These features can translate into reduced emission and maintenance cost for operators.

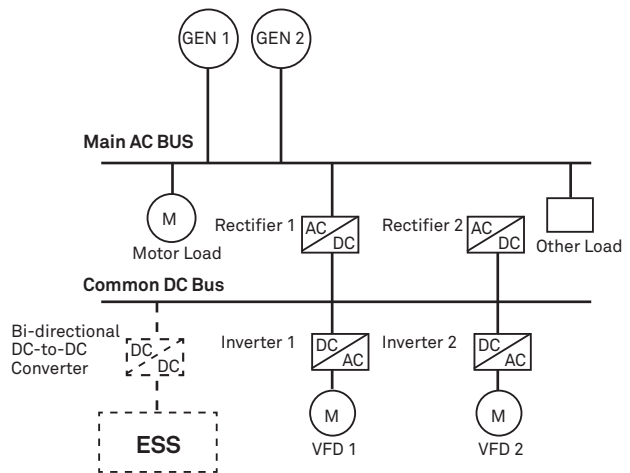


Figure 2 ESS Integration with Common DC Bus

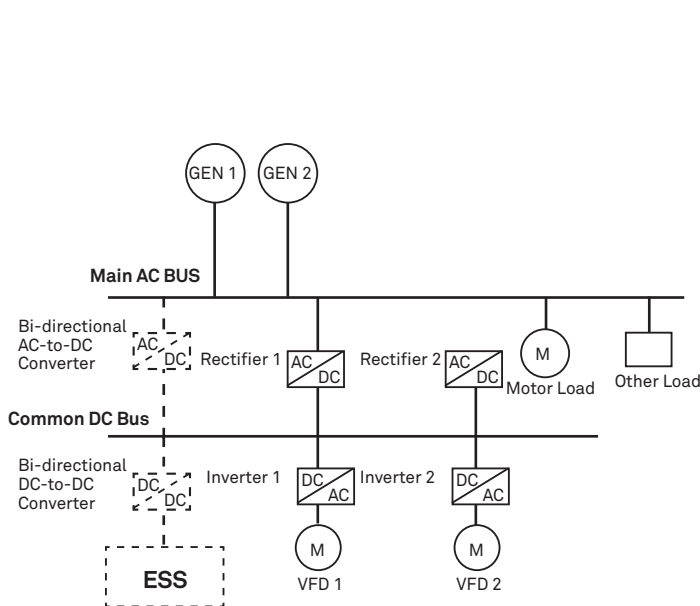


Figure 3 ESS Integration with Common DC Bus and Main AC Bus

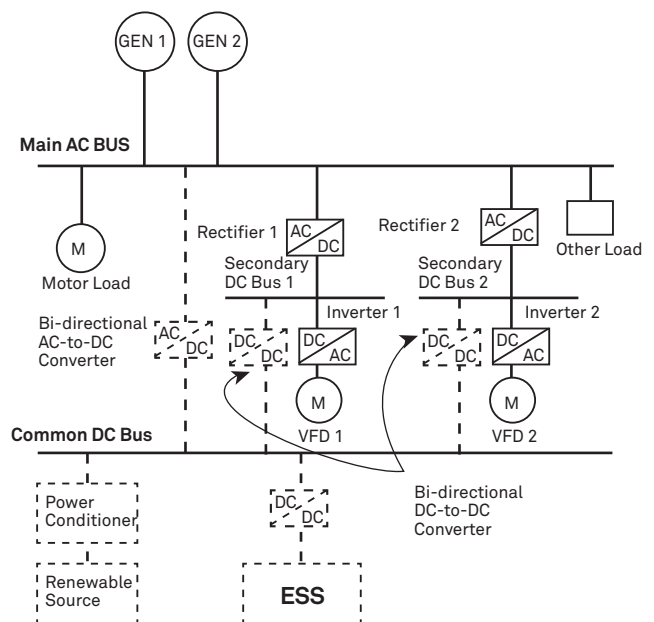


Figure 4 Power System with ESS, Common DC Bus and Renewable Source

The ESS can enable features such as jacking and drawworks regenerative energy recovery, fuel efficient operation mode, jacking inrush current reduction, reduce drilling DC power variation, optimal discharge mode and renewable input. Benefits include reduced fuel consumption, increased spinning reserve, load leveling, reduced emission and reduction in maintenance cost for operators/owners.

Table 1 ESS Features and Benefits

	ESS Features	Description	Energy Recovery + Fuel Optimisation	Power Quality & Reliability	Availability	Emissions
1	Drawworks Regenerative Energy Recovery	During tripping-in operation, the regenerative energy can be conserved and stored	✓			✓
2	Jacking Regenerative Energy Recovery	When the hull or leg(s) is being lowered regenerative energy can be absorbed and stored	✓			✓
3	Fuel Efficient Operation Mode	The ESS can bring the engines to the next fuel efficient level which can result in fuel savings and more efficient running of the engines	✓		✓	✓
4	Jacking Inrush Current Reduction	The ESS can discharge energy for direct-on-line starting of the motors		✓		
5	Reduce Drilling DC Power Variation	Smoothing of the DC power fluctuation during drilling operations		✓	✓	
6	Optimal Discharge Mode	Using the ESS, load variations on AC bus can be optimised through outputs of generator sets and/or ESS		✓	✓	
7	Renewable Input	Renewables such as solar energy can be included onto the Common DC Bus	✓			✓

References

- [1] Patent Application No.: 10201609106X: Power Storage and Supply Method and System for a Drilling Rig

Author's Contact

- | Bernard.how@komtech.com.sg
- | afshar.shaikh@komtech.com.sg
- | jinxiang.koh@komtech.com.sg

Enhancing Business Capabilities through Future Digital Rigs : Keppel RigCare™

| FOO Kok Seng*, PhD, KOMtech

| Bernard HOW*, PhD, KOMtech

| LIM Yak Yang#, B.Eng, Keppel FELS

| LEE Wey Lii, B.Eng, Keppel FELS

| Shawn YEO#, B.Eng, Keppel FELS

* Keppel Offshore & Marine Technology Centre

Keppel FELS

This paper describes a future digital world envisaged for the marine and offshore industry and the Keppel RigCare™ Platform to assist customers to reduce their OPEX, increase the reliability and availability of the equipment and provide a one-stop concierge service for asset lifecycle needs.

Introduction

In our future digital world, the market is becoming more competitive. Rig owners are looking into digital solutions to reduce their operational costs. The technology trend is to move towards a digital world which is becoming more data centric, with real time acquisition of data from sensors to monitor operations and conditions on the rig. There will be more data transactions and data analytics will play a major role in providing more optimised operations.

RigCare™ Platform

Leveraging Keppel's experience as a World Class designer, builder and integrator of rigs, Keppel embraced this trend and tailored a solution to assist Rig Owners in their operations and maintenance.

This platform enables the Rig Owners to enjoy rig care services after delivery with enhanced customer experience. The operations & maintenance data also enables analytics such as early warning for failures, running hour and event triggered maintenance alerts, remote monitoring, optimised manning and operation improvements. The RigCare™ Command and Configuration Centre (Figure. 1) provides the remote monitoring and ability to perform configuration according to the Rig Owners' preference and strategies.

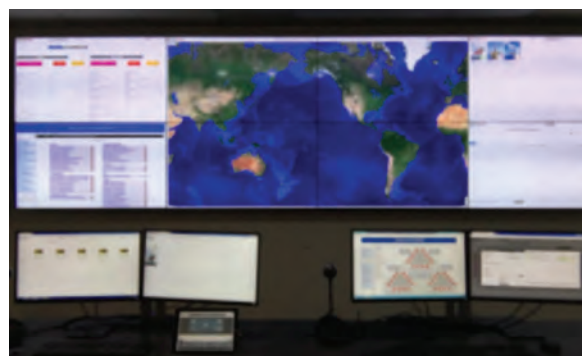


Figure 1 RigCare™ Command and Configuration Centre

The features and their advantages can be summarised in Table 1.

Conclusion

With the digital infrastructure, connectivity and security setup, a plethora of data can be acquired. This data can then be used to translate into OPEX reduction and used to increase the reliability and availability of the equipment via the RigCare™ Platform. With this platform, the rig owners are able to enjoy a one-stop full concierge service for asset lifecycle needs.

This data can then be used to translate into OPEX reduction and used to increase the reliability and availability of the equipment via the RigCare™ Platform.

Table 1 Features and Benefits of RigCare™

Feature	Benefits	Feature	Benefits
 Digital Rig	<ul style="list-style-type: none"> Digital Rig infrastructure to enable connectivity 	 Rig Information	<ul style="list-style-type: none"> Digitalisation of information and records for quick on demand access
 Asset Maintenance	<ul style="list-style-type: none"> Evidence based maintenance alerts Quick Turnaround 	 Asset Management (reliability)	<ul style="list-style-type: none"> Condition based maintenance Survey Credits enhancement Survey Downtime Cost avoidance
 Rig Analytics	<ul style="list-style-type: none"> Early Warning Increase Reliability Increase Uptime 	 Operation Optimisation	<ul style="list-style-type: none"> Reduce OPEX Operation Improvements
 Enhanced Monitoring	<ul style="list-style-type: none"> Extra Pair of Eyes Optimise Manning Quick Response 	 Concierge Service	<ul style="list-style-type: none"> One stop part & service Diverse Range of Product Selection with Competitive Price

Author's Contact

| kokseng.foo@keppelom.com

Improving Cargo Handling on Floating Platforms Using Dynamic Lift Monitoring and Predictive Decision Support System

| FOO Kok Seng*, PhD

| Bernard HOW*, PhD

| Umair SULTAN**, MSc

| Satish MENON**, B.Eng

| WANG Sheng Yin*, PhD

* *Keppel Offshore & Marine Technology Centre*

** *Offshore Technology Development*

The Dynamic Lift Monitoring System (DLMS) is a customised solution for crane operators to improve decision making required during cargo handling on floating platforms in rough and harsh offshore environment. During vessel to vessel lifting operations, the crane operator exercises judgment to lift and land the cargo based on his experience taking into the motions of both vessels. A judgment error may result in impact, causing damage to the payload. This system measures and provides real time dynamic motion to crane operators. A predictive algorithm is used to support the decision of the operators for dynamic lift operations.

Introduction

For vessel to vessel lifting operations, both vessels will be moving in six degrees of freedom and also relative to one another due to the offshore environment (wind, wave, swell and current). The dynamic motions of the vessel during the vessel to vessel lifting operation and the degrees of freedom are illustrated in Figure 1.

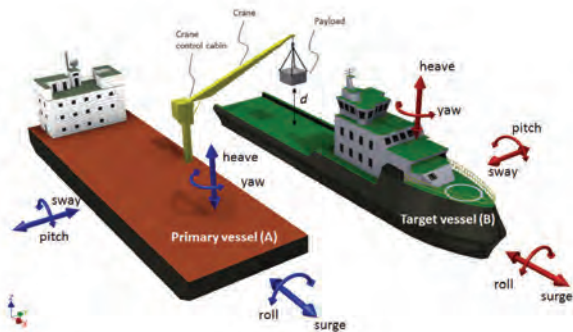


Figure 1 Dynamic motions of vessels and payload

For safe operations, the restriction on relative motions to conduct lifting operation is defined in Class rules and API standards [1-4]. For vessel to vessel lifts, relative vertical motion between crane hook and object should be carefully evaluated before the commencement of the lift. The crane operator in the cabin typically has to rely on his own judgment of the environment and his instinct to make decisions on the time to lift and land the cargo safely and with minimal impact.

Dynamic Lift Monitoring System

The Dynamic Lift Monitoring System (DLMS) interfaces multiple sets of motion sensors at different locations with wireless connectivity. The monitored data is displayed on

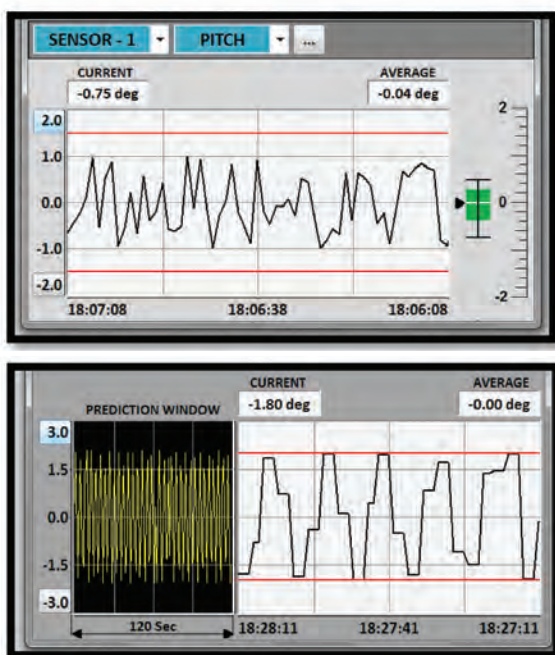


Figure 2 (top) Motion with limits and statistical box plot and (bottom) with motion and prediction window

Human Machine Interface (HMI) on a laptop and can be placed near the hoisting system to assist the operator. The motion sensors transmit the data to HMI panel through wireless communication and can be deployed instantly for any required operation. Based on the captured data, the system is able to predict the motion for operators. Taking into account the vessel motions and lift dynamics, the DLMS can provide a recommendation to support the operator decision on the time to start lifting and landing operation. The simulations for motion prediction and lifting / landing are discussed in the next section.

Simulations

In this simulation study, the panel code WAMIT was used to investigate the motions of a multi-body system involved in a lift operation in the frequency domain, while the numerical computing software MATLAB was applied to obtain the time-domain results from the frequency domain data. The lift operation was assumed to be under a sea state with a significant wave height of 2m and a zero-upcrossing period of 5s. The random wave amplitudes in the time domain were determined by the JONSWAP wave spectrum.

Example: Lift Operation of a Crane Vessel

The crane and target vessels used in this study are shown in Figure 3. The relative vertical motions of the crane vessel were shown in Figures 4 and 5, in which the barge is either on the weather side or the lee side.

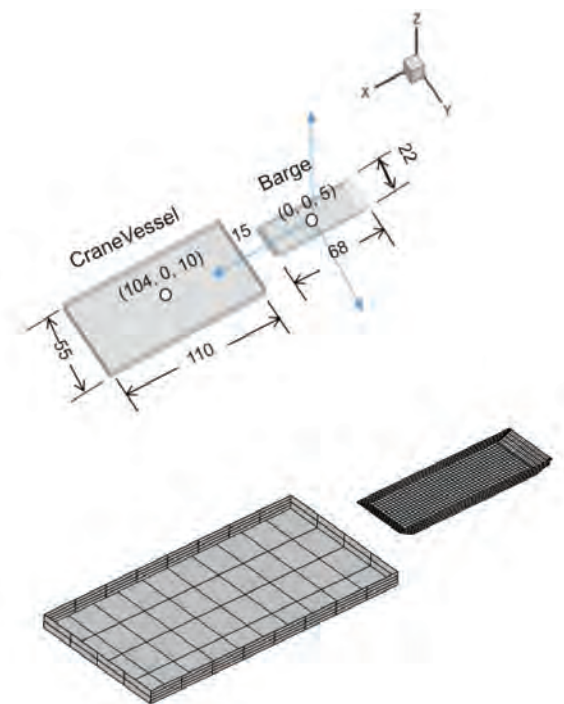


Figure 3 A Crane Vessel and a Barge in Lift Operation (top) dynamics and (bottom) mesh for hydrodynamic simulations.

The motion sensors transmit the data to HMI panel through wireless communication and can be deployed instantly for any required operation.

Based on the prediction of the motions, the accuracies is calculated to be around 7% which is satisfactory for random wave simulation (refer to table 1). The zoom in comparison of the simulated vs predicted motions are shown in 6 and 7. The comparison of the simulated predictive relative heave motions and velocities are shown in Figure 8 and 9 respectively.

Landing operations are simulated based on the case where landing is activated every second. The mean impact forces for both the simulated and predicted are found to be 71 kN and 75 kN, respectively (Figure 10).

Table 1 Comparison of the 3-hour Maximum Relative Heave Motion Predictions

	Frequency Domain Approach	Time Domain Approach	Error
Barge on Weather Side	2.4 m	2.53 m	5%
Barge on Lee Side	1.82	1.70	7%

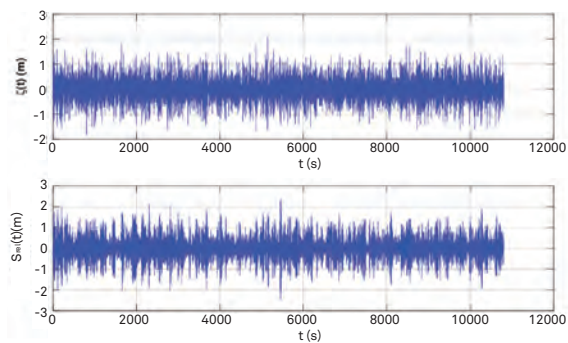


Figure 4 Relative Heave Motion Response (Barge on the Weather Side)

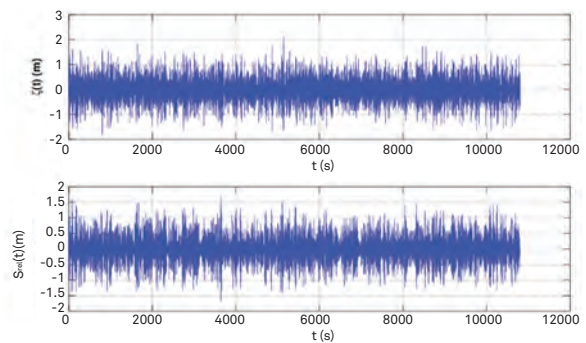


Figure 5 Relative Heave Motion Response (Barge on the Lee Side)

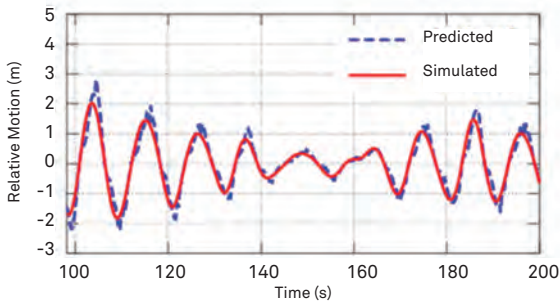


Figure 6 Comparison of the Predicted and Simulated Relative Heave Motions (Local View)

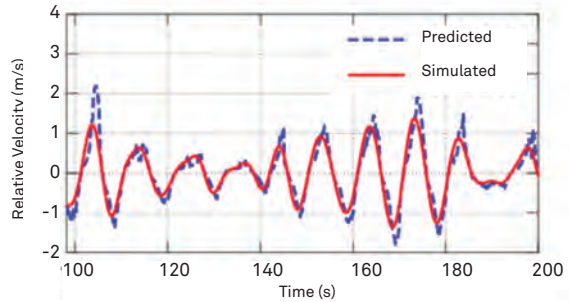


Figure 7 Comparison of the Predicted and Simulated Relative Heave Velocities (Local View)

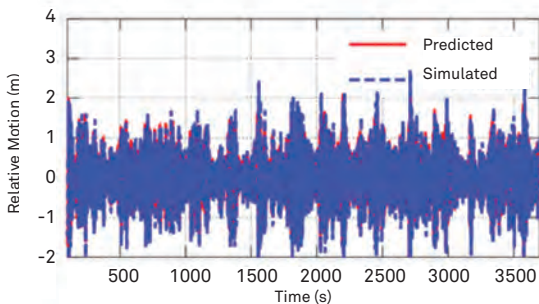


Figure 8 Comparison of the Predicted and Simulated Relative Heave Motions

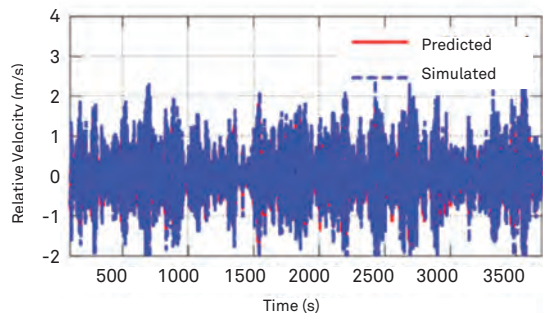


Figure 9 Comparison of the Predicted and Simulated Relative Heave Velocities

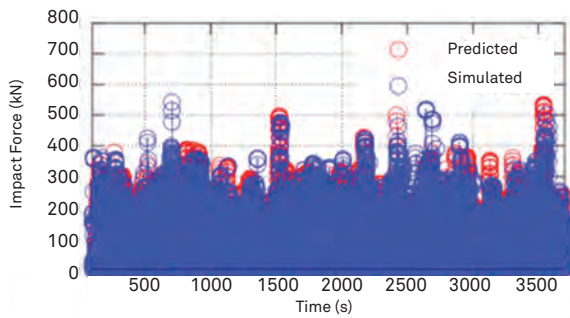


Figure 10 Comparison of the Impact Forces with landing activated every second. (Mean Impact Force ~ 70kN)

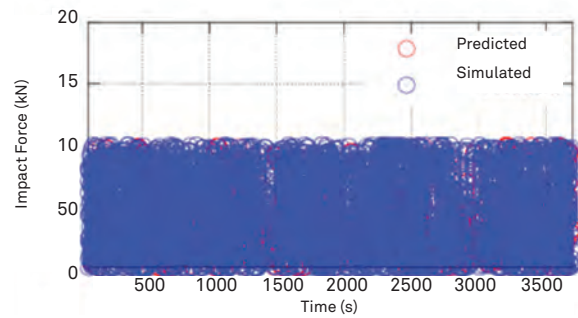


Figure 11 Comparison of the Impact Forces based on selected recommendations times (Mean Impact Force ~ 4kN)

Using the predicted motion and recommendation, the number of operations will be reduced to a set of the original operations shown in Figure 11. This new set of operations has a much lower mean impact force of around 4kN (Figure 11) than the original with a mean impact force of around 70kN. This shows that a significant improvement can be achieved.

System Benefits

The system helps to increase lifting availability of crane, optimise cargo handling, and reduce non-productive waiting time required to get for favourable weather conditions. The system is design to handle any types of cranes working on stationary, floating or mobile platforms in rough and harsh offshore environment.

The system provides the following benefits to end user:

- Unique predictive decision support feature for lift operations
- Real-time monitoring of relative motion between vessels.
- Allow operator to compute the measured data for precise handling and monitoring of load.
- Maximum utilisation of the load capacity based on the actual vessel motion instead of significant wave height
- Contact less instrumentation.
- Fast deployment of system on vessel.
- Less dependency on weather for lifting operation.
- Ideal for heavy lifting operations.
- In-build data logging of critical parameters.
- Single solution for all types of cranes and supply vessels.

Beside lifting applications, the DLMS can be used in variety of offshore and marine operations as a simple motion monitoring system such as Heavy structure movement, Heavy structure Decommissioning, Rig move and Rig recovery.

Conclusion

The Dynamic Lift Monitoring System provides real-time monitoring of relative motion between vessels. From the simulations, the decision support recommendation can significantly reduce the mean impact force of landing a load. This can help increase lifting availability of crane, optimise cargo handling, and reduce non-productive waiting time required for favourable weather conditions.

References

- [1] "Specification for offshore pedestal mounted cranes", API SPECIFICATION 2C, SIXTH EDITION, MARCH 2004
- [2] "Modeling and analysis of marine operations", DNV-RP-H103, APRIL 2011
- [3] "Lifting operations", DNV-OS-H205, APRIL 2014
- [4] "Crane lifting and slinging safe operation procedures", UKCS-SOP-043, AUGUST 2003

Author's Contact

| kokseng.foo@keppelom.com

Introducing a Novel Mechanical System for Coupling Two Offshore Floating Structures

| Amit JAIN*, MSc, B.Tech

| Peter Francis Bernad ADAIKALARAJ*, MSc, B.Tech

| Anis HUSSAIN*, MSc, B.Eng

* Keppel Offshore & Marine Technology Centre - Deepwater Technology

This paper focuses on the design and development of a new mechanical system for coupling the TADU (Tender Assisted Drilling Unit) and a production platform. The system consists of several rigid coupling arms, flexible elastomeric joints, pneumatic/hydraulic pistons and skidding assembly, which allows all the six degrees of freedom between the TADU and the Floating Production Platform. The system also has a connection/ disconnection assembly that allows the TADU to be quickly freed from the production platform and move away in extreme weather conditions.

Introduction

TADU alongside a fixed platform has been around for several decades. However, in recent years TADS (Tender Assisted Drilling Semisubmersibles) have been employed in Deeper waters alongside Tension Leg Platforms (TLPs), Spars and Compliant Piled Towers (CPT) in areas such as Offshore West Africa, Offshore Brazil and in South East Asia. There is a huge potential of TADU operations in areas such as in Gulf of Mexico, Offshore Australia etc. For TADU operations alongside a production platform (A TLP or a Spar), the two floating structures need to be connected. Current techniques allow the TADU to stay connected with production platforms through hawser systems (Nylon Ropes). Main drawback of the hawser system is that it requires certain minimum length of hawser for full development of non-linear stiffness needed for coupling two bodies. This imposes practical limitations in terms of having to deploy the hawser system in areas where its accessibility and maintainability is challenging. In addition, the hawser system has proved itself to be efficient in benign environments; but it may have limitations in harsher environments. Moreover, the system also ensures a minimum clearance between two floating platforms for normal operational requirements and prevents the TADU from colliding with the production platform in the event of a mooring line failure of the TADU.

This paper includes a system description and initial parametric study done to determine the configuration of number of joints and component dimensions.

System Description

During operation, Nylon flexible Hawsers couples the TADU and TLP as shown in Figure 1a. The TADU is moored and hold back lines hold the TLP. This new concept replaces the Hawsers by a mechanical coupling arm as shown in Figure 1b.

TADU is equipped with mud system, power system, large pipe rack deck space and accommodation thus significantly minimises wellhead Platform size required for Drilling Equipment. Reduced footprint on the seabed, hence minimal disruption to the Marine eco-system. While operating, the TADU- TLP need to come as close as five metres, though the usual operation separation is around 20-25 metres. Thus, the coupling arm length should be around 20-25 metres with capability of retracting 15 -20 metres. In the event of a storm and hurricane or cyclone, the TADU can move away from TLP by means of a quick disconnecting mechanism in the arm. Since the coupling arm has a disconnection mechanism it could be designed to remain connected for environmental load of one year return period or more.

The coupling arm has flexible elastomeric bending joints, a hydraulic piston and a skidding assembly (see Figure 1b); together these components absorb all the six degrees of

The piston and the skidding assembly absorb the surge motions. The heave, pitch, roll, sway and yaw motions are taken care by the flexible joints. The separation between the TADU and TLP is adjusted by tightening and loosening the mooring lines, the piston and the skid assembly stroke length is such that they can accommodate 15-20 metres of stroke length of the coupling arm.

freedom of relative motions. The piston and the skidding assembly absorb the surge motions. The heave, pitch, roll, sway and yaw motions are taken care by the flexible joints. The separation between the TADU and TLP is adjusted by tightening and loosening the mooring lines, the piston and the skid assembly stroke length is such that they can accommodate 15-20 metres of stroke length of the coupling arm.



Figure 1a Shows a TAD and TLP coupled by Nylon Hawsers

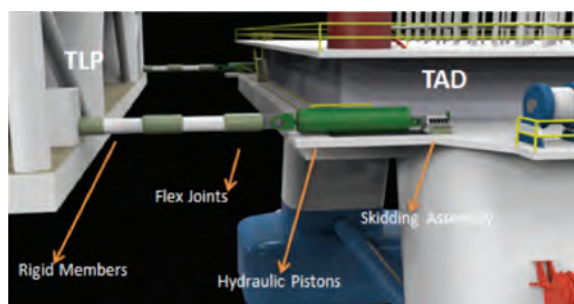


Figure 1b Shows a TAD and TLP coupled by Mechanical Coupling Arm

Moreover, the system also ensures a minimum clearance between two floating platforms for normal operational requirements and prevents the TADU from colliding with the production platform in the event of a mooring line failure of the TADU.

Preliminary Analysis

Preliminary Analysis has been done for the requirement of number of joints and the dimension of the main joints of the arms. Industry available off the shelf flex joints have been used for the stiffness and the permissible rotation and bending capacity for the analysis. Several

configurations of the coupling arm with different joint lengths and number of joints are shown in below figure. The geometric specification of the several coupling arms is listed in Table 1. The joint length measurement is done assuming each arm joint and the adjacent flex joints as one joint.

Table 1 Different Geometric configuration of the coupling arm considered for analysis

Case	Joint 1 (m) Connected to TLP	Joint 2 (m)	Joint 3 (m)	Joint 4 (m) Connected to TADU		Total length (m)	
				Fully stroke in	Fully extended	Fully stroke in	Fully extended
1	4.975	4.35	-	7.675	12.675	17	22
2	4.475	3.85	4	4.675	6.675	17	19
3	4.975	4.35	4.35	5.675	8.675	19.35	22.35
4	4.975	4.35	4.35	7.675	12.675	21.35	26.35
5	5.975	5.35	-	7.675	12.675	19	24
6	4.975	4.35	4	5.675	8.675	19	22
7	5.975	5.35	5.35	5.675	8.675	22.35	25.35
8	5.975	5.35	5.35	7.675	12.675	24.35	29.35
9	6.975	6.35	6.35	5.675	8.675	25.35	28.35

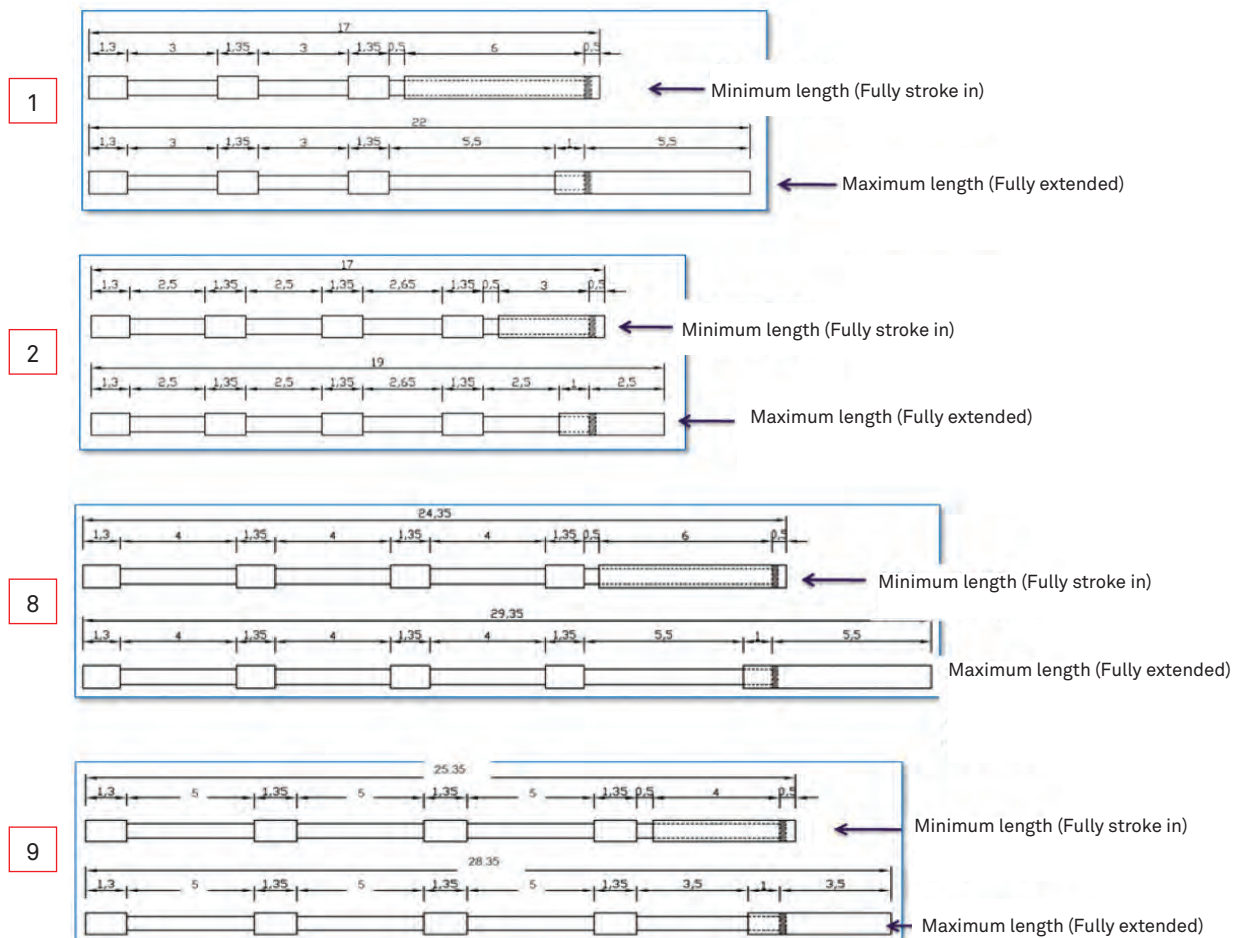


Figure 2 Different Geometric configuration of the coupling arm

Design Criteria and Analysis Methodology

Criteria

Below parameters are used to check the behaviour of the coupling arms.

Table 2 Design criteria for Coupling arm

Parameter	Symbol	Criterion	Remarks
Von Mises stress ratio	VMSR	$VMSR \leq 0.67 \text{ yield strength}$	
Max rotation of end flex joint	EFJ _{max}	$EFJ_{max} \leq 10^\circ$	Equipment limit
Max rotation of intermediate flex joint	IFJ _{max}	$IFJ_{max} \leq 20^\circ$	Equipment limit

Analysis Methodology

The objective of this study is to determine the size of the coupling arm system connecting a TADU and a TLP. The analysis was performed using FLEXCOM, which is a popular Finite Element Method (FEM) analysis software package used in offshore industry. The mass of the FlexJoints (7000Kg each) and main joints are significant and were included in the study to observe self-weight induced deflection of the arm. In reality, two arms couples the motions of two vessels. For simplification, this study only considers one single arm as shown in Figure 3.

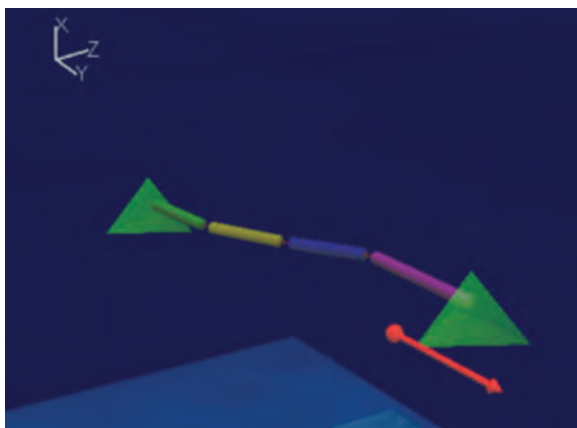


Figure 3 FE Model of a single arm in Flexcom

Sensitivity Analysis

The sensitivity analysis is conducted in two stages to determine the optimum number of joints and joint lengths for the coupling arm. Initially, a static analysis was performed by applying displacements and rotations at the TADU end as can be seen in Figure 4. Secondly, dynamic analysis was carried to check for any maximum value of stresses and rotations in the coupling arm using time history displacement inputs, obtained from coupled hydrodynamic analysis. Nine static analysis cases of the arm configuration with different joint lengths and number of joints as given in Section 3 were modelled. The arm comprises several main joints and flexible joints as shown in Figure 3. One end of the arm, which is connected to the TLP, is fixed in six DOFs whilst the other end is applied with a four-metre displacement in sway and a two-degree rotation in yaw. The displacement has been determined as the worse motion for single line mooring failure from time domain coupled analysis carried for TADU and TLP. The analysis cases are compared in terms of the von Mises stress in the main joints and the allowable rotations of the flexible joints.

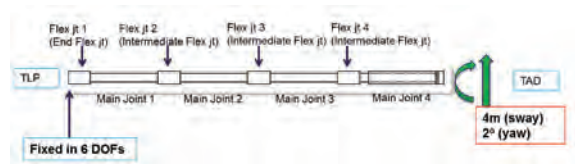


Figure 4 Sensitivity analysis with static displacements

Dynamic Analysis

For the dynamic analysis, the end, connected to the TADU of the selected arms from the sensitivity analysis is then applied with the three hour relative vessel motions, obtained from the time domain coupled body analysis. To represent piston stroke at the TADU end, a spring with stiffness value of $4.20 \times 10^4 \text{ N/m}$ is considered in this study. The Mises stress and rotations are checked with the yield strength of the main joint and the rotation limit of the flexible joints. Figure 5 shows schematic of the coupling arm model with boundary conditions and loadings.

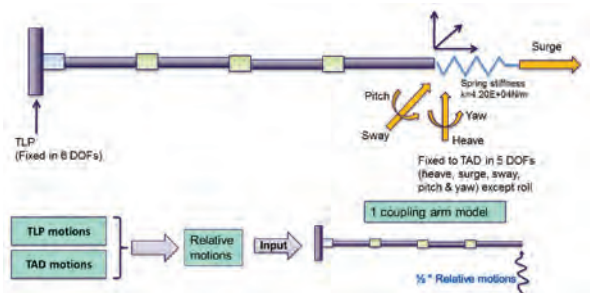


Figure 5 Dynamic analysis with series of vessel motion time trace

It is noted that these vessel motions were obtained for the system with two vessels connected by hawsers (not the coupling arms). For further study, a more precise motion analysis should be conducted for the two vessels connected by a coupling arm system.

Results and Way Forward

Sensitivity Analysis Results and Discussion

A comparison of the rotation of the flexible joints of nine analysis cases is presented in Figure 5. Flex Joint 1 (End Flex Joint) is located at 0m. As shown in Figure 5, only Cases 7, 8 and 9 gives acceptable rotations of the flexible joints. Low stresses are also noticed for Cases 7, 8 and 9. The 3-joint arms give larger rotations of the flexible joints and larger stresses in the main joints compared to the

4-joint arms. As the number of FlexJoints increased from three to four, the coupling arm becomes more flexible and resulting in small rotations. In addition to that, the von Mises stresses in the main joints are also reduced significantly as shown in Figure 6. Von Mises stress is exceeding the allowable limit of 67% of yield capacity for case 1 with three FlexJoints as can be seen in Figure 6, but only 30% for case 9.

Dynamic Analysis Results and Discussion

From the static analysis results, three analysis cases selected for the dynamic study (Cases 7, 8 and 9) with the 3-hour relative vessel motions applied at the end of the arm, which is connected to the TADU. Figure 8 – Figure 12 show time history of von Mises stress in the main joints and the relative rotation of each flexible joint when the relative

vessel motions for the mooring intact condition are applied at one end of the arm. As shown in Figure 7, the stress in the main joints is under the allowable limit (0.67% of yield strength) for all three cases. Von Mises stress utilisation along the coupling arm in Figure 7 shows that dynamic stresses in case 7, 8 and 9 are all under the allowable limit (67% of σ_y). A steep increase in the FlexJoints rotations can be seen in Figure 8 – 11 due to initial drift and self-weight of the FlexJoints. The maximum Mises stress in the arm noticed at both ends. From the dynamic analysis results, the rotation of Flex Joints 2 and 3 of Case 9 is under the limit of 20 degrees while the rotation of Flex Joint 1 almost meets the limit of 10 degrees. The rotation of Flex Joint 4 of all cases exceeds the limit of 20 degrees. It should be noted that the rotations of the FlexJoints and stresses on the coupling arm are mainly depending on the magnitude of the relative motions obtained from hydrodynamic analysis. In this study, the specifications of the FlexJoints were directly taken from supplier without any modifications. To withstand such very large displacements at the ends of the coupling arm the FlexJoints can be designed with high rotational limits (25 degrees).

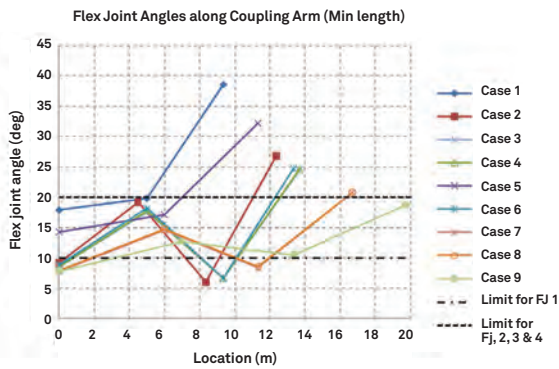


Figure 6 Bending subtended at different Flex Joints

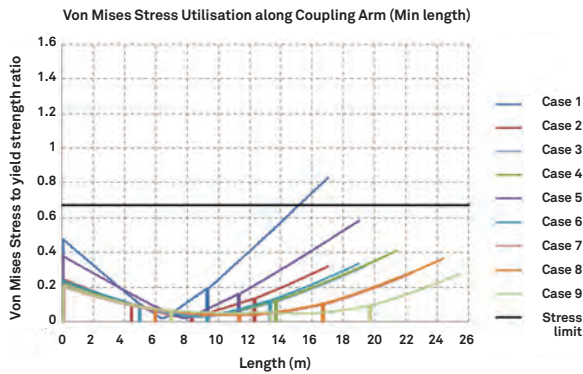


Figure 7 Stresses at different flex joints of the Coupling Arm

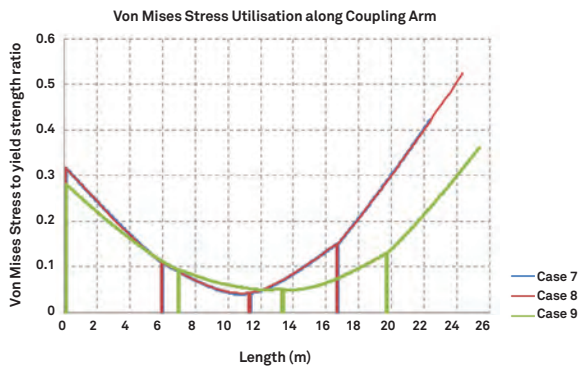


Figure 8 Von Mises Stress utilisation along coupling arm (Limit 0.67)

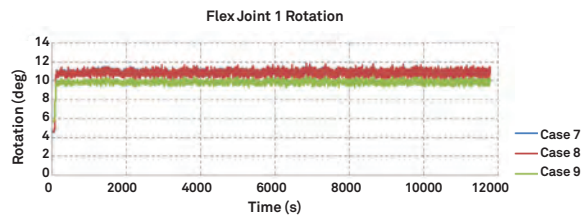


Figure 9 Flex Joint 1 (End Flex Joint) rotation (Limit: 10°)

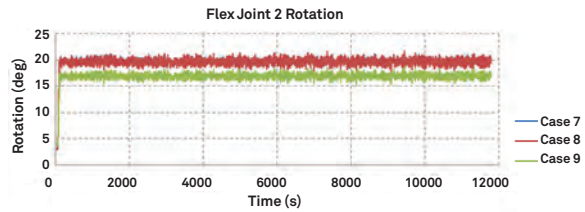


Figure 10 Flex Joint 2 (Intermediate Flex Joint) rotation (Limit: 20°)

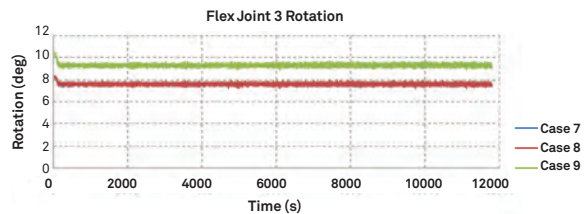


Figure 11 Flex Joint 3 (Intermediate Flex Joint) rotation (Limit: 20°)

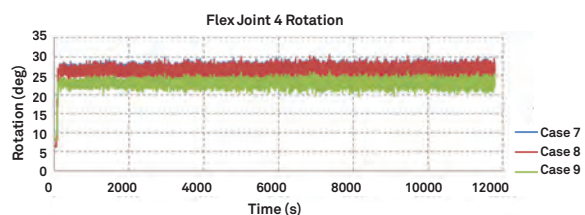


Figure 12 Flex Joint 4 (Intermediate Flex Joint) rotation (Limit: 20°)

Conclusion

The design, operation principle, and FE analysis of a new coupling arm system is briefly presented in this paper. The analysis results show that increase in the number of joints and the joint lengths results in reduction in the stress in the arm and the rotation of the flexible joints. However, this lead to increase in self-weight induced deflection and stresses. The 3-joint options give significantly large rotations at the flexible joints and high stresses at both ends of the coupling arm compared to the 4-joint options, albeit larger spaces on the TADU are required to accommodate longer 4-joint coupling arms.

From the initial analysis, the 4-joint coupling arm, i.e. Case 9, turns out to be the best option of all analysis cases that can take large relative vessel motions. As a final point, relative motions envelope of two floating structures and operating environment will dictate the Flexjoint rotations and von Mises stresses in the coupling arm. It may be used for further detailed study of the coupling system.

Way forward : Keppel- NUS Corporate Laboratory

Presently the system is being studied under the aegis of Keppel – NUS Corporate Laboratory, with research focusing on following three sub-themes

- a. To develop a methodology for non linear time domain Coupled Hydrodynamic Analysis incorporated with non-linear properties of the Coupling Arm incorporated and experimental validation of the methodology.
 - b. To prepare an interface for interaction of the hydrodynamic analysis with the Structural FEM analysis and prediction of the structural performance of the Coupling arm using industry based FEA tools and benchmarking of the results by scaled lab tests.
 - c. Development of sensors for structural health monitoring of the Coupling Arm system.
-

References

1. American Petroleum Institute (API). Recommended Practice for Design of Risers for Floating Production Systems (FPSs) and Tension-Leg Platforms (TLPs). API RP 2RD, June 1998.
2. Oil States Industries, Inc. Drilling Products. Technical Data Sheets for Diverter, Intermediate and Subsea FlexJoints.
3. Deepwater Technology Group (DTG). Coupled Mooring Analysis: TLP with SSDT3600E. 10 Jul 2012.

Author's Contact

- | amit.jain@komtech.com.sg
 - | Bernad.Peter@komtech.com.sg
 - | anis.hussain@komtech.com.sg
 - | aziz.merchant@keppelom.com
-

Technology Review 2017

Acknowledgement

The editorial committee would like to thank the following organisations for their strong support towards the publication of this technology review:

- Keppel FELS Ltd
- Keppel Shipyard Ltd
- Keppel Singmarine Pte Ltd
- Deepwater Technology Group Pte Ltd
- Offshore Technology Development Pte Ltd
- Keppel FELS Brasil S.A.
- American Bureau of Shipping
- DNV GL
- Llyod's Register
- Maritime and Port Authority of Singapore
- National University of Singapore
- Nanyang Technological University
- Ocean Mineral Singapore Pte Ltd
- f(K)N
- Laboratório de Ondas e Correntes

We also wish to acknowledge the help of everyone involved in this technology review publication, especially the authors and reviewers. We thank the authors for their time and effort contributed to the articles. We thank the reviewers for their guidance and expertise in ensuring the quality, coherence, and content presentation of the paper submissions.

Keppel Offshore & Marine
Technology Centre

31 Shipyard Road

Singapore 628130

Tel: (65) 6591 5450

Fax: (65) 6265 9513

Email: KOMtech@keppelom.com

Co Reg No: 200615559N